

This item was submitted to Loughborough University as a PhD thesis by the author and is made available in the Institutional Repository (<https://dspace.lboro.ac.uk/>) under the following Creative Commons Licence conditions.



For the full text of this licence, please go to:
<http://creativecommons.org/licenses/by-nc-nd/2.5/>

Pilkington Library

Author/Filing Title ONG, F.R.

Accession/Copy No.

Vol. No.	Class Mark <u>T</u>
---------------	---------------------------------

LOAN COPY

0402084845



**ANALYSIS OF BONE DRILLING CHARACTERISTICS FOR THE
ENHANCEMENT OF SAFETY AND THE EVALUATION OF BONE STRENGTH**

by

FOOK RHU ONG

A Doctoral Thesis


submitted in partial fulfilment of the requirements

for the award of

The Degree of Doctor of Philosophy of the Loughborough University

July 1998

© Fook Rhu Ong, 1998

 Loughborough University PL Library
Date May 99
Class
Acc No. 060208484

K0645004

ABSTRACT

Bone drilling is a major part of modern orthopaedic surgery associated with the principles of internal fixation of fractured bones. At present, information related to drilling forces, rate of drill bit penetration and drill bit rotational speed is not available to orthopaedic surgeons, clinicians and researchers as bone drilling is performed manually. This research demonstrates that orthopaedic surgery involving the drilling of bone can greatly benefit from the technology of automation/mechatronics, which allows the collection and storage of the drilling data for analysis as well as for the improvement of the drilling procedure. The research also represents a significant contribution to the development of a drilling system for the enhancement of safety and/or as a diagnostic tool for the evaluation of bone strength. A novel automated experimental rig, which enables drilling tests to be carried out in a controlled environment, has been developed.

The investigation for the enhancement of safety involves the detection of drill bit break-through on a femoral shaft in the presence of system compliance and inherent fluctuation of drilling forces. Since these two factors affect the detection of drill bit break-through, a robust and reliable method based on a modified Kalman filter has been developed. When applied to the force difference between successive samples and the rotational speed, the modified Kalman filter has been found to be very effective in establishing trends and ironing out major fluctuations caused by the system compliance and inherent drilling force fluctuation.

The evaluation of bone strength related to the cancellous bone at the proximal femur has resulted in the establishment of a positive relationship between the average drilling force and bone mineral density (BMD), obtained from bone densitometry, which is used to estimate bone strength in clinical practice. The correlation has been found to depend on the direction of drilling. This is indicated by a linear relationship obtained in the anterior-posterior direction (perpendicular to the cervical axis), which is not interchangeable with the relationship in the direction of the cervical axis. Findings of this research have indicated that analysis of bone drilling forces has the potential to provide additional information about the strength of bone.

ACKNOWLEDGEMENTS

I would like to express my gratitude to Dr. K. Bouazza-Marouf for the supervision of this research and for his support and advice.

The opportunity to carry out this research has been made possible by the financial support provided by the Overseas Research Students (ORS) Award and the Departmental studentship. I am grateful to the Committee of Vice-Chancellors and Principals of the Universities of the United Kingdom (CVCP) for the ORS Award, and to the Wishbone Trust of the British Orthopaedic Association and the Department of Mechanical Engineering for the studentship.

I would like to thank the members of the technical staff of the Department of Mechanical Engineering who have contributed towards the development of the drilling experimental rig and the robot for surgery assistance, the machining of mechanical components and the interfacing of electronic components.

I would also like to thank Eddie Baileys of Loughborough and the formerly Butchery of Residential Organisation for the supply of porcine bones for the experiments. Thanks also go to Mrs. A. C. McKinnon of BUPA Hospital Leicester for providing densitometric measurements of the bones.

I would like to extend my appreciation to my parents and Miss M. T. Dang for their constant encouragement and moral support. Finally, my appreciation is also extended to Dr. K. T. K. Toh for his invaluable comments with regards to the thesis during the course of writing-up.

DEDICATION

To my parents,
for their love, support and encouragement

CONTENTS

ABSTRACT	i
ACKNOWLEDGEMENTS	ii
DEDICATION	iii
CONTENTS	iv
CHAPTER 1 INTRODUCTION	1
CHAPTER 2 PROJECT BACKGROUND	4
2.1 Orthopaedic Surgery	4
2.1.1 Difficulties Related to Orthopaedic Surgery	
2.2 Robotic Systems for Surgery Assistance	7
2.2.1 Application of Robotics in Medicine	
2.2.2 Robotic System for Orthopaedic Surgery Assistance	
2.3 Drilling of Bone	13
CHAPTER 3 SCOPE OF THE RESEARCH	14
3.1 Statement of the Problem	14
3.1.1 The Enhancement of Safety	
3.1.2 The Evaluation of Bone Strength	
3.2 Research Aims	16
3.3 Research Objectives	16
3.4 Scope of the Research	17
3.4.1 Literature Review	
3.4.2 The Detection of Drill Bit Break-through	
3.4.3 The Evaluation of Bone Strength	
3.4.4 Experimental Rig Design and Tests	
3.4.5 Experimental Results	
CHAPTER 4 REVIEW OF THE LITERATURE	20
4.1 The Drilling of Bone	20
4.2 Bone Drilling Performance	21
4.2.1 Effects of Thrust Force and Torque	
4.2.2 Effects of Temperature	
4.3 Strength of Bone	34
4.3.1 Mechanical Properties of Bone	
4.3.2 Bone Densitometry	
4.3.3 Correlation of Mechanical Properties and Bone Densitometry	
4.3.4 Bone Drilling	
4.4 Automation of the Bone Drilling Process	48
4.5 Conclusion	51

CHAPTER 5	THE DETECTION OF DRILL BIT BREAK-THROUGH	52
5.1	The Drilling of Bone	52
5.2	Configuration of the Drilling Unit	53
5.3	The Enhancement of Safety	54
5.4	Present Detection Methods of Drill Bit Break-through	54
5.4.1	The Effects of System Compliance	
5.4.2	The Effects of Inherent Drilling Force Fluctuation	
5.5	Proposed Detection Method of Drill Bit Break-through	59
CHAPTER 6	THE EVALUATION OF BONE STRENGTH	62
6.1	The Strength of Bone	62
6.2	Bone Drilling Analysis in the Evaluation of Bone Strength	63
6.2.1	Drilling Force Profiles of the Proximal Femur	
6.2.2	Proposed Method for Correlation of Bone Strength	
CHAPTER 7	EXPERIMENTAL RIG DESIGN AND DRILLING TESTS	72
7.1	Experimental Method for Detection of Drill Bit Break-through	72
7.1.1	Experimental Rig and Instrumentation	
7.1.2	Data Acquisition, Input and Output Interface	
7.1.3	Experimental Set-up	
7.2	Experimental Method for Evaluation of Bone Strength	82
7.2.1	Experimental Rig and Interface	
7.2.2	Bone Densitometry Measurement	
7.2.3	Experimental Set-up	
7.2.4	Correlation between Average Drilling Force and BMD	
CHAPTER 8	RESULTS AND DISCUSSION: THE DETECTION OF DRILL BIT BREAK-THROUGH	87
8.1	Effects of System Compliance	87
8.1.1	Experimental Tests Using an Industrial Twist Drill Bit	
8.1.2	Experimental Tests Using a Surgical Drill Bit	
8.1.3	Discussion on the Effects of System Compliance	
8.2	Application of a Modified Kalman Filter	101
8.2.1	Kalman Filtered Results of an Industrial Twist Drill Bit	
8.2.2	Kalman Filtered Results of a Surgical Drill Bit	
8.2.3	Discussion on the Application of a Modified Kalman Filter	
8.3	Control Strategy for the Detection of Drill Bit Break-through	113
CHAPTER 9	RESULTS AND DISCUSSION: THE EVALUATION OF BONE STRENGTH	116
9.1	Correlation in the Direction of Anterior-Posterior	116
9.1.1	Correlation at the Proximal Femur	
9.1.2	Correlation at the Femoral Shaft	
9.2	Correlation in the Direction of the Cervical Axis	123
9.2.1	Profiles of the BMD	
9.2.2	Profiles of the Average Drilling Force	
9.2.3	Correlation between Average Drilling Force and BMD	
9.3	Discussion	134

CHAPTER 10 CONCLUSIONS	137
10.1 Contribution of the Research	137
10.2 Conclusions from the Research	138
CHAPTER 11 RECOMMENDATIONS FOR FURTHER WORK	140
11.1 The Enhancement of Safety	140
11.2 The Evaluation of Bone Strength	141
REFERENCES	143
APPENDICES	
Appendix 1 Exemplar of Orthopaedic Surgical Procedures for Femoral Fracture Fixation	150
A1.1 Fractures of the Femur	
A1.2 Internal Fixation of Proximal Femur Fractures	
A1.3 Internal Fixation of Femoral Shaft Fractures	
Appendix 2 Description of the Robotic System for Orthopaedic Surgery Assistance	156
A2.1 Prototype Robot Manipulator and Controller	
A2.2 Vision Interface System	
A2.3 Procedure of Robotic Assisted Orthopaedic Surgery	
Appendix 3 Bone	161
A3.1 The Functions of Bone	
A3.2 The Chemical Composition of Bone	
A3.3 Bone Cells	
A3.4 The Structural Composition of Bone	
A3.5 The Microstructure of Bone	
A3.6 Fracture Healing Process of Bone	
A3.7 The Physical Properties of Bone	
Appendix 4 Modelling of Drilling Unit Bone Support System	171
Appendix 5 Modelling of Cross-Sectional Chip Area at Drill Bit Break-Through	173
Appendix 6 A Recursive Kalman Filter	177
Appendix 7 Journal Paper to be published in the Proc. Instn Mech. Engrs, Part H, Journal of Engineering in Medicine, Vol. 212, 1998	181
Appendix 8 Experimental Results related to Chapter 9	195
A8.1 BMD Measurements at the Greater Trochanter and the Femoral Head	
A8.2 BMD Measurements at the Femoral Shaft	
A8.3 BMD Measurements at Sections aligned with the Cervical Axis	
A8.4 Actual Profiles of Drilling Force in the Direction of the Cervical Axis	
Appendix 9 Mechanical Design - Drawings	208
A9.1 The Pan Joint with Brake Unit	
A9.2 The End Effector	
A9.3 A Calibration Frame	
A9.4 The Drilling Experimental Rig	

CHAPTER 1

INTRODUCTION

The importance of bone drilling is reflected in two main areas of interest: (i) orthopaedic surgery and (ii) biomechanical engineering, shown in figure 1.1. In orthopaedic surgery, the drilling of bone is extensively carried out for the fixation of fractured bones related to the principles of internal fixation using implants and screws. These techniques of fixation, which are less traumatic, have been shown to achieve excellent fracture stabilisation and allow for early recovery of the patient's mobility. It is, therefore, very crucial to produce holes of the correct size at prescribed positions with the minimum of effort during surgery. The amount of mechanical and thermal damage to the surrounding bone during drilling should also be kept to a minimum.

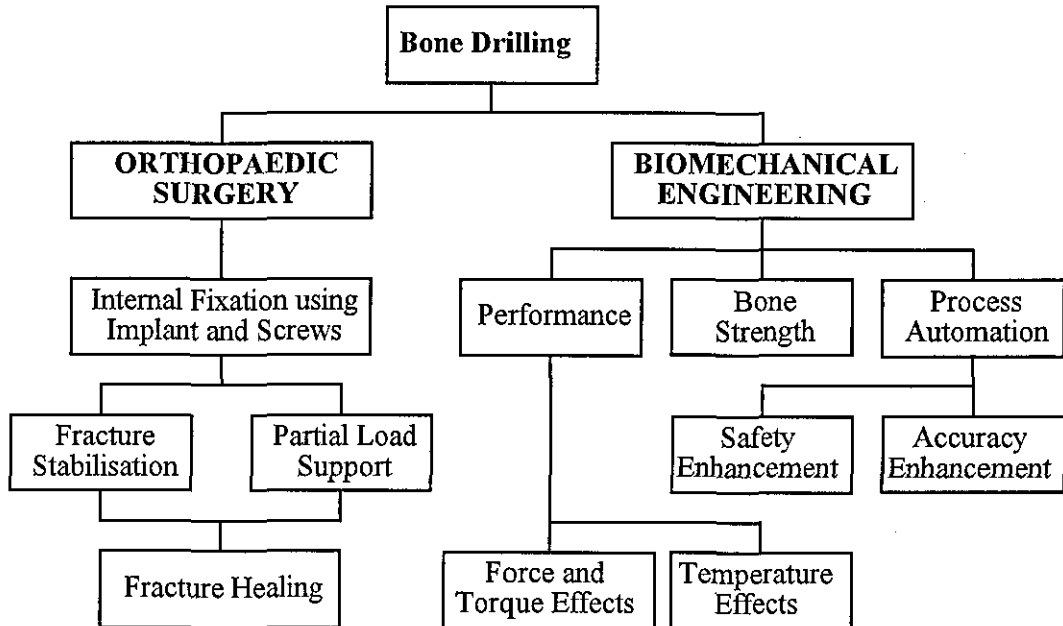


Fig. 1.1 Applications of bone drilling

The need to study and to improve the process of bone drilling associated with orthopaedic surgery has been the driving force behind the research into the area of biomechanical

engineering. This area can further be classified into: (i) the drilling performance, (ii) the mechanical strength of bone, and more recently, (iii) the automation of the drilling process. The effectiveness of producing the 'correct' hole for internal fixation is primarily governed by the drilling performance of drill bits, which is directly linked to the design of the drill bit shape and the operating conditions. Therefore, optimisation of the drilling performance based on measurable parameters, such as thrust force, torque, rotational speed and temperature, is essential for the improvement of the process of bone drilling. The evaluation of bone strength using bone drilling data and the automation of the drilling process are the objectives of this research, and are presented in the following section.

At present, information on bone drilling which is related to drilling forces, rate of drill bit penetration and rotational speed, is not available to orthopaedic surgeons, clinicians and researchers, as drilling is performed manually. Furthermore, there is no means of acquiring these data with the current available drilling equipment. The potential benefits from these drilling data can be: (i) safety enhancement of the surgical drilling procedure, (ii) providing an indication of bone strength and (iii) building a knowledge base for clinical studies. In order to gain these potential benefits, the technology of automation or mechatronics has to be incorporated into the present bone drilling process. The automation technology enables the drilling data to be collected and stored for either immediate or future analysis as well as for clinical studies.

This research emphasises the contribution of automation to the process of bone drilling associated with robotic/mechatronic assisted orthopaedic surgery. A major aspect of the work is to investigate the characteristics of bone drilling for the enhancement of safety of the mechatronic assisted orthopaedic drilling process. This thesis describes the development of a robust technique for the detection of drill bit break-through on a femoral shaft in the presence of system compliance. The work also involves the consideration of inherent drilling force fluctuation resulting from the variation of the bone structural density. The second major aspect of the research is to investigate the relationship between bone strength of the proximal femur derived from drilling mechanics and bone mineral density (BMD) measured by bone densitometry. The resulting relationship is considered to be a contribution to the strength evaluation of the proximal femur because the bone structure at this skeletal site is critically related to the bone mineral density or mass.

Chapter 2 of this thesis relates to the background for the research project into bone drilling and it describes the sequence of events leading to the start of the research. This includes the problems related to orthopaedic surgery and the application of robotics in medicine such as a robotic system for assisted orthopaedic surgery developed in the Department of Mechanical Engineering of Loughborough University.

Chapter 3 presents the scope of research which includes the problem statement and the identification of the research aims and objectives. The scope also covers a detailed description of the work to be carried out in order to achieve the research objectives.

The literature review of bone drilling in Chapter 4 consists of three main sections in accordance with the application of bone drilling on biomechanical engineering, as shown in figure 1.1. A detailed discussion on the current developments related to bone drilling is provided. Established methods of evaluating bone strength related to strength of materials and bone densitometry are also discussed.

Chapter 5 provides a critical review of the present methods of drill bit break-through detection for the enhancement of safety. It also presents details of the research methodology in order to achieve the aim of safety enhancement. Chapter 6 presents the method of correlation between drilling mechanics and bone densitometry used to achieve the second research aim of evaluation of bone strength.

In order to verify the proposed methods of safety enhancement and evaluation of bone strength, an experimental rig has been designed and appropriately set-up in order to gather relevant measurement data for analysis. This is presented in Chapter 7. Results and discussions of the experimental tests in relation to Chapter 5 and Chapter 6 are presented in Chapter 8 and Chapter 9 respectively with accompanying graphical presentation of the results.

The conclusions from the research are drawn in Chapter 10, and Chapter 11 presents the recommendations for further work.

CHAPTER 2

PROJECT BACKGROUND

This chapter provides an overview of robotic applications in medicine, particularly in the field of assisted orthopaedic surgery where the Department of Mechanical Engineering of Loughborough University has been actively involved. The difficulties related to orthopaedic surgery are highlighted in order to justify the development of a proposed robotic system for surgery assistance in planning of the drilling trajectory. General discussions on the overall developments of the project and issues associated with stringent safety and sterility requirements for the robotic system are also included in this chapter. Since the robotic system partly involves drilling, the investigation associated with bone drilling is also briefly discussed.

2.1 Orthopaedic Surgery

Orthopaedic surgery encompasses the correction of deformities and the treatment of diseases and injuries of the musculoskeletal system that includes bones, joints, muscles, tendons and nerves. In the eighteenth and nineteenth century, orthopaedic practitioners were known as bone setters (Dandy, 1989). Modern orthopaedic surgery, however, is more sophisticated and requires knowledge of other disciplines such as rheumatology, neurology and community services, as well as the application of biomechanical principles. Furthermore, having a wide range of skills and techniques in orthopaedic surgery is essential since there are a wide variety of instruments available for various techniques of fixation.

In modern orthopaedic practice, the traditional prolonged traction and plaster-casting of fractured bones have mostly been replaced by principles of internal fixation. This is also known as osteosynthesis, which involves reducing the fracture to restore bone fragments to their anatomical locations before using nails or plates, and screws to achieve fracture stabilisation. These techniques of internal fixation have been shown to achieve excellent results in fracture

stabilisation and healing, restoring full functional capability of the fractured bone, and allow for early mobilisation (Müller *et al.*, 1991).

The advantages of internal fixation have been shown to be evident in the repair of hip fractures associated with elderly people. Excellent fracture stabilisation and early mobilisation offered by internal fixation are essential to achieve maximum functional independence and to prevent secondary complications (Perez, 1994).

2.1.1 Difficulties Related to Orthopaedic Surgery

Difficulties associated with orthopaedic surgery relate, in general, to the difficulty in visualising the drilling trajectory on a partly exposed bone (Bouazza-Marouf *et al.*, 1995). This is due to the minimal invasive nature of the techniques of internal fixation, which requires orthopaedic surgeons to use x-ray images taken from a mobile x-ray unit (C-arm) as guidance. In order to highlight the difficulties encountered by orthopaedic surgeons, surgical procedures related to the fracture fixation of the hip (neck and trochanter) and the femoral shaft, as described in Appendix 1, are chosen.

The difficulty in visualising the drilling trajectory is a consequence of the use of only two near orthogonal x-ray images, taken from a C-arm, to represent a three-dimensional object. In addition, only a small part of the fracture site is adequately exposed during surgery in order to reduce intra-operative blood loss, risk of wound infections and other complications. Without direct visualisation of the fracture site, surgeons have to estimate the location and the orientation of the fractured bone based on x-ray images. Also, surgeons have to rely heavily on intra-operative fluoroscopic guidance provided by the x-ray unit to monitor the progress of the drilling procedure. As a result, surgeons and patients are exposed to the hazards of x-ray radiation, and the level of exposure depends on the number of x-rays taken to give a satisfactory guidance, especially in placing distal locking screws for fixation of shaft fracture. The amount of radiation exposure has been found to be more pronounced among surgically inexperienced surgeons due to the necessary long learning curve (Coetzee & Van Der Merwe, 1992). At present, there are no conclusive findings on the extent of radiation effects in orthopaedic surgery. Although quantitative studies have indicated that levels of x-ray exposure are well

within the maximum yearly limit (Riley, 1989; Sanders *et al.*, 1993), radiation exposure is a cumulative process and it has no safe threshold (Kwong *et al.*, 1990).

Orthopaedic surgeons are also faced with difficulties in estimating the desired drilling depth due to unknown position of the drill bit and bone thickness. If the drilling procedure is not stopped in time, excessive drill bit over-travel can occur, which could result in serious damage to the surrounding tissue. For instance, the treatment of femoral neck fractures has been shown to suffer excessive protrusion of guide wires into the pelvis (Feeney *et al.*, 1997) and that over-travel of as much as 20 mm may not be detected (Noordeen *et al.*, 1993). Fluoroscopic images provide guidance only and therefore, measurement of the drilling depth and bone thickness would require suitable calibrated references.

Manual drilling is also limited by the level of accuracy to which a surgeon can achieve. For instance, insertions of distal locking screws for shaft fracture fixation and pedicle screws for spinal stabilisation are demanding tasks and require a high level of accuracy, good technical skill and great effort. To effectively achieve these tasks would place heavy reliance on the usage of fluoroscopic guidance.

The size of the drilled hole is critical when it comes to the holding power of screws as failure of either bone or screw could occur because of incorrect hole sizes. On the one hand, too large a diameter leaves insufficient material for holding, but on the other hand, too small a diameter creates undue stress to both the bone and the screw. The holding power of screws also depends on bone strength as well as on bone thickness, and at present, such information is not obtainable in manual drilling. Knowledge of strength and thickness of the bone can provide some measure of the fixation's success rate. This is especially crucial for internal fixation of femoral neck fractures since the success of such fixation depends largely on the mechanical behaviour and architecture of cancellous bone (Martens *et al.*, 1983).

Most of these problems can be addressed by robotic/mechatronic systems for orthopaedic surgery assistance. However, the possible implementation of such a system in the future depends very much on its safety which is of paramount importance, and on the confidence shown by the medical/surgical profession and the patient.

2.2 Robotics Systems for Surgery Assistance

This section presents a general application of robotics in medicine and briefly describes the robotic system developed in the Department of Mechanical Engineering of Loughborough University for orthopaedic surgery assistance.

2.2.1 Application of Robotics in Medicine

Robots have been applied primarily in the manufacturing industries for the enhancement of productivity because they offer the advantages of performing complex movements with accuracy and repeatability, and suffering from no effects of tiredness, hunger and temperament. Moreover, the emergence of more powerful computers and the advances in sensor technology have enabled dynamic interaction between robots and their environment, and expanded the range of robot applications such as in medicine.

The progression of robotics in manufacturing to robotics in medicine has been rather cautious due to the transition of robot culture from being isolated for safety to close human interaction. As a result of this enormous transition, the current safety issues on robots have to be completely restructured to ensure absolute human safety when interacting with robots (Preising *et al.*, 1991). The success of developing medical robots will, therefore, require not just the knowledge and the synthesis of engineering, medicine and robotics, but also adequate safety features due to the close vicinity of the robot with the patient and medical personnel.

The applications of robotics in medicine can generally be classified into five areas: (i) laboratory, (ii) rehabilitation, (iii) hospital (transportation and patient transfer), (iv) assistance to surgery, and (v) micro-robotics or bio-robotics (Preising *et al.*, 1991; Kassler, 1993; Dario *et al.*, 1994). Development of robotics for surgery assistance is a relatively new field, and as a consequence of the potential benefits outlined above, the Department of Mechanical Engineering of Loughborough University has taken the initiative to develop an image guided robotic system for orthopaedic surgery assistance in drilling trajectory planning.

2.2.2 Robotic System for Orthopaedic Surgery Assistance

The project, known as MEDROSA (MEchatronic Design of a Robot for Orthopaedic Surgery Assistance), was funded by the Wishbone Trust of British Orthopaedic Association. The main objectives of this project, shown in figure 2.1, were to alleviate the difficulties encountered by surgeons in current orthopaedic surgical procedures involving the usage of fluoroscopic guidance in planning the drilling trajectory and to improve the success rate of the operation. Assistance in trajectory planning reduces the number of drilling attempts to one and thus results in the reduction of x-ray exposure, and has the potential of reducing the duration of the operation. Also, robotic assistance ensures optimum implant placement. The overall benefits are improved post-operative recovery and improved success rate.

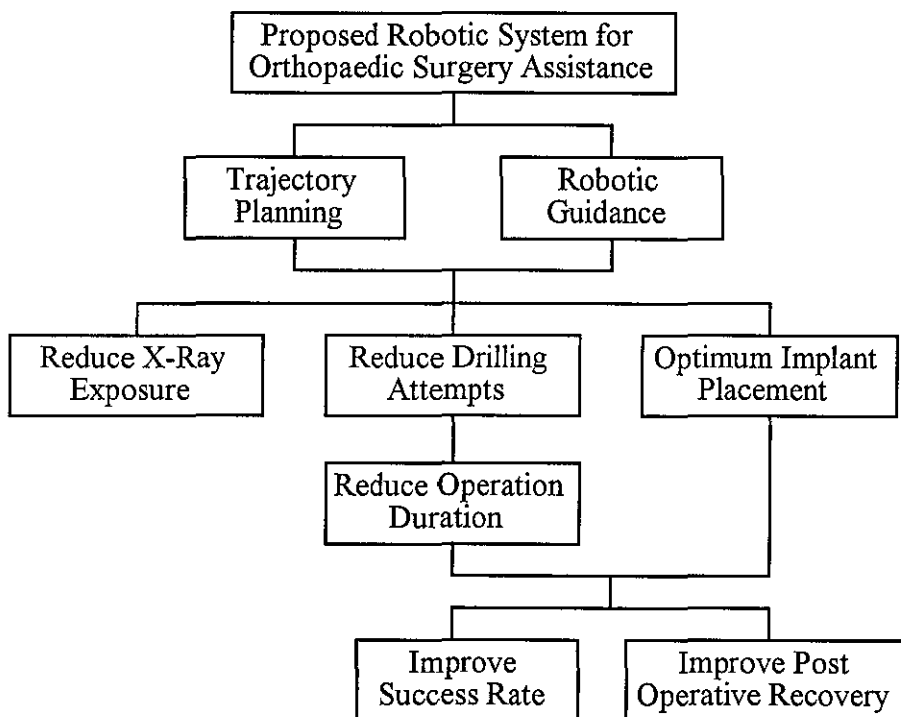


Fig. 2.1 Objective tree of a proposed robotic system for orthopaedic surgery assistance

A novel robotic system with image guidance has been developed for orthopaedic surgery assistance. In order to demonstrate the potential of this system, two orthopaedic surgical procedures involving internal fixation of fractures of the hip and the femoral shaft, shown in figure 2.2, have been selected as exemplar. A brief description of these surgical procedures is found in Appendix 1. Repairs of the hip and the femoral shaft fractures, are common orthopaedic procedures and hence generate a considerable need for robotic assistance.

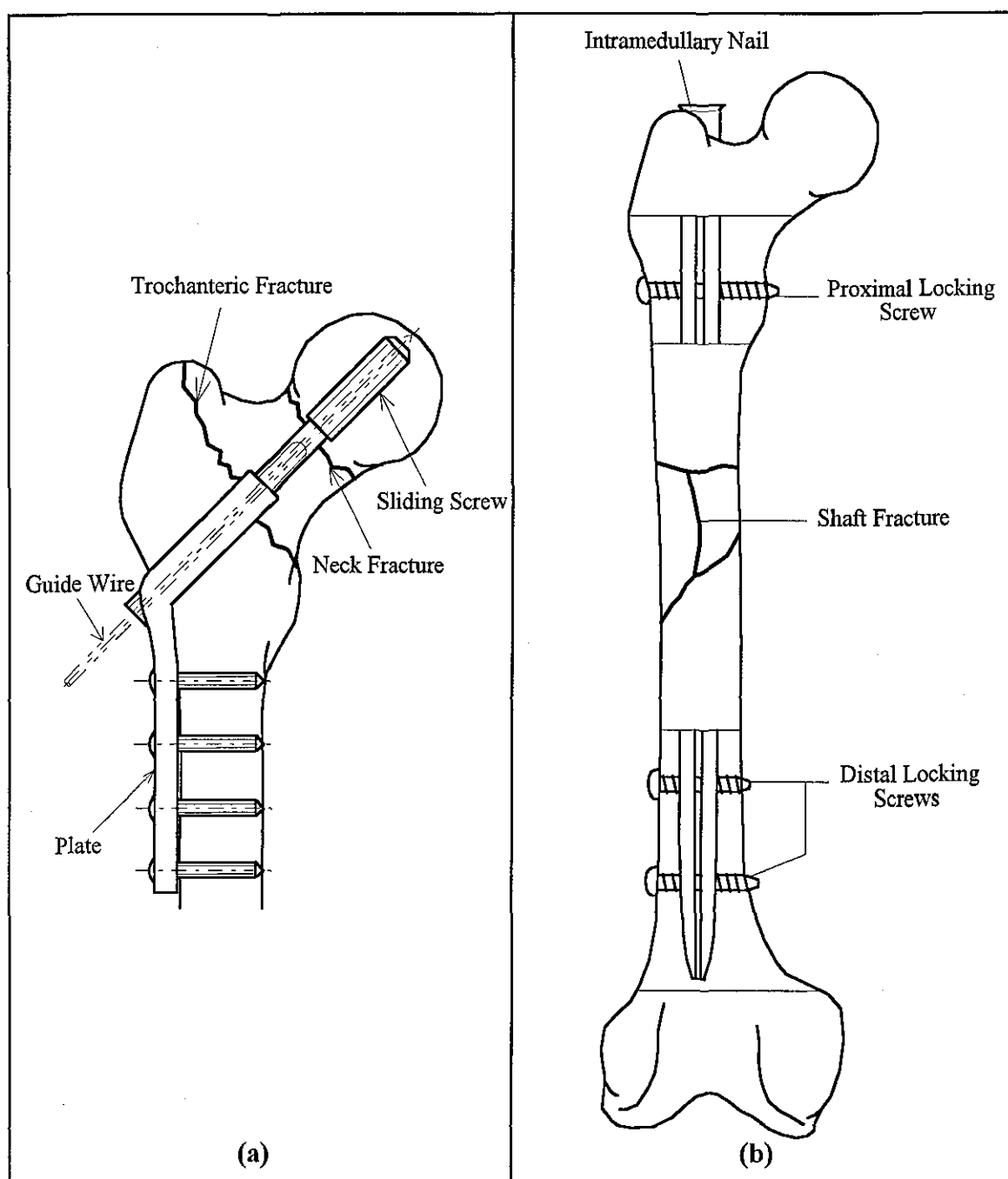


Fig. 2.2 Fracture fixation of the femur: (a) hip fracture, (b) shaft fracture

There are two methods for providing orthopaedic surgery assistance, the first is by modifying an industrial robot and the second is by designing a robotic device that is compatible with the environment of the operating theatre. Both methods need to satisfy the stringent criterion of safety and hygiene. The cost of modifying an industrial robot to meet the safety and hygiene standards may be high although there is a variety of robot configurations (degrees of freedom) available. Designing a new robotic device, however, requires the safety and hygiene constraints

to be considered throughout the design process; this also permits the construction of an optimum robot configuration for the operating theatre environment.

The proposed MEDROSA project is to be carried out in three phases. The first phase is the feasibility study to gauge the potential of a robotic system as an orthopaedic surgical assistant based on existing setting/environment of the operating theatre. Findings from the feasibility study have established that it is more favourable to develop a new robotic device, which includes the design and manufacture of a prototype manipulator, the development of a vision system and user interface, and the development of a control protocol for safety. In addition, the robotic system has to be developed to comply with current orthopaedic practice and the use of existing medical equipment with minimum modification. Based upon these specifications, a prototype robotic system for orthopaedic surgery assistance, shown in figure 2.3, has been developed. The integration of the complete system and laboratory tests have also been carried out. This phase of development concentrates on two types of orthopaedic procedures related to the repair of proximal femur (hip) fractures and femoral shaft fractures as benchmarks for further potential applications and for the realisation of a generic system (Bouazza-Marouf *et al.*, 1995).

The second phase is the design and manufacture of a robotic system for hospital trials based on the findings from the feasibility study. Finally, in the third phase, the new system will be used in clinical trials.

As mentioned earlier, the proposed robotic system, shown in figure 2.3, consists of three main developmental areas: a robot manipulator and controller, a vision system and user interface, and a safety control protocol. A mobile x-ray (C-arm) unit is also part of the system's set-up for full system integration. The purpose of the manipulator is to position the drill bit according to motion commands generated using the vision system, which is responsible for processing the x-ray images taken from the x-ray unit to give the desired drilling trajectory.

In the specification for manipulator design, several factors, such as the safety of both the patient and surgeon, accuracy and precision, physical size, sterility and cost, have been taken into consideration. The manipulator, shown in figure 2.4, is designed to have four degrees of freedom (DOF) for the positioning of a drill bit (or a drill bit guide) along any line in three-

dimensional space, plus an additional DOF for advancing the drill bit. The four DOF consist of two cartesian (linear) and two rotational joints. The linear motions are horizontal (joint 1) and vertical (joint 2), while the rotational motions are pan (joint 3, rotation about the vertical axis) and tilt (joint 4, rotation about the horizontal axis). The additional DOF (joint 5) is a linear joint. A further description of the manipulator as well as the vision system is presented in Appendix 2. This appendix also includes the operating procedure for the robotic assisted orthopaedic surgery.

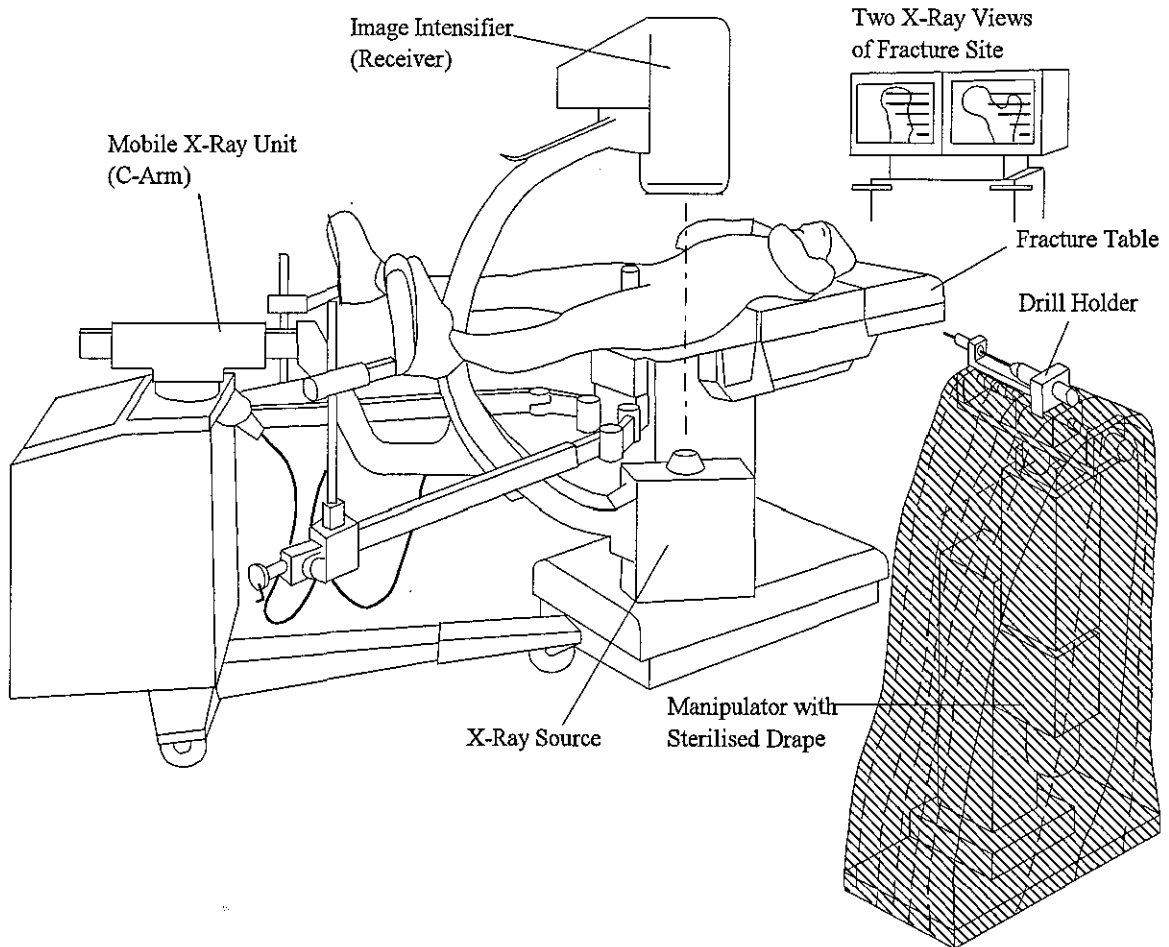


Fig. 2.3 Robotic system for orthopaedic surgery assistance

In open surgery, the reduction of the risk of wound infection places a major emphasis on proper sterilisation of the surgical equipment and implants, clothing of the surgical team and the construction of the operating theatre. The aim of sterilisation is to remove or destroy all micro-organisms from a contaminated item. It has been found that infection rates related to internal fixation can be as high as 40% depending on the type of wound and the extent of tissue damage (Matthews *et al.*, 1994). The sources of contamination can be categorised into airborne and

incomplete sterilisation of the surgical tools and implants. In order to reduce the infection rate, a positive pressure air flow which moves radially outwards away, known as 'exponential' flow air pattern, from the wound and the surgical team must be used in operating theatres (Howorth, 1980). In addition, total body exhaust systems can be worn by members of the surgical team. Since it is not often practical to sterilise the manipulator, the best option is to isolate the manipulator from the patient and the surgical team. This can be achieved by covering the manipulator with a sterilised drape currently used in operating theatres, as shown in figure 2.3. Only the drill holder, which is mounted on the drill feed unit (joint 5), is in direct contact with the surgeon and the patient. Therefore, the drill holder is specially designed to withstand sterilisation by steam (autoclaving¹) using suitable materials for both standard and manufactured components. Further description of the drill holder is given in Section 7.1.1 paragraph 2 and in Appendix 2.1.

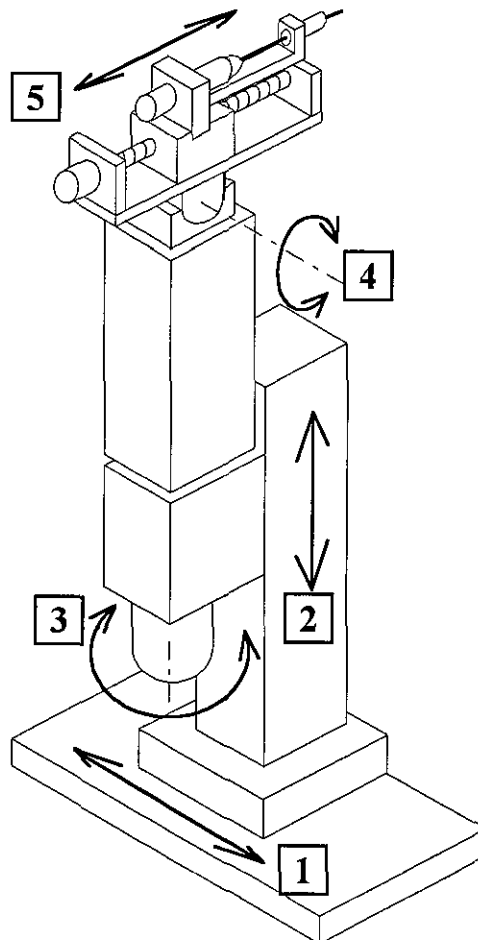


Fig. 2.4 Prototype robot manipulator

¹ Autoclaving, which is easily available and relatively inexpensive, is an effective method of killing all types of micro-organisms (Gardner & Peel, 1979).

2.3 Drilling of Bone

The current development of a robotic system for orthopaedic surgery assistance is associated with planning of the drilling trajectory in order to reduce the heavy dependence of intra-operative fluoroscopic guidance. In addition, a robotic system will not be complete without the knowledge of the effects of drilling into bones, which is very crucial to the development of a safety protocol and the analysis of the bone's characteristic. Since modern orthopaedic surgery involves multiple drilling operations, the analysis of drilling data such as drill bit displacement, thrust force, rate of penetration and drill bit rotational speed can also provide valuable information in the form of bone strength and bone thickness to surgeons. Although the investigations into drilling of bone have been well established in the literature, these have been primarily aimed at developing a suitable drill bit in order to optimise the drilling thrust force and torque, as well as to prevent or reduce thermal damage to the bone. Chapter 4 provides a comprehensive review of the bone drilling literature.

This research into the drilling of bone concentrates on the analysis of continuous drilling profiles of force, penetration rate and rotational speed with the aims of enhancing the safety of the drilling procedure, and estimating the bone strength in association with bone densitometry. However, it should be noted that this is not an investigation into the effects of drill bit geometry on force, penetration rate and rotational speed when drilling into bones. In order to achieve the objectives of this research, the drilling process is automated to enable data to be collected automatically and stored for subsequent analysis. The next chapter introduces the statement of the problem and the basis for the investigation of bone drilling.

CHAPTER 3

SCOPE OF THE RESEARCH

A major part of the development of a surgical assistance robotic system requires research into the effects of drilling into bones in terms of drilling thrust force, rate of penetration and drill bit rotational speed. This chapter highlights the major research issues and identifies the research problem. A detailed description of the research aims and objectives is subsequently given. Finally, the scope of research is presented to identify the major areas of work to be carried out.

3.1 Statement of the Problem

In general, the research reported in this thesis can be broadly divided into (i) the enhancement of safety and (ii) the evaluation of bone strength. The problems associated with these two aspects will now be discussed in detail to identify the impetus for carrying this major piece of research.

3.1.1 The Enhancement of Safety

In clinical situations, the presence of system compliance is a result of the extreme difficulty in securing the specific part of the anatomy in a rigid manner. This presents a major challenge for the detection of drill bit break-through in the drilling of bone. When drilling procedures are performed manually, the effects of system compliance could be brought under control by the feel of movement. At the start of drilling, an initial force has to be applied on the bone before the drill bit penetrates into the bone surface. A high initial force is normally associated with a high system stiffness. At the commencement of drill bit break-through (which in this case, is the exit of the drill bit from the material/bone), the reduction in the drill bit rotational speed is detectable, and appropriate action is normally taken by the surgeon to prevent or minimise excessive over-travel of the drill bit. In order to further improve the safety of the procedure,

these features, which are clearly evident in drill bit break-through, should be extracted in the form of drilling force and rotational speed profiles using an automated/mechatronic drilling tool.

There are two important factors, namely system compliance (mentioned earlier) and inherent drilling force fluctuation, to be considered in the detection of drill bit break-through. The fluctuation in the drilling force, which is normally caused by the variation in the bone structural density, can give a premature indication of drill bit break-through.

There are potential benefits of automated bone drilling in the enhancement of safety. However, before these potential benefits can be realised, there is a need to devise an automatic technique for the identification of imminent drill bit break-through when drilling into the shaft of long bones. The results from this investigation will be very beneficial when implemented in the design and development of a drilling tool for mechatronic/robotic assisted orthopaedic surgery.

3.1.2 The Evaluation of Bone Strength

Surgical drilling is a major part of orthopaedic surgery. However, as stated in Chapter 1, the information of drilling forces or rate of advancement is, at present, not attainable in manual drilling. Results from this research could prove to be valuable for evaluating bone strength especially when the process of internal fixation using plates and screws involves bone affected by low bone density/mass or disease such as osteoporosis.

In order to study the bone strength based on drilling mechanics, a preliminary correlation with established methods of bone strength determination has to be substantiated. One method of determining bone strength is related to basic engineering principles of evaluating mechanical properties, distribution of material and applied loads. However, this method involves a large amount of sample preparation which is difficult to carry out. The accuracy of the results is also limited by the size of the bone specimen. Bone densitometry, which is non-invasive and measures the bone mineral density *in vivo*, is the second method of evaluating bone strength and it is widely used in clinical practice for the evaluation of osteoporosis. The limitation of bone densitometry is related to the size of the area or region being scanned and the thickness of the

bone. It is in the author's opinion that an estimation of bone strength could also be obtained by analysing drilling data.

Studies have been carried out to correlate mechanical properties with densitometric measurements. Therefore, a method of determining a correlation between drilling data and densitometric measurement is required. The proximal femur is chosen for bone strength investigation since it can be singled out as an important skeletal site where the bone structure and density are most critically related. Results of this investigation will contribute towards the development of a potentially powerful alternative and/or complementary method of evaluating and identifying diseased bones, assessment of success rate associated with treatment using internal fixation and suggestion of appropriate post-operative management.

3.2 Research Aims

There are two principal aims to be achieved in this research of bone drilling. The first aim is provide a reliable technique for the identification of imminent drill bit break-through when drilling into the shaft of long bones for the enhancement of safety. This is related to mechatronic/robotic assisted orthopaedic surgery. The second aim is to make a significant contribution towards the evaluation of bone strength by investigating the correlation between drilling data and bone densitometric measurement.

3.3 Research Objectives

From the aims, a number of objectives for the research have been established. These are given as:

- (i) To critically review the current progress of bone drilling and identify contributions of automation/robotics technology to orthopaedic surgery related to bone drilling.
- (ii) To develop a drilling experimental rig which can cater for both the enhancement of safety and the evaluation of bone strength. This development also involves interfacing of the rig

with a personal computer, and software programming for the activation of the drilling procedure and data acquisition.

- (iii) To devise a robust and reliable technique for the detection of drill bit break-through when drilling into the shaft of long bones (femoral shaft), taking into consideration the effects of system compliance and inherent drilling force fluctuation for safety enhancement purposes.
- (iv) To study the correlation of bone strength of the proximal femur, derived from drilling mechanics, with bone densitometric measurements.
- (v) To critically analyse the results obtained from the experimental tests in order to verify the technique for safety enhancement and the correlation of drilling data with densitometric measurements.

3.4 Scope of the Research

The identification of the objectives for the research has led to the scope of the research to be drawn out. The scope of research is highlighted in the following sections.

3.4.1 Literature Review

In order to support the research, the literature review has to cover three areas of bone drilling related to the performance of drilling, the strength of bone and the automation of the bone drilling process. The drilling performance, which highlights the shape of the drill bit, reviews the effects of thrust force and torque and the effects of temperature. In the area of bone strength, the literature review includes the determination of mechanical properties, strength evaluation based on bone densitometry and the correlation between the two methods. The use of bone drilling for bone strength evaluation is also to be discussed. Automation of the bone drilling process is relatively new and its potential, especially in the detection of drill bit break-through, is discussed in this review.

3.4.2 The Detection of Drill Bit Break-through

Surgery assistance in orthopaedic procedure using mechatronic or robotic technology has to meet stringent safety criteria in order to ensure safety of the patient and the surgeon. The present techniques of safety enhancement associated with the detection of drill bit break-through in the literature of bone drilling are to be evaluated critically. The present detection methods have been greatly influenced by the effects of system compliance and inherent drilling force fluctuation. As a result, a more robust and reliable method of break-through detection in the presence of these two effects must be developed. This technique, which is to be developed, should also be capable of estimating the imminence of drill bit break-through.

3.4.3 The Evaluation of Bone Strength

The evaluation of bone strength associated with correlation between different methods of strength measurements is a contentious issue. A novel approach of correlating drilling data with bone densitometric measurement must be developed as an intermediate method in order to establish a strength relationship. This method of bone strength evaluation will be well supported since both the drilling process and densitometric measurement are widely used in clinical practice in the areas of orthopaedic surgery and evaluation of osteoporosis respectively. The methodology for the study of this relationship requires dimensional and statistical analyses. This study, therefore, is to highlight the importance of the drilling process in evaluating bone strength.

3.4.4 Experimental Rig Design and Tests

The aim of experimental rig design and instrumentation is to provide a controlled environment for drilling experiments in order to achieve the research aims which are the enhancement of safety and the evaluation of bone strength. This developmental work involves mechanical design of the rig together with appropriate sensors, interfacing of the rig with a personal computer and software programming for controlling the drilling procedure and data acquisition.

Since there are two types of drilling experiments (one for the safety enhancement and the other for the bone strength evaluation), the experimental set-up must be developed to cater for both experiments. In addition, the experimental set-up for the evaluation of bone strength must take into consideration the standard set-up for measuring bone mineral density.

3.4.5 Experimental Results

The main focus of this work is for the realisation of the methods associated with the detection of drill bit break-through and the correlation of bone strength. Analyses of the results obtained from the drilling experiments are to be performed using the proposed methods outlined in Sections 5.5 and 6.2.2. In addition, a number of graphical presentations of the profiles of drilling data with accompanying analysis has to be generated and discussed in detail. This includes statistical analysis for the correlation of drilling data with densitometric measurements.

CHAPTER 4

REVIEW OF THE LITERATURE

The previous chapter has discussed problems associated with bone drilling in orthopaedic surgery and the potential benefits of automating the drilling process in terms of safety enhancement and bone strength evaluation. The main objective of this chapter is to comprehensively review the literature and to discuss current developments related to the drilling of bone. Established methods of evaluating bone strength are also discussed due to their relevance to this investigation.

4.1 The Drilling of Bone

Bone drilling in biomechanical engineering is categorised into three main areas of investigation, the drilling performance, mechanical strength of bone and the automation of the drilling process, as shown in figure 1.1. Firstly, various studies have been carried out to describe the bone drilling performance based on measurable parameters such as force, torque, rotational speed, temperature and hole accuracy. The aim is to optimise factors affecting the drilling performance, which are the drill bit shape and drilling conditions, in order to provide recommendations for the design of suitable drill bits and drilling instruments for clinical applications. The second area of bone drilling investigations is related to the determination of mechanical bone strength by means of correlating drilling data to mechanical properties. Finally, the most recent development emphasises the automation of the surgical drilling process as part of a device or a system for surgery assistance in order to improve the accuracy and the safety of the procedure.

4.2 Bone Drilling Performance

In the engineering industry, the extensive use of drilling has led to a substantial effort into research for the purpose of improving the efficiency and hence the performance. There are five main technical factors that influence the drilling performance, namely the drill bit, the workpiece, the machine, the drilling conditions and the cutting fluid (Galloway, 1957). However, most of the technical factors, such as machine type and cutting fluid are not applicable to bone drilling since the operation is performed manually by surgeons and does not involve high production volume. The criteria involved in evaluating drilling performance include the rate of penetration, drill life, efficiency of material removal, hole accuracy and hole surface finish.

The effect of drill bit on drilling performance depends upon its shape and material. Since all surgical bits are made from high grade stainless steel, the main concern is on the drill bit shape which covers the diameter and the geometry. The most common bit shape used is the conventional twist drill bit shown in figure 4.1 (Oxford Jr., 1955). However, the chisel edge of a conventional twist bit has a significant effect on its locating ability and the drilling thrust force. The absence of self-centering action of the chisel edge causes the drill bit to walk to one side of the hole and lose its locating ability. Furthermore, the chisel edge causes severe deformation of the work material. As a result, the chisel edge accounts for more than 50% of the total thrust force and the increase in the temperature generated, regardless of the work material. Modification on the drill bit tip has, therefore, been made to improve the locating ability and reduce thrust force. Typical modified point shapes of twist drill bits found in the literature are the spiral point (Ernst & Haggerty, 1958) and the split point (Oxford Jr., 1955) or four-facet point, as shown in figure 4.2.

The other applicable factor to bone drilling performance is the workpiece, consisting of the hole depth, either through or blind hole, and the workpiece material and its rigidity. In most clinical cases, the drilling of bone is blind in nature and the hole depth is unknown. Although fluoroscopic images are the only means to provide guidance for surgeons, the depth of hole cannot be measured without appropriate calibrated references. In addition, increased frequency in fluoroscopic imaging for monitoring may not be acceptable. The workpiece material in the case of bone drilling can either be cortical, or a combination of cortical and cancellous bones.

The composition of bone is given in Appendix 3. However, the mechanical properties of cortical and cancellous bones vary considerably (Evans, 1973). Added to the difficulty of blind drilling are the slippery nature of the uneven bone surface and the irregular angle of approach which cause the drill bit to deflect from the desired trajectory. Rigidity can be considered to be the most important element since it is extremely difficult to fix the specific part of the anatomy rigidly in clinical situations. Therefore, this presents another problem, the influence of system compliance on drilling performance.

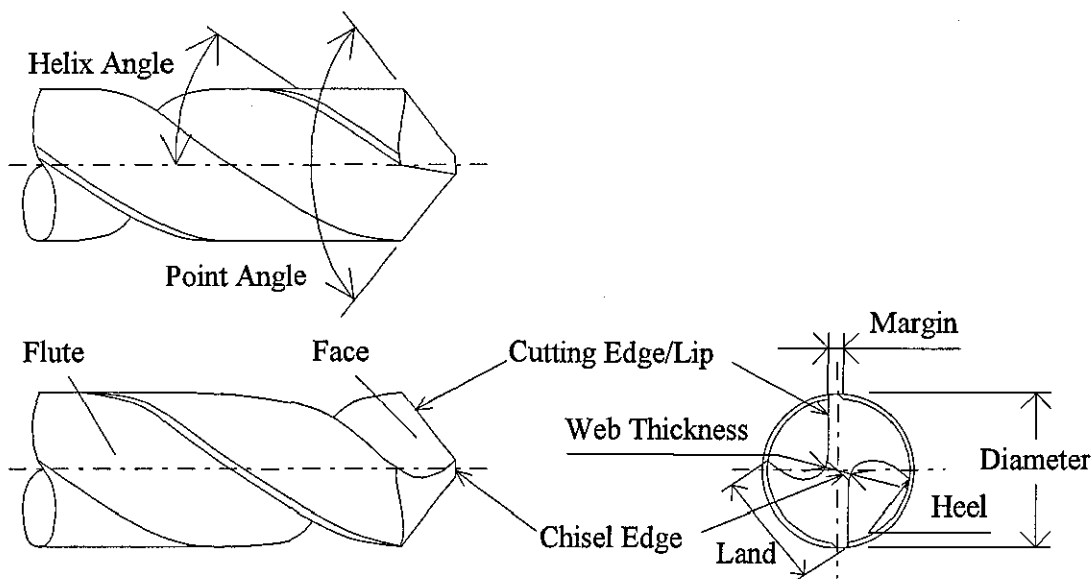


Fig. 4.1 A conventional twist drill bit

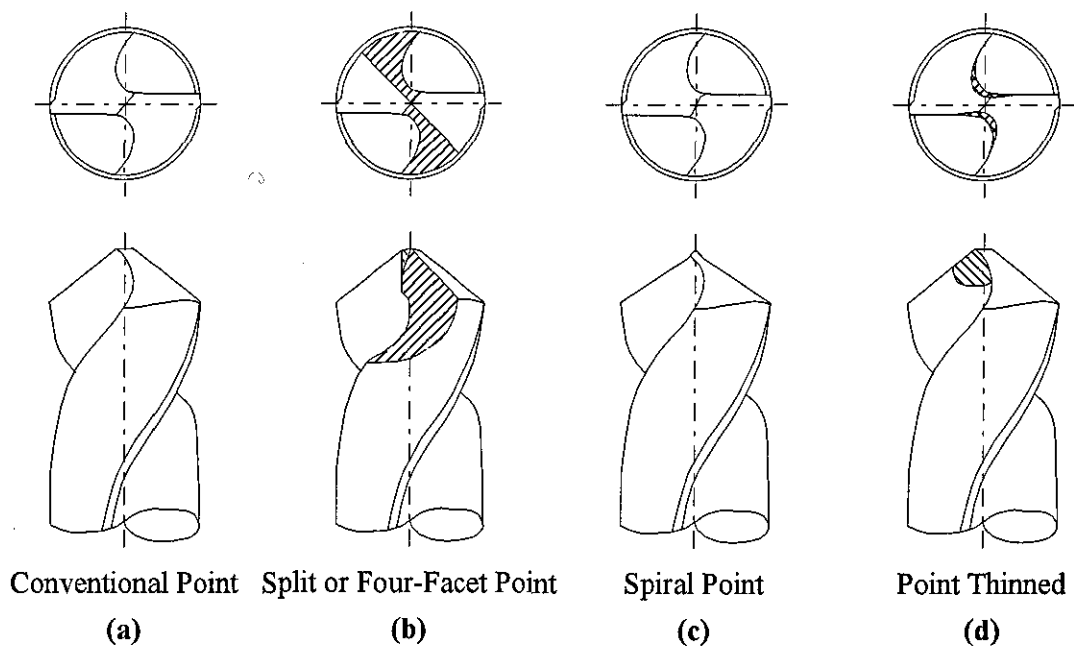


Fig. 4.2 Typical point/tip shapes of twist drill bits

As for the drilling conditions, the parameters involved are rotational speed and constant feed rate or applied force. In actual surgical procedure, constant applied force is assumed to be a more accurate representation as compared to constant feed rate (Wiggins & Malkin, 1976).

In order to describe the factors affecting bone drilling performance, it is common to measure drilling force and torque. There are many established literature on the drilling of metals where force and torque are used to analyse the drilling performance and to model the drilling process (Galloway, 1957; Shaw & Oxford Jr., 1957; Williams, 1974). Alternative measurements of temperature, hole accuracy and rate of penetration in bone drilling have been reported (Matthews & Hirsch, 1972; Farnworth & Burton, 1974; Wiggins & Malkin, 1976). Several studies have also been attempted to relate these measurements to the mechanics of drilling. These investigations have been aimed at developing a suitable drill bit that optimises drilling force and torque, as well as prevents or reduces thermal damage to the bone. The effects of thrust force and drill bit torque, as well as the effects of temperature on bone drilling performance are discussed below.

4.2.1 Effects of Thrust Force and Torque

The effects of the chisel edge has led to many early investigations into the modification of drill bit geometry in order to reduce both the drilling force and torque. One of the common modifications on twist drill bits is the spiral point geometry shown in figure 4.2c. This minimises the chisel edge effect and introduces a self-centering action. The effectiveness of the spiral point was first demonstrated by Ernst and Haggerty (1958) on a hip pinning operation of a fractured femoral head without the problem of drill bit slipping or 'walking'. Furthermore, the spiral point was reported to reduce the thrust force by 15% to 34% when drilling into steel workpieces with greater improvement at lower feed rates.

Sneath (1964) and Farnworth and Burton (1974) also recommended the spiral point geometry based on findings associated with drilling force, torque, penetration rate and temperature generated. Sneath (1964) made the recommendation after investigating the drilling performance of three different bit shapes, namely four-facet point, spiral point and point-thinned shown in

figure 4.2. Each of the three bit shapes comprised bits with and without cutting lands. However, no results were presented on the investigation which was carried out on bovine bones.

Farnworth and Burton (1974) conducted a more comprehensive investigation on the effects of drill bit geometry using porcine femoral shafts. Drilling performances on two groups of 6.35 mm diameter general twist drill bits with various geometries were evaluated in terms of thrust force and torque under constant feed rate, and in terms of penetration rate under constant applied thrust force. Both groups included three types of helix angle: fast, normal and slow. The first group was represented by three point shapes of radial relief, four-facet and spiral point, with web thickness 17.5% of bit diameter and point angles between 80° to 150°. The second group had radial relief shape with point angle of 118° and web thickness varying from 0.74 mm to 1.60 mm. In addition, observations were made on the locating ability and the snatching effect of the drill bit point during break-through. The findings of this investigation showed that the most desirable drilling performance came from the spiral point drill bits with point angles of between 120° and 140°, in conjunction with normal helix angle of approximately 27°, web thickness up to 18% of the drill bit diameter and clearance angle of 15°. Although fast helix drill bits appeared to have the best performance, the tendency to catch upon break-through has been observed when compared to normal and slow helix drill bits. In addition, drill bits with small point angles between 80° and 90° were found to have tendency to jam during break-through.

In a study by Jacobs *et al.* (1976), seven drill bits of different point shapes and geometries in twelve combinations were used to determine the effects of drilling speed on thrust force and torque under a specified constant feed rate. The experiments were carried out on mature bovine tibiae which were kept wet and lubricated constantly. The drilling conditions applied were constant feed rates of 25.4, 50.8 and 127.0 mm/min, and nine different drill bit rotational speeds varying from 100 to 2360 rev/min. However, only results from a feed rate of 50.8 mm/min using four drill bit shapes, with different point and helix angles, labelled as 'M', 'Y', 'Q' and 'O' were presented. In general, both the drilling force and torque decrease, to a minimum level, as the speed increases. The 'Q' type bit, which had a point angle of 110° and a helix angle of 24° was shown to be the best drill bit configuration, and produced the lowest thrust force and torque of approximately 14.1 N and 0.89 Ncm respectively. Whereas, the 'O' type bit, which

had a point angle of 90° and a helix angle of 23° , and had been blunted to give an effective negative rake angle between 1° to 3° , produced a high thrust force and the highest torque of approximately 23.4 N and 5.21 Ncm respectively. The 'Y' type bit of point angle of 86° and helix angle of 17.2° produced the highest thrust force of 26.2 N. In addition, the 'Q' type bit was observed to have little thermal effects, while the 'O' type bit suffered severe heating effects indicated by steam ejected from the hole. Based on these findings, recommendations were presented for the design and use of orthopaedic drill bits.

In contrast, Wiggins and Malkin (1976) measured parameters of penetration rate, torque and specific cutting energy (total energy per unit volume) over a range of fixed thrust loads for evaluating the drilling performance. The experiments were carried out on a human cadaveric male femur. Three different drill bits were used for the investigation: (i) a surgical twist drill bit of diameter 2.77 mm with 60° point angle, 20° helix angle and constant zero rake angle, (ii) general purpose twist bits of various diameters with 118° point angle, 28° helix angle, and a rake angle of -30° near the chisel edge increasing to 30° at the bit periphery, and (iii) a special spade drill bit of diameter 3.66 mm with 90° point angle and zero rake angle. The general purpose twist drill bits were operated at rotational speeds of 40 rev/min and 1150 rev/min, whereas the surgical bit and the spade drill bit were operated at 40 rev/min. For each type of drill bit, the drilling performance was categorised by power function (law) relationships using log-log coordinates. It was also found that the specific cutting energy was less when drilling at higher feed rates which could be explained by the larger applied thrust force. When compared to the general purpose twist drill bits, the surgical bit had better penetrating ability, but required higher torque and hence higher specific cutting energy. In the investigation associated with drill bit rotational speed, the drilling performance of the general twist bits under constant force was found to be independent of the rotational speed, implying that the performance depended primarily on the drill bit geometry. In addition, the tendency of clogging was attributed to the increasing depth of hole, which incidentally caused an increase in both the torque and the specific cutting energy.

Further investigation by Saha *et al.* (1982) to improve the drilling performance involved the use of the split point geometry, shown in figure 4.2b, which was similar to that reported by Oxford Jr. (1955). This bit geometry minimises the chisel edge through the provision of two additional cutting edges with positive rake angle. The split point bit shape used in this investigation had

118° point angle, 34°-36° helix angle and a parabolic flute design. Consequently, a reduction of approximately 40% of the total thrust force was achieved when drilling into bovine bones at a constant feed rate of 120.32 mm/min and a drill bit rotational speed of 940 rev/min. This was comparable to the reduction in thrust force achieved by a standard metal cutting drill bit of the same point angle and 15° helix angle when drilling into bovine bones with a pilot hole of the chisel edge length. Further drilling experiments were carried out on bone cement to compare the drilling performance between the split point geometry and surgical drill bits with 90° point angle and 24°-27° helix angle under a constant applied force of 45 N and a drilling speed of 940 rev/min. There was no significant difference found in terms of drilling force and torque between the standard metal cutting and split point geometry bits. The penetration rate was, however, significantly lower using surgical bits. It was also reported that the split point geometry produced cleaner and better quality holes, and eliminated bit 'walking' as well as minimised the problem of clogging. Furthermore, it was stated that the split point bit showed promising results in a clinical trial based on drilling thrust force and temperature developed, but no results were presented.

The issue of drill bit shape was not included in a study carried out by Abouzgia and James (1995). Instead, the effects of applied force on the drilling rotational speed and energy consumption were looked into using a medical drill bit of diameter 2.5 mm. The drill bit was driven into fresh bovine femoral shafts at a rotational speed range of 10000 to 100000 rev/min under a constant applied load of between 1.5 and 9.0 N. The applied force was found to affect the rotational speed only at speeds above 50000 rev/min by reducing the speed when a load was applied. However, the drilling time and energy consumed were significantly less with increased load and speed.

Drilling of bone also involves other types of drill bits which are very different from conventional and surgical twist drill bits. These different drill bits, known as guide wires and Kirchner wires (K-wires), shown in figure 4.3, are used for drilling pilot holes and as a guide for cannulated drill bits. The tips of these guide wires are in the shape of either two or three bevelled surfaces and come with either plain or threaded ends. There are no flutes to carry the bone chips from the hole and therefore, drilling force and torque involved will be relatively higher than expected. Three types of guide wires with diameter 2.5 mm, namely plain, threaded and a prototype point shape were used to conduct drilling experiments to determine the thrust forces generated

(Shuaib & Hillery, 1995). The guide wires were driven at feed rates of 40, 60 and 80 mm/min with seven different rotational speeds ranging from 400 to 1600 rev/min in steps of 200 rev/min. Human femoral heads were used for the drilling experiments. The results have indicated that the threaded guide wire generated the highest drilling forces while the plain guide wire had the lowest forces for all three feed rates at rotational speed of 400 rev/min. In general, higher drilling forces were associated with increases in feed rate, except those forces generated by the threaded guide whereby feed rate had little impression. Furthermore, the rotational speed had little effect on the forces generated. However, the forces were far higher by several orders of magnitude when drilling into cortical bone than cancellous bone. The significant difference came from the threaded guide wire which was shown to produce less thrust force with increasing feed rate as opposed to increase of force shown by the plain and prototype guide wires. Drilling forces in cortical bone were found to have a downward trend with increasing rotational speed and this trend was more extreme for threaded guide wire.

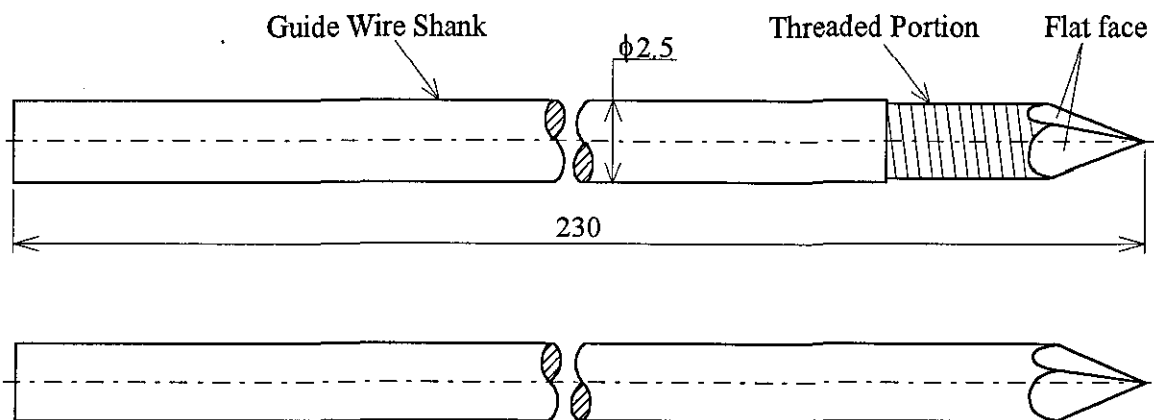


Fig. 4.3 Typical guide wire or Kirchner wire (K-wire) shapes (Shuaib & Hillery, 1995)

The studies discussed so far indicate mainly the drilling performance of various drill bits in different operating conditions by experimental analyses. In order to characterise the drilling performance, analytical relationships and knowledge of drilling mechanics are required. The basis of drilling mechanics is described by an orthogonal (two-dimensional) cutting process which involves a single edge cutting tool that is perpendicular to the direction of the relative motion between the tool and the work material, as shown in figure 4.4. A conventional twist drill bit can be considered to have two single cutting edges on a common axis. However, the variation of rake angle along the cutting edge and the chisel edge results in a complex three-dimensional (oblique) cutting action. Since the cutting action also differs significantly between

the main cutting edge and the chisel edge, separate analyses on both the edges are carried out in order to derive general equations for estimating drilling force and torque.

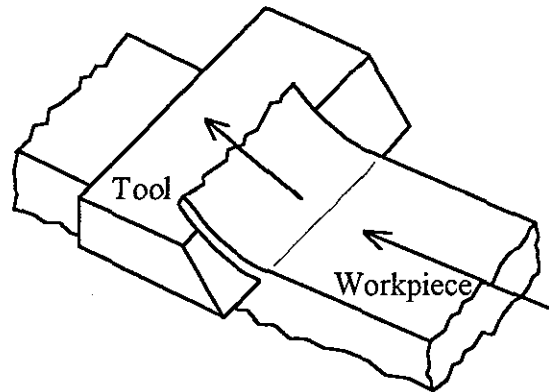


Fig. 4.4 Orthogonal Cutting

Drilling mechanics

Several studies have been carried out to analyse bone drilling mechanics, but the operating conditions and the drill bit shape were different in each study. Jacobs *et al.* (1976) developed an approximate theoretical model for drilling by using Cook's equations for single edge cutting tools based on shear failure criteria. Using specific energy together with geometric considerations of the bit point, the force and the torque models compared favourably to the experimental results.

On the other hand, Wiggins and Malkin (1976) found that the drilling performance of three different drill bits (defined earlier in this section: a surgical drill bit, a general purpose drill bit and a special spade drill bit) could be characterised by different power functions. Linear relationships with high correlation coefficient were obtained using log-log coordinates of feed rate against thrust pressure, torque and specific cutting energy.

Davis *et al.* (1980) attempted to predict the feed rate at constant applied force on human cortical bones using empirical coefficients based on experimental results obtained from bovine bones. These empirical coefficients were derived from orthogonal cutting tests in the longitudinal and transverse directions of the shafts of bovine long bones. From the results of drilling into human bones, it was shown that the feed rate followed a downward trend with increasing drill bit point angle. This trend was similar to the predicted trend using empirical constants but differed in terms of magnitude. However, a statistical analysis was not carried out

to verify the magnitudinal correlation between the predicted and the experimental results. Among the reasons for not carrying out the statistical analysis were: anisotropy of the bone material, different species of bones were used, empirical constants obtained from drilling bovine bones were based on one drill bit point angle, and effects of storage on mechanical properties of the human bone were not taken into consideration.

In summary, the investigations carried out using drill bits with different geometries and sizes were aimed at developing an optimum drill bit for bone drilling. However, findings from the experimental analyses of various bone drilling investigations differed significantly from the recommendations given by Bechtol *et al.* (1959), which were followed by most of the surgical bit manufacturers. In these recommendations, Bechtol *et al.* (1959) stated that the drill bit should not 'walk' on the bone surface, and the drill bit geometry should include 90° point angle and zero rake angle. This geometry was actually meant to reduce the chipping of the bone and to prevent the drill bit from snatching the bone during break-through, based on observations made when drilling into plastic material. Unfortunately, these recommendations did not take cutting forces into consideration, and experimental analyses by other researchers found that this bit geometry required higher cutting forces and energy, as well as generated a higher temperature. A comprehensive summary of the literature on bone drilling mainly related to the effects of force and torque on the drilling performance is given Table 4.1.

4.2.2 Effects of Temperature

In addition to evaluating drilling force and torque, the drilling performance can also be assessed through the measurement of temperature. Heat is generated by the friction between the drill bit and the bone, and the fragmentation of bone particles at the cutting edge of the drill bit. The main concern of temperature effects is the heat generated at temperatures above 50°C during the drilling operation. This temperature (50°C) is considered to be the threshold for thermal damage or bone death (osteonecrosis), especially when combined with long duration of exposure. The higher the temperature, the shorter is the duration required to cause thermal damage to the bone. Bonfield and Li (1968) have shown that bone structure suffers irreversible change after being subjected to deformation at temperatures above 50°C.

Author	Year	Bone Type	Drill Bit Type	Drill Bit Geometry (Angle in degrees)			Penetration or Feed Rate (mm/min)	Drill Bit Speed (rpm)	Thrust Force (N)	Drill Bit Torque (Nm)
				Point	Rake	Helix				
Ernst H. & Haggerty W.A.	1958	Bovine & Human Femoral Proximal End	Surgical Twist Bit	<i>Resharpened to Spiral Point with Point Angle of 72°</i>			Faster Penetration Rate	-	-	-
				<i>Conventional Surgical Drill Bit</i>			Slower P. R.	-	-	-
Sneath R.S.	1964	Bovine Diaphysis/Shaft	General Metal Cutting Twist Bit	60° to 160°	<i>Spiral point shape, with & without cutting lands.</i>		Faster Penetration Rate	-	Constant	-
					<i>Four-facet, pt. thinned, with & without lands.</i>		Slower Penetration Rate			
Farnworth G.H. & Burton J.A.	1974	Porcine Femoral Diaphysis	Spiral Point (φ6.35 mm)	80° - 150°	<i>Web thickness - 17.5% of bit diameter</i>	(φ6.35 mm General Twist Bit)	Const Feed Rate 46.512	456	20 - 60	0.15 - 0.21
							Penetration Rate 2.5 to 12.5		Constant 19.6	-
			Four Facet Point (φ6.35 mm)				Const Feed Rate 46.512		50 - 125	0.18 - 0.20
				80° - 150° and 118°	<i>Web 17.5% and 0.74 mm - 1.6 mm</i>	Slow, Normal & Fast Helix Angle	Penetration Rate 0.45 to 5.0		Constant 19.6	-
			Radial Relief Point (φ6.35 mm)				Const Feed Rate 46.512		60 - 120	0.14 - 0.20
							Penetration Rate 0.29 to 5.0		Constant 19.6	-
Jacobs C.H. et al.	1976	Bovine Tibiae Diaphysis	M (φ3.2 mm)	113°	13.5°	13.5°	Constant	100 to 2360	22.8	4.67x10 ⁻²
			Y (φ3.2 mm)	86°	17.2°	17.2°	Feed Rate		26.2	4.50x10 ⁻²
			Q (φ3.2 mm)	110°	24°	24°	50.8		14.1	0.89x10 ⁻²
			O (φ3.2 mm)	90°	-1° to -3°	23°			23.4	5.21x10 ⁻²
Wiggins K.L. & Malkin S.	1976	Human Femoral Diaphysis	Surgical (φ2.77 mm)	60°	0	20°	Penetration Rate, $f = 3.8 \times 10^{-4} p^{2.2}$	40	Constant Force	$T = 1.6 \times 10^{-2} f^{0.39} A$ $f = \text{penetration rate}$
			General (Various φ)	118°	-30° to +30°	28°	$f = 3.7 \times 10^{-4} p^{1.8}$ $p = \text{thrust force}$	40 & 1150		$T = 1.4 \times 10^{-2} f^{0.37} A$ $A = \text{area}$
			Spade (φ3.66 mm)	90°	0	-	$f = 3.9 \times 10^{-3} p^{1.3}$	40		$T = 2.5 \times 10^{-3} f^{0.66} A$
Davis J.K. et al.	1980	Bovine Diaphysis	General (φ4.76 mm)	118°	19°, 20°, 21°, 22°	23°	-	-	-	-
		Human Femoral Diaphysis	Surgical ASIF (φ3.2 mm)	80° to 140° steps of 10°	-	-	Penetration Rate (Graph)	800, 1500, 2000, 2500	Constant 20	-
Karalis T. & Galanos P.	1982	Human Tibiae Diaphysis & Femoral Head	-	<i>'Q' type as in Jacobs et al., 1976.</i>			Advance Ratio (Graph)	1200-1380	Constant	-
Saha S. et al.	1982	Bovine Diaphysis	General (φ6.35 mm)	118°	Lip Relief 6°-10°	15°	Constant Feed Rate	940	70	-
			Split Point (φ6.35 mm)	118°	Lip Relief 15°-18°	36°	120.32		46	-
Chagneau F. & Levasseur M.	1992	Human Femoral Head	3-Lipped Twist Bit (φ4.0 mm)	<i>A flat front and a preliminary tip as a guide. Drill shank reduced to 2 mm diameter.</i>			Constant Feed Rate 10	350	Force Profile	-
Bouazza-Marouf K. et al.	1995	Porcine Femoral Diaphysis	Threaded Guide Wire (φ2.5 mm)	<i>Three-facet point with a threaded end smaller than the drill bit shank.</i>			Constant Feed Rate 132	3300	Force Profile (Max 17)	-
Dario P. et al.	1995	Porcine Femoral Diaphysis	General (φ3.5 mm)	120°	-	25°	Constant Feed Rate 50, 75, 100	1500, 1800 & 2000	Force Profile (Max 38)	0.055 (Max)
Shuaib I. & Hillery M.	1995	Human Femoral Head	Threaded Guide Wire (φ2.5 mm)	<i>Three-facet point with a small threaded end and 60° point angle.</i>			Const Feed R. 40	400	Mean 13.8	-
							60		Mean 15.6	
							80		Mean 15.6	
			Plain Guide Wire (φ2.5 mm)	<i>Three-facet point with 60° point angle.</i>			40		Mean 3.5	
							60		Mean 8.7	
							80		Mean 10.4	
			Prototype Guide Wire (φ2.5 mm)	-			40		Mean 5.2	
							60		Mean 8.7	
							80		Mean 15.6	
Abouzgia M.B. & James D.F.	1995	Bovine Femoral Diaphysis	Surgical (φ2.5 mm)	-			Faster Rate of Penetration at Higher Speed and Force.	20000 - 100000	Constant 1.5 - 9.0	-

Table 4.1 Effects of Force and Torque in Bone Drilling - Summary of Experimental Data

Bone undergoes two processes during healing: bone resorption (removal) and bone formation. Details of these two processes are given in Appendix 3.3. Bone healing is, therefore, affected by the rate of the two processes. An increase in bone resorption or a slower rate of bone formation as a result of thermal damage would have a negative effect on bone healing. According to Matthews and Hirsch (1972), increased bone resorption might be the cause of occasional failure of stable fixation using screws. Similar argument was made by Van Egmond *et al.* (1994) that osteonecrosis might be the contributing factor towards the loosening of K-wires and infections. However, Albright *et al.* (1978) argued that the evidence of screw loosening due to increased resorption of bone was not proven. Apart from thermal damage, excessive heat generated also chars bone tissue and this may prevent the removal of debris when the drill bit flute is blocked by the charred tissue (Sneath, 1964).

There are generally three factors, namely applied force, rotational speed and drill bit geometry that affect bone drilling temperatures. An investigation into the effects of constant applied force and drill bit rotational speed on temperature generated was carried out by Matthews and Hirsch (1972) using a standard ASIF (Association for the Study of Internal Fixation) surgical drill bit of diameter 3.2 mm on human cadaveric femoral shafts. Measurements of temperature and duration of temperatures above 50°C at distances of 0.5, 1.0, 2.0 and 3.0 mm from the hole wall were made at constant applied forces of 2, 6 and 12 kgf, and rotational speeds of 345, 885 and 2900 rev/min in all combinations. It was found that rotational speed had little influence on the heat generated (maximum temperature), but the duration of temperature above 50°C was significantly shorter at higher speeds. Whereas the applied force was found to have a significant effect on both the temperature elevation and the duration. Higher applied forces were found to be associated with lower temperatures and shorter duration of temperatures above 50°C. Incidentally, the highest average maximum temperature was 93.1°C obtained from a force of 2 kgf and a speed of 2900 rev/min. An increase in the applied force resulted in a higher penetration rate which allowed drilling to be completed with fewer rotations, and thus less cutting by the drill bit. High penetration rate coupled with the possible redistribution of heat to the chips might be the reason behind the significant reduction in the magnitude and the duration of temperature elevation (Matthews & Hirsch, 1972). Similar findings related to specific cutting energy in drilling were reported where a higher penetration rate produced by a higher thrust force resulted in a lower cutting energy which was related to reduced temperature elevation (Jacobs *et al.*, 1976; Wiggins & Malkin, 1976).

Drill bit geometry was shown, by Saha *et al.* (1982), to have a significant effect on heat generated. Using twist drill bits with modified split point geometry (as defined in Section 4.2.1, Paragraph 6 and shown in figure 4.2b), a reduction of 41% was achieved when compared to surgical drill bits of the same diameter of 3.2 mm under a constant force of 93.4 N and a rotational speed of 940 rev/min. This finding emphasised the importance of reducing the chisel edge length of surgical drill bits to minimise heat generated.

Apart from factors related to drill bit and drilling conditions, bone thickness also has an effect on heat generated. This was reported by Eriksson *et al.* (1984) when measuring drilling temperatures *in vivo* on both live animals and human patients undergoing internal fixation procedures using twist drill bits of 3.0 mm diameter running at 20000 rev/min. It was found that higher drilling temperatures were related to greater bone thicknesses. A temperature of 96°C, which greatly exceeds the bone threshold for thermal damage, was recorded on a human subject with the thickest cortical bone. The increase heat generation with the increase in depth of drilling might be linked to drill bit clogging and the difficulty of coolant reaching the drilling point.

There are several surgical techniques to minimise or prevent excessive temperature elevation in bone drilling (Albright *et al.*, 1978). Irrigation has been found to be one of the most effective methods to help dissipate heat, but it has to be applied directly at the point of penetration (Matthews & Hirsch, 1972). The condition of the drill bit also has a considerable effect on temperature elevation, therefore, only sharp drill bits should be used. Another method to limit temperature elevation can be achieved by eliminating the chisel edge effect through pre-drilling of a smaller diameter hole prior to the drilling of a hole of the desired diameter, or modifying the drill bit geometry to, for instance, the split point geometry.

Apart from surgical and standard metal twist drill bits, bone drilling also involves the use of pins such as K-wires and Steinmann pins. These pins have different point geometry to surgical twist drill bits, but are driven at similar rotational speeds. There are two commonly used point shapes: a diamond point which has two bevelled surfaces, and a trocar point with three surfaces. Pins with a trocar point are more suitable for drilling cortical bone. Furthermore, pins do not

have the flutes of twist drill bits and therefore, more heat is generated as debris produced during drilling cannot be cleared (Albright *et al.*, 1978; Van Egmond *et al.*, 1994).

A study carried out by Van Egmond *et al.* (1994) measured drilling forces and temperatures at tips of K-wire when drilling into human cadaveric bones of the thumb and fingers (phalanges). A trocar point K-wire of diameter 1.1 mm with a built-in thermocouple (at the tip of the K-wire) was used and it was driven at a drilling speed of 600 rev/min. The temperature elevation was found to be influenced by bone orientation, where higher temperatures were measured when drilling in the transverse axis of the phalanx than in the longitudinal axis. The maximum average temperature was 133°C at the middle phalanx in the transverse axis, which incidentally had the longest drilling time. In addition, the production of heat was found to decrease with the reduction in speed, but resulted in longer drilling time. However, temperatures measured by Van Egmond *et al.* (1994) were far higher than those measured by Zegunis *et al.* (1993) at 0.5 mm from the hole on cortical bones of ox, pig and sheep. The contrasting temperatures recorded may be explained by the measurements taken from two different mediums. Van Egmond *et al.* (1994) measured temperatures at the tip of a K-wire with a built-in thermocouple and Zegunis *et al.* (1993) obtained temperature measurements from the bone. Furthermore, the thermal conductivity is far higher in the K-wire than in the bone.

The investigation carried out by Zegunis *et al.* (1993) also looked into an alternative insertion of K-wires by hammering instead of conventional drilling. It was found that hammering K-wires into bones generated less heat than drilling. An average maximum temperature of 34°C was recorded for all bones when hammering was used to insert a 1.6 mm trocar point K-wire, while a temperature of 54°C was recorded when drilling was performed using the same K-wire at a rotational speed of 850 rev/min.

Similar to twist drill bits, the pin-point geometry was shown to affect the heat generation in a study by Matthews *et al.* (1984) on large pin insertion. The temperature effects of drilling rotational speed and pre-drilling were also included in this study. Five point configurations, one of which was a trocar point, of diameter 3.9 mm were used. Temperatures for all the pins were measured on fresh human cadaveric tibiae based on rotational speeds of 300 rev/min and 700 rev/min, and also on hand-drilling. In general, drilling at 700 rev/min produced the highest maximum temperature, while 300 rev/min produced the lowest temperature. However, the

duration of temperatures above 55°C was lowest at 700 rev/min and highest using hand-drilling. The trocar point was found to have the highest average maximum temperature of 115°C and the second longest average duration above 55°C. Pre-drilling was shown to reduce the maximum temperature by more than 50%.

The temperature generated during drilling has been shown to be very severe around the interface between the drill bit and the bone. Temperatures in excess of 100°C have been reported adjacent to the hole in *in vitro* studies by Matthews and Hirsch (1972), and an average temperature of 89°C has been recorded in an *in vivo* clinical study conducted by Eriksson *et al.* (1984). In general, heat generated in bone drilling depends on the bit geometry, the applied force and the rotational speed. The point geometry of both twist drill bits and pins has a significant effect on the heat produced. Surgical twist bits with geometry recommended by Bechtol *et al.* (1959) have been shown to generate more heat (Saha *et al.*, 1982). As for the force applied, higher forces are related to reduced temperature generation and reduced duration of temperatures above 50°C (Matthews & Hirsch, 1972). Although rotational speed has little influence on temperature generated when applied to twist drill bits (Matthews & Hirsch, 1972), pins such as K-wires generate less heat at lower rotational speeds (Matthews *et al.*, 1984; Van Egmond *et al.*, 1994). However, longer durations of temperatures above 50°C are associated with lower rotational speeds regardless to whether twist drill bits or pins are used (Matthews & Hirsch, 1972; Matthews *et al.*, 1984; Van Egmond *et al.*, 1994). A comprehensive summary of the literature on bone drilling related to the effects of temperature on the drilling performance is given Table 4.2.

4.3 Strength of Bone

A huge interest has been generated in finding the most appropriate technique or method to estimate bone strength. It may be seen from the literature that there are two general methods of evaluating bone strength. As shown in figure 4.5, the first is based upon basic engineering principles which relate the material strength to mechanical properties (density and elasticity), structural properties (architecture and quality) and to loading conditions (direction, magnitude and rate). Structural properties are intimately related to the mechanical properties. The second method of strength measurement is bone densitometry. This method is non-invasive and

determines the amount and the density of bone present (Faulkner *et al.*, 1991). Both of these methods have a primary aim of studying the strength of bone, especially cancellous (trabecular/spongy) bone, for the evaluation of fracture risk. In addition to these two methods, drilling of bone has also been used for the evaluation of bone strength. However, the present literature on bone drilling for the evaluation of bone strength is limited, and little is known about the relationship of drilling mechanics with mechanical strength and/or bone densitometry.

Author	Year	Bone Type	Drill Bit Type	Drill Bit Geometry (Angle in degrees)			Feed Rate (mm/min)	Drill Bit Speed (rpm)	Thrust Force (N/kgf)	Temperature (measured at hole vicinity)	
				Point	Helix	Rake					
Matthews L.S. & Hirsch C.	1972	Human Femoral Diaphysis	ASIF Surgical (φ3.2 mm)	-			-	345, 885 & 2900	Constant 2 kgf	82°C at 0.5 mm 71°C at 1.0 mm	
									Constant 6 kgf	68°C at 0.5 mm 54°C at 1.0 mm	
									Constant 12 kgf	51°C at 0.5 mm 45°C at 1.0 mm	
Saha S. <i>et al.</i>	1982	Bovine Diaphysis	Surgical (φ3.18 mm)	90°	24°	Lip Relief 12°-15°	-	940	Constant 93.4 N	55°C at 1.0 mm	
			(φ4.76 mm)		25°						53°C at 1.0 mm
			Split Point (φ3.18 mm)	118°	34°	Lip Relief 15°-18°				32°C at 1.0 mm	
			(φ3.97 mm)		-						38°C at 1.0 mm
			(φ6.35 mm)		36°						
			Eriksson A.R. <i>et al.</i> (<i>in vivo</i>)	1984	Rabbit Femoral Diaphysis	Surgical (φ3 mm)				118°	30°
Canine Femoral Diaphysis	56°C at 0.5 mm (Max 65°C)										
Human Femoral Diaphysis	89°C at 0.5 mm (Max 96°C)										
Matthews L.S. <i>et al.</i>	1984	Human Tibial & Femoral Diaphysis	5 Fixation Pins of φ3.97 mm : Trocar, Spade, Hoffman, Half Drill, Modified Half Drill	-			-	Hand Drill	60 to 120 N	109°C at 0.5 mm 88°C at 1.0 mm	
								300		100°C at 0.5 mm 82°C at 1.0 mm	
								700		121°C at 0.5 mm 100°C at 1.0 mm	
Zegunis V. <i>et al.</i>	1993	Ox Cortical	φ1.6 mm Trocar Point and φ2.0 mm Diamond Point	-			-	850	-	51°C at 0.5 mm 43°C at 1.0 mm	
		Porcine Cortical								58°C at 0.5 mm 51°C at 1.0 mm	
		Sheep Cortical								Kirschner Wire (K-wire)	51°C at 0.5 mm 45°C at 1.0 mm
Van Egmond D.B. <i>et al.</i>	1994	Human Phalanges Transverse dir.	φ1.1 mm Trocar Point K-wire		-		-	600	-	133°C	
		Human Phalanges Longitudinal dir.								65°C	

Table 4.2 Effects of Temperature in Bone Drilling - Summary of Experimental Data

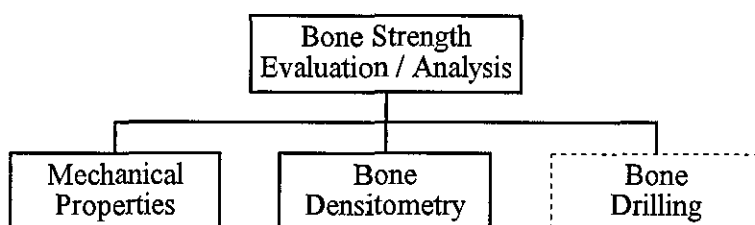


Fig. 4.5 Evaluation of Bone Strength

4.3.1 Mechanical Properties of Bone

Methods used in determining mechanical properties of bone are similar to those of engineering materials, as shown in figure 4.6. For example, tensile, compressive and bending tests are carried out to determine respective strength or stress, and to determine modulus of elasticity based on the stress and strain relationship. However, certain formulae for characterising homogeneous and isotropic materials may not be appropriate since bone is a composite and anisotropic material (Evans, 1973; Jacobs *et al.*, 1976). Bone anisotropy, which has a major effect on the determination of mechanical properties, is characterised by the organisation and the orientation of bone architecture in the direction of loading. As a result, the distribution of strength and density in the bone varies according to the anatomic location, for example in cancellous bone of the proximal femur. Because the significance of these factors is more pronounced in cancellous bone, coupled with the storage method and testing conditions, immense variation in the determination of mechanical properties has been reported (Martens *et al.*, 1983; Goldstein, 1987). Other contributions to this large variation include the non-physiologic boundary conditions of the bone specimen and the effect of bone specimen geometry in mechanical testing (Linde *et al.*, 1992; Keaveny *et al.*, 1993). In addition, the accuracy of mechanical testing is limited by the size of the bone specimen.

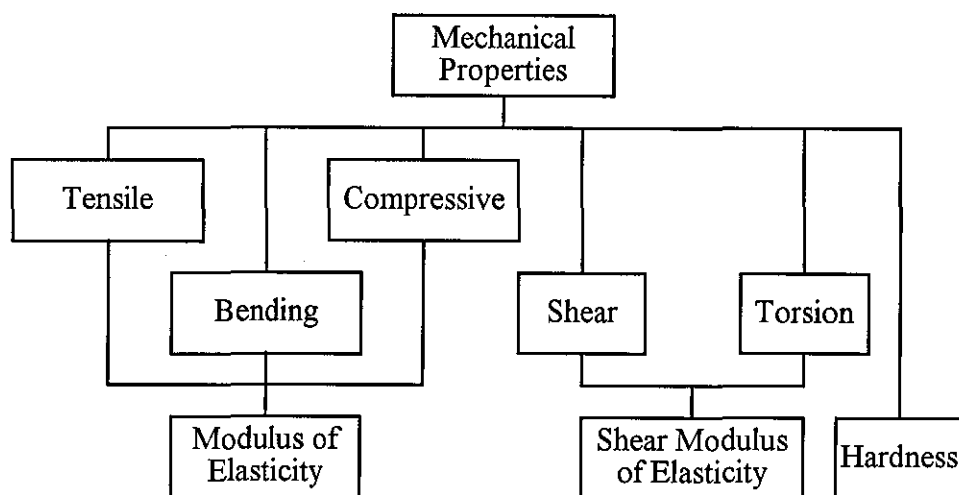


Fig. 4.6 Mechanical properties of bone (Evans, 1973)

The literature on the mechanical properties of both cortical and cancellous bones is well established and reflects a better understanding of the functional adaptation of bones. Most of

the early investigations have been concentrated on the mechanical properties of cortical bone (Yamada, 1970; Evans, 1973). The importance of mechanical behaviour of cancellous bone is reflected in the understanding of the effects of metabolic and degenerative diseases, such as osteoporosis and osteoarthritis, on bone strength. Osteoporosis, for instance, is commonly associated with the elderly population. It is characterised by the reduction in both the quality and the quantity (mass) of cortical and cancellous bones, consequently there is an increased risk of bone fracture due to reduced load capacity. Since cancellous bone has a higher metabolic rate due to its greater surface area of porous structure, it becomes more responsive to changes in mineral storage (Cooper, 1990). Therefore, bone loss caused by diseases such as osteoporosis affects cancellous bone more quickly than cortical bone.

The hip and the vertebrae, which consist mainly of cancellous bone, are two common areas where osteoporotic fractures occur. These type of fractures are generally treated with internal fixation. Therefore, the success of internal fixation depends, to a certain extent, on the knowledge of the mechanical properties and bone architecture. This knowledge is also beneficial to treatment associated with total hip and knee replacement since a section of cancellous bone is replaced by a prosthesis or an implant.

Studies have shown that the proximal femur (upper femoral region) is where the bone structure and density are most critically related and, therefore, it is an important skeletal site for determining the mechanical characteristics. Although the cancellous bone in the proximal femur is highly anisotropic, linear correlation has been found between compressive strength and elastic modulus (Brown & Ferguson, 1980; and Goldstein, 1987). Other studies obtain power function relationships which are quite close to a linear relationship (Martens *et al.*, 1983; Hodgkinson & Currey, 1993 and Keller, 1994). This kind of relationship enables the strength of cancellous bone to be predicted based on its modulus of elasticity. However, there is little validity in predicting strength and elastic modulus of cortical bone by means of extrapolation from cancellous bone (Rice *et al.*, 1988; Keller, 1994). This can be explained simply by the microstructural orientation and properties of the bone tissue. Cortical bone has concentric lamellae of bone tissue oriented parallel to the shaft of long bones, while cancellous bone consists of fragmented superimposed lamellae, as described in Appendix 3.5. Therefore cortical bone cannot be assumed to be a dense cancellous bone.

Positive relationship of strength and modulus to apparent density of cancellous bone has also been reported (Goldstein, 1987; Brear *et al.*, 1988; Rice *et al.*, 1988). Apparent density is the dry weight of bone per unit volume. The correlation between mechanical properties and apparent density favours the use of a power function instead of a linear function. Moreover, compressive strength has been shown to have better correlation with the apparent density than the modulus of elasticity (Brear *et al.*, 1988; Keller, 1994).

The unique trabecular architecture of the proximal femur, as shown in figure 4.7, has been subjected to several studies which relate to spatial and directional effects on values obtained for mechanical properties. The spatial variation in strength and elastic modulus within the specimen have been found to be extremely large (Brown & Ferguson, 1980; Martens *et al.*, 1983). Even within the femoral head alone, a wide spatial distribution of strength along axes parallel to the cervical axis has been reported (Schoenfeld *et al.*, 1974). In general, the femoral head region has the highest strength and stiffness as compared to neck and inter-trochanteric regions.

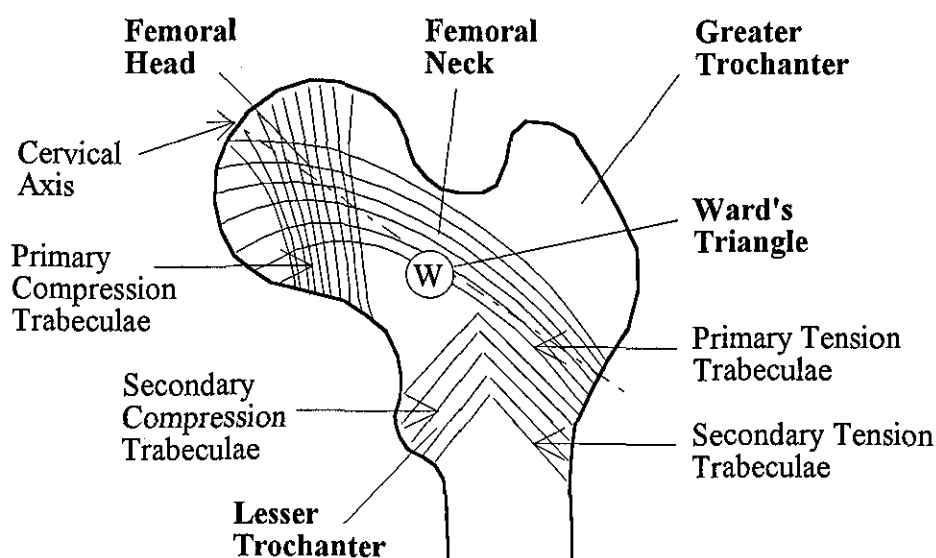


Fig. 4.7 Trabecular orientation of the proximal femur (Wahner & Fogelman, 1995)

The directional effects also account for the variation in the values of mechanical properties. Mechanical testing by compression of the proximal femur has been carried out in three orthogonal axes with respect to two reference axes of either the medial-lateral (horizontal) axis (Brown & Ferguson, 1980) or the cervical axis (Martens *et al.*, 1983), as shown in figure 4.8. Loading in the anterior-posterior (AP) direction has been found to produce the weakest overall strength and modulus of elasticity, as compared to those loaded in the direction of the cervical

axis and in the direction perpendicular to the cervical axis (Y-Axis shown in figure 4.8) (Martens *et al.*, 1983). Based on reference to the medial-lateral axis, the overall strength and modulus of elasticity have been found to be the highest when loaded in the superior-inferior direction (Brown & Ferguson, 1980). In addition, the loading direction also has an influence on the mechanical properties at specific regions of the proximal femur. For instance, the neck region has been found to have a higher overall strength and stiffness than the inter-trochanteric region when loaded along the cervical axis but the opposite is true when loaded in the direction of Y-Axis (Martens *et al.*, 1983).

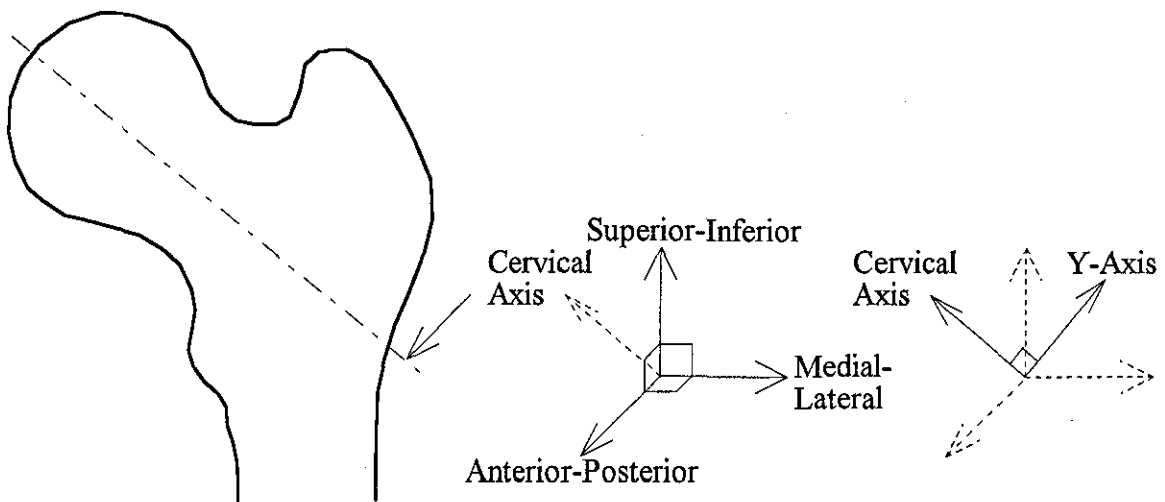


Fig. 4.8 Axes of the proximal femur

Apart from material properties related to mechanical behaviour and architecture, it is also important to consider the microstructural characteristics of cancellous bone in the evaluation of bone strength. One of the microstructural parameters relates to the measure of local or structural anisotropy known as fabric. It has been found that fabric has a significant correlation with both ultimate compressive strength and elastic modulus (Goulet *et al.*, 1994). Since cancellous bone has an irregular structure of inter-connecting plates and columns of trabeculae, the thickness, the spacing and the connectivity of trabeculae also affect the bone strength. These correlations from apparent density and microstructural characteristics can be useful in predicting the mechanical properties of bone.

Although, the determination of the mechanical properties plays an important role in the evaluation of cancellous bone strength, it depends on many factors related to the specimen, testing condition and storage method. Mechanical testing requires a large amount of bone samples, and also meticulous specimen preparation due to the intricate cancellous bone

structure. Since the specimen is removed from the bone, testing is carried out under non-physiologic boundary conditions. To a certain extent, the size of the specimen represents a limit in terms of accuracy that can be achieved by mechanical testing. These factors, therefore, limit the clinical value of using mechanical methods in the evaluation of bone strength. However, the positive relationships of apparent density with the mechanical strength and modulus of elasticity link to the use of another method of bone strength evaluation called bone densitometry. This method measures bone mineral density as an indication of strength.

4.3.2 Bone Densitometry

The clinical importance of bone densitometry is in the area of osteoporosis where it assists in the prediction of fracture risk, the selection of patients for hormone replacement therapy (HRT), monitoring and optimising therapy and improving compliance of therapy (Sartoris, 1994). It has been established that low bone density measured by densitometry is associated with increased risk of fracture (Marshall *et al.*, 1996). In general, bone density has been found to decline linearly after the age of 55 years (De Laet *et al.*, 1997). Since osteoporosis is a major cause of hip and vertebral fractures and has certain resistance to treatment once established, early detection of bone loss is important in the prevention of this disease and its complications (Heidrich, 1993). Hip fractures, in particular, are responsible for considerable disability, morbidity and mortality of the elderly people, and create an enormous burden to both public health and health-care finance (Adams, 1992; Compston *et al.*, 1995).

In densitometry, bone strength is determined through bone mineral content (BMC), bone mineral density (BMD), true bone mineral density, broadband ultrasonic attenuation (BUA), speed of sound (SOS) or magnetic resonance. There are several techniques of measuring BMC and BMD in either g/cm or g/cm²: (i) single-photon absorptiometry (SPA), (ii) dual-photon absorptiometry (DPA), (iii) dual energy x-ray absorptiometry (DXA or DEXA), and (iv) quantitative computed tomography (QCT) (Hagiwara *et al.*, 1994; Wahner & Fogelman, 1995). QCT also provides true bone mineral density in g/cm³. The techniques of bone densitometry are summarised in figure 4.9.

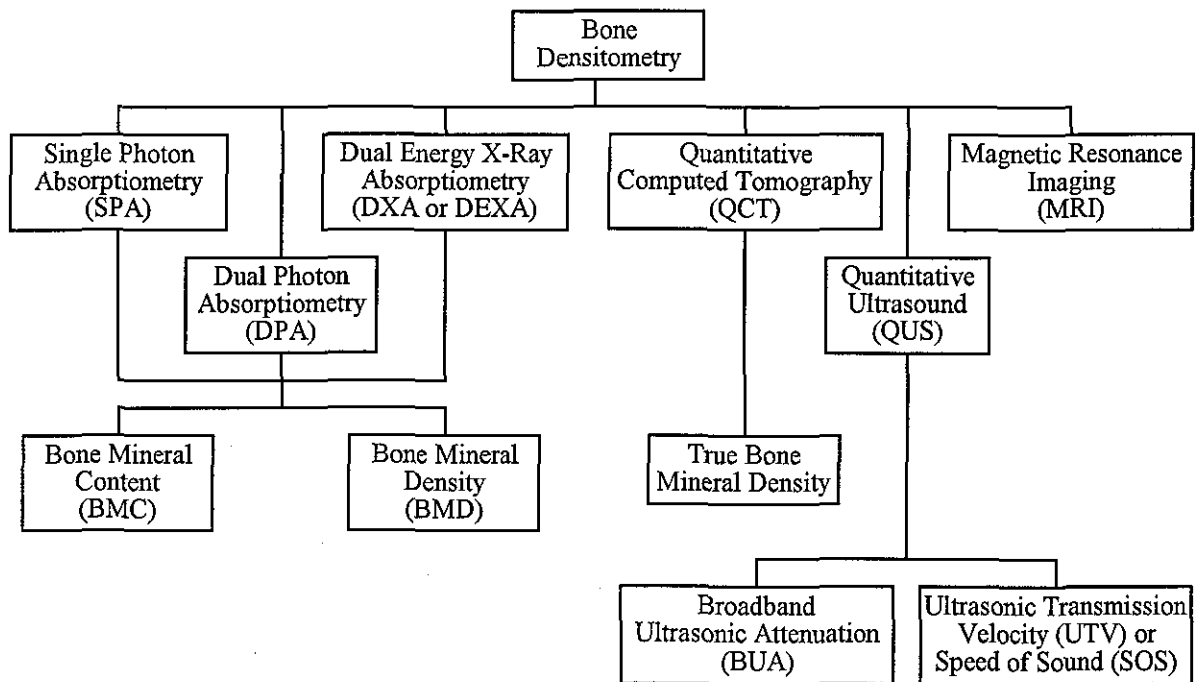


Fig. 4.9 Bone densitometry (Wahner & Fogelman, 1995 and Hagiwara *et al.*, 1994)

One of the earliest methods of quantitative bone mineral analysis is radiographic absorptiometry (RA or radiogrammetry). However, this technique suffers from poor accuracy and precision and thus, its usage is now limited to appendicular bones (phalanges and metacarpal). Subsequently, SPA, which measures BMD, was developed in place of RA. SPA uses only one photon of energy and as a result, it can only measure BMD accurately at peripheral skeletal sites, such as distal radius (forearm), humerus, calcaneus (heel) and distal femur, where soft tissue thickness is relatively constant. The effects of soft tissue thickness can be corrected using the DPA technique with two photon energy levels but at the expense of accuracy and precision. Bone density measurement by DPA is derived from the relative attenuation of the two photon energy levels, higher and lower, between the bone and the soft tissue.

The most widely used technique for BMD measurement is the dual energy x-ray absorptiometry (DXA or DEXA) which has a similar operating principle to DPA except for the replacement of the photon source with an x-ray source. Due to higher photon flux produced by the x-ray source, DXA offers improved accuracy and precision as well as reduced scanning times as compared to DPA. Besides measuring areal density (g/cm^2), QCT is the only established method capable of providing BMD as a true mineral density in g/cm^3 . Measurement of BMD has been reported to account for 70% of the bone strength (Chesnut III, 1993). At present, BMD is the most widely used parameter for the evaluation of bone strength and risk of fracture.

Alternative techniques such as quantitative ultrasound (QUS), which measures BUA and SOS, and magnetic resonance imaging (MRI) are currently being developed for bone strength measurement. Both techniques are free from ionising radiation, and QUS equipment has further advantages of being relatively inexpensive and more portable.

The diagnosis of osteoporosis or bone loss is generally based upon bone density measurements of cancellous bone at a specific location such as the calcaneus (heel), forearm, hip, spine and tibia. However, densitometry measurement of one location does not reflect the measurement of another, and the degree of osteoporosis may vary at different locations within the patient (Wahner & Fogelman, 1995). The measurement of BMD is also affected by the thickness of soft tissue and fat around the measured site, as well as the bone distance from the table and its positioning. Moreover, an optimal site for the assessment of bone density has not been established for the prediction of fracture risk (Compston *et al.*, 1995). In the prediction of hip fractures, densitometric measurements of the hip have been reported to be the best predictor as compared to spine measurements (Cummings *et al.*, 1993; Marshall *et al.*, 1996). Therefore, fracture prediction using densitometry is very site specific. Densitometric measurements have also been shown to have a large overlap between patients with and without fractures in case control studies of hip fractures (Marshall *et al.*, 1996).

Comparison of BMD measurements between DXA (g/cm^2) and QCT (g/cm^3) has not produced any conclusive findings on the method with the most effective predictor of fracture risk related to low bone mass (Duboeuf *et al.*, 1995; Cody *et al.*, 1996). Standardisation of bone density measurements through cross-calibration using phantoms has been attempted in order to facilitate longitudinal studies and multi-centre trials associated with osteoporosis (Adams, 1992). This is because densitometric measurements between equipment of different manufacturers using the same technique are not interchangeable for studying individual patients (Tothill *et al.*, 1995).

Investigations into the use of QUS for evaluating bone strength has produced promising results which indicate that QUS parameters of BUA and SOS could provide information on the bone structural aspect and quality besides bone density (Glüer *et al.*, 1993; Moris *et al.*, 1995). Although assessment of bone strength using QUS is confined to sites with minimum amount of soft tissue around bones such as the calcaneus and the tibia, BUA and SOS have been found to

have conflicting correlations with BMD of the calcaneus, femoral neck, spine and tibia. In one of the studies, calcaneus QUS was found to correlate significantly with lumbar spine BMD by DXA (Moris *et al.*, 1995). Whereas other studies have found weaker correlations between calcaneus QUS and densitometric measurements at femoral neck and lumbar spine (Turner *et al.*, 1995; Cunningham *et al.*, 1996). The common conclusion from these studies indicates that QUS is capable of evaluating bone strength and fracture risk. There is, however, no superiority in terms of performance for the prediction of low bone density and fracture risk between DXA and QUS. Unlike DXA, the use of QUS as a clinical tool for evaluating bone strength has yet to be established.

In addition to bone densitometry, the trabecular pattern of the proximal femur, which is characterised by the Singh Index based on a radiograph, has been found to relate to the degree of bone loss as a result of osteoporosis (Singh *et al.*, 1970). However, the dependency of this method on the quality of the radiograph and the consistency of the observation has resulted in mixed findings with regards to the reliability and the reproducibility of the Singh Index in the assessment of bone strength (Smith *et al.*, 1992; Smyth *et al.*, 1997).

4.3.3 Correlation of Mechanical Properties and Bone Densitometry

Many investigations have been targeted either at the correlation between mechanical properties related to apparent density, compressive strength and modulus of elasticity or between bone densitometric measurements of DXA, QCT and QUS. It has been well established that the relationships between apparent density, compressive strength and elastic modulus are strong with consistently high correlation coefficients (Goldstein, 1987). In comparison, establishing relationships between densitometric measurements has been subjected to more recent investigations due to wider availability of clinical densitometry equipment. Since bone densitometry is, at present, the only *in vivo* method of evaluating bone strength for the prediction of fracture risk associated with low bone mass, it has started to generate an ever increasing interest in bone strength especially in the correlation between densitometric measurements and mechanical properties.

Studies have shown that correlations between densitometric measurements and mechanical properties of cancellous bone had contrasting results. The most basic comparison between apparent density and BMD has produced positive correlations ranging from moderate to high (Leichter *et al.*, 1988; Lotz *et al.*, 1990; Rho *et al.*, 1994). An investigation carried out by Cody *et al.* (1996) has found that *in vitro* densitometric measurements from DXA and QCT of the human proximal femur had poor correlation with the mechanical properties related to elastic modulus, but moderate correlation with ultimate stress. In addition, there was no advantage of using QCT over DXA in the correlation between densitometric and mechanical measurements. Conflicting findings were presented by Lotz *et al.* (1990) where both apparent density and BMD by QCT of the proximal femur had strong power relationships with compressive strength and elastic modulus of the bone. Moderate correlations were also obtained by Leichter *et al.* (1988) between BMD by SPA and mechanical properties related to compressive strength and modulus of elasticity at the greater trochanter of the proximal femur.

Studies were also conducted to determine relationships between breaking strength, or average shear stress at failure, of the femoral neck and density measurements. A moderate correlation was found between femoral neck BMD by DPA and measured breaking strength (Beck *et al.*, 1990). The BMD by QCT was also found to have a moderate correlation with the fracture load of the femoral neck (Smith *et al.*, 1992). However, specimen apparent density and BMD by SPA of the greater trochanter correlated rather poorly with the average shear stress at failure of the femoral neck (Leichter *et al.*, 1988). A significant correlation did exist between the average shear stress at failure and the overall mass density of the intact greater trochanter.

These results reinforce the findings on the effects of trabecular orientation, as shown in figure 4.7, and bone density on the determination of the mechanical properties. However, densitometric measurements (BMD) by DXA and QCT give only an average mineral density over a region (ROI) or a volume (VOI) of interest regardless of the trabecular orientation and the density variation within. Although BMD, which accounts for approximately 70% of the bone strength, is a major determinant of fracture risk, bone quality and bone architecture are also responsible for the loss of bone strength. These two latter determinants are not considered to be measurable by BMD.

Apart from the proximal femur, cancellous bones from the vertebrae were also used for *in vitro* correlation purposes between mechanical properties and densitometric measurements. In an investigation by Edmondston *et al.* (1994), vertebral compressive strength was found to correlate moderately with BMD by DXA, but no significant relationship was found with true mineral density by QCT. On the contrary, results from Rho *et al.* (1994) have shown that compressive strength and its elastic modulus correlated moderately with densitometric measurements by QCT but rather poorly with BMD by DPA. Furthermore, the correlations of apparent density with BMD and true mineral density by QCT were moderate at best, while the relationship between BMD and true mineral density was very poor.

The mechanical behaviour of cancellous bone depends on bone density, as well as on bone architecture and bone quality, which can be described by the elastic modulus, and microstructural properties such as the fabric, trabecular thickness and trabecular spacing. QUS has been reported to be able to characterise both bone architecture and bone quality besides bone density. QUS parameters of BUA and SOS have been found to relate significantly to elastic modulus (bone quality) and bone density respectively (Grimm & Williams, 1997). Further discussion on the evaluation of bone strength is given in Section 6.1.

4.3.4 Bone Drilling

Bone drilling measurements using small diameter drill bits have been proposed as an alternative method for evaluating bone strength (Karalis & Galanos, 1982; Chagneau & Levasseur, 1992). The level of resistance produced by bone drilling can indicate not just the density, but also bone orientation and quality. Furthermore, force profiles produced during drilling are only limited by the drill bit diameter and, therefore, provide better spatial resolution or accuracy than densitometric or mechanical measurements.

An investigation was carried out by Karalis and Galanos (1982) to show the interrelationship between the penetration rate of a drill bit, drilling strength (defined as the ratio of energy input to volume of bone broken), tri-axial strength and hardness of bone based on mathematical analyses associated with rock mechanics. Tri-axial strength is obtained from a mechanical test, in which two principal stresses are equal, usually $\sigma_1 > \sigma_2 = \sigma_3 > 0$ (Jaeger & Cook, 1979). A

principal stress is a normal stress acting on a principal plane in a defined principal direction. The investigation by Karalis and Galanos (1982), however, was not aimed at studying the mechanical properties of bone related to quality, location, age and sex. The drilling experiments were carried out on human cadaveric cancellous bone of the femoral head and cortical bone of the tibial shaft. The drill bits used were the 'Q' type recommended by Jacobs *et al.* (1976), with drilling speeds in the range of 1200-1380 rev/min at constant applied force. A linear correlation was found between the tri-axial compressive strength and the drilling strength of both the femoral head cancellous bone and the cortical bone. A linear relationship was also found between the rotational speed and the penetration rate. The cortical bone exhibited a slower penetration rate than cancellous bone for a given rotational speed. Since bone is an anisotropic material, hardness was shown to have no linear relationship with the drilling strength for both cortical and cancellous bones. It was further mentioned that drilling would be widely utilised if correlations could be made to distinguish normal bone from diseased bone caused by, for instance, osteoporosis.

Drilling force and torque measurements are normally quantified in terms of an average value. However, this type of measurement is not applicable to cancellous bone, especially in the proximal femur, due to its large variation in both structure and density within the bone. A continuous measurement of drilling force or torque would therefore be more useful to represent changes in density, and hence the strength along a specific drilling trajectory. Based on this technique, Chagneau and Levasseur (1992) introduced a method of mechanical testing called dynamostratigraphy. It is a measurement of penetration strength (thrust force) and torque developed with respect to drill bit penetration displacement during drilling using a pre-set drill bit rotational speed and feed rate. This technique enables the thickness and the mechanical resistance of the material, especially fragile, fibrous or laminated materials, to be measured to a high degree of precision. Drilling data can also be acquired through dynamostratigraphy in quick and simple form without any risk of error.

Chagneau and Levasseur (1992) proposed that dynamostratigraphy could be used to study the morphology of bone structure and to define its mechanical resistance. They applied dynamostratigraphy on human cadaveric femoral heads using a 4.0 mm diameter three-flipped drill bit. The drill bit rotational speed and the feed rate were fixed at 350 rev/min and 10 mm/min respectively, while the thrust force and the displacement were recorded automatically.

For the purpose of comparison, punching tests were also conducted using a cylindrical steel rod of diameter 4.0 mm. The results from dynamostratigraphy showed clear changes in the resistance of the cancellous bone across the femoral head at different drilling trajectories. A two-dimensional force mapping was also presented to show the force characteristics of the femoral head. When compared to results from drilling test, higher forces were obtained by punching; this could be attributed to the deformation forces associated with compliance of the porous cancellous bone structure before failure by shear. Correlation between drilling and punching forces was not presented.

In addition to bone drilling, another method proposed by Hvid *et al.* (1984) utilised a needle under a constant feed rate to penetrate cancellous bones for strength measurements of human cadaveric knees. The penetration forces with respect to the needle displacement were obtained from an instrument known as osteopenetrometer. Continuous changes in the penetration forces with respect to the depth were observed, hence indicating the strength variation of cancellous bone at the knee. It was found that, using a power function, average penetration strength (penetration force/projected area of the needle) had a good linear correlation with ultimate compressive stress. Furthermore, Bentzen *et al.* (1987) and Petersen *et al.* (1996) have found that penetration strength using osteopenetrometer had significant linear relationships with densitometric measurement and mechanical properties.

All the investigations discussed above share a common goal of *in vivo* evaluation of bone strength and assessing the effects of metabolic diseases such as osteoporosis and osteomalacia on bone strength. However, these bone drilling investigations have not been able to provide an applicable method for the evaluation of bone strength. As a result, the relationship of drilling data with mechanical properties and densitometric measurements has not been statistically established. Furthermore, drilling experiments on cancellous bone have been carried out only on the head of the femur (Karalis & Galanos, 1982; Chagneau & Levasseur, 1992). Although osteopenetration strength has been found to relate to the strength of bone, the use of a penetration needle is not a common procedure in orthopaedic surgery. The osteopenetration forces involved is also higher than drilling forces for a given feed rate. Further discussion on bone drilling for the evaluation of bone strength is presented in Section 6.2.

The additional knowledge of bone strength through drilling offers a possible guide to surgeons in selecting appropriate treatment of fracture fixation, in indicating the use of bone cement or in suggesting the need for more protective post-operative management (Smith *et al.*, 1992). Since bone drilling is a common procedure of fracture fixation in orthopaedic surgery, it is practical to automate bone drilling suitable for collection of drilling data for bone strength analysis. To the author's present knowledge, investigations into the feasibility of using bone drilling for bone strength evaluation have not been carried out.

4.4 Automation of the Bone Drilling Process

The automation of the surgical drilling process is the most recent development. This is to take advantage of the flexibility, the accuracy and the precision offered by automated devices for the purpose of enhancing the drilling accuracy and safety, and thus the success rate of the procedure. Data such as drilling forces, drill bit displacement and rotational speed, which are not available to surgeons at present, can be automatically collected during drilling operations for immediate analysis as well as stored for follow-up or future analysis. Analysis of such can help in implementing a control algorithm to predict and to affect or control the outcome of a drilling procedure for safety enhancement. The usage of drill bits with regards to bit shape for bone drilling also becomes more flexible as automation provides measurement and control to help minimise drilling force, torque and temperature generated. In addition, the usage of drill bit with regards to bit shape for bone drilling also becomes more flexible as automation provides measurement and control to help minimise drilling force, torque and temperature generated.

One particular application of automation is the detection of drill bit break-through when drilling into the shaft of long bones for the fixation of shaft fractures, such as in the insertion of interlocking screws for intramedullary nailing. At present, this type of bone drilling procedure requires good manual skills and relies heavily on radiographic guidance. Break-through detection is aimed at minimising the over-travel of the drill bit through the bone and thus reducing tissue damage. Moreover, any anomaly in the conventional drilling data, such as an unexpected increase in drilling force, can be detected instantly, hence allowing the drilling procedure to be duly stopped and the trajectory checked.

One such system for drill bit break-through detection is being developed by Allotta *et al.* (1995) for drilling into long bones as part of a mechatronic tool design for drilling in orthopaedics. The proposed break-through detection method would allow the hole to be completed with minimal protrusion and hence minimal tissue damage. The experiments were carried out on porcine femoral shafts using a dc-motor powered drill prototype mounted on a testing machine and a standard metal drill bit of diameter 3.5 mm. Both the force and torque were measured under feed rates of 50, 75 and 100 mm/min, and drill bit rotational speeds of 1500, 1800 and 2000 rev/min. The results of drilling force and torque indicate two prominent peaks at the two cortical walls as a result of sharp changes on entry and exit of the walls. Using a force derivative algorithm, these sharp changes are detected with appropriate lower and upper thresholds to identify the onset of bit break-through. The force derivative algorithm is given as:

$$\frac{dF(t)}{dt} = -K_s f^2 n \sin\left(\frac{\beta}{2}\right) \tan\left(\frac{\beta}{2}\right)$$

where: $F(t)$ is the drilling force (N) which varies with time t (s), K_s is the specific cutting energy (Mpa or N/mm²), n is the rotational speed (rev/s), f is the feed rate (mm/rev), and β is the drill bit point angle.

However, as fixed thresholds cannot be used since the forces and their derivatives are functions of drill bit diameter, feed rate and cutting speed, the lower and upper threshold values have been determined by using the drilling force data of the first cortical wall to set the thresholds for the second cortical wall. Theoretical models of the drilling thrust force and the torque at drill bit break-through have also been presented. The break-through model of thrust force has been shown to compare well with the experimental data. The expressions used for the drilling force break-through model are:

$$F(t) = 2K_s CSA(t) \sin\left(\frac{\beta}{2}\right) \quad \text{and}$$

$$CSA(t) = \begin{cases} \frac{Df}{4} - \frac{f^2}{2} n^2 t^2 \tan\left(\frac{\beta}{2}\right) & 0 < t < \frac{1}{2n} \\ \frac{Df}{4} - \left[\frac{f^2}{2} n t \tan\left(\frac{\beta}{2}\right) - \frac{f^2}{8} \tan\left(\frac{\beta}{2}\right) \right] & \frac{1}{2n} < t < \frac{D}{2fn} \cot\left(\frac{\beta}{2}\right) + \frac{1}{2n} \end{cases}$$

where: $CSA(t)$ is the chip area (mm²) which varies with time t (s), D is the drill bit diameter (mm), and the other terms are defined as above.

The use of a derivative function is limited to drilling forces with minimum amount of inherent fluctuation for the detection of drill bit break-through. Furthermore, the determination of the lower and higher thresholds requires the estimation of the specific cutting energy from the force derivative. Detection methods of drill bit break-through are further discussed in Section 5.4.

A different method of break-through detection has been proposed by Brett *et al.* (1995) for drilling through a stapes footplate using a burr drill bit in accordance with the stapedotomy procedure of the middle ear. The stapes is a tiny compliant bone in the middle ear, and stapedotomy, which is a part of the stapedectomy procedure, is carried out to recover the loss of hearing, due to immobilisation of the footplate of the stapes, by producing a hole for the attachment of a piston prosthesis. In the experiments both the thrust force and the torque along with the displacement of the drill bit were measured using a feed rate in the range of 0.2 to 1.0 mm/min and a drill speed of 120 rev/min. At the start of drilling, both the force and the torque increase steadily as a result of the advance rate being greater than the penetration rate; this causes the stapes footplate to deflect. On the verge of break-through, there is first a gradual fall in force, which is followed by a rapid fall in force and a rapid increase in torque. The characteristics of the force and torque associated with the break-through process are shown to be always present when drilling into stapes footplate. Only the magnitudes of maximum force and torque vary with the stiffness of the stapes, drill feed velocity and drill bit sharpness. These bit force and torque characteristics are then applied to the automatic detection of break-through by identifying the persistent increase in the torque over six samples period while the force decreases. When this condition, which occurs before bit break-through, is true, the drill rotation is stopped and the drill bit is retracted until zero feed force is obtained. At this point, the stapes footplate returns to the original position. The information obtained from the force reduction, corresponding to the deflection of the stapes when retracting the drill bit, is then used to estimate the stiffness of the stapes footplate. Subsequently, a second advance of the drill bit is initiated to achieve a fully formed hole with minimum bit protrusion. The peak force in the second drilling phase is lower than the first, while the peak torque is higher due to the decreased deflection of the stapes footplate.

Automation gives bone drilling the capability to measure and store drilling data such as forces and drill bit displacement in real time, and to implement appropriate control strategies for predicting and affecting the outcome of drilling such as the detection of drill bit break-through.

The two detection methods of drill bit break-through reviewed above are affected by inherent fluctuation of drilling force. Therefore, there is a need to devise a more reliable break-through detection method for the enhancement of safety. Further discussion of the present detection methods are presented in Sections 5.3 and 5.4.

4.5 Conclusion

This review has drawn together the literature of bone drilling and discussed methods of evaluating bone strength. Two novel areas of investigation have been identified, and these are the drilling process automation related to safety enhancement and bone strength evaluation based on bone densitometry. The improvement of safety of the drilling operation can be achieved by devising a robust and reliable method of drill bit break-through detection in the presence of system compliance and inherent fluctuation of drilling force, and by the evaluation of drilling profile characteristics. The present detection methods of break-through lack the reliability because the effects of system compliance and inherent drilling force fluctuation are not taken into consideration. Results of this investigation could be implemented in the design and development of a drilling tool for mechatronic/robotic assisted surgery.

The current studies of bone drilling have not established a suitable method for the evaluation of bone strength associated with correlations between bone drilling and mechanical properties and/or between bone drilling and bone densitometry. Since both bone drilling and bone densitometry are extensively used in orthopaedics surgery and clinical evaluation of bone strength respectively, the drilling data from the proximal femur can be correlated with the densitometric measurements. This is to investigate the effects of bone mineral density (BMD) on the drilling data and to study the feasibility of the correlation method. The following two chapters will provide a critical discussion on the present work and outline the research methodology for bone drilling to achieve the objectives of safety enhancement and the evaluation of bone strength.

CHAPTER 5

THE DETECTION OF DRILL BIT BREAK-THROUGH

Two areas of investigation have been identified as a result of the literature review. These are the detection of drill bit break-through and the analysis of drilling data for the evaluation of bone strength. The purpose of this chapter is to provide a critical discussion of the present methods of drill bit break-through detection, as well as a detailed description of a novel robust detection method. This involves discussions on the effects of system compliance and inherent fluctuation of drilling force on the break-through detection.

5.1 The Drilling of Bone

Early investigations related to bone drilling were primarily aimed at developing a suitable drill bit in order to optimise the thrust force and torque, as well as prevent or reduce thermal damage to the bone. Therefore, heavy emphasis was placed on the drilling conditions and on the design of drill bit shape. Comparative studies have been difficult due to the lack of standardisation in the testing methods employed. Differences in the results are, therefore, expected due to variation in the drilling conditions, and also force and torque measurements are functions of drill bit type and diameter. Moreover, most of the recommendations made by different researchers with regard to surgical drill bit design have not been fully implemented at the clinical level.

Two areas associated with bone drilling, namely process automation and bone strength evaluation, have been identified as the areas of research and contributions to the literature. The automation of bone drilling in this investigation focuses on the safety enhancement of surgical drilling procedures and also plays an important role in determining bone strength. As stated in Section 3.1.1, the system compliance, especially from the bone, and the inherent drilling force fluctuation can affect the method of drill bit break-through detection when drilling into long bones such as the femoral shaft.

5.2 Configuration of the Drilling Unit

The effects of system compliance would depend on the amount of drill bit advancement relative to the bone being drilled. When the drilling unit and the bone are two independent objects, the advancement of the drill bit, as shown in figure 5.1a, will be affected by the system compliance. An example of this configuration is a floor or an operating table mounted robotic device. The critical factor of the system compliance is the tendency to cause excessive protrusion of the drill bit at break-through due to the spring-back effect. On the other hand, system compliance would have negligible effect when the drilling unit is in constant contact with the bone via an external applied force when advancing the drill bit, as shown in figure 5.1b. An example of this configuration is a hand-held mechatronic drill which is pressed against the bone by the surgeon. In order to achieve negligible effect of system compliance, a constant external force is required. Furthermore, this constant force which is applied to the drilling unit must be greater than the drilling force of the bone.

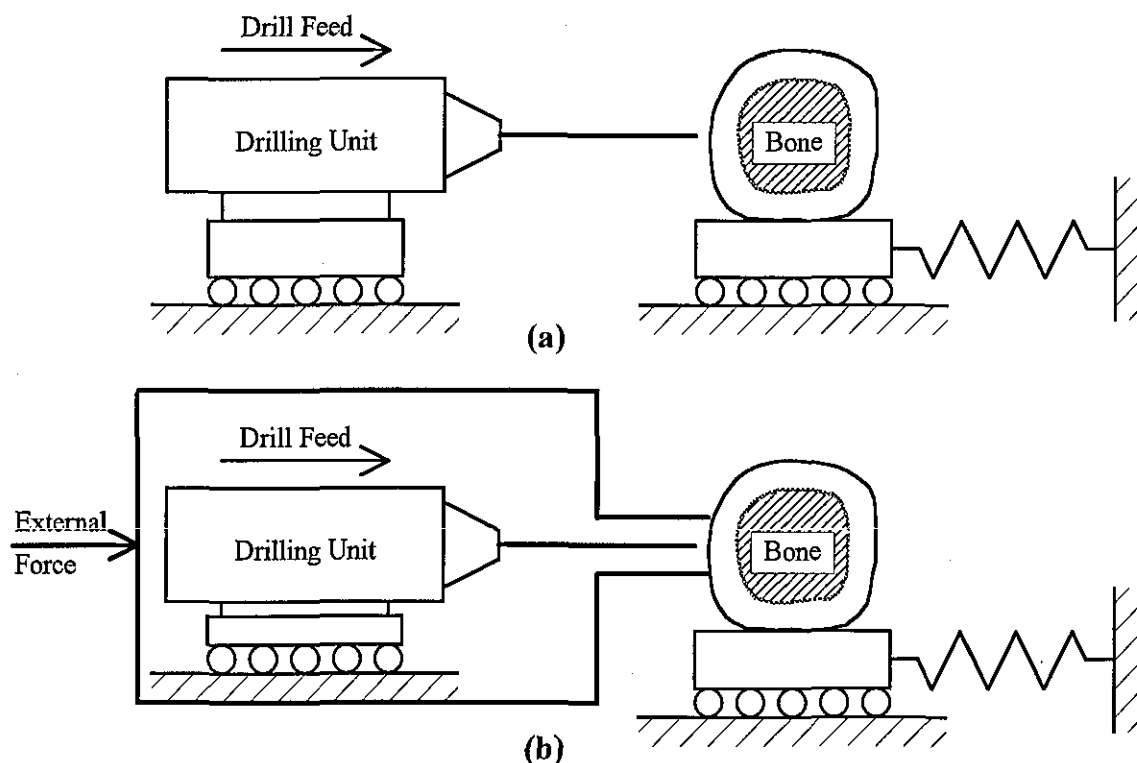


Fig. 5.1 Configuration of the drilling unit relative to the bone: (a) the drilling unit and the bone are independent objects, (b) the drilling unit is constantly pressed against the bone

5.3 The Enhancement of Safety

Investigation into devising a robust and reliable technique of drill bit break-through detection that is immune to system compliance and, to a certain extent, to the inherent drilling force fluctuation would be very important for the enhancement of safety associated with robotic/mechatronic assisted surgery in drilling of long bones. System compliance plays an important role in the break-through detection in robotic assisted orthopaedic surgery. Apart from direct contact measurement using a pointer or a probe, movement or displacement of the bone with reference to the drilling unit is difficult to measure.

System compliance in bone drilling is affected by the magnitude of initial bone penetration force. The initial penetration force is the force required to overcome the system stiffness and the bone deformation before the start of actual cutting or drilling. This initial force is difficult to estimate without drilling. In contrast, the stiffness coefficient can be estimated by advancing a non-rotating drill bit or a probe onto the bone surface and measuring the force corresponding to the displacement. This would, however, mean an additional procedure which could be time consuming in the drilling process. The presence of soft tissue and the slippery bone surface may affect the estimation of system stiffness. Furthermore, system compliance estimated without drilling may not necessarily apply to the actual drilling process when bone material is being removed.

Automation of bone drilling can also allow for progressive analysis of drilling profiles based upon typical stored profiles in order to estimate the direction and location of the drill bit. This type of analysis could prove to be valuable in minimising misplacement of fixation implants and preventing excessive drill bit over-travel so as not to penetrate other organs. For instance, the penetration of the pelvic organ by guide wires (guiding drill bits) through the femoral head is not infrequent during fixation of hip fractures even with routine use of fluoroscopic guidance during the operation (Feeney *et al.*, 1997).

5.4 Present Detection Methods of Drill Bit Break-through

Two particular studies by Allotta *et al.* (1995) and Brett *et al.* (1995), discussed in Section 4.4, are dedicated to the detection of drill bit break-through. However, both studies differed in terms of break-through control strategy and types of bone being drilled. In addition, theoretical

models of the drilling thrust force and torque have been presented by both studies for the purpose of predicting the drill bit break-through. Brett *et al.* (1995) modelled the profiles of force and torque for the simulation of drill bit entry and break-through of the stapes footplate, while Allotta *et al.* (1995) presented only the break-through profile models of drilling force and torque with reference to femoral cortical bone. Both modelling methods have been based upon chip formation or tool contact area. The drawback of this kind of modelling is the difficulty of obtaining a general model because the model will depend very much on a specific feed rate, drill bit diameter, drill bit geometry, rotational speed and system compliance, as well as the bone strength. Furthermore, the drilling force model of break-through presented by Allotta *et al.* (1995) does not accurately represent the stages of chip area formation. During break-through, the cross-sectional chip area varies according to three stages, not to two as presented by Allotta *et al.* (1995). A more accurate chip area representation of the break-through model, the derivation of which is detailed in Appendix 5, is given by:

$$CSA(t) = \begin{cases} \frac{Df}{4} - \frac{f^2}{2}n^2t^2\tan\theta & 0 < t \leq \frac{1}{2n} \\ \frac{Df}{4} - \frac{f^2}{2}nt\tan\theta - \frac{f^2}{8}\tan\theta & \frac{1}{2n} < t - \frac{1}{2n} \leq \frac{D}{2fn}\cot\theta \\ \frac{1}{2}\tan\theta\left(\frac{f^2}{4} - f^2nt + (fnt)^2\right) & \frac{D}{2fn}\cot\theta < t - \frac{D}{2fn}\cot\theta \leq \frac{D}{2fn}\cot\theta + \frac{1}{2n} \end{cases}$$

where: $CSA(t)$ is the chip area (mm^2) which varies with time t (s), D is the drill bit diameter (mm), n is the drill bit rotational speed (rev/s), f is the feed rate (mm/rev), and θ is the half drill bit point angle.

The drill bit break-through detection method proposed by Allotta *et al.* (1995) when drilling into long bones uses appropriate thresholds on a force derivative function to detect sharp changes on entry and exit of the cortical walls. The system compliance is not involved since the drilling tool is in constant contact with the bone. This configuration is shown in figure 5.1b. However, the detection method can only be activated after the occurrence of drill bit break-through regardless of any theoretical models. Furthermore, the inherent drilling force fluctuation due to changes in the bone structural density has not been taken into account. Changes in the bone structural density is expected since bone is a porous non-homogeneous material and these changes can cause inherent fluctuation in both the profiles of drilling force and torque. This fluctuation is represented by multiple peaks and troughs on the drilling force

profiles, and as a result, premature indication of drill bit break-through may be given by a derivative function with a fixed threshold. Variation in bone structural density of long bones can also be interpreted as a sign of increased bone porosity or decreased bone strength that could ultimately affect the holding power of bone to implants and screws.

System compliance, which has an element of uncertainty, adds to the difficulty in devising a robust detection method in order to reduce or prevent excessive drill bit break-through. A contributing factor for a successful break-through detection is the estimation of the system compliance. Brett *et al.* (1995) estimated the stiffness of the stapes footplate by measuring the reduction of force with the corresponding deflection of the stapes during the retraction of the drill bit. System compliance can be also obtained before the commencement of drilling, but this may not be an accurate representation during the drilling process.

The break-through detection methods proposed by Allotta *et al.* (1995) and Brett *et al.* (1995) can be greatly affected by both system compliance and the inherent fluctuation of drilling force. Furthermore, the drilling depth is unknown which makes it difficult to model the drilling process at drill bit break-through. It is, therefore, more appropriate to devise a method of break-through detection that is unaffected by the system compliance and to a certain extent, the inherent drilling force fluctuation, and without the need for measuring the drilling depth.

5.4.1 The Effects of System Compliance

Figure 5.2 shows the effects of system compliance on drilling force profiles across a porcine femoral shaft. The force profiles of low system stiffness (high system compliance) and high system stiffness have been obtained from experiments using spring stiffness coefficients of 2.80 N/mm and 18.44 N/mm respectively. Experimental set-up for these tests is given in Section 7.1.3. The values in bracket represent actual cross-sectional measurement of the femoral shaft, while the values not in bracket represent actual drill bit displacement. Drilling under the influence of low system stiffness is shown to require a larger drill bit displacement to complete the hole. Moreover, the characteristics of the two force profiles differ significantly from each other in both the first and second cortical walls. At low system stiffness, the magnitude of initial bone penetration force is indicated by the initial rapid rise of drilling force. The subsequent change in the force profile represents the amount of displacement due to the system compliance.

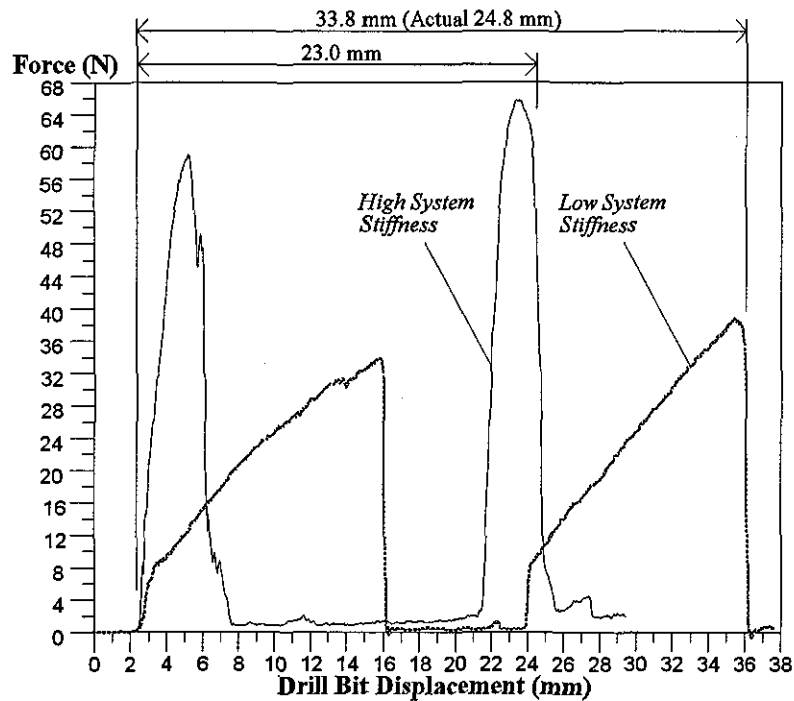


Fig. 5.2 Profiles of drilling force at low (stiffness coefficient of 2.80 N/mm) and high (stiffness coefficient of 18.44 N/mm) system stiffnesses using an industrial drill bit of diameter 2.5 mm (Feed Rate = 90 mm/min; Rated Speed = 1000 rev/min)

Figure 5.3 shows the difference in the force profiles between the actual/true penetration displacement relative to the bone and to the feed displacement of the drill bit. At high system compliance, as much as 10 mm or even more of the drill bit may protrude from the second cortical wall during break-through. This is caused by the spring-back effect.

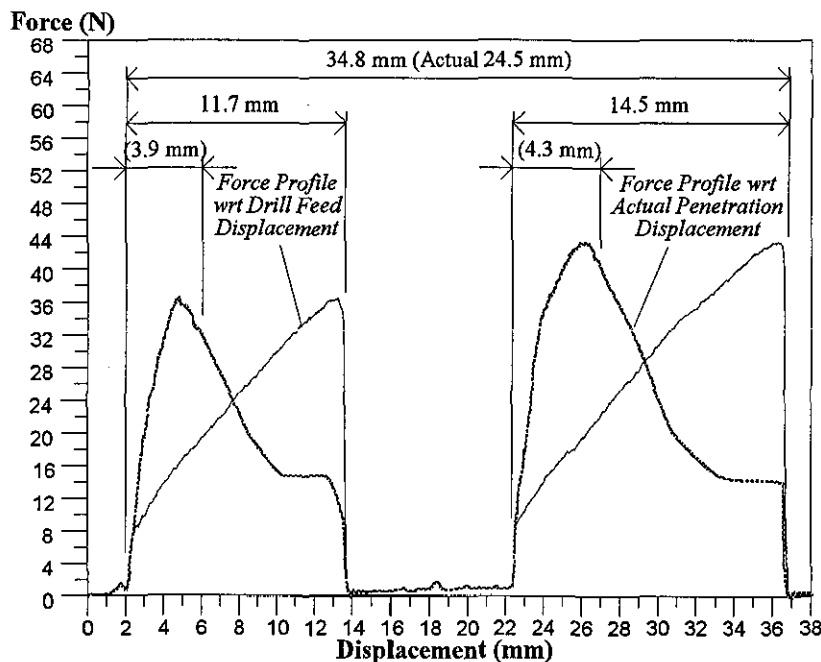


Fig. 5.3 Profiles of drilling force with respect to actual penetration and drill feed displacements of a porcine femoral shaft using an industrial drill bit of diameter 2.5 mm (Feed Rate = 90 mm/min; Rated Speed = 1000 rev/min)

5.4.2 The Effects of Inherent Drilling Force Fluctuation

The inherent drilling force fluctuation, which is generally caused by variation in the bone structural density, are shown in figure 5.4. The figure also includes the profiles of force difference between successive samples (FDSS), which is similar to force derivative based on a backward difference digital filter, and drill bit rotational speed. The FDSS and the rotational speed profiles shown have been filtered using a five-term averager. The profiles in this figure relate to the second cortical wall for a system without compliance (stiff system). Both the force and FDSS profiles of the second cortical wall show multiple peaks and troughs. Using FDSS with fixed thresholds, the variation in the bone density results in a false or premature detection of drill bit break-through. In this case, the effect of premature detection is not safety critical since drill bit break-through has not occurred. In addition, the thresholding technique related to the derivative function or FDSS can be implemented only after drill bit break-through has occurred. With the extra effects of compliance, especially when compliance is high, excessive break-through can occur as a result of spring-back effect by the time drill bit break-through is detected by the FDSS algorithm.

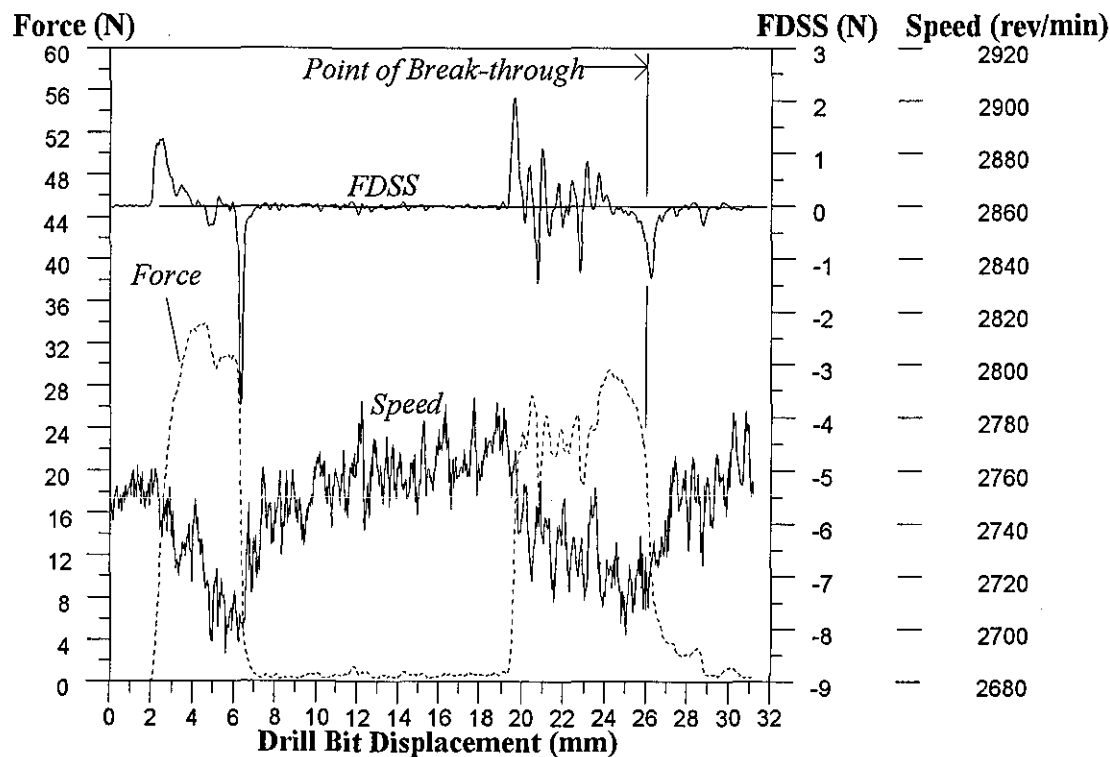


Fig. 5.4 Profiles of drilling force, force difference between successive samples (FDSS) and rotational speed of a porcine femoral shaft for a stiff system using an industrial drill bit of diameter 2.5 mm (Feed Rate = 132 mm/min; Rated Speed = 3300 rev/min)

5.5 Proposed Detection Method of Drill Bit Break-through

The major factors to consider in detection methods of drill bit break-through associated with robotic assisted orthopaedic surgery are system compliance and inherent fluctuation of drilling force or speed. By devising a reliable detection method, the advancement of the drill bit can be controlled so as not to cause excessive protrusion upon break-through. The proposed drill bit break-through detection method is based on a Kalman filter (Bozic, 1979). This type of filter is a digital linear time varying estimator designed to remove random fluctuations and to establish long term trends by smoothing any sudden or abrupt changes in the input. In order to derive the Kalman filter, a first-order recursive algorithm is used and is given by:

$$\hat{y}(n) = a(n)\hat{y}(n-1) + b(n)x(n) \quad (5-1)$$

where: $\hat{y}(n)$ represents the best estimate of $y(n)$ which is the actual output, $x(n)$ is the input data to be processed, and $a(n)$ and $b(n)$ are two time-varying parameters.

The algorithm shows that the current estimated output is the sum of two weighted terms. The first term is taken as the weighted previous best estimated output; the second is the weighted current input. In order to determine the best estimate for $y(n)$, the relationship between the two time-varying parameters, $a(n)$ and $b(n)$, has to be established. This is achieved through the minimisation of the mean-squared error. The mean-squared error, $\rho(n)$, is given as:

$$\rho(n) = E[(\hat{y}(n) - y(n))^2] \quad (5-2)$$

where: E represents the operation to evaluate the mean or expected value of a data set.

Through this minimisation of mean-squared error process, as detailed in Appendix 6, the relationship between $a(n)$ and $b(n)$ becomes:

$$a(n) = a[1 - cb(n)] \quad (5-3)$$

where: a is the system parameter, and c is the measurement parameter. Both parameters are related to the model of random signal generation and measurement, as presented in Appendix 6.

Therefore, the optimum recursive algorithm of the Kalman filter, as shown in figure 5.5, is:

$$\hat{y}(n) = a\hat{y}(n-1) + b(n)[x(n) - a\hat{y}(n-1)] \quad (5-4)$$

The algorithm shows that the present estimated output is the sum of two weighted terms. The first term is taken as the previous best estimated output; the second is taken as a correction term which depends on the current measurement/input, $x(n)$, which can be affected by noise, and the previous estimate. Although the gain parameter, $b(n)$, is time-varying, it can be assumed that it

converges to a constant value as the Kalman filter reaches a steady-state operation when the mean-squared error, $\rho(n)$, is time-invariant or known.

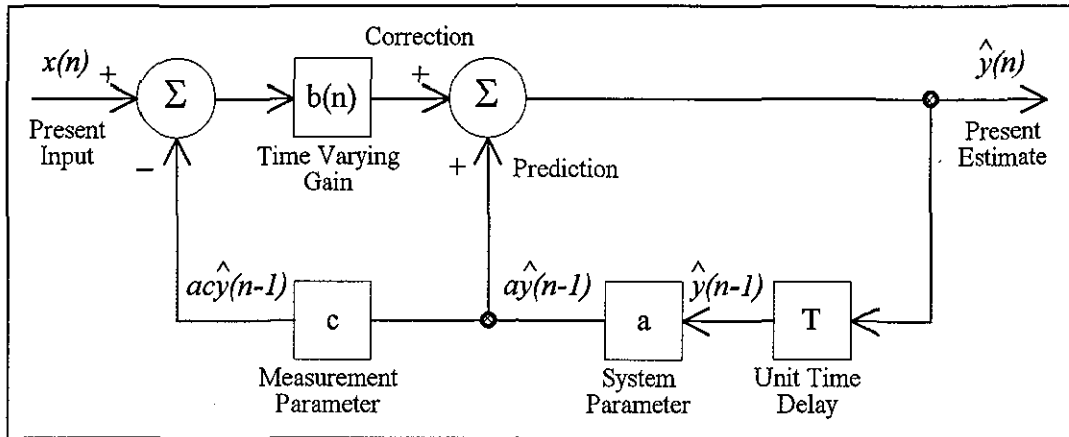


Fig. 5.5 Recursive Kalman filter in system block diagram (Bozic, 1979)

The Kalman filter may be expressed as an elementary first-order low pass recursive filter. Therefore, the Kalman filter can be modified to a simpler version (Hutchings, 1995):

$$y(n) = 0.99y(n-1) + 0.009x(n) \quad (5-5)$$

To ensure that the modified Kalman filter remains stable, the sum of the coefficients for $y(n-1)$ and $x(n)$ must be less than unity. As a consequence of the small weighting placed on the input, there is sufficient time to smooth out the abrupt changes, thus allowing the input trends to be established. This simpler modified form of the Kalman filter is applied to two types of drilling data, namely the FDSS (similar to the force derivative obtained by a backward difference digital filter (Allotta *et al.*, 1995)) and the drill bit rotational speed to establish trends, because these data display fluctuation. Through the analysis with a modified Kalman filter, the imminence of drill bit break-through can be predicted (Ong & Bouazza-Marouf, 1998 - in Appendix 7).

The modified Kalman filter (equation 5-5) used in the detection of drill bit break-through algorithm is similar to a first-order low pass recursive filter. It reduces to a difference equation approximation of a first-order filter using the backward rectangular approximation, as shown below. Consider the transfer function of a first-order filter:

$$G(s) = \frac{Y(s)}{X(s)} = \frac{1}{1+\tau s} \quad (5-6)$$

where: $X(s)$ and $Y(s)$ are the input and output in Laplace transform respectively, and τ is the system time constant. Rearranging equation 5-6 gives:

$$Y(s) + \tau s Y(s) = X(s) \quad (5-7)$$

or (in the time domain):

$$y(t) + \tau \frac{dy(t)}{dt} = x(t) \quad (5-8)$$

The backward rectangular approximation of $\frac{dy(t)}{dt}$ is:

$$\left. \frac{dy(t)}{dt} \right|_{t=nT} = \frac{y(n) - y(n-1)}{T} \quad (5-9)$$

where: T is the sample time/interval in seconds.

Therefore, the difference equation approximation of the differential equation 5-8 is:

$$y(n) + \tau \frac{y(n) - y(n-1)}{T} = x(n) \quad (5-10)$$

or

$$y(n) = \frac{\tau}{T + \tau} y(n-1) + \frac{T}{T + \tau} x(n) \quad (5-11)$$

Comparing equation 5-11 with equation 5-5 gives:

$$\frac{\tau}{T + \tau} = 0.99 \quad (5-12)$$

and

$$\frac{T}{T + \tau} = 0.009 \quad (5-13)$$

Both equations 5-12 and 5-13 give approximately the same value of τ :

$$\tau = 99T \text{ from equation 5-12, and } \tau = 110T \text{ from equation 5-13}$$

The sample time, T , was measured as 0.025 s. Therefore, using equation 5-12, the time constant can be approximated to:

$$\tau \approx 2.5 \text{ s}$$

This shows that the modified Kalman filter used here is a difference equation approximation of a first-order low pass filter with a long time constant.

This proposed technique of automatic drill bit break-through detection is, at present, limited to drilling into the shaft section of long bones. In addition to enhancing safety in automatic drilling processes, the robustness of the modified Kalman filter allows this adopted technique to be applied to different types of drill bits, such as standard metal cutting and surgical drill bits. This is presented in Section 8.2.

CHAPTER 6

THE EVALUATION OF BONE STRENGTH

This chapter relates to the second research aim, which is to investigate the contribution of bone drilling to the evaluation of bone strength. It provides a critical discussion of the present methods of bone strength correlation and demonstrates the potential analysis of drilling forces in characterising the mechanical resistance of the bone. A detailed description of a method for determining the correlation between drilling forces and densitometric measurements to achieve the aim of evaluating bone strength is also presented.

6.1 The Strength of Bone

A linear relationship of a high correlation coefficient has been found between strength and elastic modulus of bone, even though cancellous bone is a highly anisotropic material and large variations in the mechanical properties have been reported (Goldstein, 1987). Furthermore, apparent density has been found to have a significant relationship with mechanical properties (Rice *et al.*, 1998). When correlating densitometric measurements such as BMD with mechanical properties, the significance in the relationship has, generally, not been strong. At times, there has been no conclusive significance in the correlation (Cody *et al.* 1996). QUS parameters of BUA and SOS, which have been found to correlate with both mechanical properties and bone density, may offer an alternative method of evaluating bone strength (Grimm & Williams, 1997).

Mechanical properties of cancellous bone and densitometric measurements can be said to represent two extreme methods for the evaluation of bone strength. Not only does mechanical testing require a large amount of bone samples, it also involves specimen preparation where tests must be carried out under non-physiologic boundary conditions. In contrast, bone densitometry is a non-invasive method and BMD is measured *in vivo*. Although QUS offers the

advantages of portability and is free from radiation, measurement is restricted to sites with a minimum amount of soft tissue. Therefore QUS measurements cannot be made at the hip and at the vertebrae, where densitometric measurements are directly related to bone strength.

It has been found, from Section 4.3 of the literature review, that research into bone strength has concentrated either towards bone densitometry or strength of materials. Little research has been involved in using the combination of these two methods to improve the prediction power of bone strength and fracture risk. It has been reported that both the mechanical properties and densitometric measurements have been found to have a large overlap between healthy and diseased bones (Hodgkinson & Currey, 1993; Marshall *et al.*, 1996). Therefore, a novel approach of employing bone drilling as an intermediate method to bridge the gap between mechanical testing and bone densitometry has been proposed in this thesis. The use of bone drilling is highly significant in this research since bone drilling is a major part of orthopaedic surgery. Furthermore, drilling can provide better spatial resolution or accuracy than densitometric and mechanical methods as it is only limited by the drill bit diameter. With the automation of the drilling process, drilling information can be easily collected, stored and analysed to establish important relationships between drilling mechanics and bone densitometry or between drilling mechanics and mechanical properties.

6.2 Bone Drilling Analysis in the Evaluation of Bone Strength

Correlation between drilling data and mechanical properties of cancellous bone is not well established, although it can be expected to have certain similarities to the correlation between penetration strength and ultimate compressive stress reported by Hvid *et al.* (1984). Karalis and Galanos (1982) have found that the drilling strength has a linear correlation to the tri-axial strength, but not to the hardness. The drilling strength, σ_D , was derived from a dimensional analysis which is given as:

$$\frac{V_L}{\omega D} = 1.5 \left(\frac{F}{D^2 \sigma_D} \right)^2 \quad (6-1)$$

where: V_L is the feed/penetration rate (m/s), D is the drill bit diameter (m), F is the thrust force (N), ω is the drill bit rotational speed (rad/s), and σ_D is the drilling strength of the bone (N/m²). The left hand side of the equation is known as the advance ratio (Karalis & Galanos, 1982).

Dimensional analysis is a method of obtaining the correct form of relationship based on non-dimensional (dimensionless) groupings of chosen physical quantities (Massey, 1986). The equation presented by Karalis and Galanos (1982) shares certain similarity to the dimensional analysis of thrust force carried out by Shaw and Oxford Jr. (1957) on the drilling of metals. This is given as:

$$\frac{F}{d^2 H_B} = \psi \left(\frac{f}{d}, \frac{c}{d}, \frac{s}{d} \right) \quad (6-2)$$

where: F is the thrust force (N), f is the feed per rev. (m/rev), d is the drill bit diameter (m), c is the chisel edge length (m), H_B is the Brinell hardness of material (N/m²), s is the mean spacing between imperfections (m), and ψ represents a function of the terms in the bracket and the evaluation of this function requires either additional analysis or experimental data.

It can be seen from the two equations, 6-1 and 6-2, of dimensional analysis that the hardness of the metal, H_B , is equivalent to the drilling strength, σ_D , of the bone. The dimensional analysis conducted by Shaw and Oxford Jr. (1957) was aimed at deriving a general equation for the drilling thrust force of material with a known value of hardness. It was found that the general equation for thrust force represents a good model for the experimental data.

Karalis and Galanos (1982) utilised dimensional analysis to determine the drilling strength of both cortical and cancellous bones. There was little significance in the coefficient of correlation although a linear relationship between the advance ratio and the drilling thrust force was presented. Furthermore, no statistical significance was given for the relationship between the drilling strength and the tri-axial strength, which was shown to be linear.

Chagneau and Levasseur (1992) presented the changes of drilling forces and punching forces (hardness) in the femoral head. However, no correlation was reported between the drilling force and the punching force. Furthermore, the punching test was found to be unsuitable for estimating bone strength as a result of excessive displacement of the punch caused by the porous structure of cancellous bone. The analogy of this excessive displacement found in the compression test was also used to account for the non-physiologic conditions of the cancellous bone specimens during compressive tests.

The proximal femur is an important site for bone strength evaluation due to its unique and critical relationship between bone architecture and density. Osteoporotic fractures are often associated with hip fractures, normally at the femoral neck. The drilling investigations carried out by Karalis and Galanos (1982) and Chagneau and Levasseur (1992) presented results on the femoral head only, and excluded critical areas in the proximal femur, namely the femoral neck, the trochanter and the Ward's triangle. It should also be noted that clinical evaluation of BMD does not apply to the femoral head because it is partially covered by the pelvis.

The limited literature on bone drilling for bone strength evaluation related to cancellous bone indicates a need to investigate the possible correlation of drilling data, such as force and penetration rate, to densitometric measurement or strength of materials. The significance of this kind of relationship is further supported by the findings by Petersen *et al.* (1996), which show a good linear relationship between penetration strength by osteopenetrometer and BMD by DXA. Bone drilling has been shown to define the bone strength along the drilling trajectory (Chagneau & Levasseur, 1992), but this has been limited to the femoral head. Furthermore, little is known about the contribution of the effects of bone architecture and density to the drilling mechanics for the evaluation of strength. In order to determine the contribution of density to the drilling data, established densitometric measurement of BMD can be utilised for correlation purposes. The contribution of bone architecture can be subsequently deduced from the correlation between drilling data and densitometric measurement. As a consequence, an alternative and/or complementary method for the evaluation of bone strength can be developed. This will lead to a possible development of a diagnostic tool for bone strength.

The knowledge of bone strength is regarded to be important to orthopaedic surgeons. This knowledge may be used as a guide to orthopaedic surgeons, when selecting an appropriate treatment of internal fixation, by indicating the need to use bone cement or suggesting the need for more protective post-operative management (Smith *et al.*, 1992). In addition, bone strength estimated by bone drilling can be applied to two types of clinical studies associated with the assessment of success rate of internal fixations. Firstly, the strength derived from bone drilling can provide some explanation about occasional failures of internal fixations, either due to the bone strength or the fixation device, or to both. Secondly, the strength derived from bone drilling can be used for comparative studies between fixation devices from different manufacturers in order to determine the most suitable to be applied to a particular fracture.

6.2.1 Drilling Force Profiles of the Proximal Femur

In order to indicate the effects of density and bone architecture of the proximal femur, force profiles of three drilling trajectories, shown in figure 6.1, are presented in figure 6.2. These three drilling trajectories were taken parallel to the cervical axis. The experimental tests were carried out on a porcine proximal femur using an industrial twist drill bit of diameter 2.5 mm driven at a feed rate of 132 mm/min and a rated rotational speed of 3300 rev/min.

All three force profiles of figure 6.2 show a peak at the start and at the end of drilling due to the presence of an outer layer of cortical bone. The spacing between the parallel drilling trajectories was 6.0 mm. A significant difference in the force profile can be observed at trajectory 3 where there is a large section of low force magnitude in the region of the neck and the Ward's triangle. This region of low force magnitude may indicate the presence of a porous trabecular region filled with red marrow and/or may be caused by the trabecular orientation being parallel to the cervical axis. At the same section, several peaks are seen at trajectories 2 and 3 which may be explained by the trabecular orientation not being parallel to the direction of drilling. Towards the end of drilling, the peaks and troughs on all three trajectories are related to the intersection of primary tension and compression trabeculae shown in figure 4.7, as well as to the epiphyseal line shown in figure 6.1.

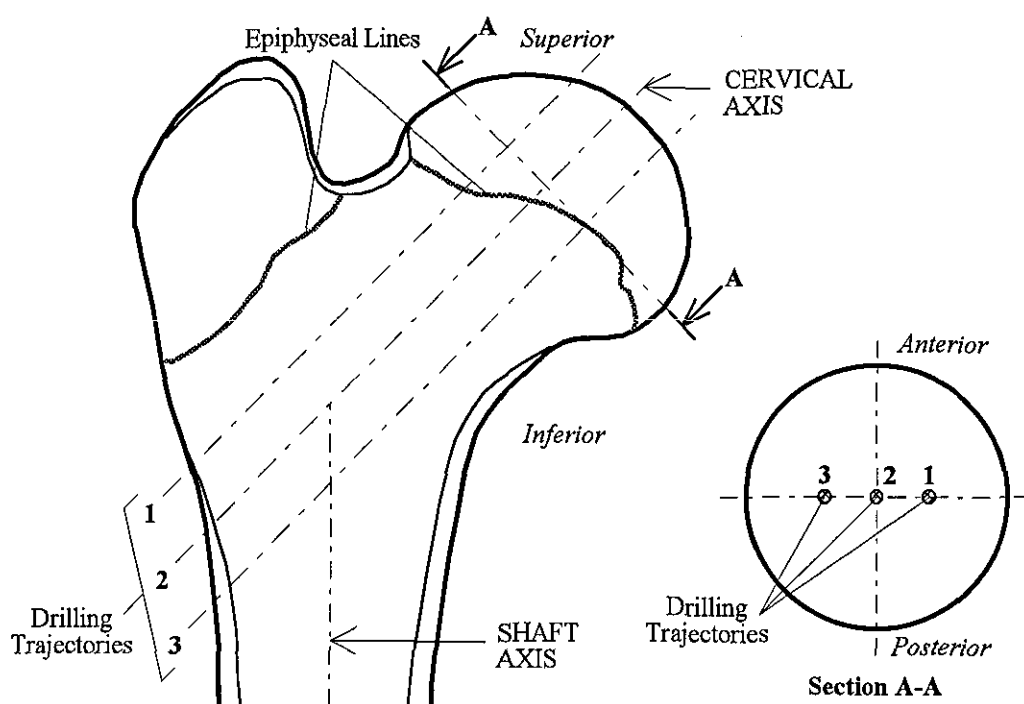


Fig. 6.1 Drilling trajectories of the porcine proximal femur

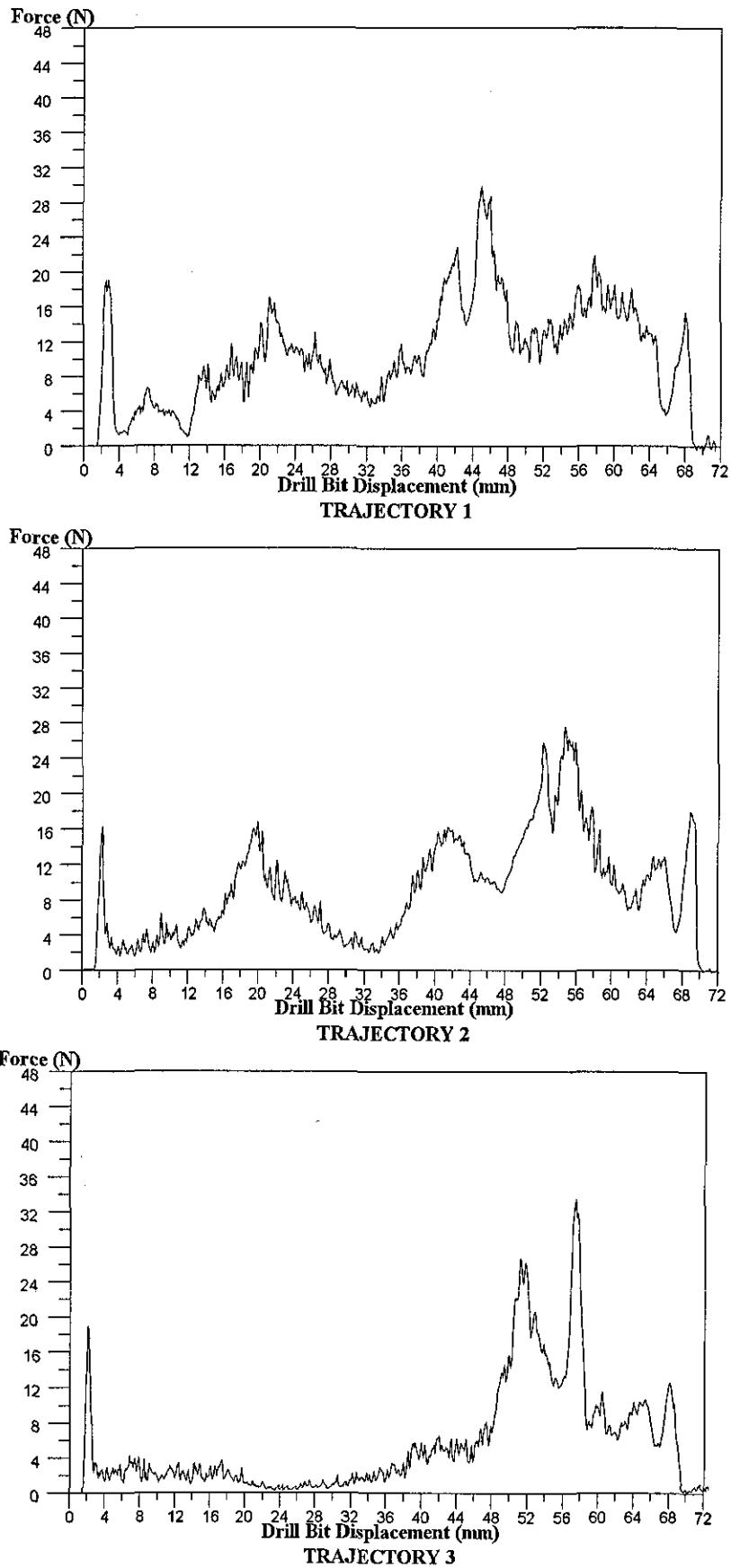


Fig. 6.2 Profiles of drilling force of a porcine proximal femur using an industrial twist drill bit of diameter 2.5 mm on a stiff system (Feed Rate = 132 mm/min; Rated Speed = 3300 rev/min)

The results show that drilling forces are sensitive to both the changes in the bone density and in trabecular orientation. The variation of drilling force due to the orientation of trabeculae could be synonymous to the variation in orthogonal cutting forces with respect to the direction of the predominant osteon (parallel to the shaft axis) in cortical bone (Jacobs *et al.*, 1974), as shown in figure 6.3. This is because the twist drill bit can be considered to be a tool with two single orthogonal cutting edges. It has been found that cutting forces parallel to the shaft axis (i.e. in the same direction of the predominant osteon orientation) are the lowest, and the highest forces are in the perpendicular or transverse direction to the shaft axis (Jacobs *et al.*, 1974).

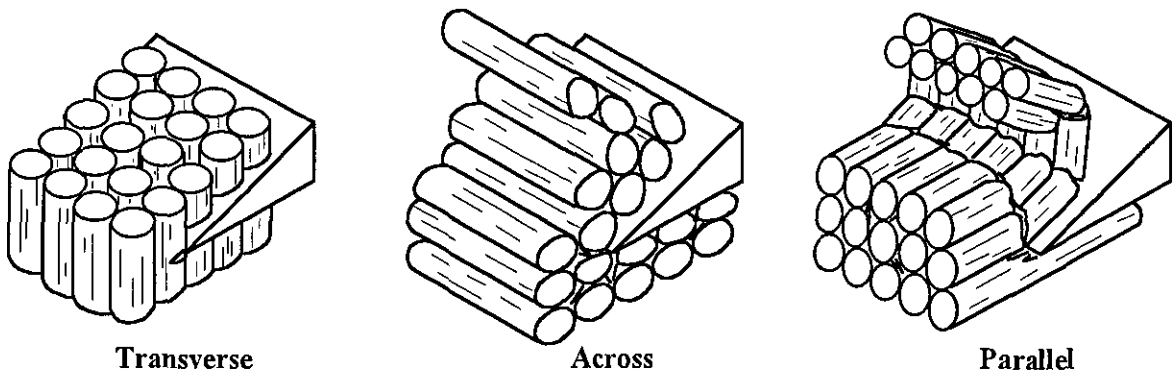


Fig. 6.3 Cutting directions in relation to predominant osteon direction (Jacobs *et al.*, 1974)

6.2.2 Proposed Method for Correlation of Bone Strength

As mentioned earlier, there are several methods that can be used for determining the correlation of bone strength related to the drilling of bone. The use of dimensional analysis is not feasible in this present research since it is not meant for deriving general equations for bone strength. Also, the use of penetration rate in equation 6-1 (when a constant force is applied) may not be suitable because it has been found that the results are inconsistent and the rate of change can be extremely high, as shown in figure 6.4. These results, which show the profiles of drill bit displacement and penetration rate, have been obtained along drilling trajectories parallel to the cervical axis shown in figure 6.1. An industrial drill bit of diameter 2.5 mm has been used and drilling has been performed under a constant applied load of 4 kgf and at a rated drill bit rotational speed of 1000 rev/min. It should be noted that the spacing between the drilling trajectories was 4.5 mm.

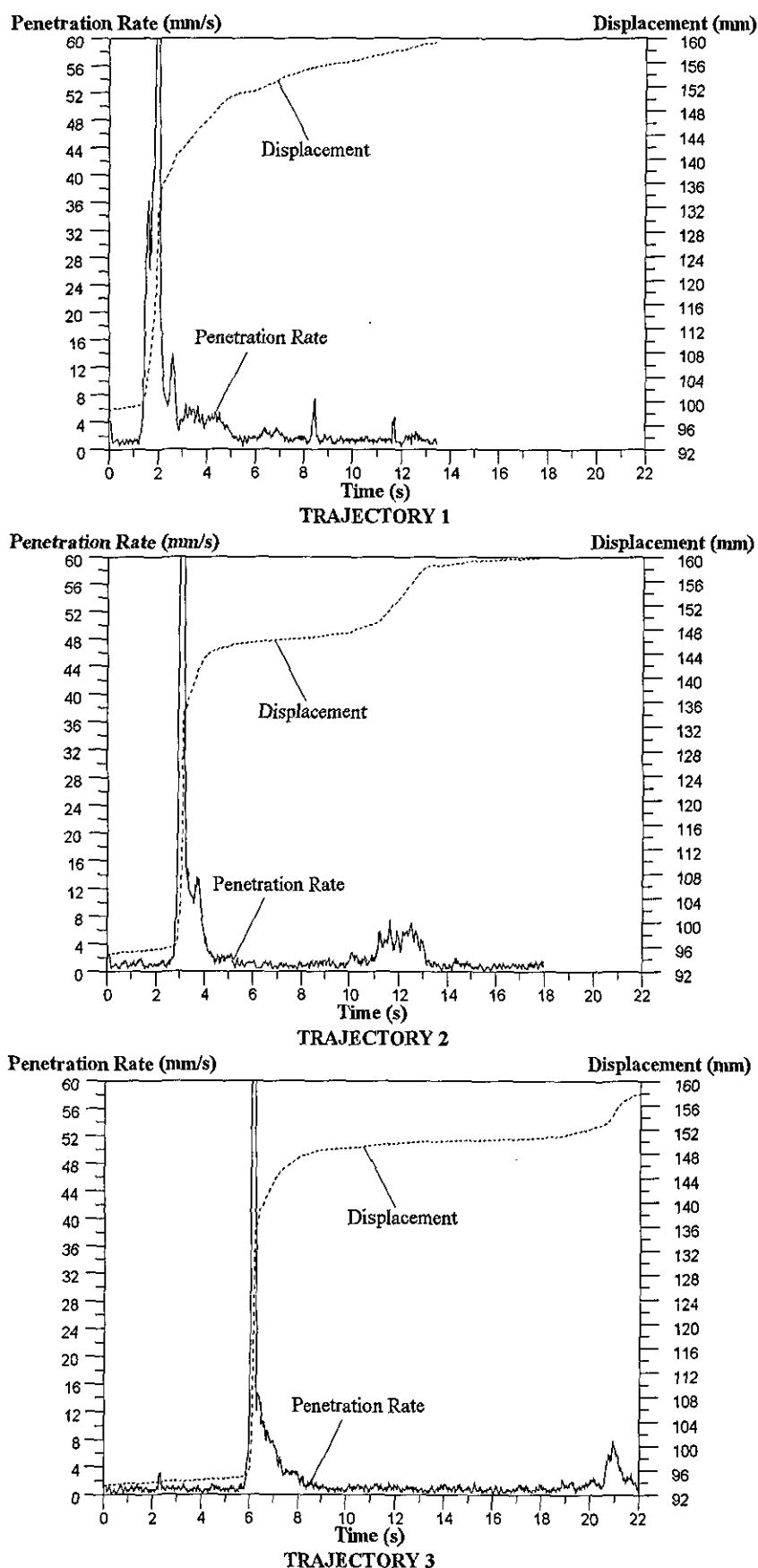


Fig. 6.4 Profiles of penetration rate and drill bit displacement at a constant applied load of 4 kgf on a porcine proximal femur using an industrial twist drill bit of diameter 2.5 mm (Rated Speed = 1000 rev/min)

Much effort has been put into determining the effects of BMD on the overall bone strength. The main reason is that BMD measurement of the bone can be readily obtained with little preparation when compared to bone drilling and mechanical testing. As a result, measurement of BMD can be considered a suitable medium for establishing relationships of bone strength with drilling mechanics and strength of materials. The following paragraphs describe a method for determining the correlation between drilling forces and BMD measurements.

The BMD measurement of bone for this research is taken by a dual energy x-ray absorptiometry (DXA) instrument. Standard evaluation of bone strength using BMD concentrates on three particular ROIs (region of interest), namely the femoral neck, the Ward's triangle and the trochanter (Wahner & Fogelman, 1995). The most reproducible ROI of the proximal femur is the femoral neck because it is the least affected by size (thickness) and position. For research purposes, the ROIs are to be applied throughout the proximal femur which includes the femoral head and the greater trochanter, as shown in figure 6.5. This flexibility increases the number of samples for analysis and enables each ROI to be analysed separately. It should be noted that the femur is to be scanned without being attached to the pelvic bone.

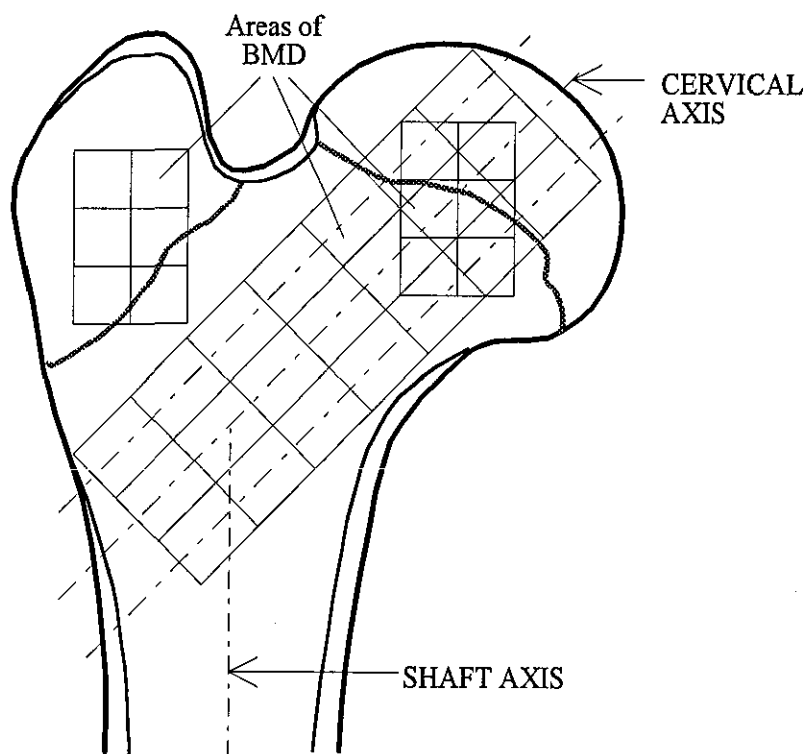


Fig. 6.5 ROIs of BMD along the cervical axis, on the femoral head and on the greater trochanter of the proximal femur for research purposes

In order to match the ROIs obtained from bone densitometry for correlation, the profiles of drilling force have to be divided or discretised into sections or sectors which correspond to the ROIs of BMD. The drilling forces within these sectors have to be taken as an average value before correlating to the BMDs. It is, therefore, important to match the drilling trajectory to the ROIs of BMD so as to minimise the error in the correlation.

There are two types of relationship to be determined in this investigation. Firstly, analysis is to be carried out to establish a correlation between the average drilling forces and the BMDs in the direction of the DXA scan (anterior-posterior direction), which involve sites at the femoral head and the greater trochanter. Although drilling in the AP direction is not performed in orthopaedic surgery, this analysis has been carried out to investigate the relationship between the drilling force and the BMD in order to provide a justification for the use of drilling force measurements in the direction of the cervical axis in the evaluation of bone strength. This is the second type of relationship to be determined. The number of ROIs or sectors has to be selected to give a reasonable accurate representation of the bone strength across the proximal femur in the direction of the cervical axis. A detailed description of the experimental method is given in Section 7.2.

The correlation between the average drilling forces and BMDs is to be obtained based on statistical analysis. Results are plotted, either from the measured quantities or by taking logarithms of the measured quantities, to derive linear expressions by best fit using the least-squares method. The statistical significance of the relationships is given by the coefficient of correlation or determination (Weiss, 1993).

The following chapters focus on a new approach towards the enhancement of safety and the evaluation of bone strength.

CHAPTER 7

EXPERIMENTAL RIG DESIGN AND DRILLING TESTS

This chapter relates to the plan of investigation in accordance with the research methodology towards achieving the two aims of safety enhancement and evaluation of bone strength, as outlined in Chapter 3. A detailed description of the drilling experimental rig and discussion of the experimental tests for both methods of research are carried out.

7.1 Experimental Method for Detection of Drill Bit Break-through

The objective of this bone drilling experimental set-up is to obtain the relevant data in order to validate the drill bit break-through detection method based on a modified Kalman filter, as outlined in Section 5.5. The effects of both system compliance and inherent drilling force fluctuation are taken into consideration in this experimental set-up. This section consists of three sub-sections which describe the implementation of the experimental method. The first part describes the mechanical design of the drilling apparatus with relevant actuators and sensors for performing drilling experiments. In order to facilitate the analysis of the drilling data, the experimental rig is interfaced to a personal computer, as outlined in the second part, for activating the drilling unit, and for collecting and displaying data. The description of the experimental set-up for drilling experiments is given in the last part.

7.1.1 Experimental Rig and Instrumentation

The complete experimental rig, which includes a control panel and a personal computer (PC), is shown in figure 7.1. The experimental drilling rig, shown in figure 7.2, consists of a constant drill feed unit, a bi-directional force sensor, a quick mount drill holder, a rotational speed sensor and a compliant bone holder. The full mechanical assembly drawings of the drill holder and the

experimental rig are given in Appendices 8.2 and 8.4. The schematic of the experimental rig is shown in figure 7.3.

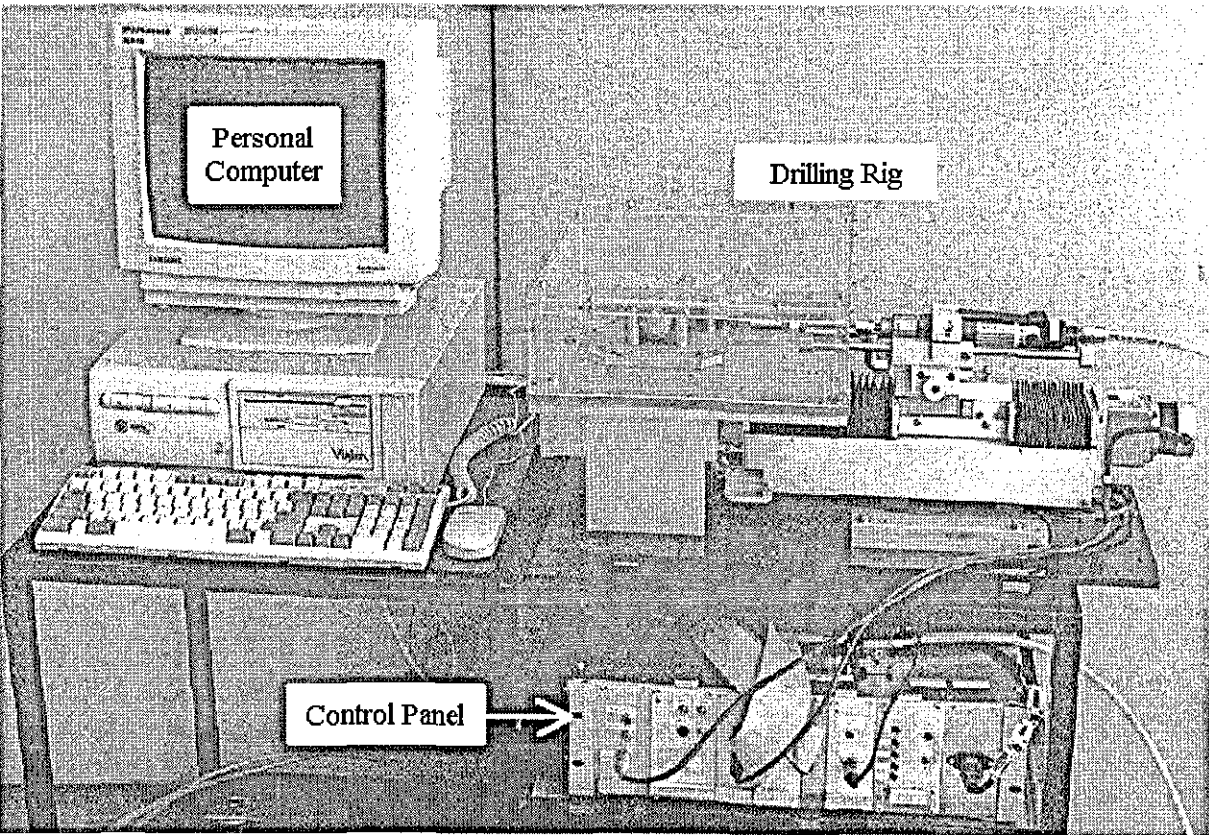


Fig. 7.1 Complete Experimental Drilling Rig

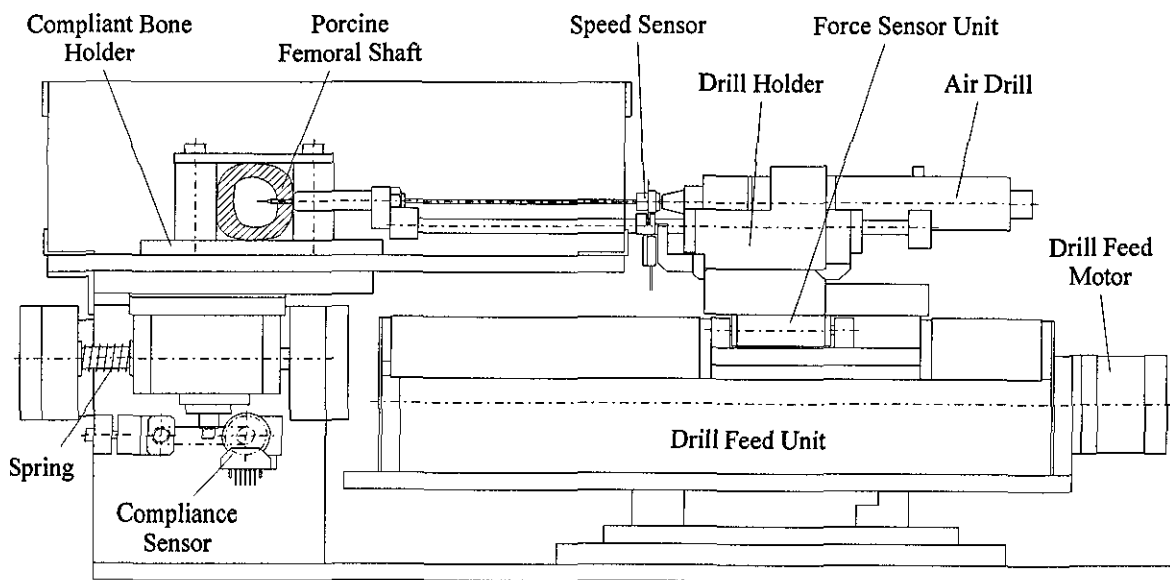


Fig. 7.2 Experimental rig for bone drilling experiments (on femoral shaft)

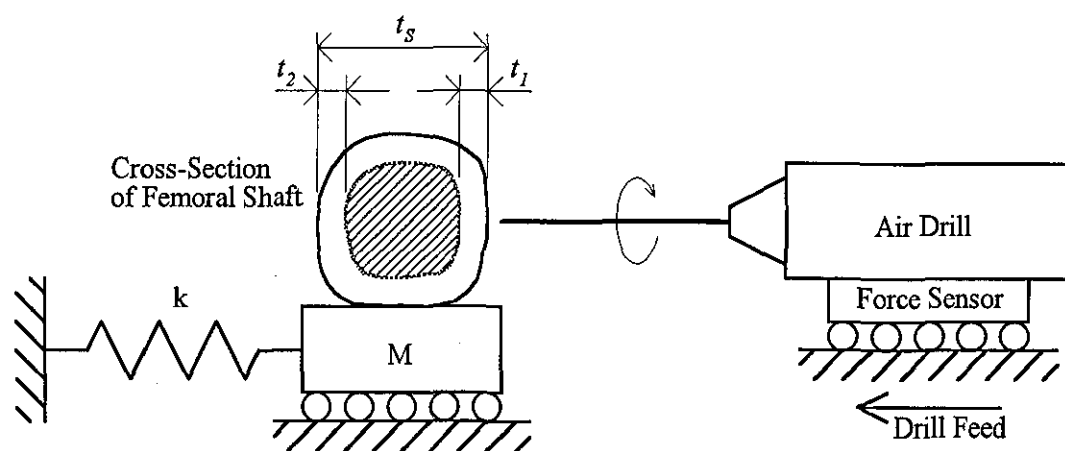


Fig. 7.3 Schematics of the experimental rig

The drill feed unit provides a constant feed rate through an anti-backlash ballscrew driven by a stepper motor. At a constant feed rate, the level of resistance is characterised by changes in the drilling force. Measurement of the drill feed displacement is by means of a linear potentiometer. In addition, limit switches are fitted at both ends of the drill feed to prevent mechanical overdrive. A bi-directional force sensor is fixed onto the carriage of this unit to measure drilling thrust force which is obtained from the change in resistance of four strain gauges arranged in Wheatstone bridge on a cantilever plate, as shown in figure 7.4. The measurement from the strain gauges is amplified 1000 times by a standard strain gauge amplifier board which is attached to the drill feed carriage. Calibration of the force sensor is carried out using known weights before and after the drilling experiments. A typical force calibration curve is shown in figure 7.5. When the force sensor was loaded at fixed increment of 0.5 kgf, output voltages (measured using a 12-bit analogue-to-digital converter (ADC)) were shown to have a linear relationship of very high correlation coefficient, r^2 , with the applied loads. It may be seen from the curve that there is a certain amount of hysteresis in the sensor when unloading the weights from the maximum value.

The drill holder provides a mounting for the air drill, and has a movable guide to prevent long drill bits from deflecting from the desired trajectory caused by slippery and uneven bone surface. It is designed to be easily located and clamped onto the drill feed unit without the loss of positional accuracy, even with a sterilised drape over the drill feed unit. In order to comply with current practice in orthopaedic surgery, industrial air drills, ARO Series 20, are used. The drill holder is also designed to withstand sterilisation by steam (autoclaving) which is readily available in hospitals and is relatively inexpensive.

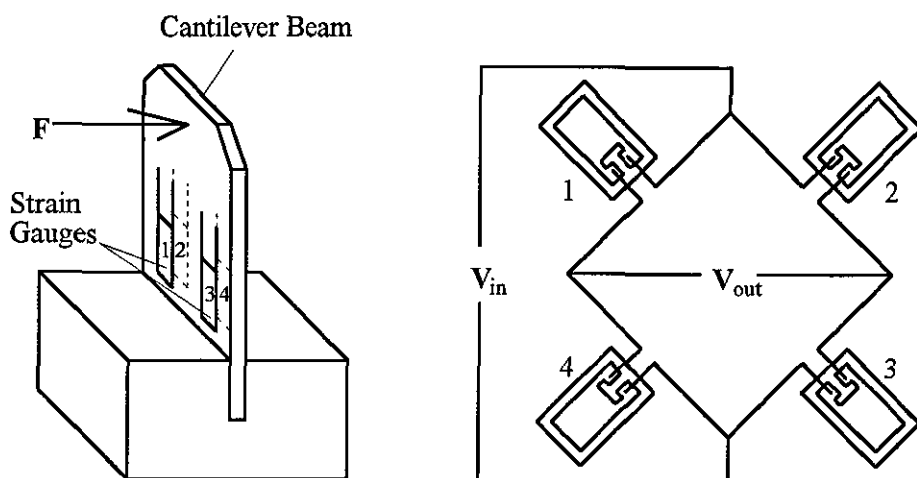


Fig. 7.4 Strain gauges arrangement (Wheatstone) of force sensor

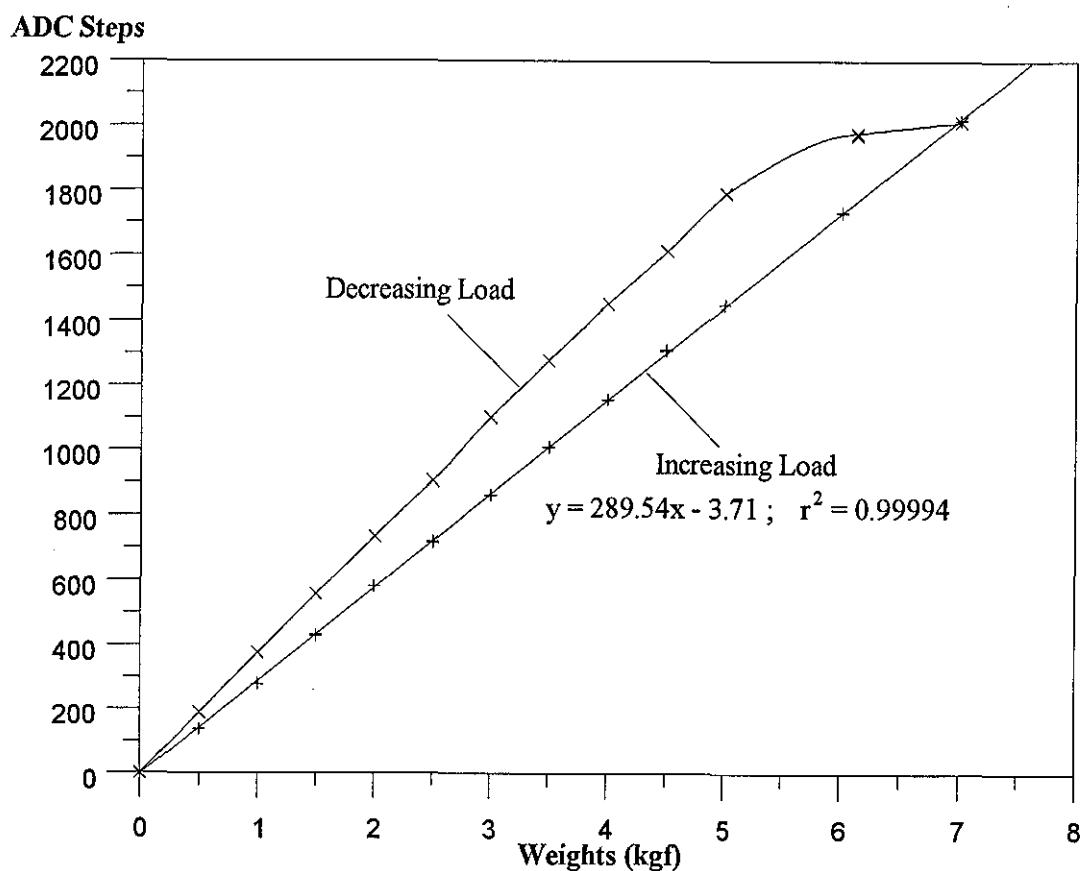


Fig. 7.5 A typical force calibration curve

The relationship between drilling force and torque is well established in the literature (Jacobs *et al.*, 1976; Wiggins & Malkin, 1976). However, torque measurements have been either derived from electrical motor current or obtained from a dynamometer mounted on a lathe or a drilling machine. In this experimental setting, measurement of drilling torque has not been

implemented. Instead, changes in torsional resistance of the bone are taken to be represented by changes in the rotational speed of the drill bit. The drill bit rotational speed sensor consists of a digital reader which is mounted onto the drill holder and a rotary encoder disc which is fixed near the drill chuck along the drill bit shank.

The bone holder clamps the bone to be drilled at the top. Depending on the type of experiments, it can be held stiff, or made compliant in the direction of drilling in a controlled manner using compression springs of various stiffness coefficients fitted to the sliding carriage. As explained in Section 5.2, the bone holder can be represented by a spring mass damper model due to inherent damping from friction in bearings and between drill bit and bone during drilling. The linear displacement caused by the system compliance is converted into angular displacement by a timing belt and pulleys before being measured by a digital reader through a rotary encoder disc, as shown in Fig. 7.2. This conversion has an accuracy of 0.06 mm. In addition, the bone holder provides the flexibility of drilling at different linear positions along the horizontal and the vertical planes perpendicular to the drilling direction as well as angular positions. A perspex cover is also included to enclose the bone and to contain the bone debris during drilling.

7.1.2 Data Acquisition, Input and Output Interface

The experimental drilling rig is interfaced to a personal computer (PC) for the purpose of data acquisition and storage as well as controlling the drilling process. The interface, which is shown in figure 7.6, consists of a controller box, two commercial plug-in boards and a custom-built board with micro-controllers. It involves analogue signals from the linear potentiometer and force sensor amplifier, digital inputs from two limit switches on the drill feed, digital outputs to the stepper motor driver and air drill solenoid valve, and digital inputs from the compliance displacement and rotational speed encoders.

The controller box performs several functions: (i) providing connections for analogue input, digital input and digital output signals, (ii) analogue signal conditioning or filtering, (iii) signal decoupling, and (iv) Automatic/Manual operation modes. In the manual mode, the drilling process is controlled by several switches on the front panel of the box. Signal conditioning is performed on the analogue signals, from the linear potentiometer and the force sensor amplifier, using fourth-order analogue Butterworth filters in order to reduce/eliminate noise and avoid

aliasing. Digital inputs from the limit switches, and outputs to the stepper motor driver and solenoid valve are decoupled from the PC using opto-isolators.

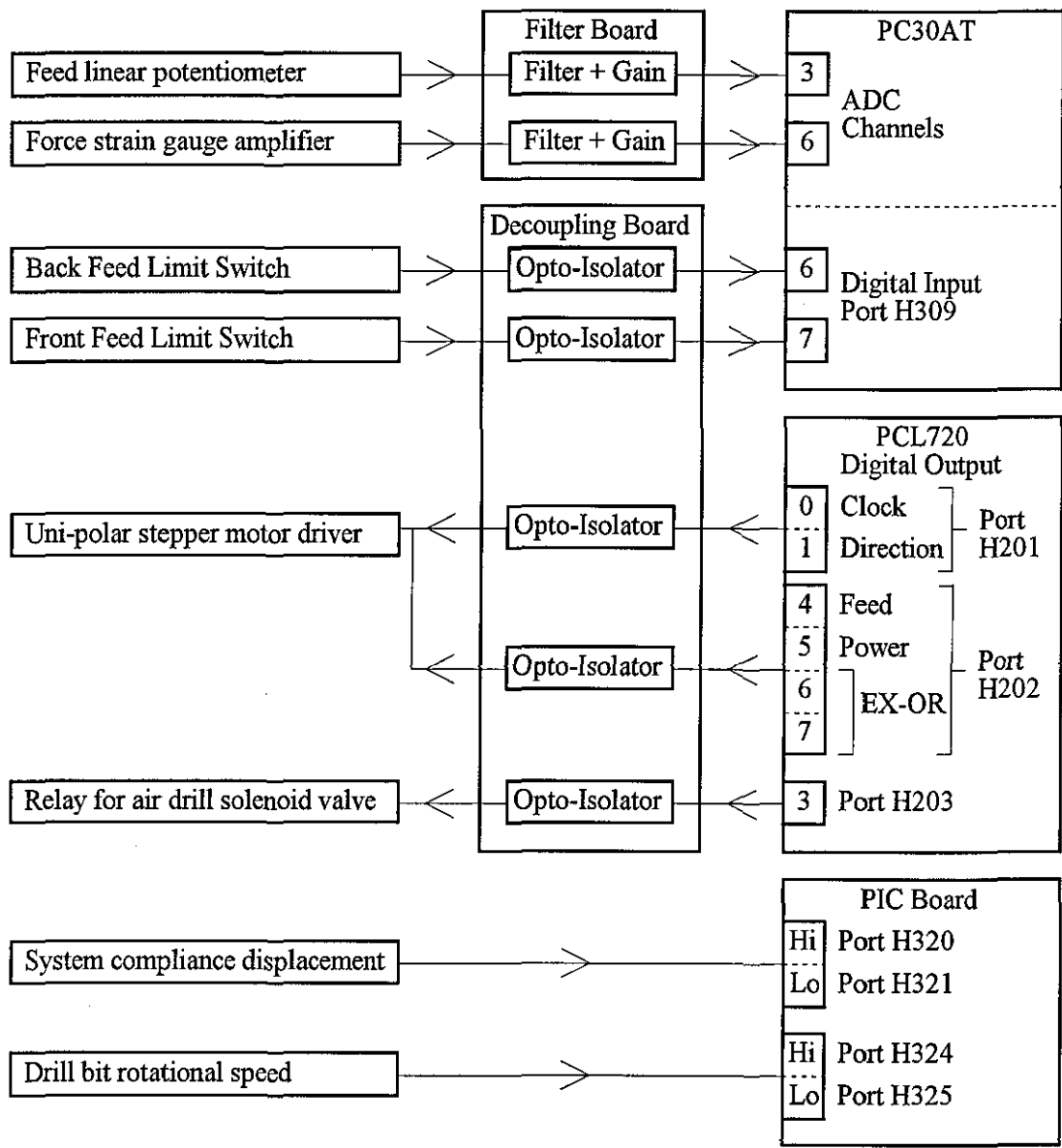


Fig. 7.6 Interface diagram

Interfacing of filtered analogue measurements with the PC is achieved through a commercial plug-in PC30AT board from Amplicon, which has a multiplexed 16-channel of 12-bit analogue to digital (A/D) conversion inputs. Only channels 3 and 6 (figure 7.6) are used for the measurement of feed displacement and drilling force respectively. The number of A/D steps corresponding to 1 mm of linear displacement and 1 N of drilling force are 26.35 and 29.3 steps respectively. The limit switches of the drill feed from the controller box are assigned to two digital inputs, bits 6 and 7, of port address H309 on the PC30AT board. Digital inputs from the

drill bit rotational speed and the system compliance displacement sensors are interfaced with the PC through PIC 17C42 micro-controllers on a custom-built board. A comparator is used to determine the rotational speed from recorded encoder counts and on-board oscillator frequency, while the compliance displacement is directly obtained from the counter.

There are two output devices, the stepper motor for feed drive and the air drill solenoid valve, to control the drilling procedure for the experiments from the PC through the controller box. A digital I/O plug-in PCL720 card is used to interface these devices with the PC. The operation of the stepper motor is controlled via two ports, H201 and H202 (Enables), of the PCL720. Bits 5 and 6 in port H202 have to be set high (1) while bits 4 and 7 are set low (0) in order to energise the feed stepper motor. Bits 0, 1, 2 and 3 are not used for drilling and are set high. The stepper motor is activated by setting the Clock of bit 0 in port H201 to high, and the direction is controlled by bit 1 where the feed is advanced forward when bit 1 is low and retracted when bit 1 is high. The other bits in port H201 are set low. Only bit 3 in port H203 controls the solenoid valve and the air drill is activated by setting bit 3 to high with the rest being set low.

Borland C++ V4.02 programming language is used for the PC interfacing in data acquisition and for activating the drilling sequence under Automatic mode. The measured data is sampled at a fixed rate based on interrupt controlled sampling provided by a 8253 timer/counter on the PC30AT board according to the feed rate. In addition, the data is displayed on screen during drilling, and stored in specified files for analysis.

7.1.3 Experimental Set-up

Drilling experiments were performed on cortical bone along the middle section of fresh porcine femoral shafts (diaphysis), where the drilling direction was perpendicular to the longitudinal axis of the femoral shaft, as shown in figure 7.7. According to the bone suppliers, the ages of the slaughtered animals were between six to eight months. As in all long bones, the medullary cavity, which is filled with soft yellow marrow, is surrounded by cortical bone. The thickness of the first and second cortical walls are indicated by t_1 and t_2 respectively, while the cross-sectional thickness of the femoral shaft is indicated by t_s .

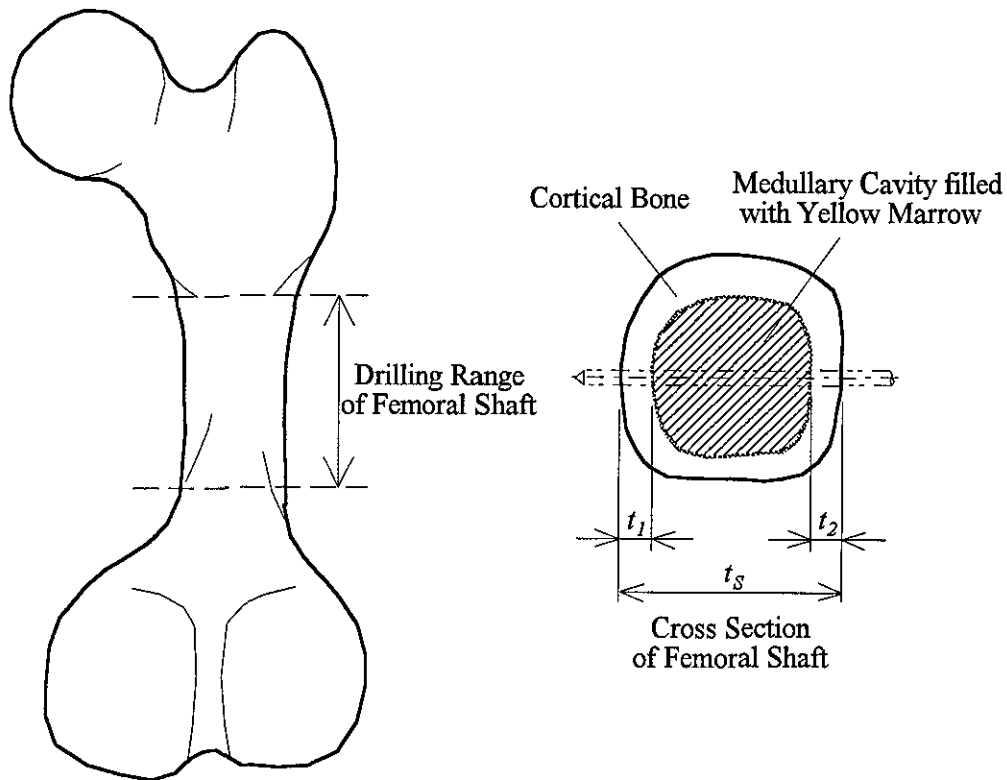


Fig. 7.7 Drilling range and cross-section of a porcine femoral shaft

The whole femur, which was fresh and stripped of all soft tissue, was clamped rigidly onto the bone holder to ensure that the system compliance was only caused by the springs used in the 'compliant bone holder' (figure 7.2). It must be noted that there is a negligible compliance displacement caused by the deflection of the force sensor's cantilever plate. Four springs with stiffness coefficients of 2.80, 5.68, 10.90 and 18.44 N/mm were used to vary the system compliance of the bone holder. All the springs were preloaded by approximately 3 mm from the free length to provide a positive contact force. Drilling experiments were also carried out using a stiff system in addition to those with system compliance.

Different drilling positions were set by adjusting the bone holder horizontally along the shaft axis, while the vertical position was fixed approximately at the middle cross-section of the shaft (figure 7.7). Two types of drill bits with diameter 2.5 mm were used to carry out the drilling experiments. The first type was a standard metal cutting (industrial) twist drill bit (figure 4.1) with a point angle of approximately 118° , and the second type was a Synthes surgical drill bit, shown in figure 7.8, from STRATEC Medical with a point angle of approximately 75° and a specially ground tip shape. The industrial bit has a length of approximately 160 mm with a flute

length of 100 mm, while the lengths of the surgical drill bit and its flute are approximately 180 mm and 30 mm respectively. Both types of drill bits were driven at three drilling conditions: a feed rate of 90 mm/min and a rated free rotational speed of 1000 rev/min, 90 mm/min and 1900 rev/min, and 132 mm/min and 3300 rev/min. The use of drill bit rotational speed rated at 1000 rev/min is within the range of speeds generated by most surgical air drills. In addition to the four system stiffnesses mentioned earlier, drilling experiments using a surgical drill bit have also included system stiffness coefficients of 4.24 and 8.29 N/mm. The purpose of using different types of drill bits and drilling conditions was to verify the effectiveness and robustness of a modified Kalman filter in identifying the imminence of drill bit break-through. Furthermore, the control of drilling offered by process automation could allow for more flexibility in selecting drill bits for bone drilling.

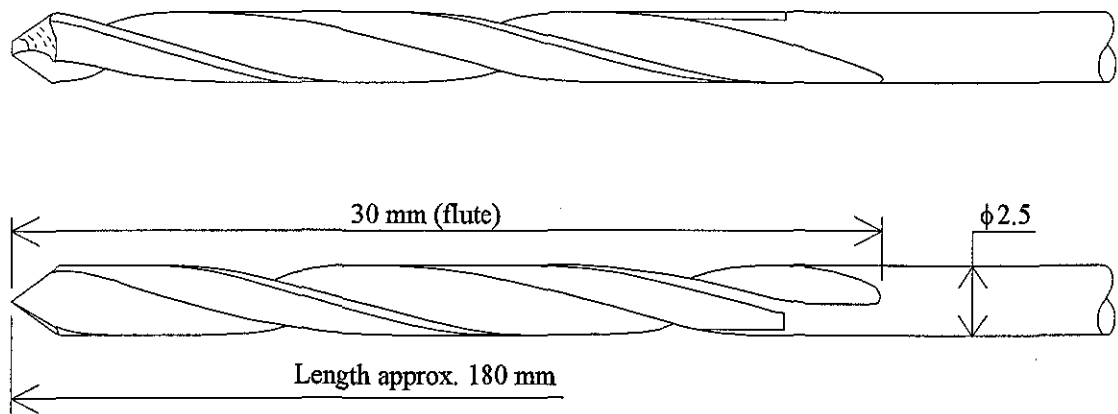


Fig. 7.8 A Synthes surgical drill bit

The simple drilling procedure with data acquisition for the experiments was controlled by the PC through the keyboard under Automatic mode. The flow chart of the drilling procedure is given in figure 7.9. At any time, the drilling process, whether advancing or retracting the drill bit, can be stopped by keyboard intervention. Thereafter, the system has to be switched to Manual mode in order to activate both the air drill and the drill feed for retraction of the drill bit using toggle switches on the controller.

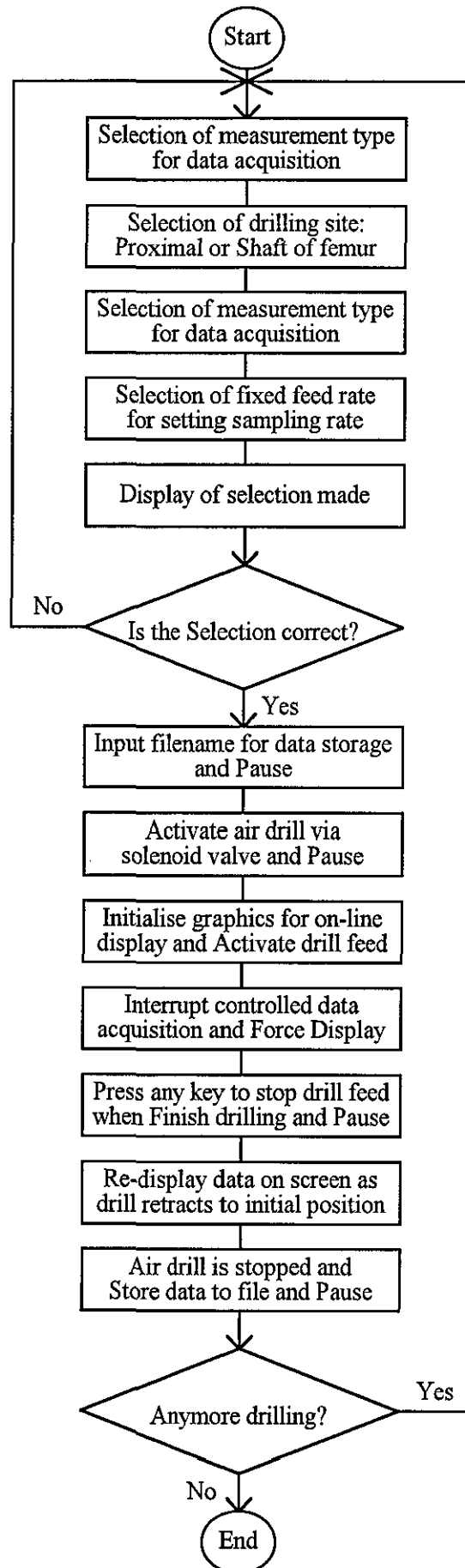


Fig. 7.9 Flow chart of the drilling procedure for experiments

7.2 Experimental Method for Evaluation of Bone Strength

The objective of this bone drilling experimental set-up is to obtain the relevant data in order to correlate drilling forces with the densitometric measurements, as outlined in Section 6.2.2. This section consists of four sub-sections which describe the implementation of the experimental method. The first sub-section briefly describes the experimental rig, while the second and third parts provide details of the set-up for bone densitometry and drilling experiments respectively. The method of correlation between drilling data and densitometric measurements is presented in the final sub-section.

7.2.1 Experimental Rig and Interface

The same drilling rig (figure 7.2) has been used for experiments related to bone strength evaluation except for the setting of the bone holder. Since the correlation of bone strength requires actual drilling forces, system compliance is not applied to these experiments. Therefore, the bone holder is rigidly secured and the sensor used for measuring displacement caused by system compliance is disconnected. An additional plate with angular adjustment is used on the bone holder to position the proximal femur appropriately for drilling. The interfacing of the drilling rig to the PC is described in Section 7.1.2 and shown in figure 7.6.

7.2.2 Bone Densitometry Measurement

Bone mineral density (BMD) in g/cm^2 of porcine femurs was measured using a Lunar DPX-alpha dual x-ray absorptiometry (DXA or DEXA) instrument at BUPA Hospital Leicester. Some details of the Lunar DPX-alpha instrument can be found in 'The evaluation of osteoporosis: Dual X-ray absorptiometry in clinical practice' by Wahner & Fogelman (1995). The scanning resolution of the Lunar DPX-alpha is given as 167 lines per 7.87" (200 mm) by 150 sample points per 7.09" (180 mm) which works out to be regions (pixel sizes) measuring 1.2 mm by 1.2 mm.

The bone was placed in a supine position, which is similar to patients being scanned, under approximately 15 cm of water to simulate body tissue around the hip. The bone was scanned from posterior to anterior. It should be noted that the anterior-posterior direction of a porcine femur is the opposite of a human one. The DXA scan of the proximal femur was performed before drilling experiments were carried out. After the drilling experiments, an x-ray image was taken to identify the different drilling trajectories or positions, and was subsequently used to identify the areas or regions of interest (ROI) where BMD measurements were ascertained. The drilling trajectories and ROIs are shown in figure 7.10. Figure 7.10a shows the ROIs of BMD according to the drilling trajectories parallel to the cervical axis of the proximal end. This means that the ROI boxes are aligned in the direction of the cervical axis. Figure 7.10b shows the ROIs of BMD at the greater trochanter, the femoral head and the femoral shaft. The size of each ROI box was set at 6 mm x 6 mm to give an area of 36 mm² (0.36 cm²). The true BMD in g/cm³ can be obtained by dividing the areal BMD by the thickness of the particular section.

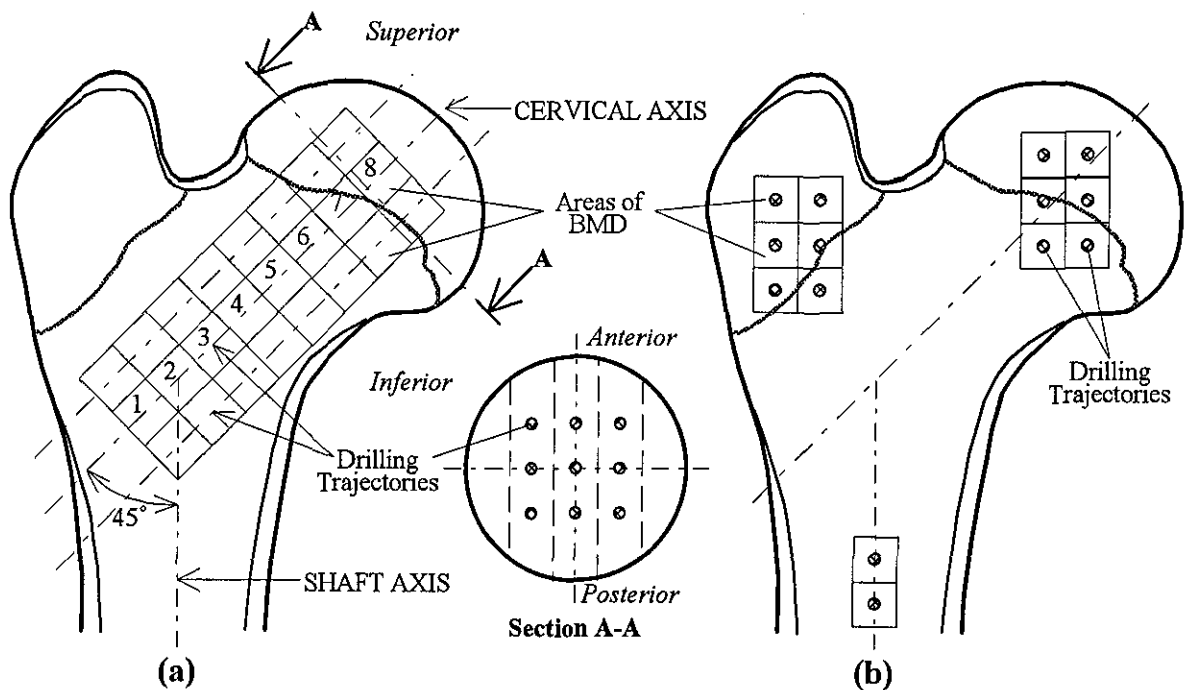


Fig. 7.10 Areas/ROIs of BMD and drilling trajectories of a proximal femur: (a) along the cervical axis of the proximal femur with ROI numbering, (b) at the greater trochanter, the femoral head and the femoral shaft

7.2.3 Experimental Set-up

Drilling experiments were performed on both the cancellous bone at the proximal end and the cortical bone along the shaft of porcine femurs. The drilling trajectories for the experiments were taken at two directions depending on the site of drilling. These directions, which are shown in figure 7.10, are: (i) in the direction of the cervical axis and (ii) in the direction of anterior-posterior (AP). The drilling trajectory in the direction of the cervical axis was approximately 135° from the shaft axis.

Experiments on the two directions were carried out on proximal femurs, while drilling in the direction of the cervical axis was not employed at the femoral shaft. At the proximal femur, the drilling trajectories have included positions parallel to the cervical axis in both the horizontal (lateral) and vertical (anterior-posterior) planes, as shown in figure 7.10a. The drilling trajectory for the femoral shaft was in the middle of the shaft cross-section and perpendicular to the shaft axis, as shown in figure 7.10b.

The whole femur was secured rigidly onto the non-compliant bone holder in accordance with the section to be drilled. Figure 7.11 shows the experimental set-up for (a) drilling the proximal femur in the direction of the cervical axis and (b) drilling in the direction of AP for the greater trochanter and the femoral head. The cervical axis of the bone was placed as parallel as possible to the drilling direction or the axis of the drill bit. Care had to be taken to prevent both movement of the bone during drilling and excessive clamping force which could influence the drilling force. The drill bit used for the experiments was an industrial twist drill bit (figure 4.1) of diameter 2.5 mm. Synthes surgical drill bits, as shown in figure 7.8, were not used because these drill bits have short drill flutes of approximately 30 mm as compared to 100 mm of the industrial bit. The problem with drill bit clogging and friction between the drill bit and the bone is, therefore, expected to be more severe. Furthermore, the surgical drill bit is designed for use on the cortical bone.

The most commonly used drill bits in the proximal femur are the guide wire or the K-wire, as shown in figure 4.3. These drill bits have a similar point shape except that the guide wire has a threaded portion at the tip. However, these types were also not used in the experiments due to the high drilling forces caused by the friction between the body of the drill bit and the bone. In

addition, the bone chips were being forced into the surrounding bone in the absence of drill flutes. The severity of this condition has often been indicated by the presence of charred bone after drilling. The guide wire even has the tendency to pull the drill bit as a result of the screw effect of the threaded portion and this can result in relatively high negative drilling forces at low feed rates.

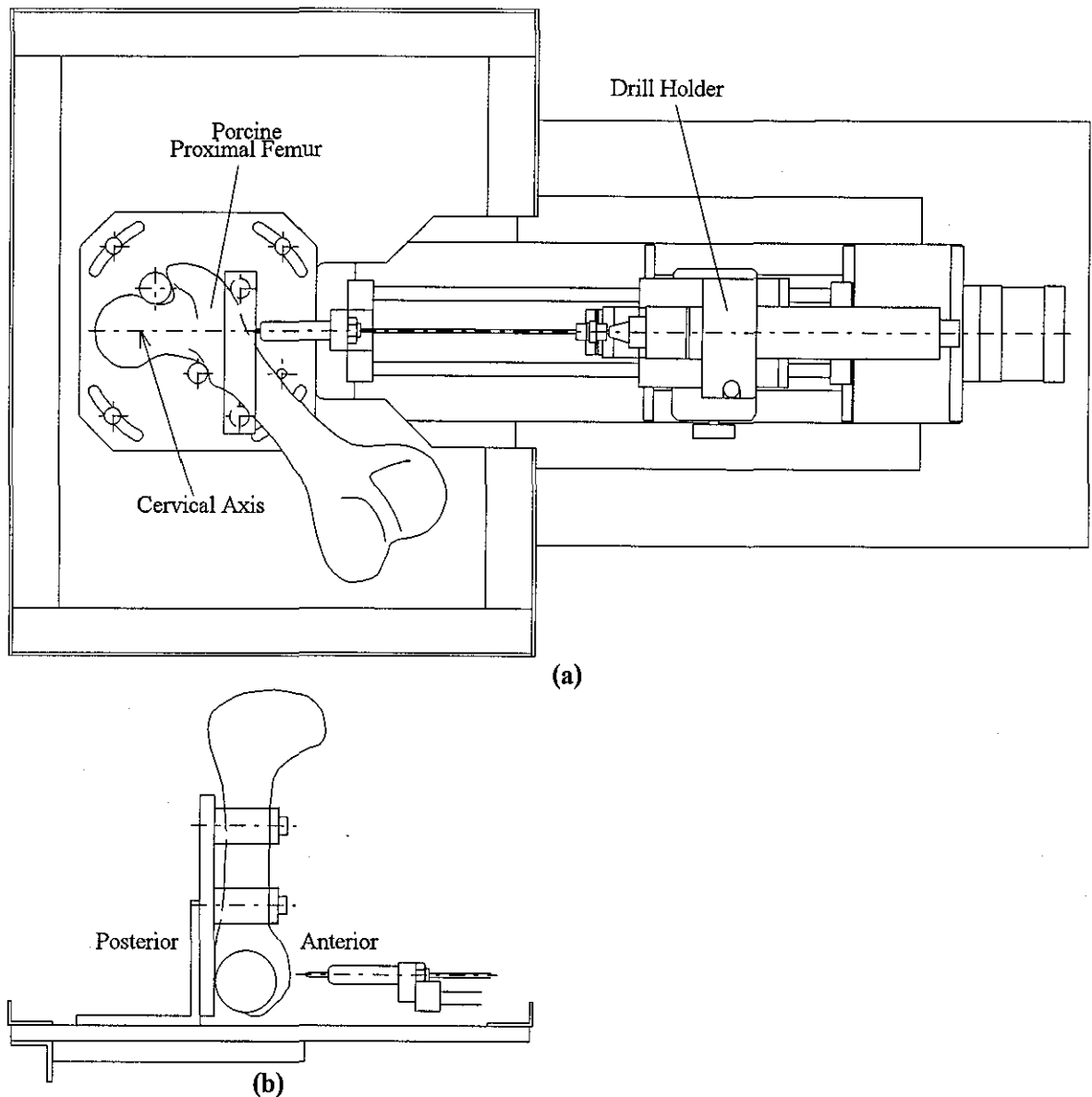


Fig. 7.11 Experimental set-up for drilling the porcine proximal femur: (a) in the direction of the cervical axis, (b) in the direction of the AP

The chosen constant feed rate for the twist drill bit was 90 mm/min and the drill bit was driven by an industrial air drill unit at a rated free rotational speed of 1000 rev/min. The simple drilling procedure was controlled by a PC through the keyboard in Automatic mode. The automatic drilling procedure for the experiments is shown in figure 7.9. At any time, the drilling process

can be stopped by keyboard intervention. Subsequently, the drill bit can be retracted using the Manual mode.

7.2.4 Correlation between Average Drilling Force and BMD

In order to correlate with BMD measurement of a specific area or ROI, an average of the drilling forces within the specific ROI was calculated. The locations of the specific ROIs for both the force and the BMD were matched as close as possible based on x-ray and BMD images to minimise matching errors of the drilling force. These errors can be assumed to be small since a relatively large number of drilling force values has been taken for averaging.

As mentioned in Section 6.2.2, there are two types of correlation between the average drilling force and the BMD. These relate to the anterior-posterior (AP) direction and the direction of the cervical axis. When correlating in the AP direction at the greater trochanter and the femoral head, the average drilling forces were calculated from the first peak at the start of drilling to the last peak just before the break-through of the drill bit.

The correlation in the direction of the cervical axis required the average drilling force to be calculated within the ROI at the trajectories above (superior to), on and below (inferior to) the cervical axis, as indicated in figure 7.10a. In addition, the proximal femur was cut with respect to the three sections to allow photographs to be taken to facilitate the measurement of the bone thickness within the ROI. These sections were further classified into regions of the trochanter, the femoral neck and the femoral head in order to establish a possible closer relationship between the average force and the BMD.

CHAPTER 8

RESULTS AND DISCUSSIONS: THE DETECTION OF DRILL BIT BREAK-THROUGH

The results obtained from the drilling experiments and their discussions are presented in this chapter with respect to the aim of achieving an enhancement of safety. These results show the effects of system compliance on drilling force profiles and the application of a modified Kalman filter in detecting drill bit break-through. Based on the modified Kalman filter, a control strategy is also presented for the detection of imminent drill bit break-through.

8.1 Effects of System Compliance

As mentioned in Section 5.1.1, the system compliance has a notable effect on the penetration rate which is the actual drill bit rate of insertion in the bone. Drill bit displacement consist of two components, one is due to the system compliance and the other is the actual drill bit penetration into the bone. The actual penetration displacement of the drill bit is obtained by deducting the displacement caused by the system compliance (compliant bone holder) from the drill feed displacement. In this study, the springs were preloaded by approximately 3 mm from the free length, as stated in Section 7.1.3, to give a positive contact force. The results obtained from the experiments using an industrial twist drill bit and a surgical drill bit (both of diameter 2.5 mm) are presented in this section in terms of drilling force, actual drill bit penetration displacement, drill feed displacement, force difference between successive samples (FDSS) and drill bit rotational speed. A five-term averager has been used to filter the FDSS and the rotational speed data. A discussion of these results is also provided.

8.1.1 Experimental Tests Using an Industrial Twist Drill Bit

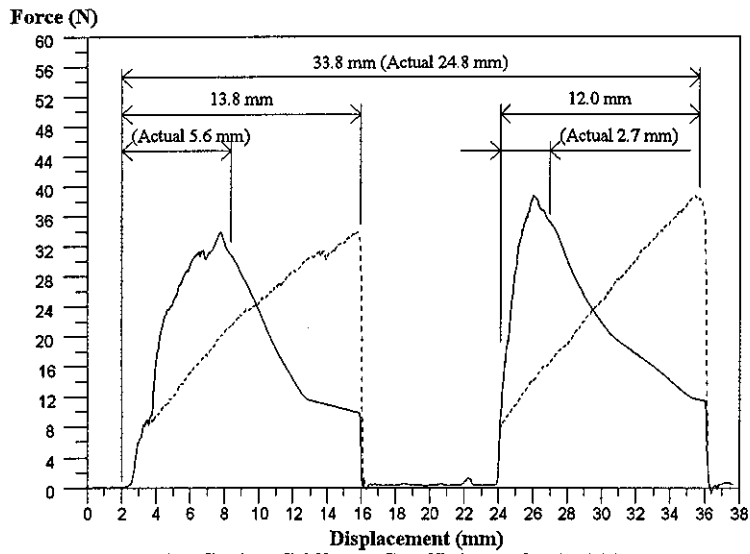
Figure 8.1 shows typical force profiles with respect to actual drill bit penetration displacement (solid lines) and drill feed displacement (dotted lines) of the drill bit while drilling into the

femoral shaft for three different system compliances. The values in brackets represent actual cortical wall thickness, whereas the values not in brackets are the drill bit displacement. At a high system stiffness, i.e. a stiffness coefficient of 18.44 N/mm as indicated in figure 5.2, the drilling force profile is considered to represent a stiff system since there is no displacement due to system compliance. A common characteristic found on all the force profiles is the rapid change in the force on entry into, and exit of the drill bit from the bone.

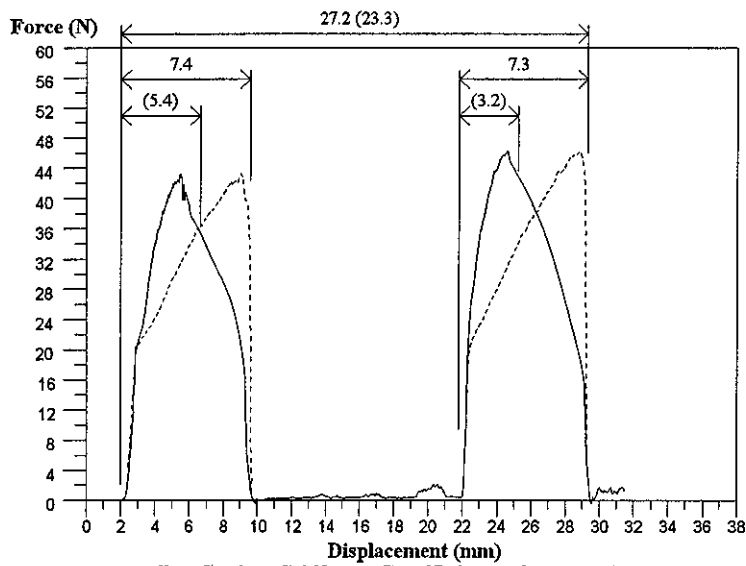
The results in figure 8.1 show that the force profiles have been significantly affected by the compliance of the bone holder in four ways. Firstly, the penetration rate is shown to vary depending on the level of system compliance, where a higher system compliance results in a lower penetration rate. Unlike a stiff system, there is a large difference between the drill feed displacement and the bone cross-sectional measurements. Instead of overcoming the drilling resistance of the bone, part of the feed displacement is taken up by the spring compression, and as a result, the force profile of figure 8.1A may be interpreted as indicating thick cortical walls and a small medullary cavity. For example, feed displacements of 13.8 mm and 12.0 mm are measured in the first and the second cortical walls of thicknesses 5.6 mm and 2.7 mm respectively, while a feed displacement of 8.0 mm instead of 16.5 mm is exhibited in the medullary cavity.

The second feature observed on the drilling force profiles is the characteristic of the rising force towards the maximum point. At the lowest system stiffness of 2.80 N/mm, shown in figure 8.1A, the initial rapid increase in the force at the start of drill bit penetration is low in magnitude. This is immediately followed by a long gradual and consistent rise to reach the maximum point across the thickness of the cortical wall. However, the initial rapid rise becomes higher in magnitude and the slope of the rising force becomes steeper, as a result of lower displacement of the bone, when the system stiffness increases, as shown in figures 8.1B and 8.1C.

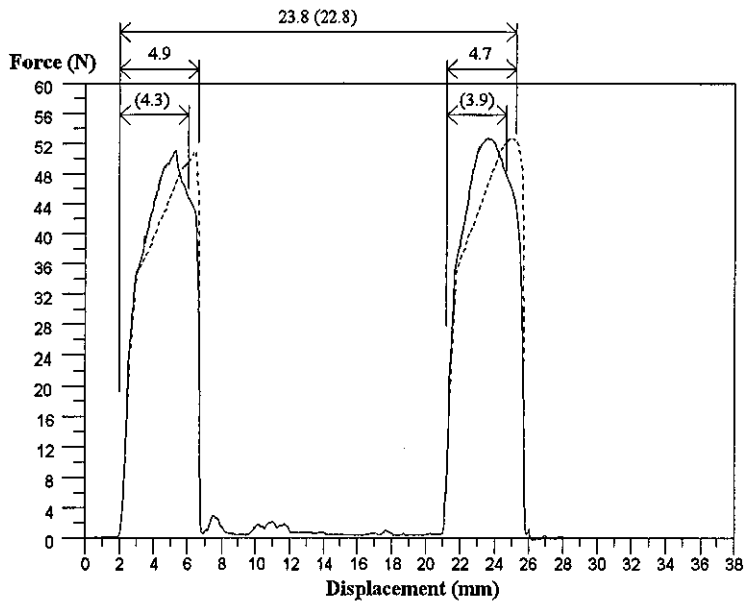
The two other effects are the magnitude of maximum force and the change in the force profile at break-through. In general, a lower system stiffness is associated with a lower magnitude of maximum force, because the compression of the spring has the effect of reducing the penetration rate and the force.



A - Spring Stiffness Coefficient of 2.80 N/mm



B - Spring Stiffness Coefficient of 5.68 N/mm



C - Spring Stiffness Coefficient of 10.90 N/mm

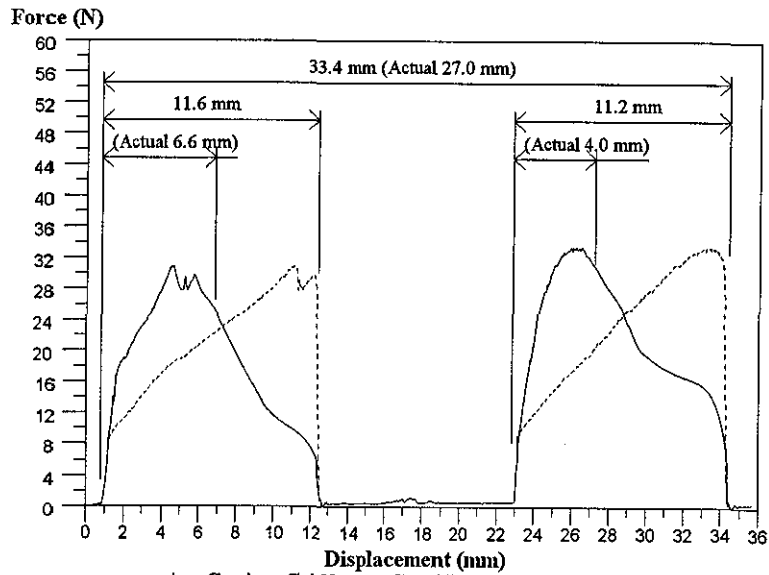
Fig. 8.1 Profiles of drilling force against actual drill bit penetration displacement (solid lines) and drill feed displacement (dotted lines) at three system stiffnesses (Feed Rate = 90 mm/min; Rated Speed = 1000 rev/min)

Upon drill bit break-through at both cortical walls, the drilling force drops sharply to zero irrespective of system stiffness. It is at the point of break-through of the second cortical wall where the system compliance can have a major effect, especially at low system stiffness, because the 'spring-back' action can cause excessive protrusion of the drill bit. Therefore, system compliance has to be taken into consideration in drill bit break-through detection.

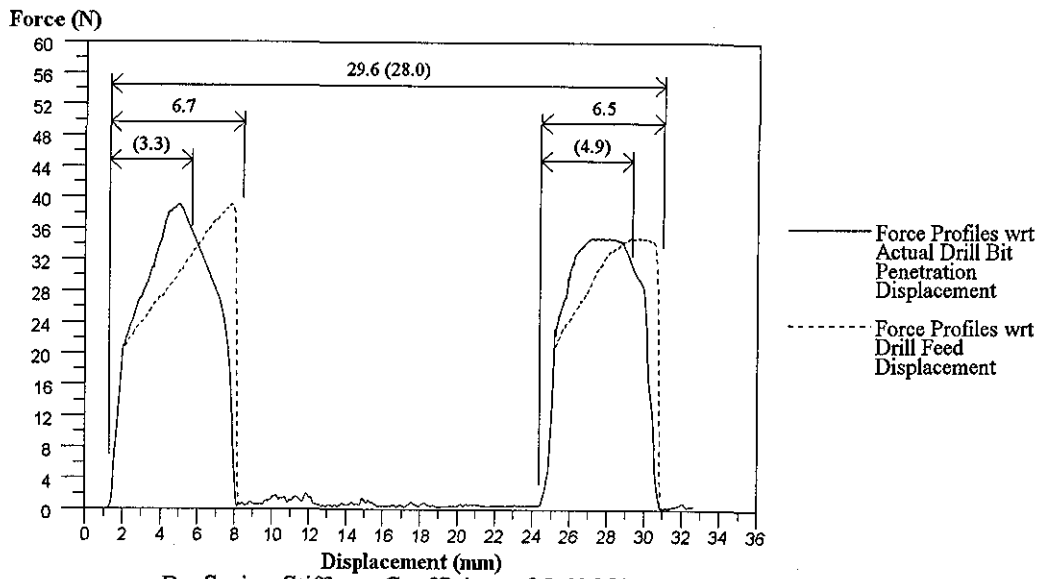
Similar results have been obtained using a feed rate of 90 mm/min at 1900 rev/min, as shown in figure 8.2. However, the dependence of drilling thrust force on the feed rate and on the rotational speed produces differences in the magnitudes of maximum force and the amount of feed displacement due to system compliance. The use of higher rotational speed has been shown to be associated with lower magnitude of maximum force, as experienced by Jacobs *et al.* (1976) and hence reduces feed displacement due to system compliance.

System compliance has also been shown to have a significant effect on both the FDSS and the drill bit rotational speed. Figure 8.3 shows typical experimental results of drilling force (dotted lines), FDSS and drill bit rotational speed, with respect to drill bit displacement, for different system compliances. The profiles of the drilling force have different characteristics in accordance with the system compliances, as mentioned earlier in this section. The rapid rise and fall of the force profile at the cortical wall interfaces have been clearly indicated by the FDSS for all system stiffnesses.

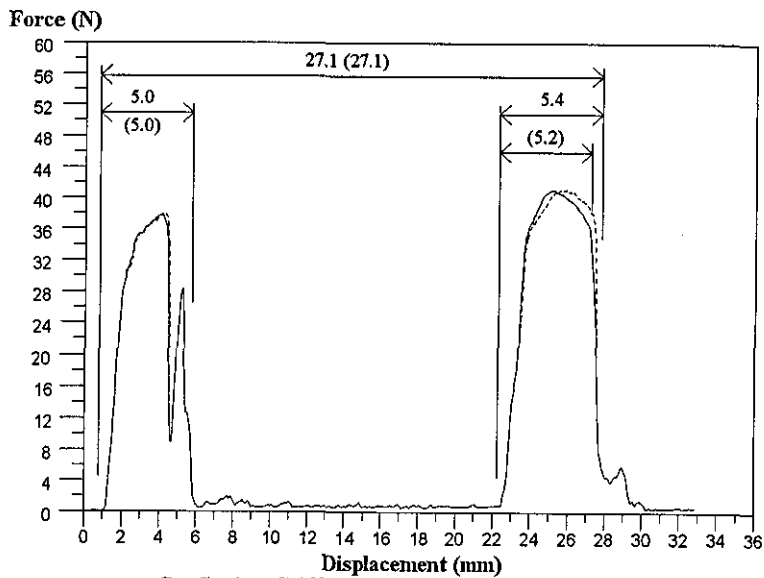
As a result of displacement due to system compliance, the difference in the FDSS is shown in the intervals between the high peaks and troughs at the cortical wall interfaces. However, the rate of force increase at the start of drill bit penetration into the cortical wall is not reflected in the magnitude of maximum FDSS at different system stiffnesses. As the system stiffness increases, the rate of force increase becomes higher which is not always the case for FDSS. The rotational speed, in general, starts to decrease as the drill bit enters the cortical bone and continues to do so across the thickness of the cortical wall regardless of whether system compliance is present or not. This is clearly shown in figures 8.4 and 8.5 for drill bit rotational speeds of 1900 and 3300 rev/min respectively. At the onset of drill bit break-through, the speed reduces to a minimum before recovering after break-through. However, at low rotational speeds in certain cases, as seen in figure 8.3B, the change in the speed is virtually undetectable.



A - Spring Stiffness Coefficient of 2.80 N/mm



B - Spring Stiffness Coefficient of 5.68 N/mm



C - Spring Stiffness Coefficient of 10.90 N/mm

Fig. 8.2 Profiles of drilling force against actual drill bit penetration displacement (solid lines) and drill feed displacement (dotted lines) at three system stiffnesses (Feed Rate = 90 mm/min; Rated Speed = 1900 rev/min)

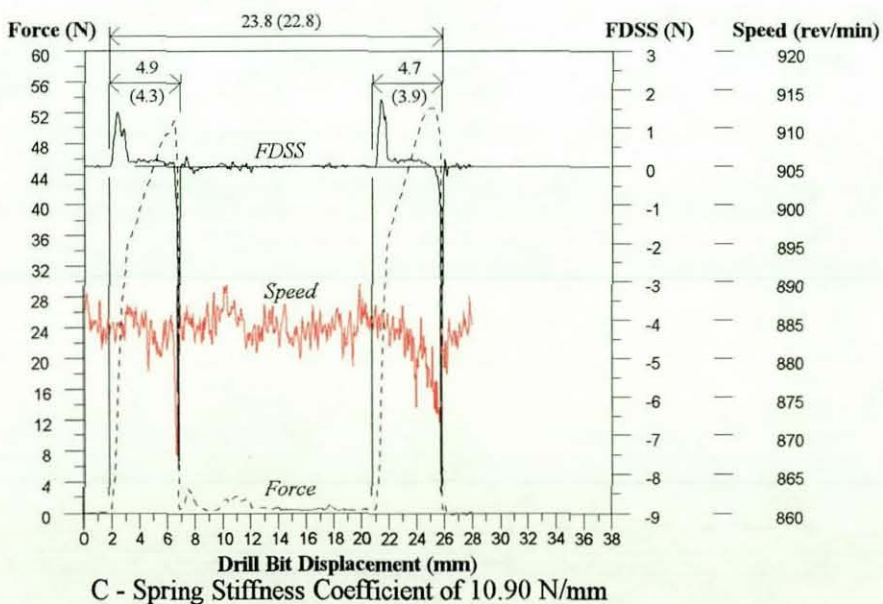
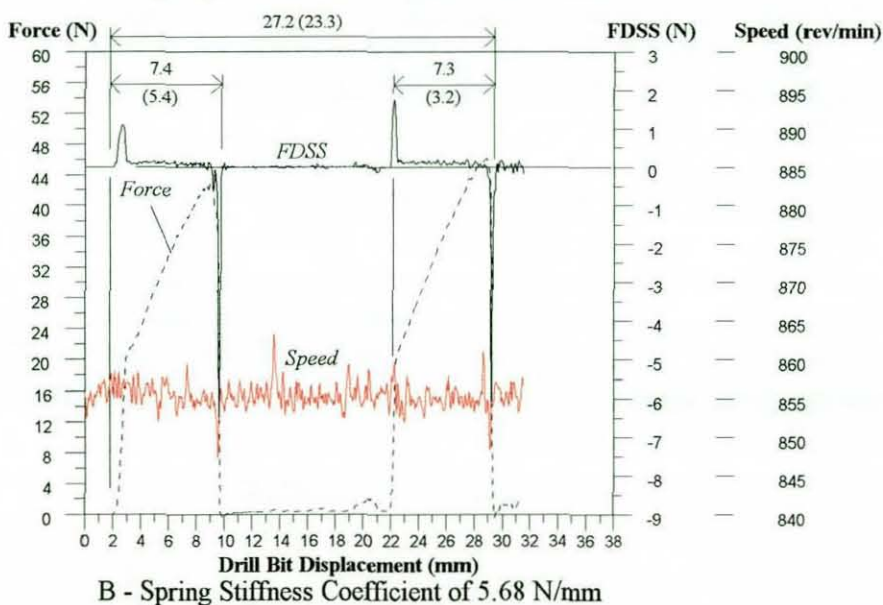
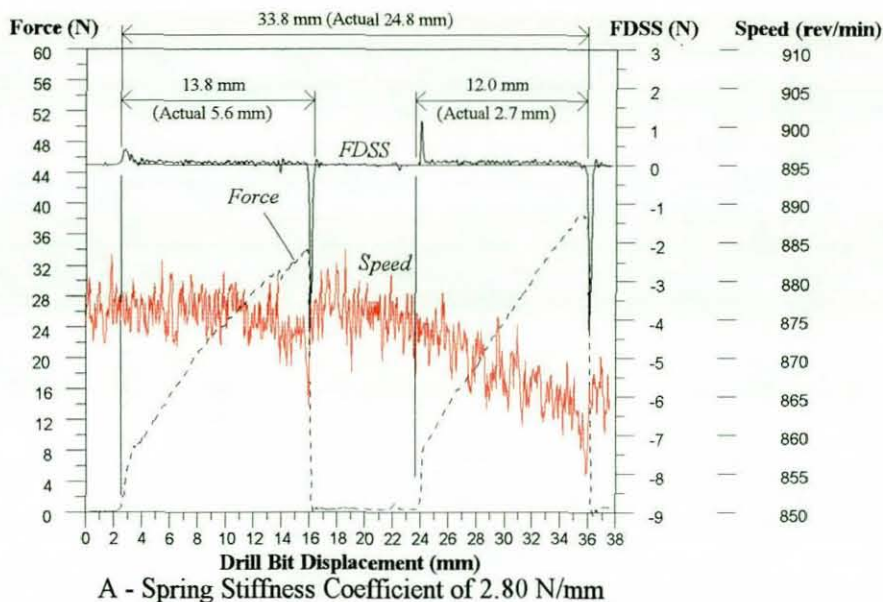


Fig. 8.3 Profiles of drilling force, force difference between successive samples (FDSS) and rotational speed of a porcine femoral shaft at three system stiffnesses (Feed Rate = 90 mm/min; Rated Speed = 1000 rev/min)

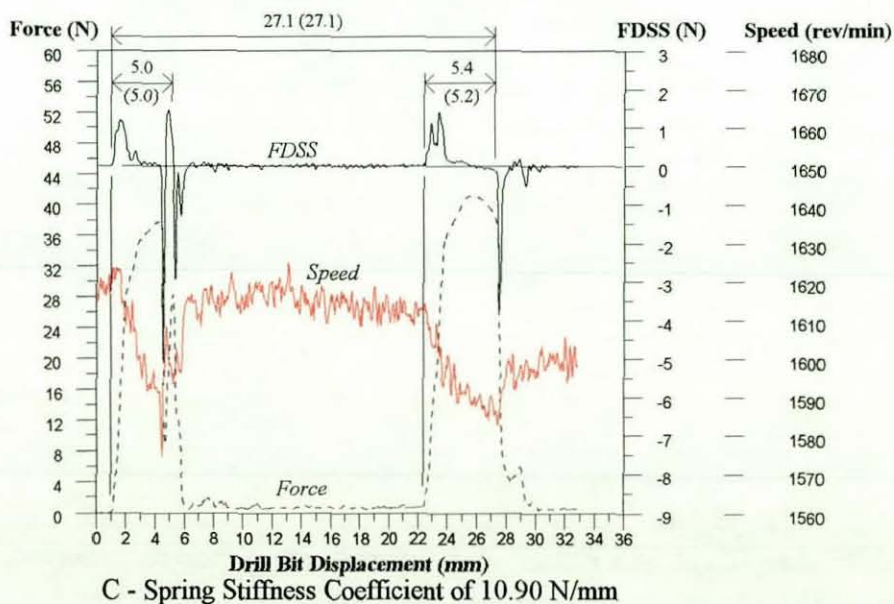
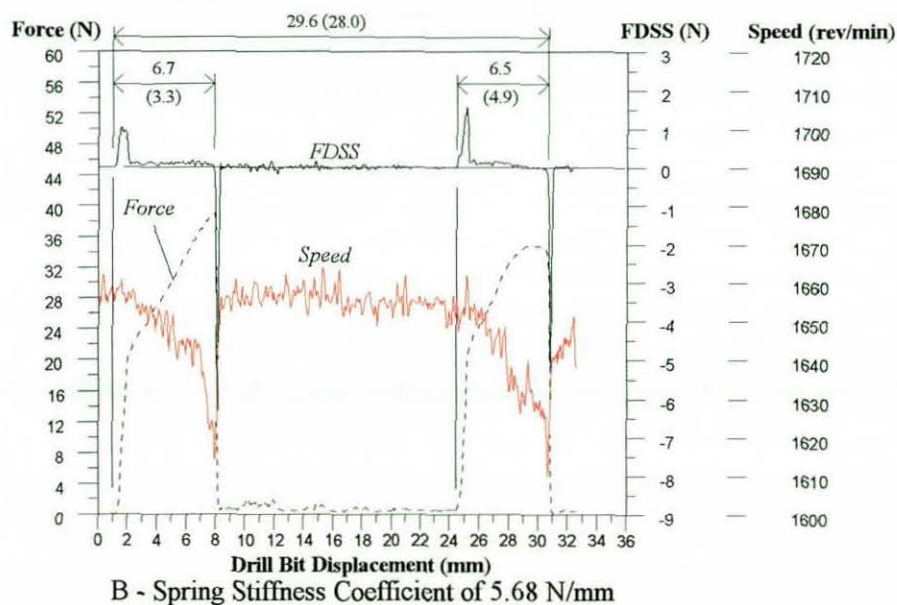
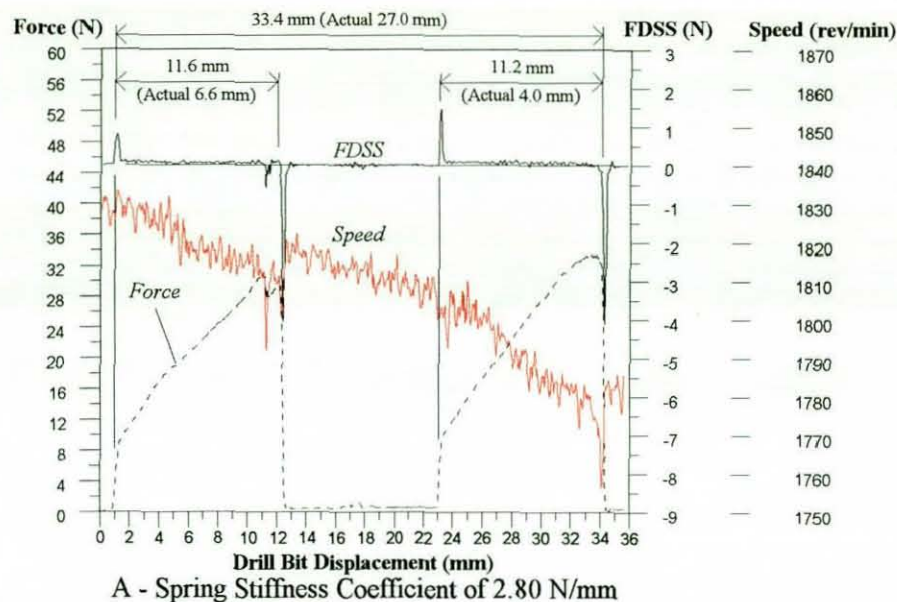


Fig. 8.4 Profiles of drilling force, force difference between successive samples (FDSS) and rotational speed of a porcine femoral shaft at three system stiffnesses (Feed Rate = 90 mm/min; Rated Speed = 1900 rev/min)

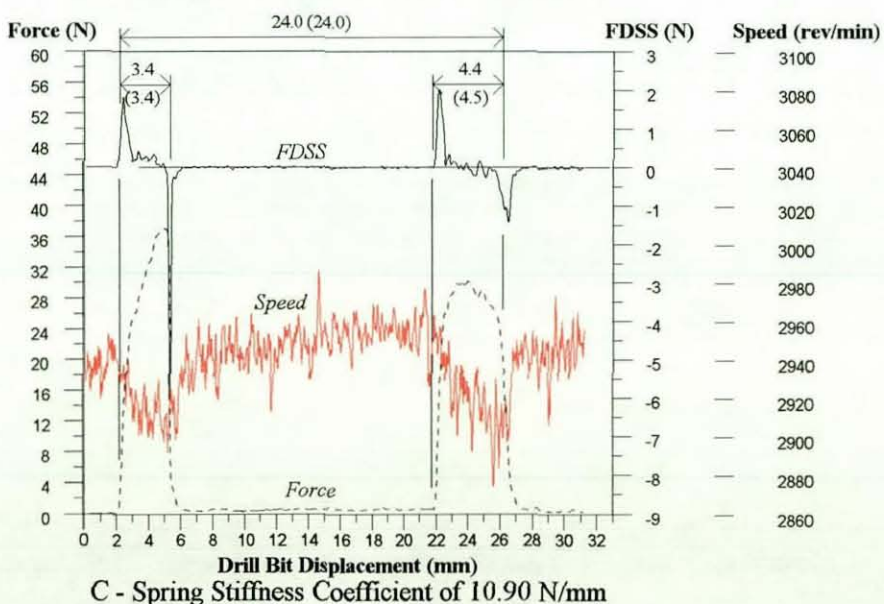
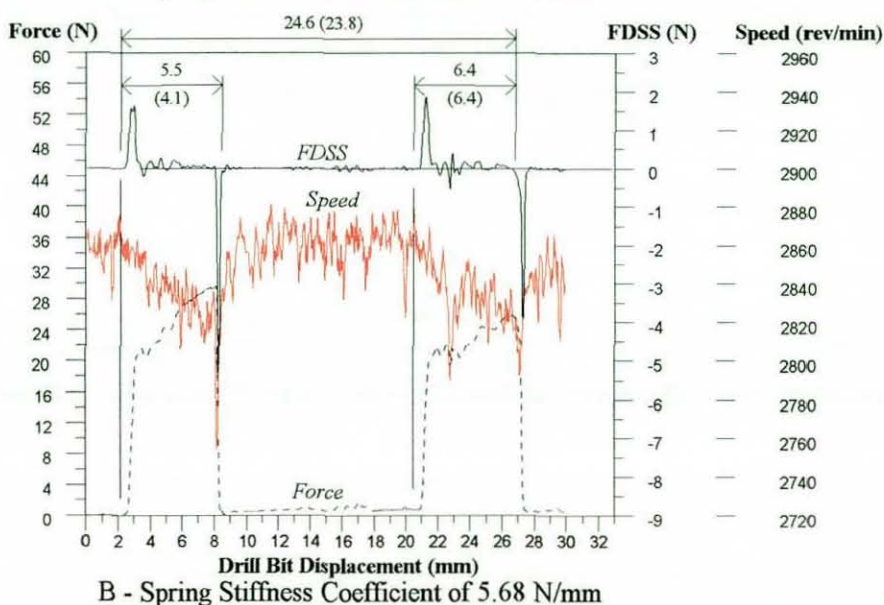
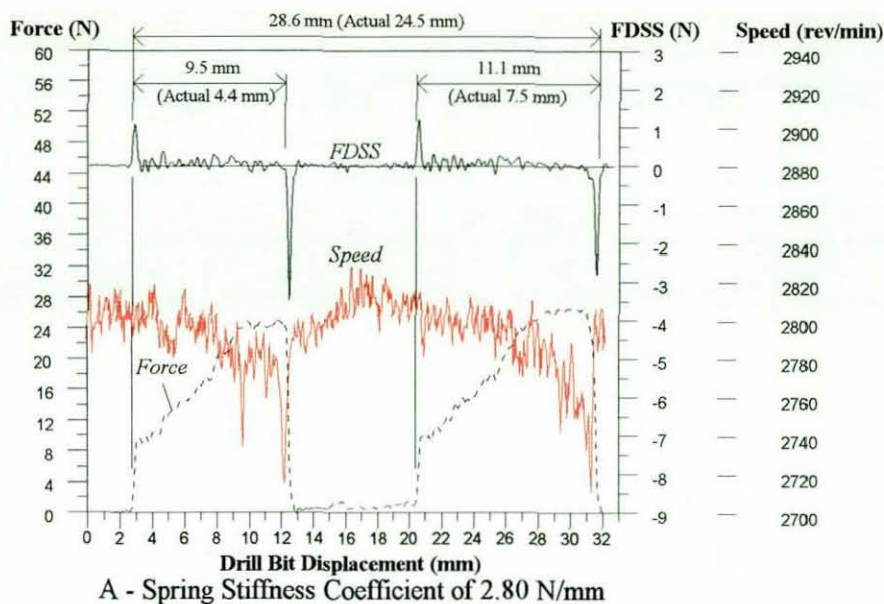


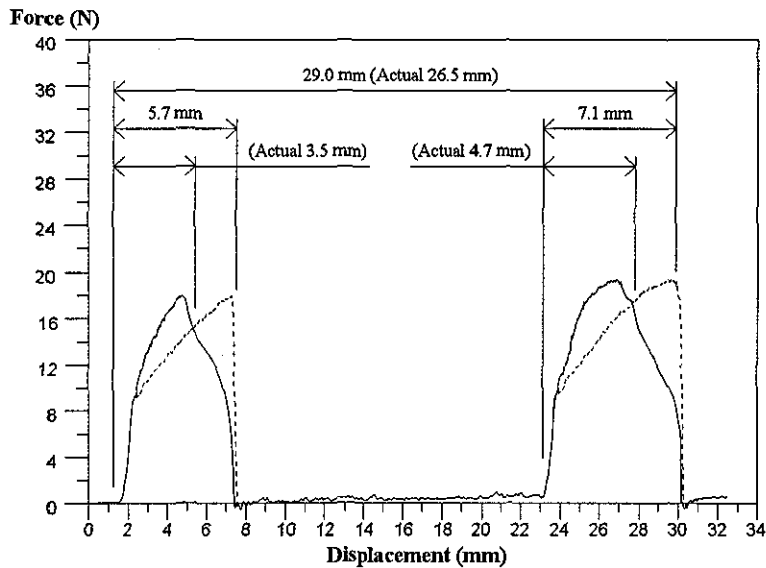
Fig. 8.5 Profiles of drilling force, force difference between successive samples (FDSS) and rotational speed of a porcine femoral shaft at three system stiffnesses (Feed Rate = 132 mm/min; Rated Speed = 3300 rev/min)

8.1.2 Experimental Tests Using a Surgical Drill Bit

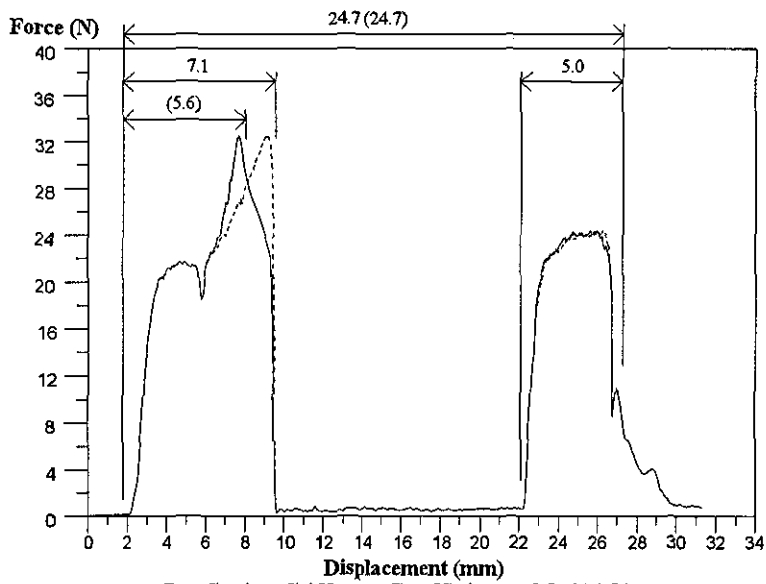
Results from experiments using a surgical drill bit have also shown similar patterns of drilling force, penetration rate, FDSS and rotational speed to those using an industrial drill bit. However, the magnitudes of maximum force and the amount of displacement due to system compliance have been found to be generally lower. This characteristic is a result of using the surgical drill bit which is specifically designed for use on cortical bones. Figures 8.6 and 8.7 show the effects of three system compliances on the penetrations rates for drilling experiments carried out at a feed rate of 90 mm/min with rated rotational speeds of 1000 and 1900 rev/min. The unexpected drop in the rotational speed, while the drill bit is travelling across the medullary cavity as seen in figure 8.9B, is a result of a drop in the supply of air pressure. This drop in speed has little effect on the drilling force, but it has a significant effect on the drill bit break-through detection when the rotational speed is used.

Similar patterns of FDSS and rotational speed, as shown in figures 8.8, 8.9 and 8.10, have been obtained from results of experiments using a surgical drill bit at the three drilling conditions. These drilling conditions consist of a feed rate of 90 mm/min with rated drill bit rotational speeds of 1000 and 1900 rev/min, and at a feed rate of 132 mm/min with a rated speed of 3300 rev/min. The magnitude of maximum FDSS provides no indication of system stiffness even though the rate of change in force is clearly visible. One distinct feature from the results obtained at a high system stiffness is the gentle drill bit break-through which makes detection difficult using threshold triggered FDSS. There is also the problem faced with detecting the change in rotational speed when operating at low speeds, as shown in figure 8.8B.

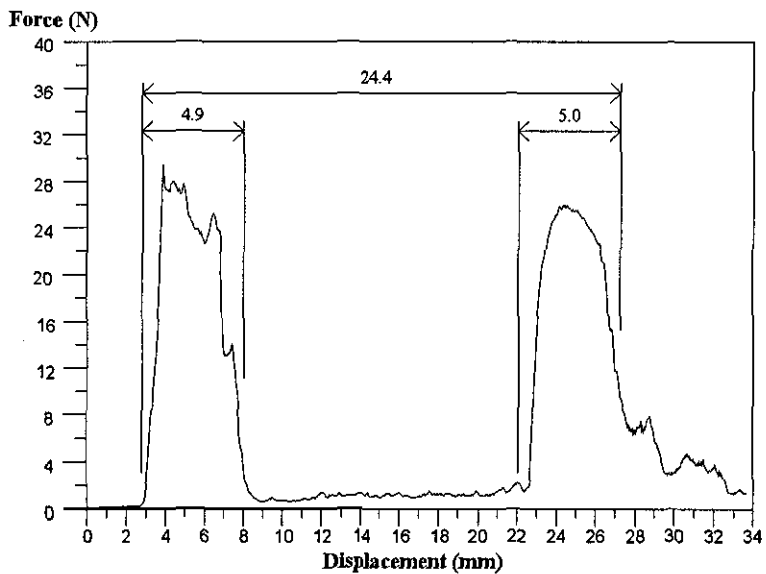
The unexpected drop in the rotational speed, while the drill bit is travelling across the medullary cavity as seen in figure 8.9B, is a result of a drop in the supply of air pressure. This drop in speed has little effect on the drilling force, but it has a significant effect on the drill bit break-through detection when the rotational speed is used. Figures 8.8C and 8.9A show speed profiles which have also been affected (but not as severe as in figure 8.9B) by the drop in the supply of air pressure. The expected profile should be similar to the rotational speed profiles shown in figures 8.8A and 8.10, which show a rise in speed after drill bit break-through of the first cortical wall, followed by a constant speed in the medullary cavity. These results have been included because such effect (caused by a fluctuation in air pressure) could occur in practice.



A - Spring Stiffness Coefficient of 2.80 N/mm

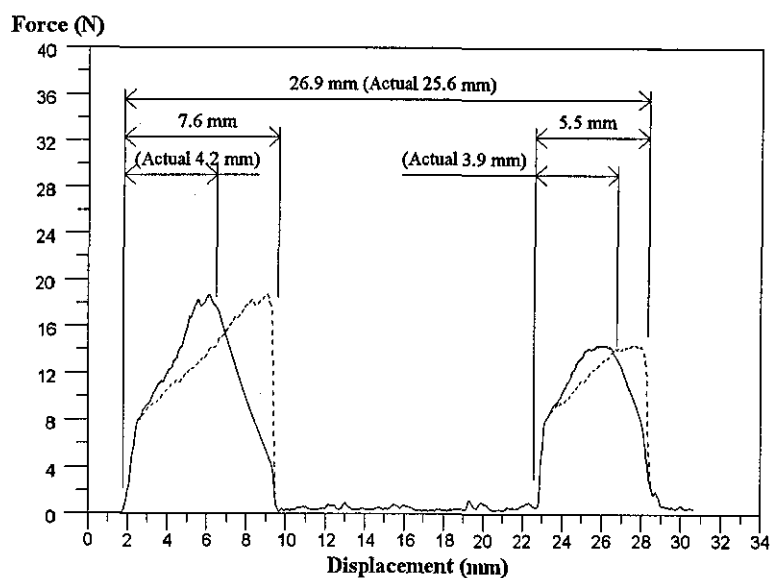


B - Spring Stiffness Coefficient of 5.68 N/mm

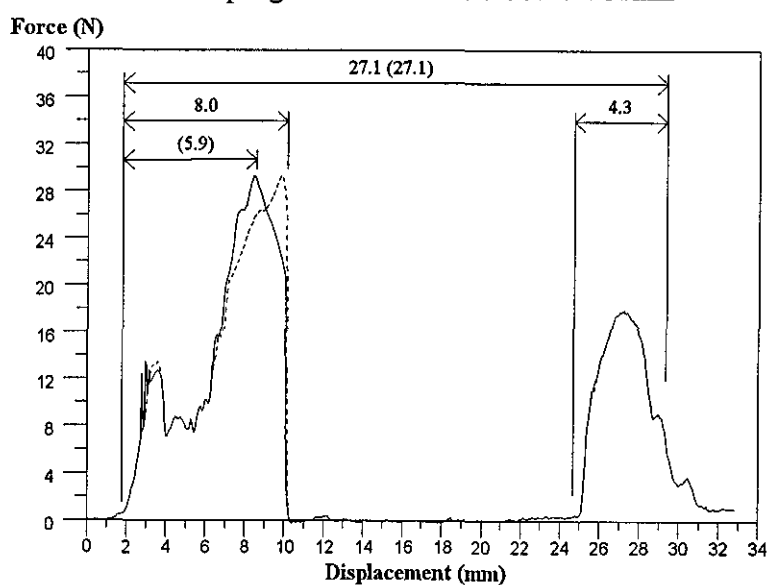


C - Spring Stiffness Coefficient of 10.90 N/mm

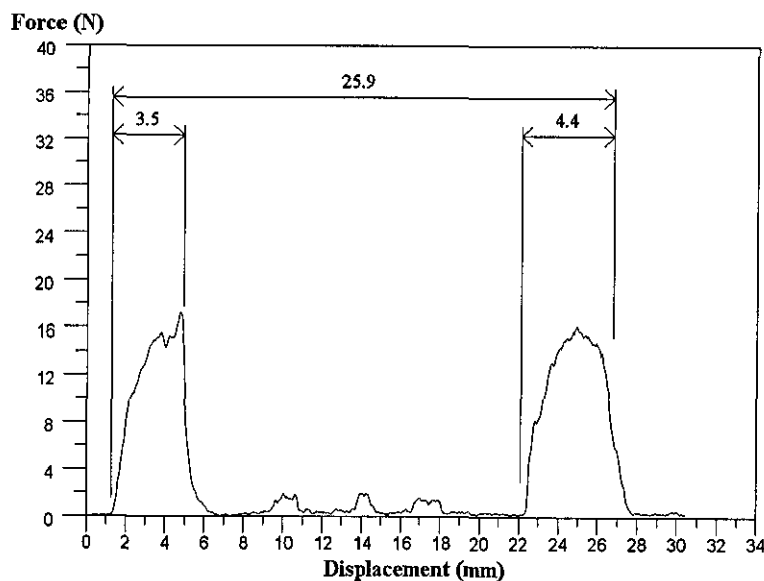
Fig. 8.6 Profiles of drilling force against actual drill bit penetration displacement (solid lines) and drill feed displacement (dotted lines) at three system stiffnesses using a surgical drill bit (Feed Rate = 90 mm/min; Rated Speed = 1000 rev/min)



A - Spring Stiffness Coefficient of 2.80 N/mm

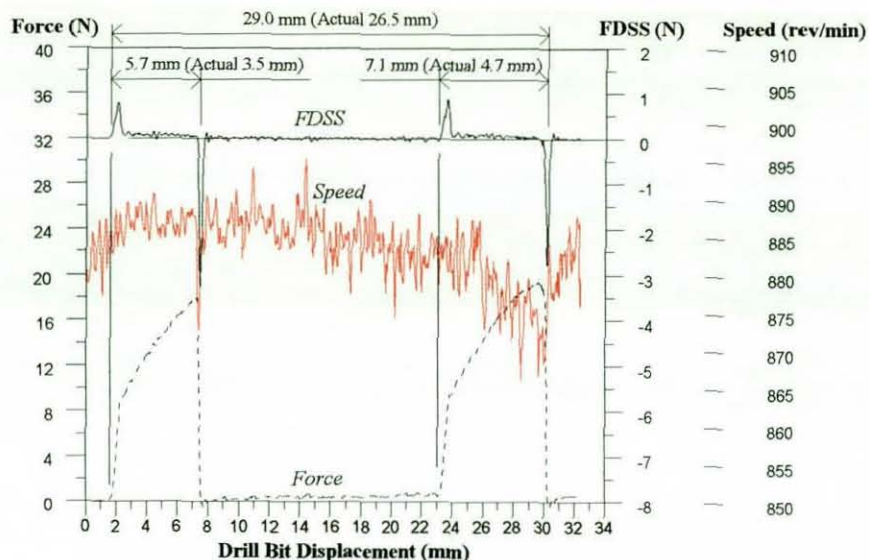


B - Spring Stiffness Coefficient of 5.68 N/mm

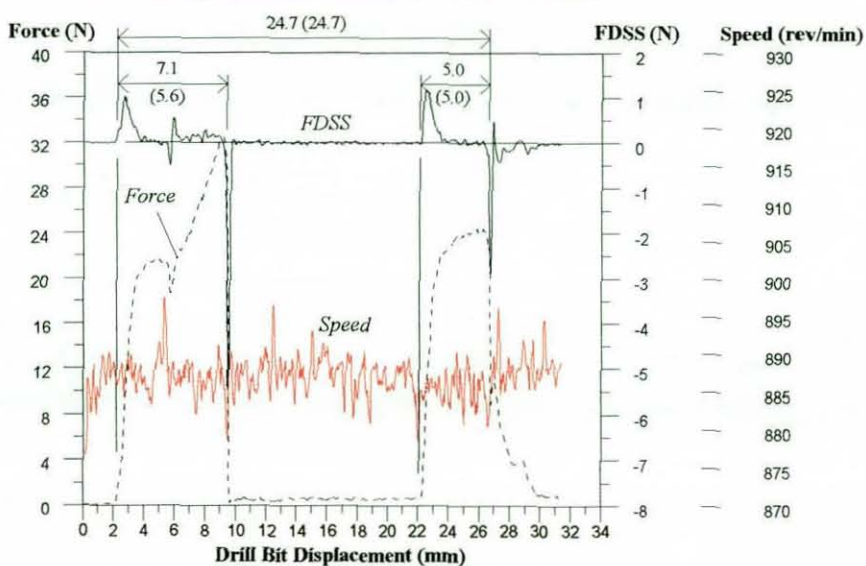


C - Spring Stiffness Coefficient of 10.90 N/mm

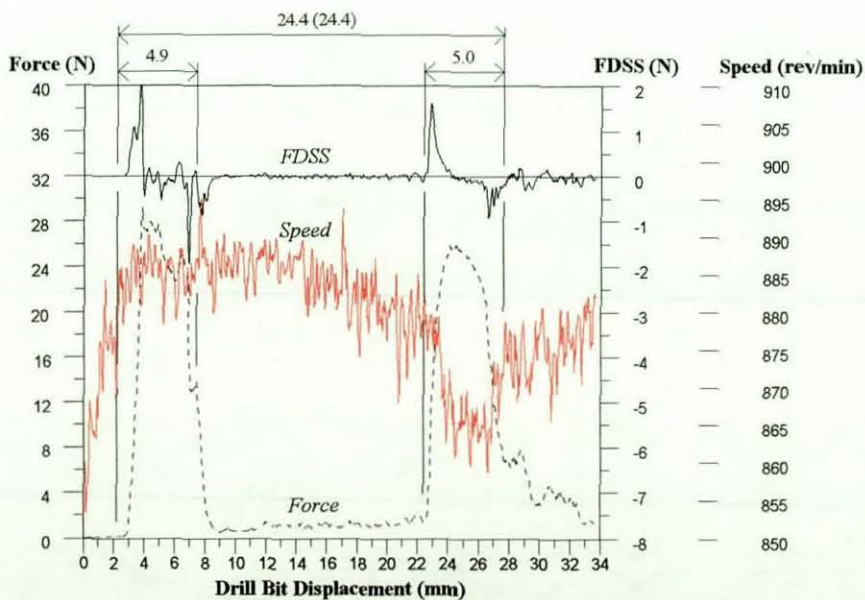
Fig. 8.7 Profiles of drilling force against actual drill bit penetration displacement (solid lines) and drill feed displacement (dotted lines) at three system stiffnesses using a surgical drill bit (Feed Rate = 90 mm/min; Rated Speed = 1900 rev/min)



A - Spring Stiffness Coefficient of 2.80 N/mm



B - Spring Stiffness Coefficient of 5.68 N/mm



C - Spring Stiffness Coefficient of 10.90 N/mm

Fig. 8.8 Profiles of drilling force, force difference between successive samples (FDSS) and rotational speed of a porcine femoral shaft at three system stiffnesses using a surgical drill bit (Feed Rate = 90 mm/min; Rated Speed = 1000 rev/min)

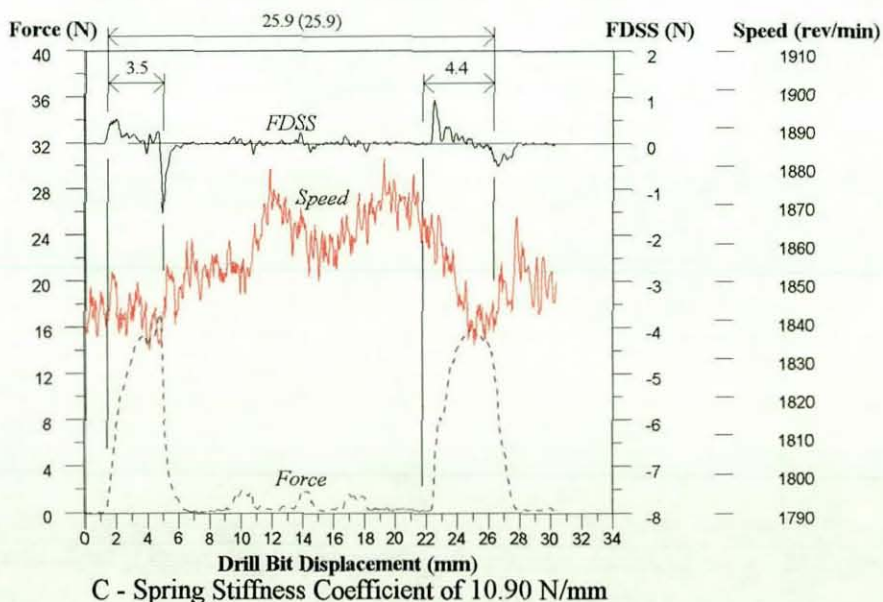
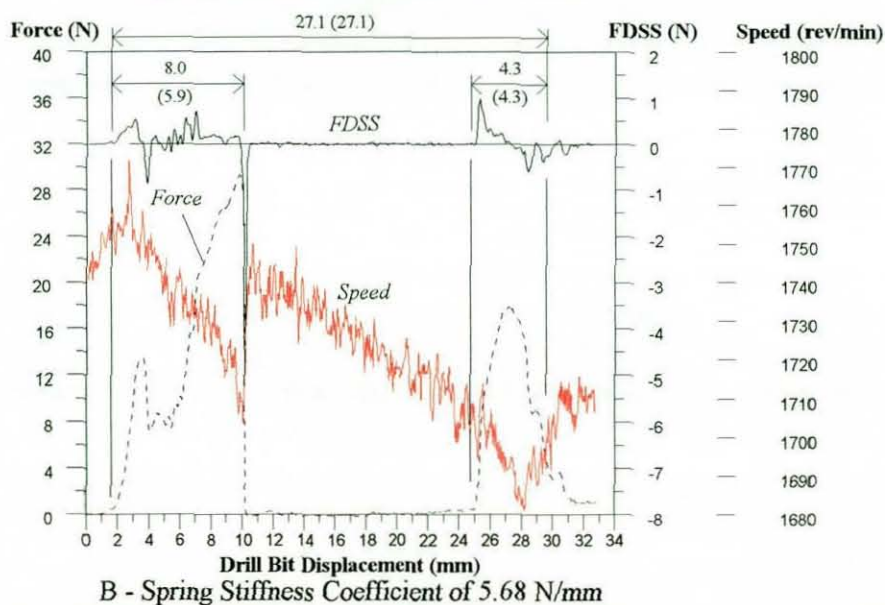
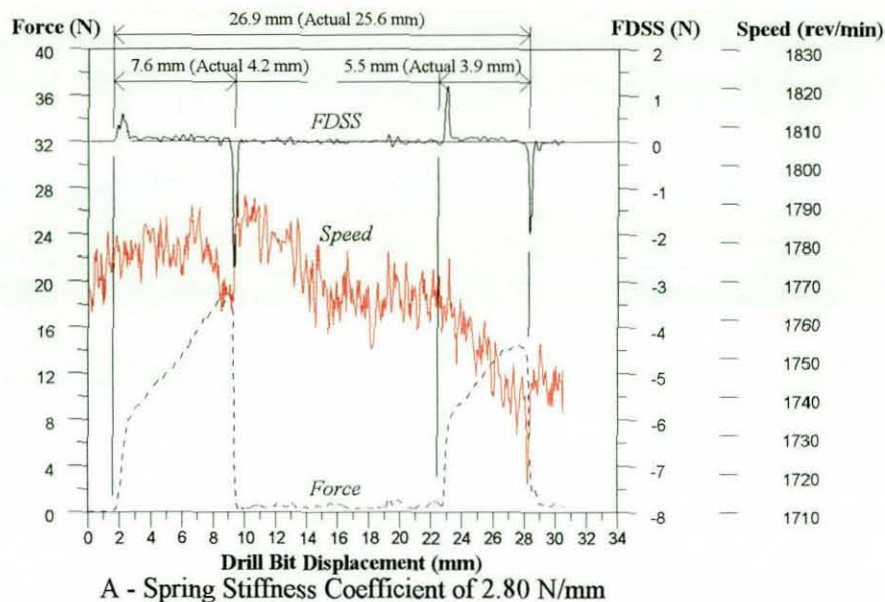


Fig. 8.9 Profiles of drilling force, force difference between successive samples (FDSS) and rotational speed of a porcine femoral shaft at three system stiffnesses using a surgical drill bit (Feed Rate = 90 mm/min; Rated Speed = 1900 rev/min)

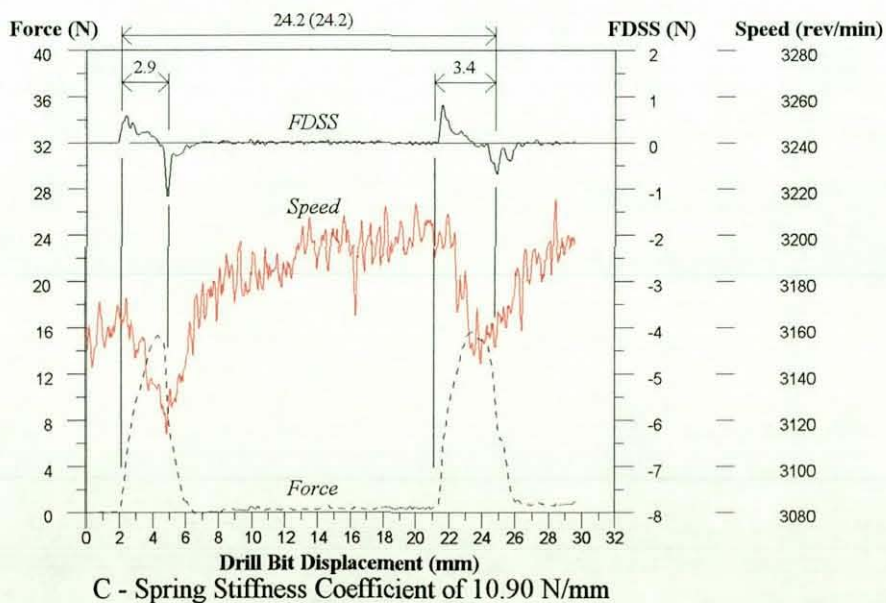
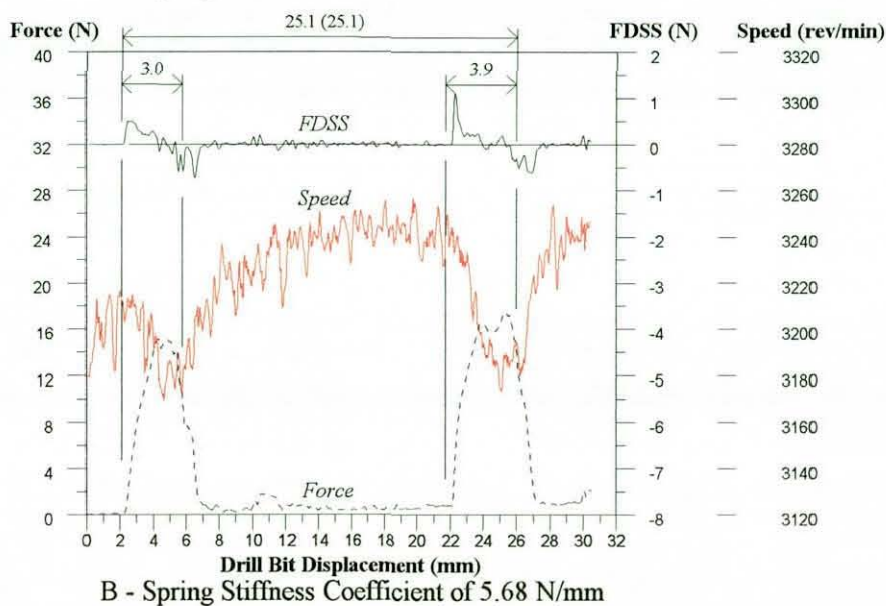
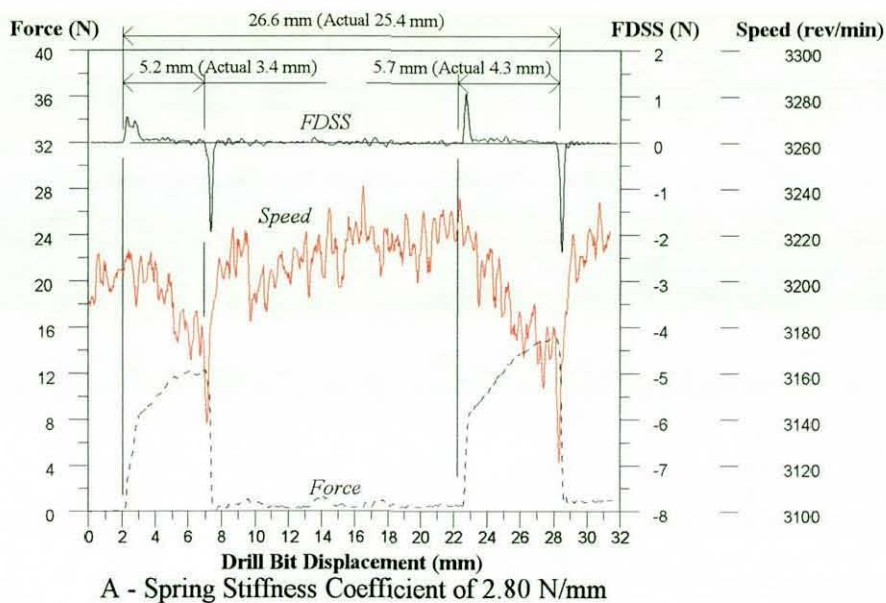


Fig. 8.10 Profiles of drilling force, force difference between successive samples (FDSS) and rotational speed of a porcine femoral shaft at three system stiffnesses using a surgical drill bit (Feed Rate = 132 mm/min; Rated Speed = 3300 rev/min)

8.1.3 Discussion on the Effects of System Compliance

The penetration rate has been found to depend on the system compliance, drilling condition and the type of drill bit. At low system stiffness, the drilling force profiles have shown certain similar characteristics to the profiles presented by Brett *et al.* (1995), although the bone involved and the drill bit used have been different. The main focus is on drilling of bone at low system stiffness where greater risk of excessive drill bit break-through is present. The results from the FDSS have been found to be similar to the results from a derivative function presented by Allotta *et al.* (1995). However, using FDSS or a derivative function would result in difficulty in setting the appropriate threshold to detect break-through particularly when the fall in the drilling force is gradual, as shown in figure 8.8C.

The measurement of rotational speed, to represent torsional resistance (i.e. torque), is significantly affected by fluctuation, especially at low rotational speeds, as shown in figures 8.3 and 8.8. The fluctuation of speed is similar to the torque fluctuation presented by Allotta *et al.* (1995). Also, similar to experimental results presented by Abouzgia and James (1995), the rotational speed reduction is relatively greater at higher rotational speeds. This is clearly shown by the greater speed reduction when drilling at a rated speed of 3300 rev/min, shown in figures 8.5 and 8.10, as compared to the speed reduction when drilling at a rated speed of 1900 rev/min, shown in figures 8.4 and 8.9. However, the reduction in speed has been shown to be virtually undetectable at low rotational speeds, as shown in figures 8.3B and 8.8B.

The drilling forces obtained from porcine femoral shafts may not represent the human cortical bone because the strength of pig bone has been found to be significantly lower (Yamada, 1970). Therefore, higher forces are to be expected when drilling into human femoral shafts and as a result, the effects of system stiffness would be more evident.

8.2 Application of a Modified Kalman Filter

The analyses of the results from Section 8.1 using the modified Kalman filter on the FDSS and on the rotational speed are presented below according to the types of drill bit.

8.2.1 Kalman Filtered Results of an Industrial Twist Drill Bit

The implementation of a Kalman filter algorithm on both the FDSS and the rotational speed has resulted in different trends with respect to the system compliance, as shown in figure 8.11. Two distinctive features can be observed from the Kalman filtered FDSS (K-FDSS). These features are the maximum magnitude of the K-FDSS, which reflects a measure of the rapid initial rise in force, and the slope of the profile after the maximum magnitude. The higher is the system compliance, the lower is the magnitude of maximum K-FDSS. As far as the slope of K-FDSS is concerned, it becomes steeper as the stiffness increases. However, the slope is difficult to determine especially at high system stiffness due to inconsistency in the force profile.

K-FDSS profiles also share a common characteristic, with FDSS profiles, of rapid rise at drill bit penetration and rapid fall during break-through at the cortical wall interfaces. Furthermore, a K-FDSS value of 0.00 N has been shown to indicate imminent drill bit break-through in both the first and second cortical walls. A break-through detection can, therefore, be established by monitoring the zero value of K-FDSS. This method is easier to implement than a threshold based derivative function as proposed by Allotta *et al.* (1995) or FDSS since the derivative threshold has to be set according to the type of drill bit and the drilling conditions. An earlier break-through detection is also possible by setting a higher threshold value for K-FDSS. For instance, a higher K-FDSS value of 0.03 N, as shown by the horizontal dashed lines in figure 8.11, provides an early indication of the commencement of drill bit break-through for all three system stiffness conditions.

The Kalman filtered speed (K-Speed) has similar trends for the three stiffness conditions at a feed rate of 90 mm/min and a rated speed of 1000 rev/min, as shown in figure 8.11. In general, the K-Speed increases steadily to a maximum value around the entry of the second cortical wall before dropping steadily. The magnitudes of maximum K-Speed are shown to vary at different system stiffness due to the difference in the levels of the measured rotational speed. Soon after the drill bit breaks through the second cortical wall, the K-Speed begins to increase. The K-Speed of the first cortical wall in this case is of little significance. When there is a difficulty in detecting the change in the measured speed, as shown in figures 8.3B and 8.8B, the K-Speed characteristic at the exit from the second cortical wall may not be present, as shown in figure 8.11B. As expected, the fluctuations of the measured speed, as seen in previous figures, have little influence on the K-Speed. This type of characteristic makes it possible to implement drill

bit rotational speed for the detection of break-through. Nevertheless, the K-FDSS must be used as the primary detection algorithm for drill bit break-through. The possible use of K-Speed in the break-through detection is by setting a threshold based upon a ratio or percentage of the maximum K-Speed value. For example, a threshold value of 99.3% of the maximum K-Speed, shown by the horizontal dash-dot-dot lines in figure 8.11, is used to identify imminent drill bit break-through. However, this threshold setting for K-Speed is not reliable at low rotational speeds, as shown in figures 8.11B and 8.11C.

The application of the K-FDSS as the primary algorithm is a robust method for the detection of drill bit break-through. The use of K-Speed complements the K-FDSS and offers an improvement in the reliability of the proposed detection method. To demonstrate the versatility of this detection method, similar results were obtained from experimental tests at a different feed rate and drill bit rotational speed. Figure 8.12 and figure 8.13 show the profiles of drilling force, K-FDSS and K-Speed for a feed rate of 90 mm/min at a rated speed of 1900 rev/min and for a feed rate of 132 mm/min at a rated speed of 3300 rev/min respectively. The characteristics of the maximum K-FDSS values for each system compliance remain rather identical. Only profiles from a feed rate of 132 mm/min at a rated speed of 3300 rev/min (figure 8.13) show higher number of ripples in both the drilling force and K-FDSS. In addition, the K-Speed profiles are easily recognisable as there is little difficulty in detecting the change in the measured rotational speed. With the same threshold settings as earlier for both the K-FDSS and K-Speed, this method gives an indication of imminent drill bit break-through.

As mentioned in Section 5.4.2, the inherent force fluctuation, generally caused by changes in bone structural density, has a significant effect on both the drilling force and the FDSS profiles indicated by the sharp changes in figure 5.4. Figure 8.14 shows the effects of force fluctuation on the K-FDSS and K-Speed. The drill bit break-through detection method based on a force derivative function proposed by Allotta *et al.* (1995) or FDSS with fixed threshold is especially prone to these changes, resulting in a premature detection of break-through. Using Kalman filter, however, a trend has been shown to be present for both the K-FDSS and K-Speed. The fluctuations of the FDSS, to a large extent, have been ironed out and this has allowed the threshold value of K-FDSS to be implemented, while the K-Speed profile has displayed a similar characteristic to a typical K-Speed profile shown earlier. Using the same previous thresholds of 0.03 N for the K-FDSS and 99.3% of the maximum value of the K-Speed, imminent drill bit break-through has been detected.

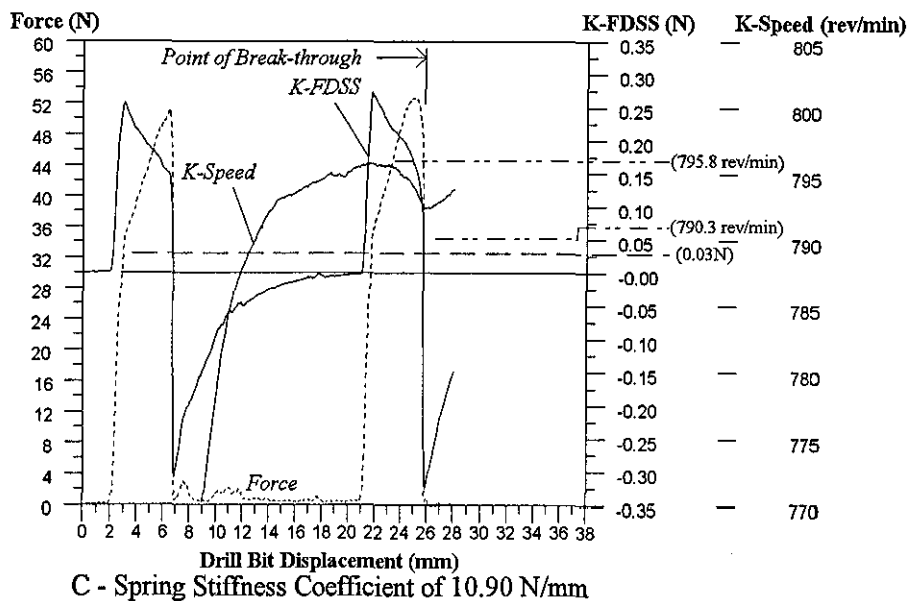
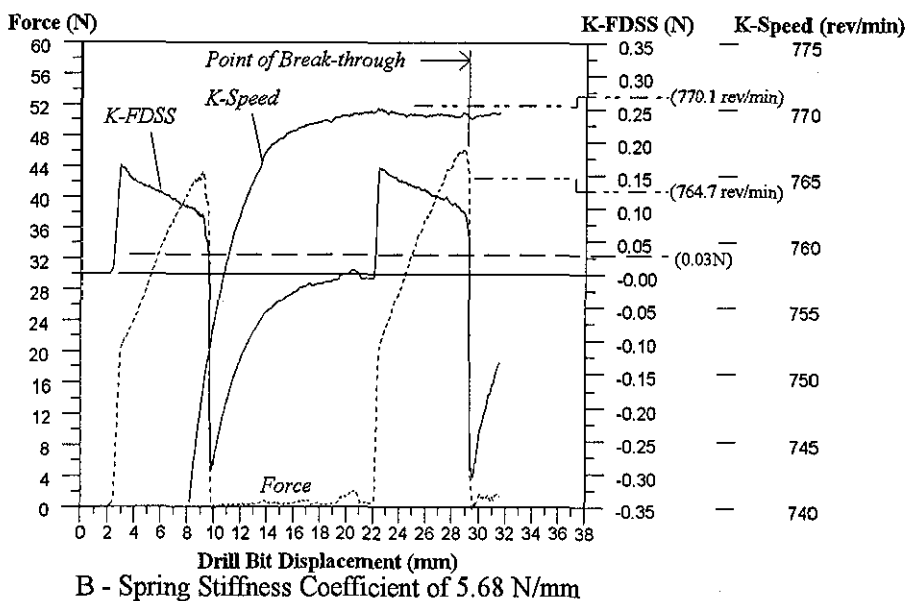
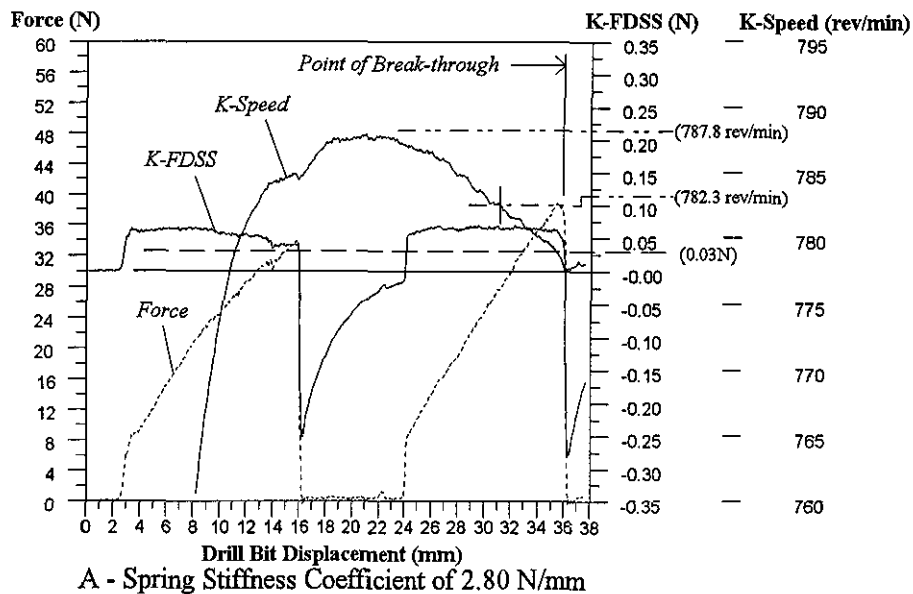


Fig. 8.11 Profiles of drilling force, Kalman processed FDSS (K-FDSS) and Kalman processed rotational speed (K-Speed) of a porcine femoral shaft at three system stiffnesses (Feed Rate = 90 mm/min; Rated Speed = 1000 rev/min)

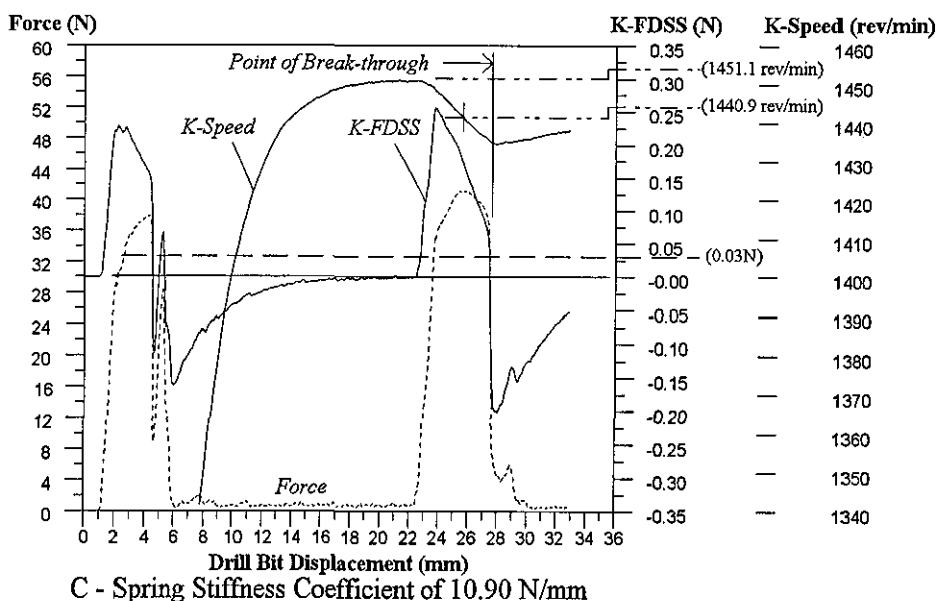
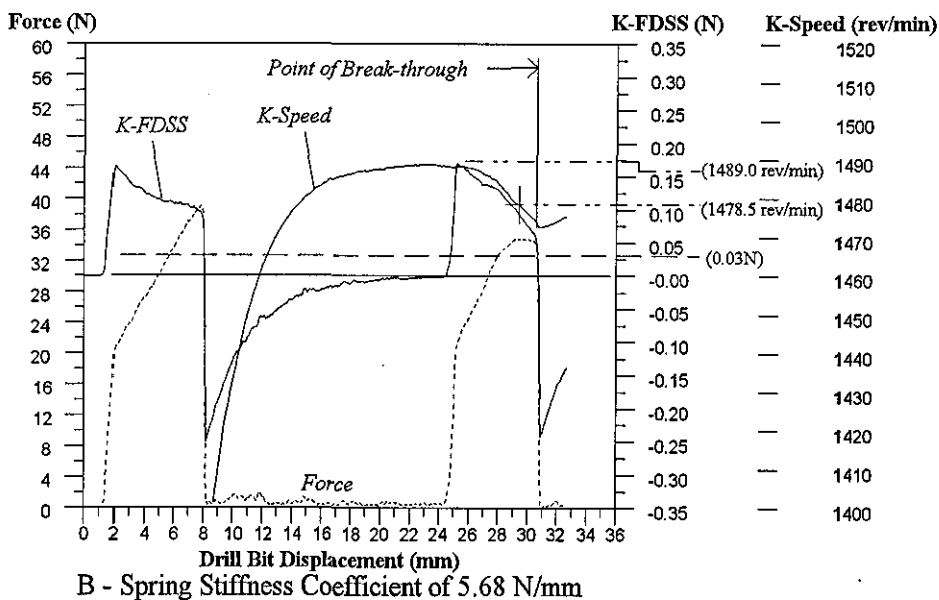
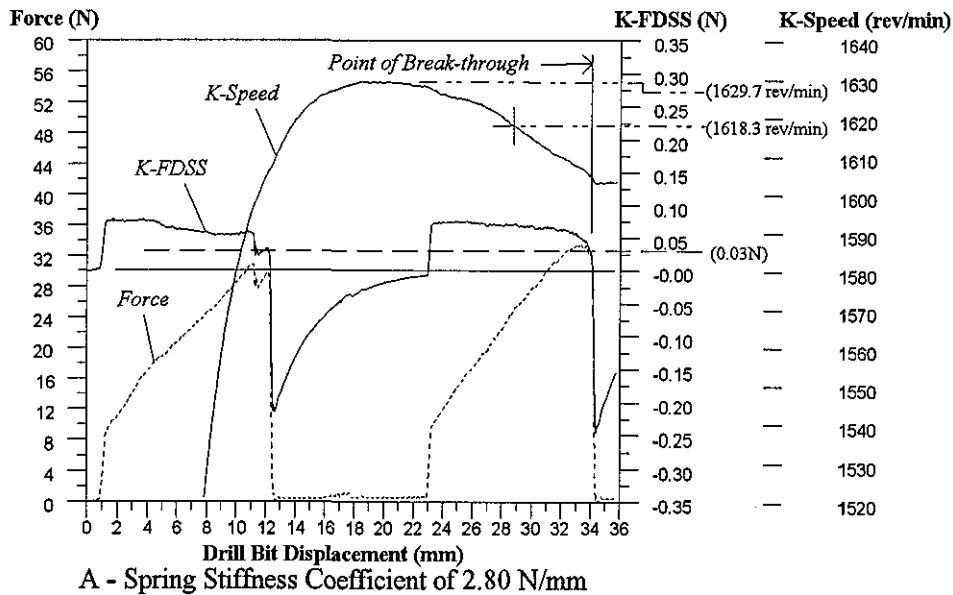
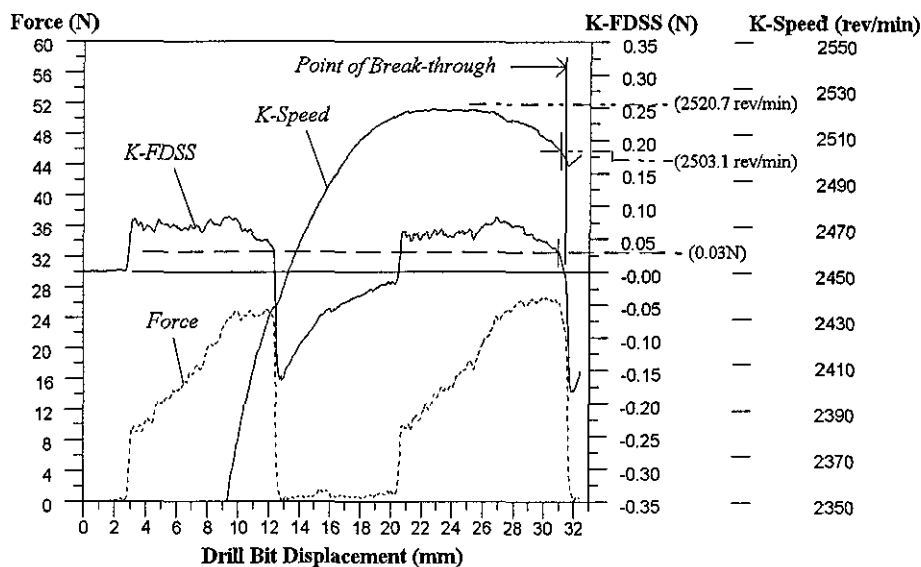
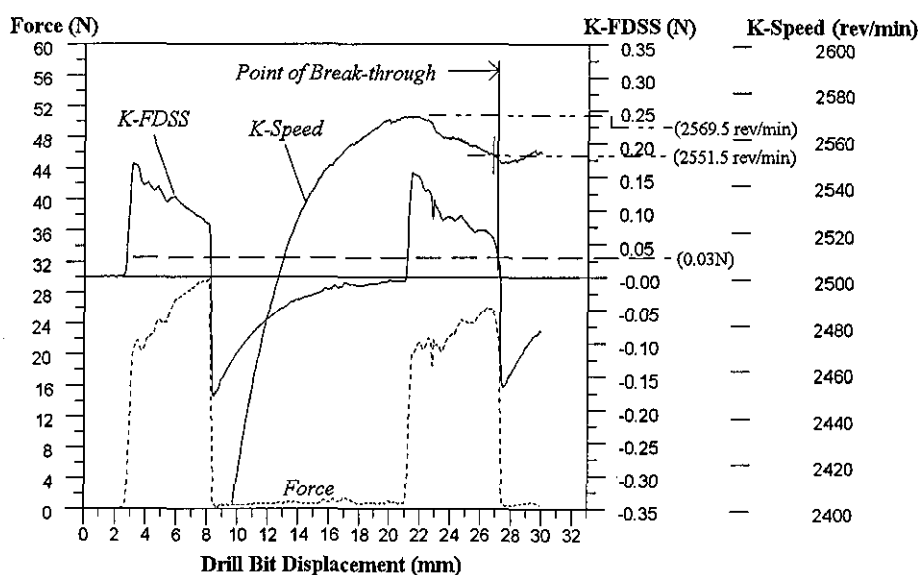


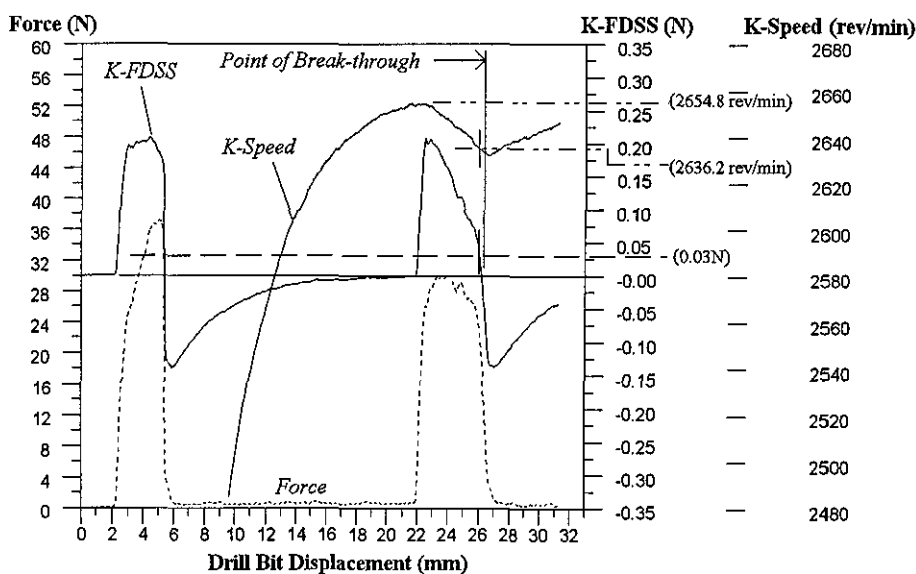
Fig. 8.12 Profiles of drilling force, Kalman processed FDSS (K-FDSS) and Kalman processed rotational speed (K-Speed) of a porcine femoral shaft at three system stiffnesses (Feed Rate = 90 mm/min; Rated Speed = 1900 rev/min)



A - Spring Stiffness Coefficient of 2.80 N/mm



B - Spring Stiffness Coefficient of 5.68 N/mm



C - Spring Stiffness Coefficient of 10.90 N/mm

Fig. 8.13 Profiles of drilling force, Kalman processed FDSS (K-FDSS) and Kalman processed rotational speed (K-Speed) of a porcine femoral shaft at three system stiffnesses (Feed Rate = 132 mm/min; Rated Speed = 3300 rev/min)

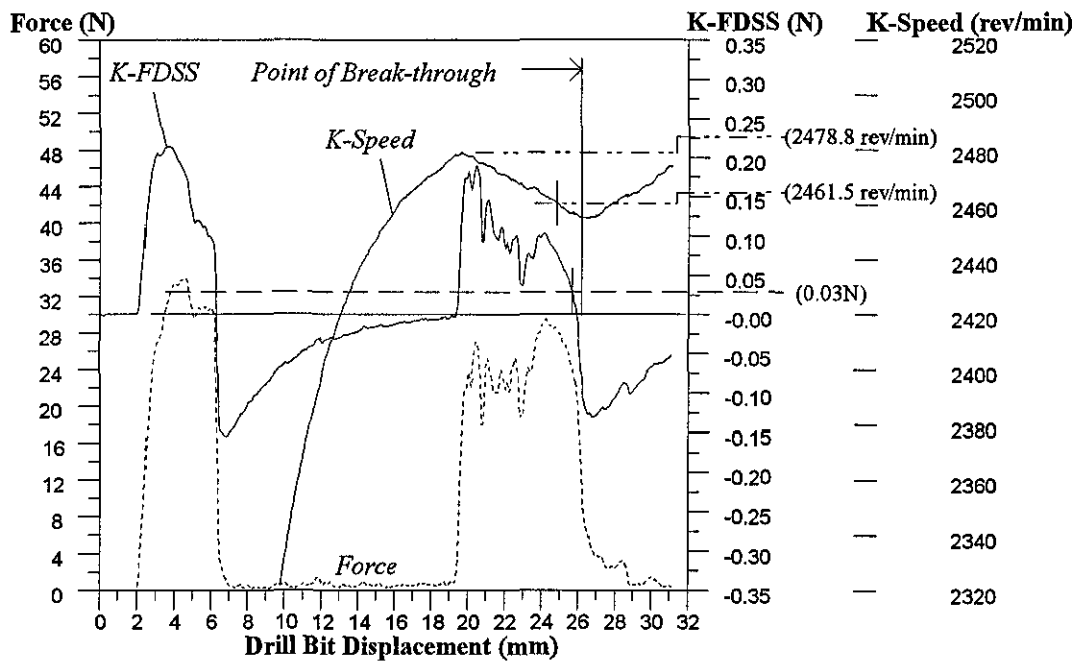


Fig. 8.14 Profiles of drilling force, Kalman processed FDSS (K-FDSS) and Kalman processed rotational speed (K-Speed) in the presence of inherent drilling force fluctuation for a stiff system (Feed Rate = 132 mm/min; Rated Speed = 3300 rev/min)

8.2.2 Kalman Filtered Results of a Surgical Drill Bit

Further verification of the proposed Kalman filter technique of drill bit break-through detection has been conducted using a surgical drill bit driven at three drilling conditions identical to the industrial drill bit. Figure 8.15 shows that the Kalman algorithm when applied to the surgical drill bit, at a feed rate of 90 mm/min and a rated speed of 1000 rev/min, produces similar patterns in the profiles of K-FDSS and K-Speed. A drop of K-FDSS to zero has also been shown to represent break-through for both the cortical walls. However, the magnitudes of maximum K-FDSS are generally lower as compared to those of an industrial drill bit. With same threshold setting of 0.03 N, the K-FDSS algorithm has successfully identified the imminent drill bit break-through. The performance of K-Speed, as expected, has not been as favourable especially at low rotational speeds (figure 8.15B). In certain cases, a higher value of threshold than 99.3% of the maximum K-Speed may be required (figure 8.15A). Nevertheless, the Kalman algorithm has been shown to be suitable for use on the surgical drill bit in predicting the imminent drill bit break-through.

Figures 8.16 and 8.17 show the consistent patterns of K-FDSS and K-Speed profiles for a feed rate of 90 mm/min at a rated speed of 1900 rev/min and for a feed rate of 132 mm/min at a

rated speed of 3300 rev/min respectively. The same K-FDSS threshold of 0.03 N has been found to apply for both drilling conditions in detecting imminent drill bit break-through. Although the K-Speed has shown a downward trend before break-through, the threshold setting of 99.3% of the maximum value has not had the same reliability in predicting break-through in advance as compared to the results obtained from an industrial drill bit. Setting to a higher threshold value than 99.3% would be appropriate for certain cases, otherwise it would prematurely detect the onset of drill bit break-through.

8.2.3 Discussion on the Application of a Modified Kalman Filter

The detection of drill bit break-through plays an important role in the enhancement of safety for systems associated with robotic/mechatronic assisted surgery in bone drilling. Without this feature, there is a risk of the drill bit protruding excessively from the exit of the bone which will cause damage to the surrounding tissue. The detection method using a modified Kalman filter can be applied to both types of drilling unit configuration, as mentioned in Section 5.2. The strategy proposed by Allotta *et al.* (1995) using a derivative function on the drilling force does detect the break-through to a certain extent when drilling into long bones. However, the appropriate threshold setting is unknown, and to set the threshold for the second wall based on the first cortical wall may not be reliable because the bone itself may vary in strength (structural density) and thickness. In addition, inherent force fluctuation further limits the capability of a derivative function in break-through detection as a result of premature break-through indication.

It can be observed that the force derivative profiles by Allotta *et al.* (1995) are relatively similar to the five-term averaged FDSS of this investigation. The second-order linear filter used by Allotta *et al.* (1995) for smoothing the force derivative has a larger bandwidth and allows a higher frequency range to pass through. When compared to the modified Kalman filter, the long time constant (as mentioned in Section 5.5) smoothes a large frequency range of the FDSS profiles and produces a more consistent profile. Therefore, the values of K-FDSS are lower than the five-term averaged FDSS values. Applying a shorter bandwidth to the second-order linear filter, in a similar way to a long time constant of the modified Kalman filter, would further smooth the force derivative. However, this would increase the phase lag of the filter and imminent drill bit break-through would not be indicated in time.

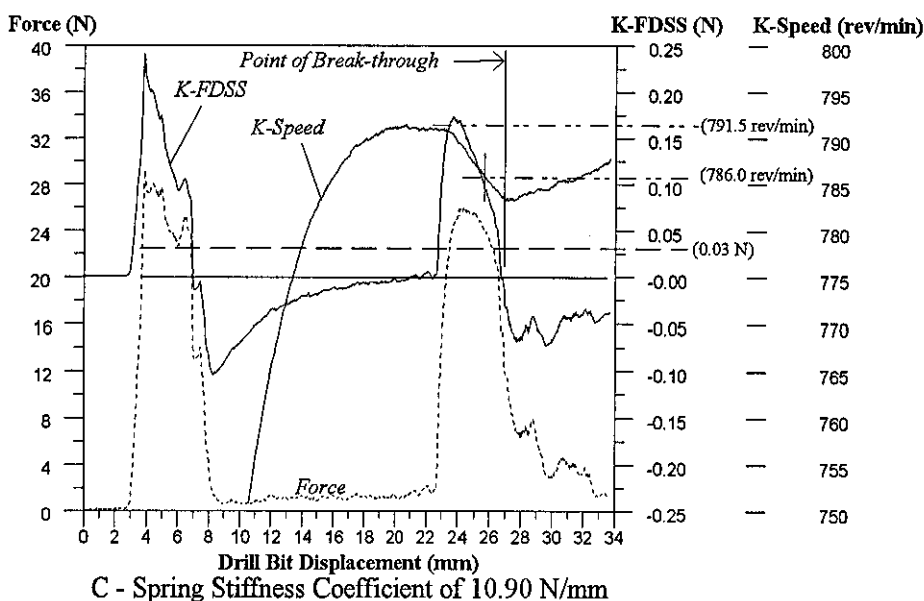
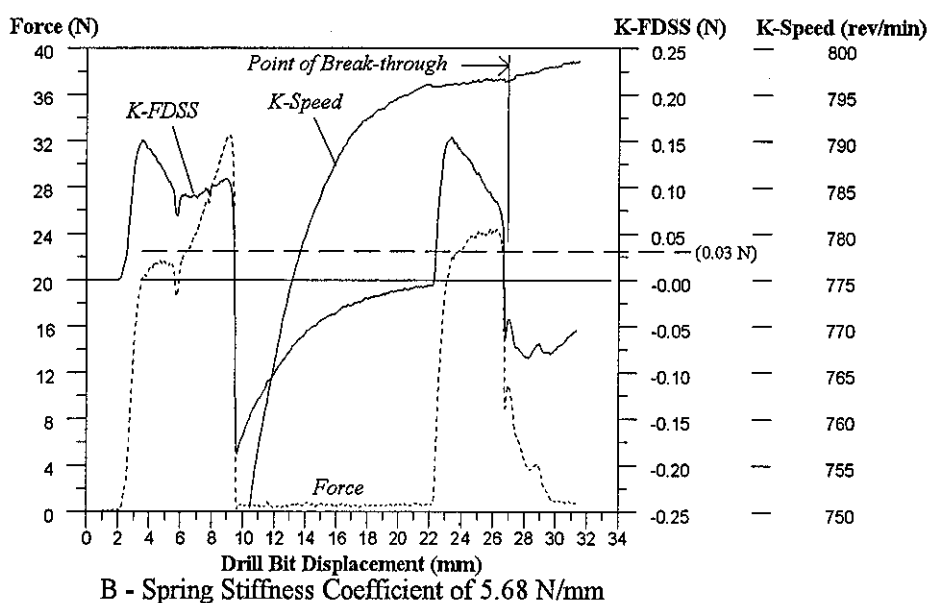
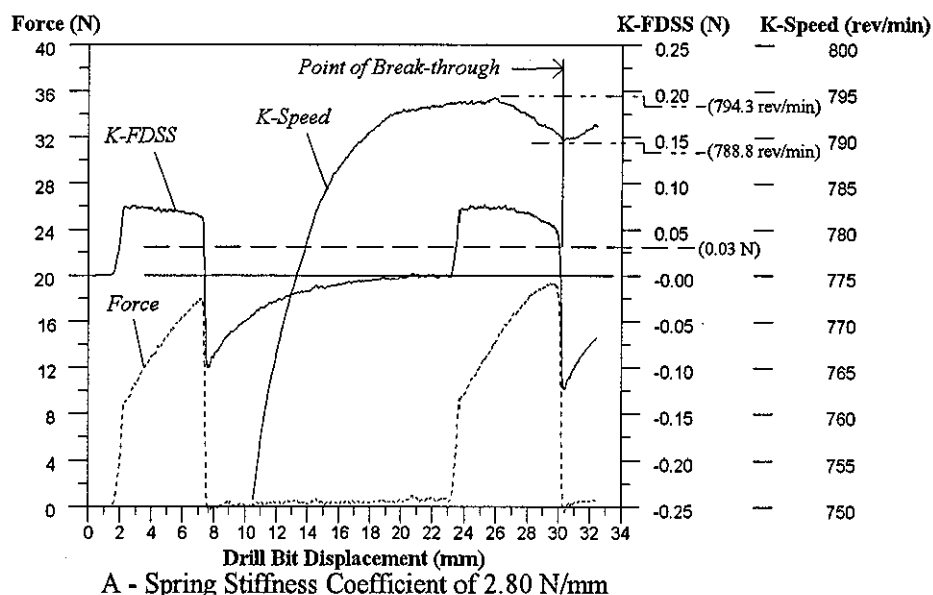


Fig. 8.15 Profiles of drilling force, Kalman processed FDSS (K-FDSS) and Kalman processed rotational speed (K-Speed) of a porcine femoral shaft at three system stiffnesses using a surgical drill bit (Feed Rate = 90 mm/min; Rated Speed = 1000 rev/min)

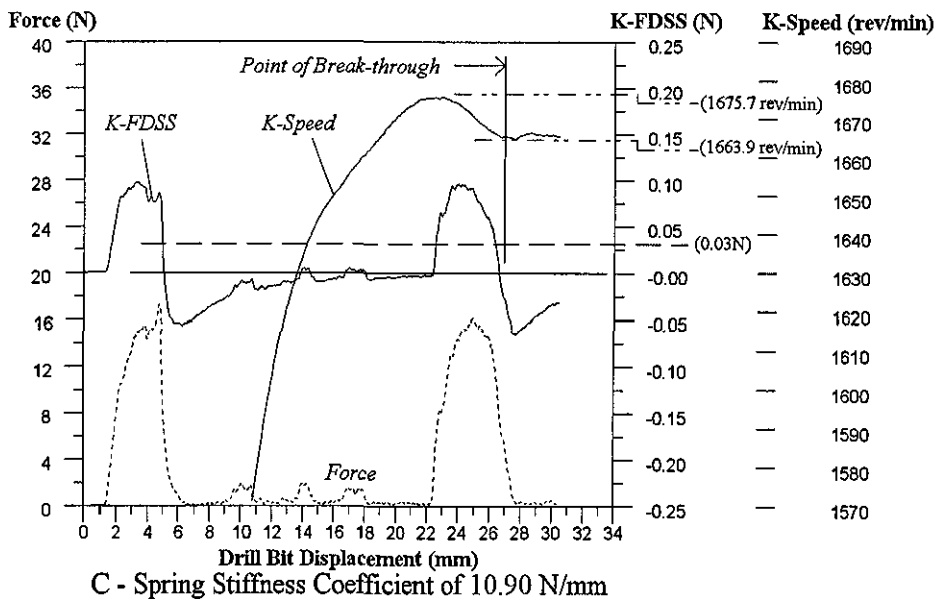
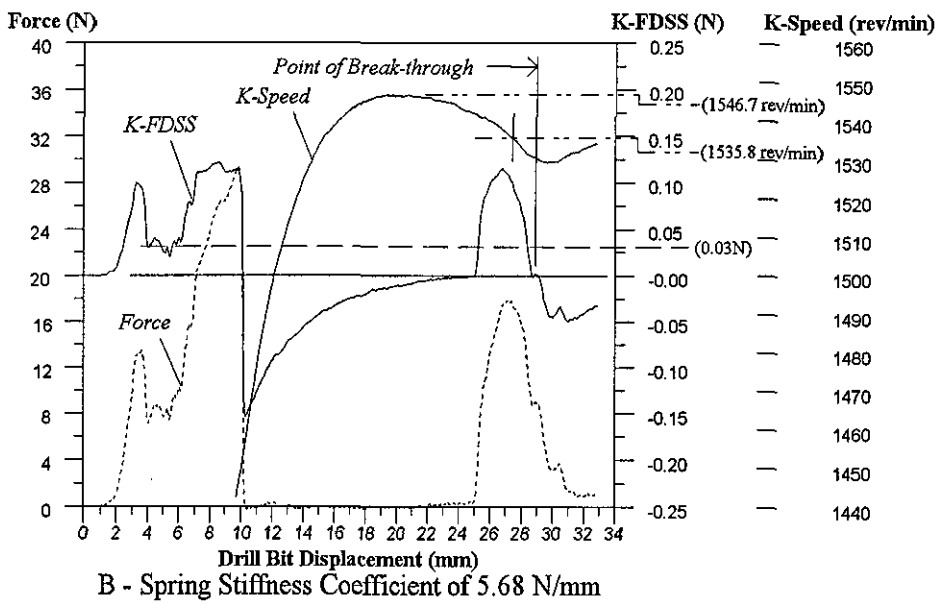
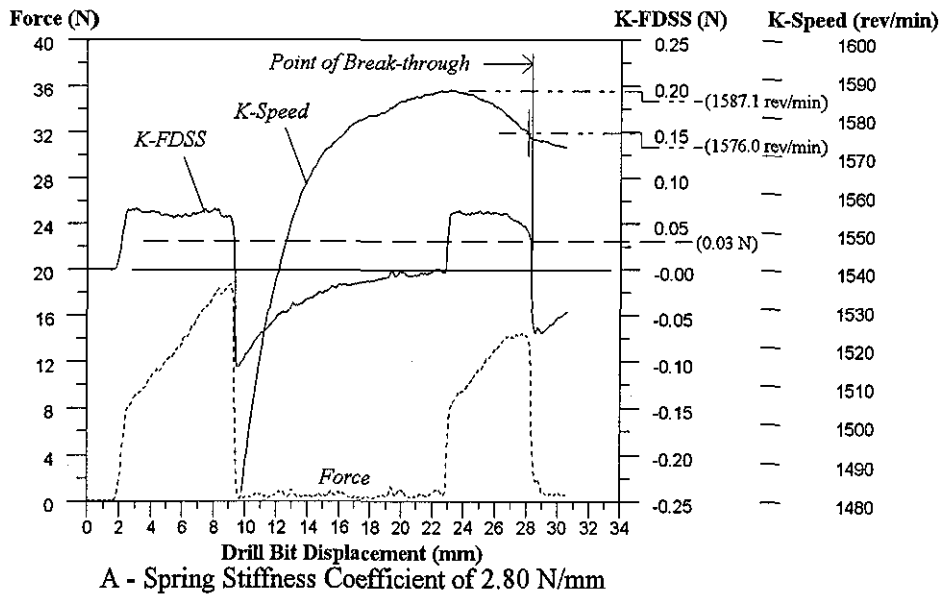


Fig. 8.16 Profiles of drilling force, Kalman processed FDSS (K-FDSS) and Kalman processed rotational speed (K-Speed) of a porcine femoral shaft at three system stiffnesses using a surgical drill bit (Feed Rate = 90 mm/min; Rated Speed = 1900 rev/min)

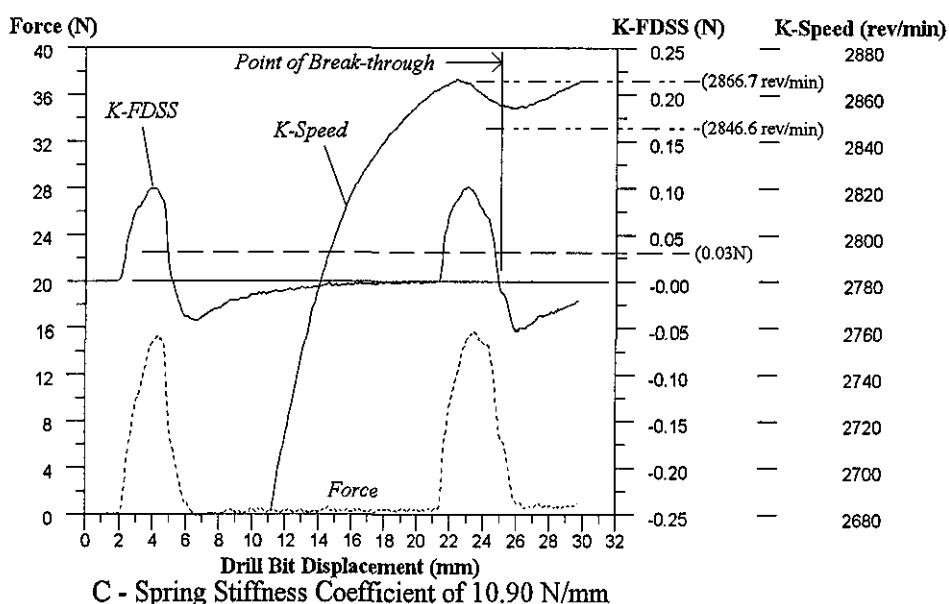
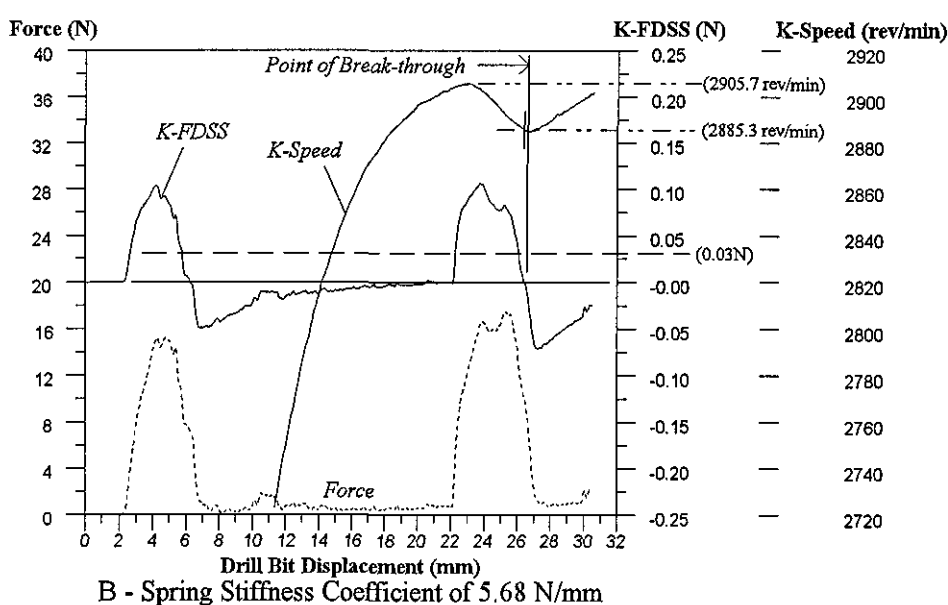
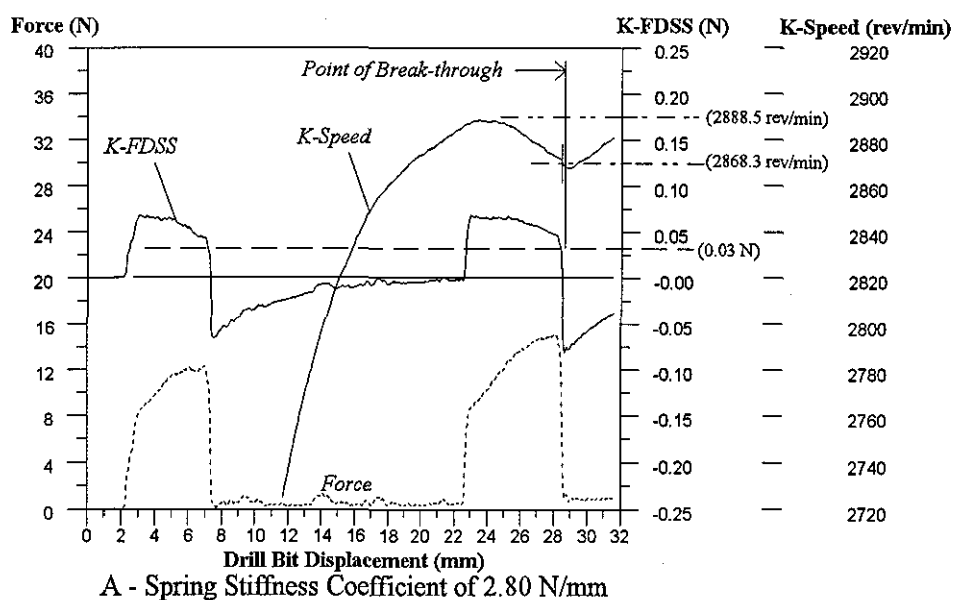


Fig. 8.17 Profiles of drilling force, Kalman processed FDSS (K-FDSS) and Kalman processed rotational speed (K-Speed) of a porcine femoral shaft at three system stiffnesses using a surgical drill bit (Feed Rate = 132 mm/min; Rated Speed = 3300 rev/min)

When compared to the drilling force, measurement of rotational speed has been shown to have more fluctuations in a similar way to the measurement of torque presented by Allotta *et al.* (1995). Brett *et al.* (1995) monitored both the force and the torque, and used a method of identifying persistent reduction in force and increase in torque over six sample periods in order to predict the onset of drill bit break-through of the stapes footplate. It is often not reliable to depend on a number of samples to register the desired characteristic because the general trend may be affected by rogue data, for example, when data is affected by noise. As a result, the sample window may not be able to provide a representative trend and the consequence of ignoring this fact could be critical. In addition, the sample window is also affected by fluctuations of the force and torque profiles caused by changes in bone structural density particularly when these fluctuations remain over the number of samples chosen.

In bone, or other similar materials, the drilling force depends on the penetration rate, as well as other factors such as drill bit geometry, drill bit sharpness and rotational speed. The penetration rate is directly dependent on the drill bit feed rate and the stiffness of the system. In general, system compliance has the effect of reducing the penetration rate and thus results in low drilling force magnitudes. At low system stiffness, however, there is a spring-back effect as soon as break-through occurs. This may result in excessive drill bit protrusion at break-through and cause tissue damage. An early and robust detection of break-through is therefore necessary.

The use of a Kalman filter on both the FDSS and the rotational speed has been very effective in overcoming the difficulties presented by the derivative function and the sample window. It has produced a simple, robust and repeatable technique for the detection of drill bit break-through which can be applied for both the industrial and surgical drill bits. Although the FDSS and the drill bit rotational speed profiles are greatly influenced by both the system compliance and inherent fluctuation of the drilling force, it is possible to generate easily recognisable and more consistent profiles with a Kalman filter. Unlike K-FDSS, the use of K-Speed for break-through detection is only applicable at higher rotational speeds than 1000 rev/min. Furthermore, the Kalman filter is potentially applicable to the torque measurement which shares similarity to the rotational speed in order to establish torque trends.

The Kalman filter irons out major fluctuations, especially force fluctuation caused by changes in the bone structural density, and creates a trend which can be implemented easily and safely in

real-time in break-through detection algorithms. The threshold setting for the Kalman filter is also easy to implement and it is applicable to different types of drill bits and over a wide range of drilling conditions. Early detection of break-through can be achieved by setting an appropriate threshold for K-FDSS above the value of 0.00 N, and for K-Speed, a threshold based on a ratio or percentage of the maximum value of K-Speed. In order to enhance the reliability of detecting imminent drill bit break-through, different levels of threshold setting have been applied to K-FDSS profile in a control strategy presented in the following section. One of the threshold levels is based on the magnitude of maximum K-FDSS.

8.3 Control Strategy for the Detection of Drill Bit Break-through

The control strategy for the detection of imminent drill bit break-through is based on the profiles of K-FDSS generated by the drilling forces. As stated earlier, a K-FDSS threshold value of 0.00 N can, in general, be used for the detection of drill bit break-through. The setting of a higher K-FDSS threshold to 0.03 N allows an early indication of imminent drill bit break-through. In normal cases, there will be four occasions when the K-FDSS goes through the threshold, upon entry and imminent exit of both cortical walls of the bone. However, a more robust control strategy is required when the profiles of K-FDSS are affected by the fluctuation of the drilling forces at the first cortical wall, as shown in figures 8.12A, 8.12C and 8.16B. In these cases, the K-FDSS profiles have been found to breach the threshold value of 0.03 N more than four times.

In order to implement an effective control strategy, it has been found that three levels of threshold for the K-FDSS are needed. The three levels are 0.00 N, 0.03 N and a maximum threshold (Max-TH) which is a proportion of the maximum K-FDSS value of the first cortical wall. For example, a factor of 0.6 of the maximum K-FDSS value from the first cortical wall can safely be used as the Max-TH, since the fluctuation of K-FDSS at the first cortical wall, after going through the K-FDSS threshold of 0.00 N, has been found to be less than half the maximum K-FDSS value. The values of K-FDSS are continuously monitored to obtain the maximum K-FDSS value for the first cortical wall. This maximum value is subsequently used to set the Max-TH for the detection of entry to the second cortical wall. The flow diagram of the control strategy for the detection of imminent drill bit break-through is presented in figure 8.18.

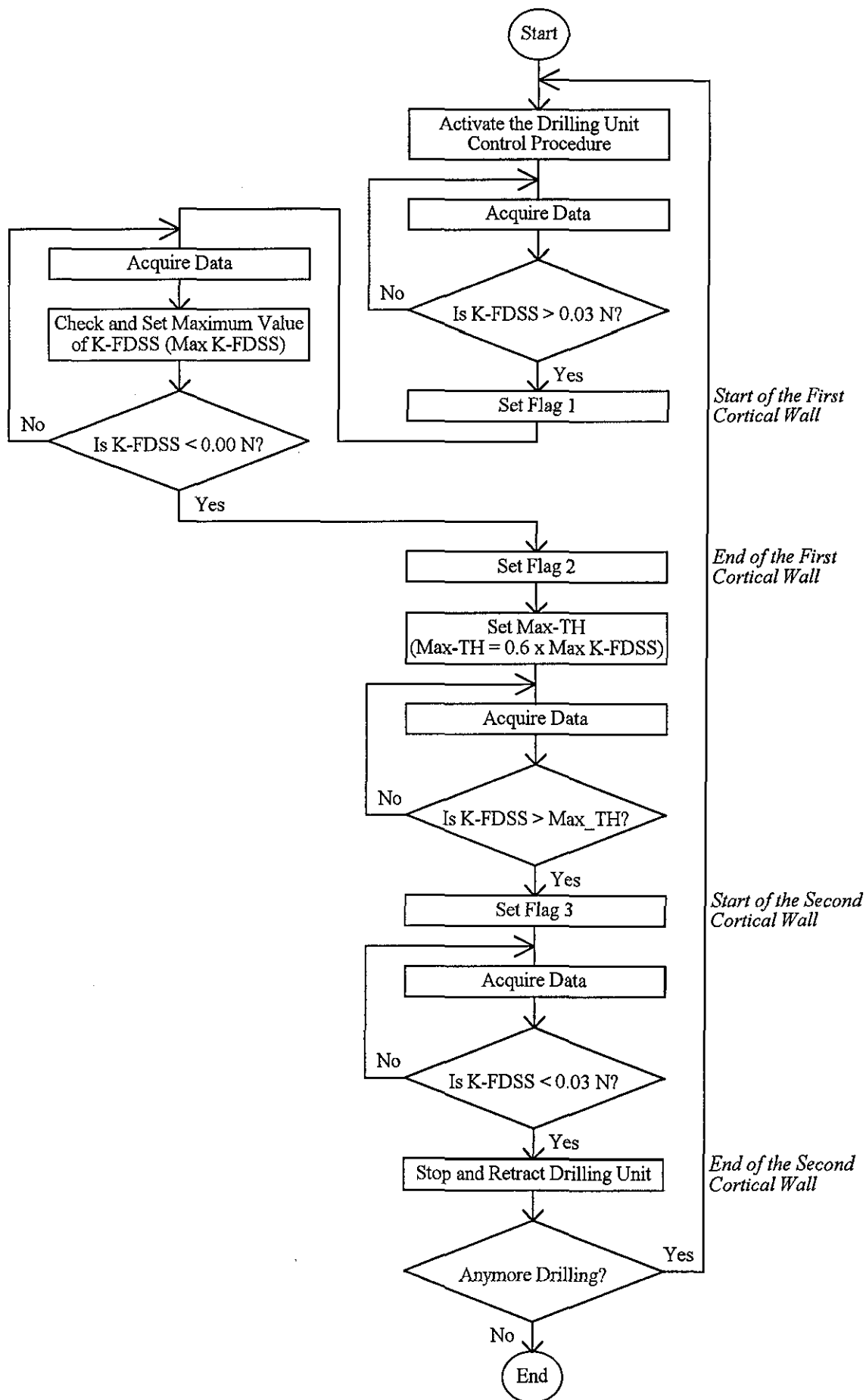


Fig. 8.18 Flow chart of the control strategy for detection of imminent drill bit break-through

In the control strategy, the first cortical wall is identified by the first two flags, as shown in figure 8.19, through the K-FDSS thresholds of 0.03 N and 0.00 N respectively. This figure is with reference to figure 8.12C. The indication of drill bit entering the second cortical wall depends on the Max-TH based on the maximum K-FDSS value in the first cortical wall. In this case, the Max-TH is set to 0.137 N (i.e. 0.229×0.6). Since the Max-TH is higher than the maximum K-FDSS fluctuation of 0.065 N at the first cortical wall, the third flag will not be triggered until the drill bit enters the second cortical wall. Finally, the imminent break-through is safely detected when the K-FDSS profile falls below 0.03 N.

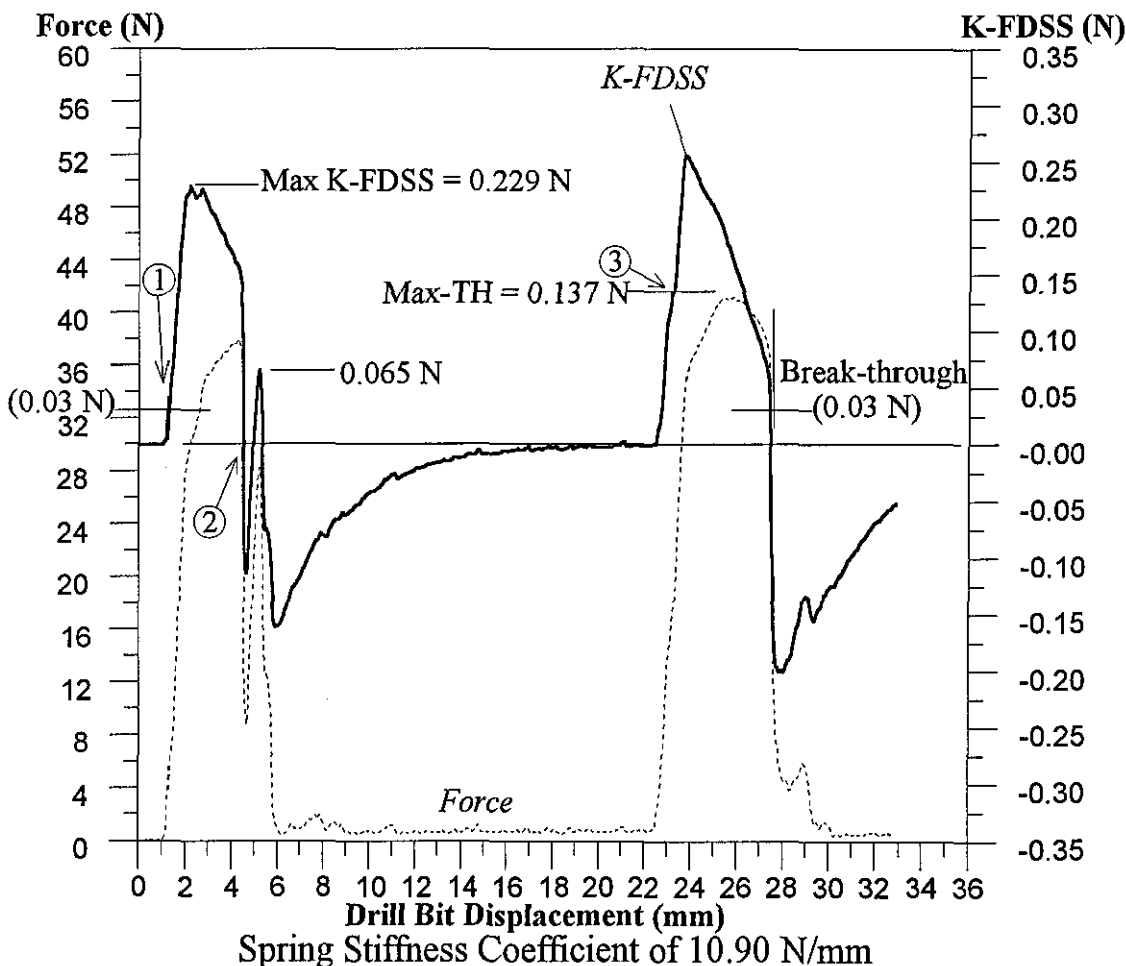


Fig. 8.19 Setting of flags according to three levels of threshold for K-FDSS and the detection of imminent drill bit break-through (with reference to figure 8.12C)

The control strategy requires only the drilling force information to carry out the detection of drill bit break-through. Unlike Brett *et al.* (1995) and Allotta *et al.* (1995), this method does not depend on the specific cutting energy required to drill the cortical bone. Furthermore, the K-FDSS, to a certain extent, smoothes out major fluctuations in the drilling forces.

CHAPTER 9

RESULTS AND DISCUSSION: THE EVALUATION OF BONE STRENGTH

This chapter presents the results obtained from bone drilling experiments and densitometric measurements of BMD and provides a discussion of the results with regards to the evaluation of bone strength. Densitometric measurements are taken in the anterior-posterior (AP) direction, and therefore, bone drilling is carried out in this direction, in the first instance, in order to correlate drilling force and BMD. However, as bone drilling of the proximal femur is usually performed along the cervical axis, drilling forces along this direction are also correlated with BMD. The results are presented in two sections based on the direction of drilling, namely the AP and the cervical axis directions. The actual bone drilling forces, based on a feed rate of 90 mm/min and a rated drill bit rotational speed of 1000 rev/min, were obtained using the experimental set-up of a stiff system. An industrial twist drill bit of diameter 2.5 mm was used in the experiments. In order to show the relationship between average drilling forces and BMDs, linear regression with coefficient of correlation is used.

9.1 Correlation in the Direction of Anterior-Posterior

In the experiments, the correlation in the anterior-posterior (AP) direction between BMD and average drilling force involves the proximal femur, which includes the greater trochanter and the femoral head, and the femoral shaft.

9.1.1 Correlation at the Proximal Femur

Significant linear relationships, shown in figure 9.1, have been found between the average drilling forces and the BMDs in the AP direction at both the femoral head and the greater trochanter sites, the trajectories of which are shown in figure 7.10b. The BMD measurements

at these sites, of a porcine proximal femur, can be found in Appendix 7.1. It should be noted that the anterior-posterior direction of a porcine femur is the reverse of a human one. However, this has no effect on the present experimental investigation. The average drilling forces are calculated from the first peak at the start of drilling to the last peak just before drill bit breakthrough. Three porcine bones were used in this investigation.

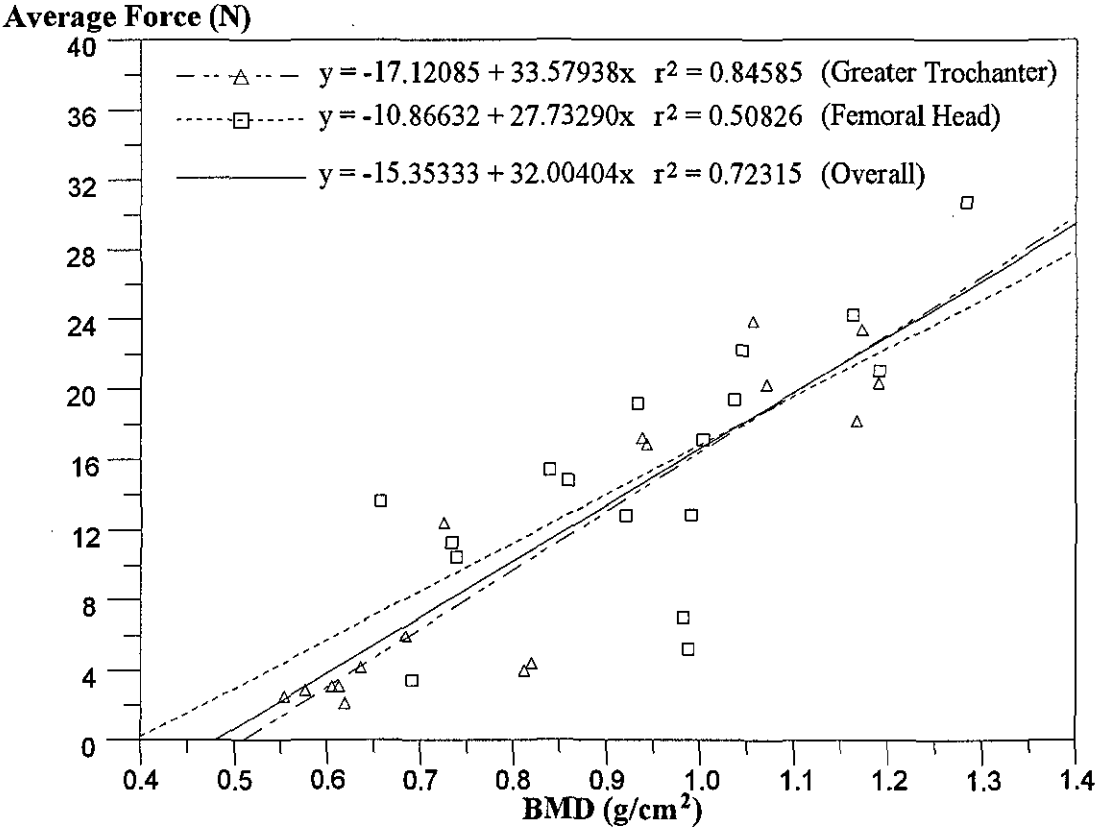


Fig. 9.1 Linear regression between average drilling forces and BMDs in the anterior-posterior direction of porcine proximal femurs

The results show that the trochanteric site produces better linear correlation with high correlation coefficient ($r^2 = 0.85$) as compared to the femoral head ($r^2 = 0.51$). There is also a difference between the slope of the relationships which may be due to the regional difference in the orientation or the structure of the trabeculae. The combination of the two sets of data shows a linear correlation with a good correlation coefficient ($r^2 = 0.72$). The use of bone thickness to obtain BMD in g/cm^3 has not been found to improve the overall correlation. Although there has been a limited number of measurements, the correlations clearly show the existence of a trend related to the evaluation of bone strength. However, the difficulty in matching the centre of a hole and the ROI may have introduced errors to the correlation.

Although the drilling forces along the drilling trajectories show a large variation, in the majority of cases, maximum forces occur at the medial-posterior (near the end of drilling) region of the trajectory. This is shown by measurements of drilling forces, which are taken at boxed locations 1 to 6 shown by the x-ray image in figure 9.2, at the femoral head and the greater trochanter. The three drilling trajectories along the cervical axis shown in figure 9.2 are used as references for matching ROIs, and therefore, should be ignored. The drilling force profiles at these locations are presented in figures 9.3 and 9.4 respectively.

It must be noted that a component of the measured drilling force is a frictional force. The amount of friction between the drill bit and the bone was found to be relatively small, at an average of approximately 0.3 N at the maximum depth of drilling. The frictional forces were obtained by advancing the drill bit into the drilled hole. Since the bone is an elastic material, some of the deformation around the drilled hole will recover sufficiently and cause friction. When drilling was performed in the reverse, i.e. PA (posterior-anterior) direction, the maximum forces for a number of cases were found to be located around the region of the medial-anterior (near the end of drilling). This characteristic is opposite to the results obtained when drilling in the AP direction. There are several factors that may help to explain this peculiar characteristic of the force profile.

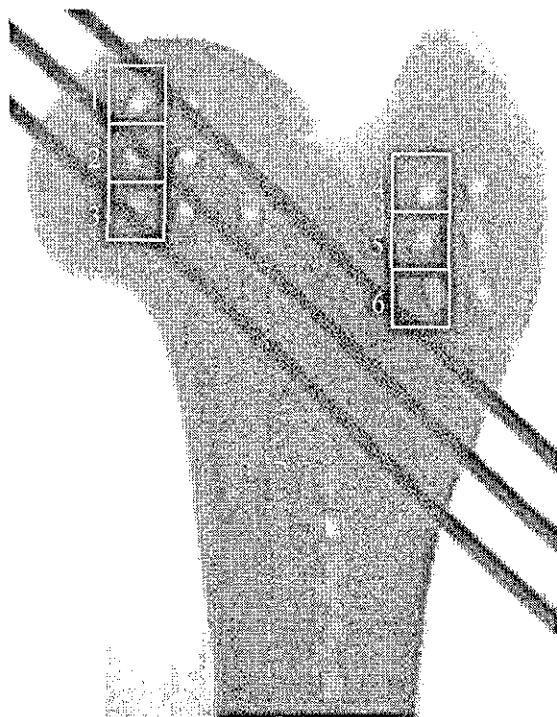


Fig. 9.2 Locations of the AP drilling trajectory at the greater trochanter and the femoral head

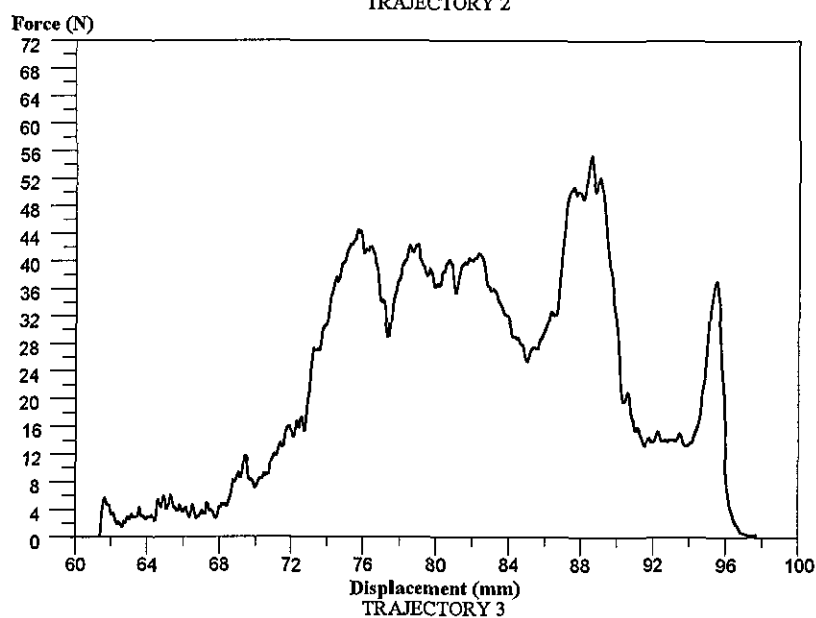
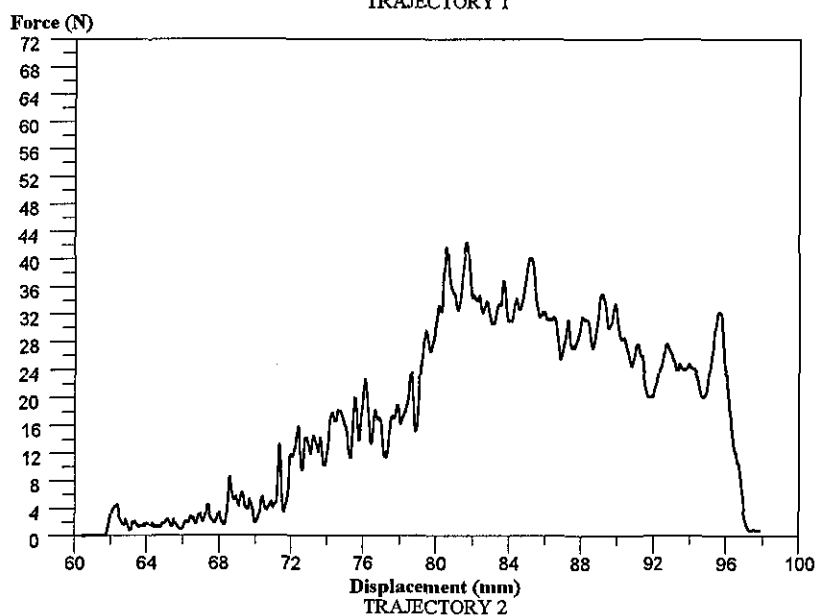
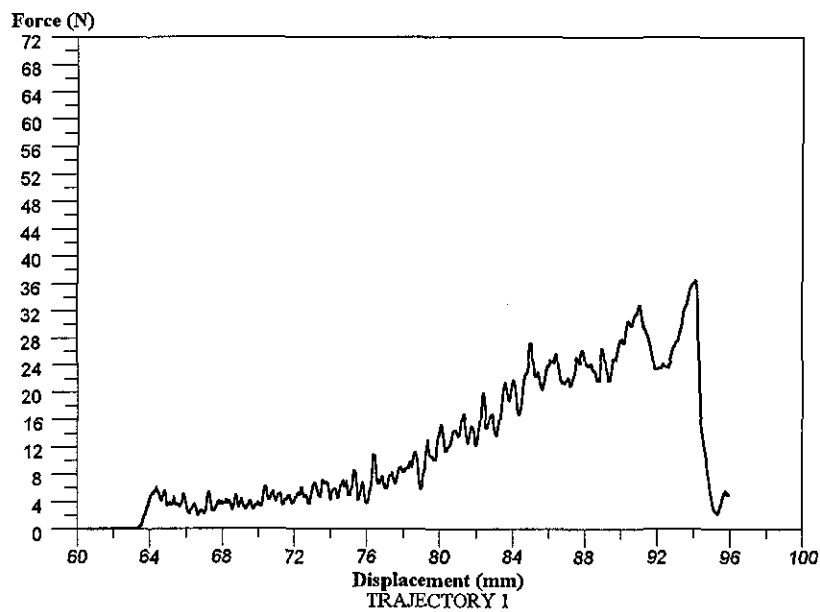


Fig. 9.3 Profiles of drilling forces at the femoral head in the AP direction

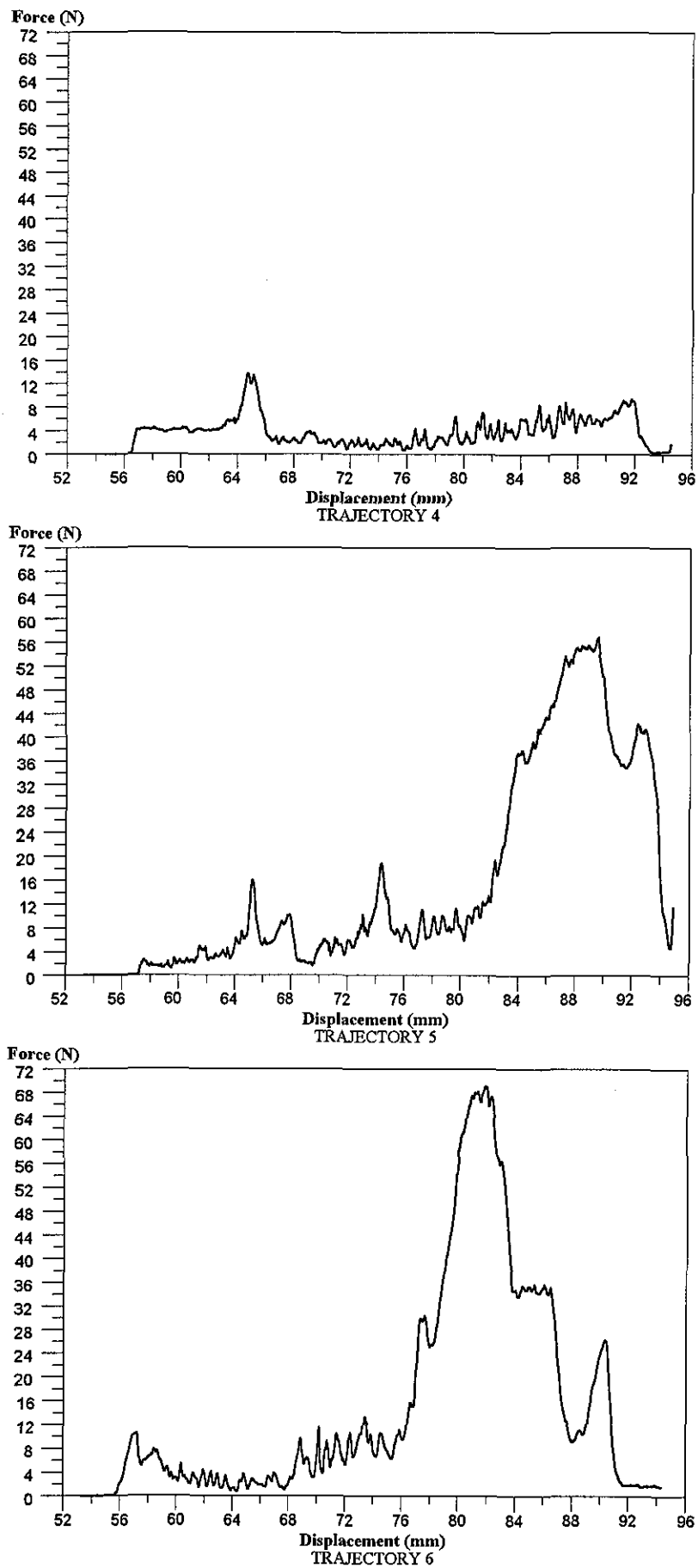


Fig. 9.4 Profiles of drilling forces at the greater trochanter in the AP direction

One of the contributing factors may be the tendency of clogging of the drill bit as a result of the large ratio between the drilling depth and the drill bit diameter. Wiggins and Malkin (1976) reported that, when drilling into the cortical bone using an industrial drill bit, an increase in both the torque and the specific cutting energy is associated with increasing depth of drilling. In general, the effect of clogging may have been indicated by a small reduction in the drill bit rotational speed. Another possible explanation relates to the influence of blood pressure during drilling which is not taken into consideration. In rock mechanics, fluid pressure in the pores affects the rate of drilling and the compressive strength of rocks (Karalis & Galanos, 1982). During the drilling experiments in this study, blood was seen flowing out from minute pores to the bone surface. This is a possible consequence of either the blood boiling due to the heat generated, or the increase in blood pressure due to drilling or both. The method of clamping, which was in the direction of drilling, may also have introduced additional compressive stresses and altered the trabecular structure.

The overall correlation between the average drilling force and the BMD has been found to be comparable or better than to those reported between osteopenetration strength and densitometric measurements using computed tomography (QCT) (Bentzen *et al.*, 1987). The osteopenetration tests and QCT measurements were obtained from the cancellous bone of human proximal tibiae. Although the proximal tibia consists mainly of cancellous bone, the structural organisation is not as complex as in the proximal femur. Another investigation carried out by Petersen *et al.* (1996) has found that both the BMD measurements by DPA and DXA had linear relationships of a high correlation coefficient with the osteopenetration strength. Although the latter correlation is better than the overall correlation of this study, osteopenetration is not a common procedure in orthopaedic surgery as compared to bone drilling. These findings reinforce the preferred usage of DXA over QCT in the evaluation of bone strength (Petersen *et al.*, 1996).

9.1.2 Correlation at the Femoral Shaft

The linear relationship between the average drilling force and the BMD at the femoral shaft has been found to be moderate, as shown in figure 9.5. The variation of the force and the BMD is relatively small in the cortical bone. In addition, the BMD measurements, which are presented

in Appendix 7.2, may have been underestimated due to the presence of yellow marrow (fat) in the medullary cavity. The average drilling forces are calculated from the drilling forces at both cortical walls only since the forces at the medullary cavity are considered to be zero. The average force at the femoral shaft has been found to be higher by a level of approximately 25 N for a given BMD when compared to the proximal femur. This finding indicates that the drilling forces of the cortical bone are not applicable to the cancellous bone and *vice-versa*.

The moderate correlation obtained at the femoral shaft may be due to a smaller number of samples used as compared to the number of samples at the proximal femur. This is further compounded by the limited range of spread of both drilling forces and BMD measurements, since cortical bone from porcine femurs of the same age has a more consistent strength and BMD compared to cancellous bone. In order to improve the correlation between BMDs and drilling forces, different age bones of the same species or bones of different species have to be used.

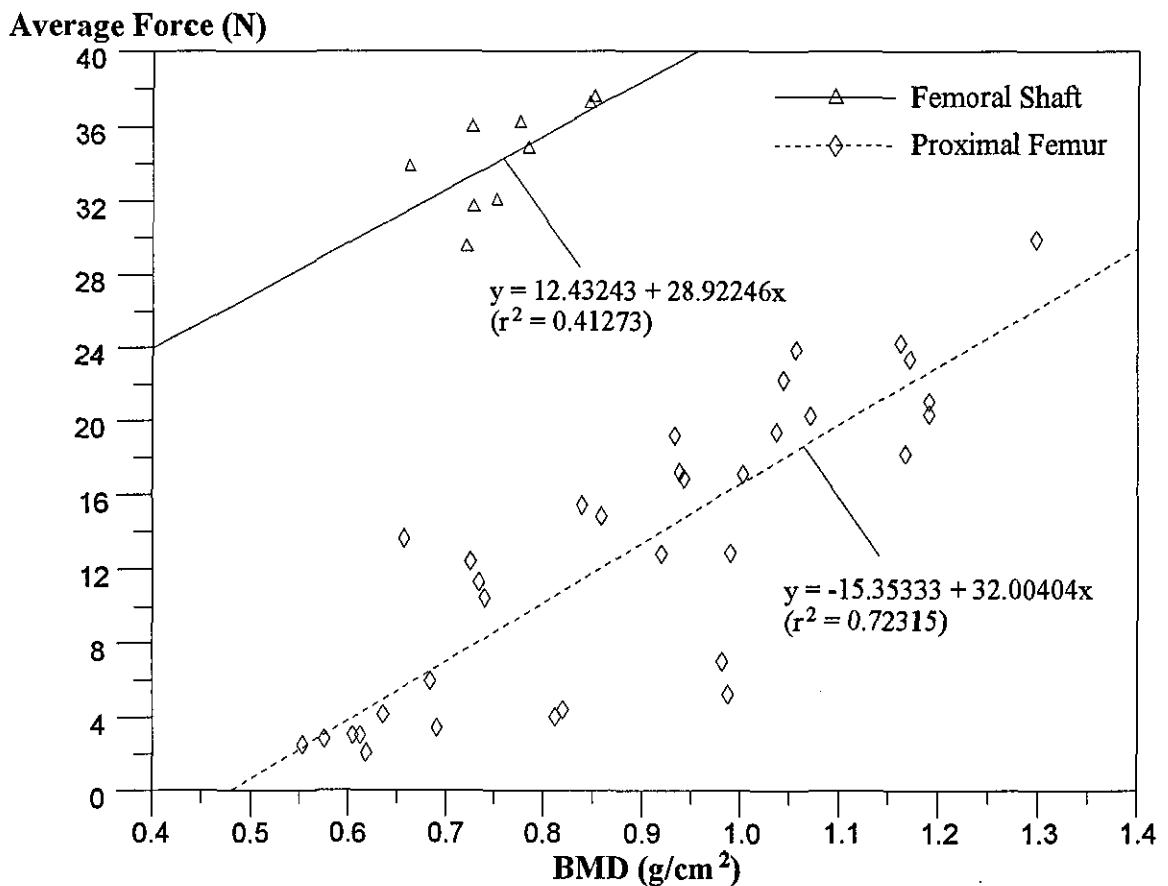


Fig. 9.5 Linear regression between average drilling forces and BMDs in the drilling direction of anterior-posterior at the femoral shaft with reference to the proximal femur

9.2 Correlation in the Direction of the Cervical Axis

This section presents profiles of the BMD and of the average drilling force with respect to the regions of interest (ROIs) as well as the correlation between these two types of measurements. The relevance of the bone thickness with respect to the ROI of BMD is also discussed in this correlation.

9.2.1 Profiles of the BMD

The levels of BMD of a porcine proximal femur at the ROIs located superior to (above), inferior to (below) and on the cervical axis, as indicated in figure 7.10a, have been found to be different. Typical profiles of the BMD are shown in figure 9.6, which includes an indication of regions of the proximal femur corresponding to the ROIs. The BMD measurements along the cervical axis of a porcine proximal femur can be found in Appendix 7.3. At the superior section to the cervical axis, the BMDs around the inter-trochanteric region have been found to be high, or the highest, in certain cases. Among the lowest of all BMDs were obtained from ROIs around the regions of the femoral neck.

The BMDs in the inter-trochanteric region of the cervical axis (medial) have been found to be high, which is similar to those at superior section of the same region. The BMDs are at the lowest in the region of the femoral neck. After this region, the BMD increases to the highest at ROIs around the centre of the femoral head before it decreases near the edge of the femoral head.

The BMDs at the inter-trochanteric region up to the subcapital femoral neck region of the inferior section have been found to be the lowest when compared to the two previous sections. In the centre of the femoral head region, the BMDs are at their highest and the profile of BMD is similar to the BMD profile at the cervical axis section.

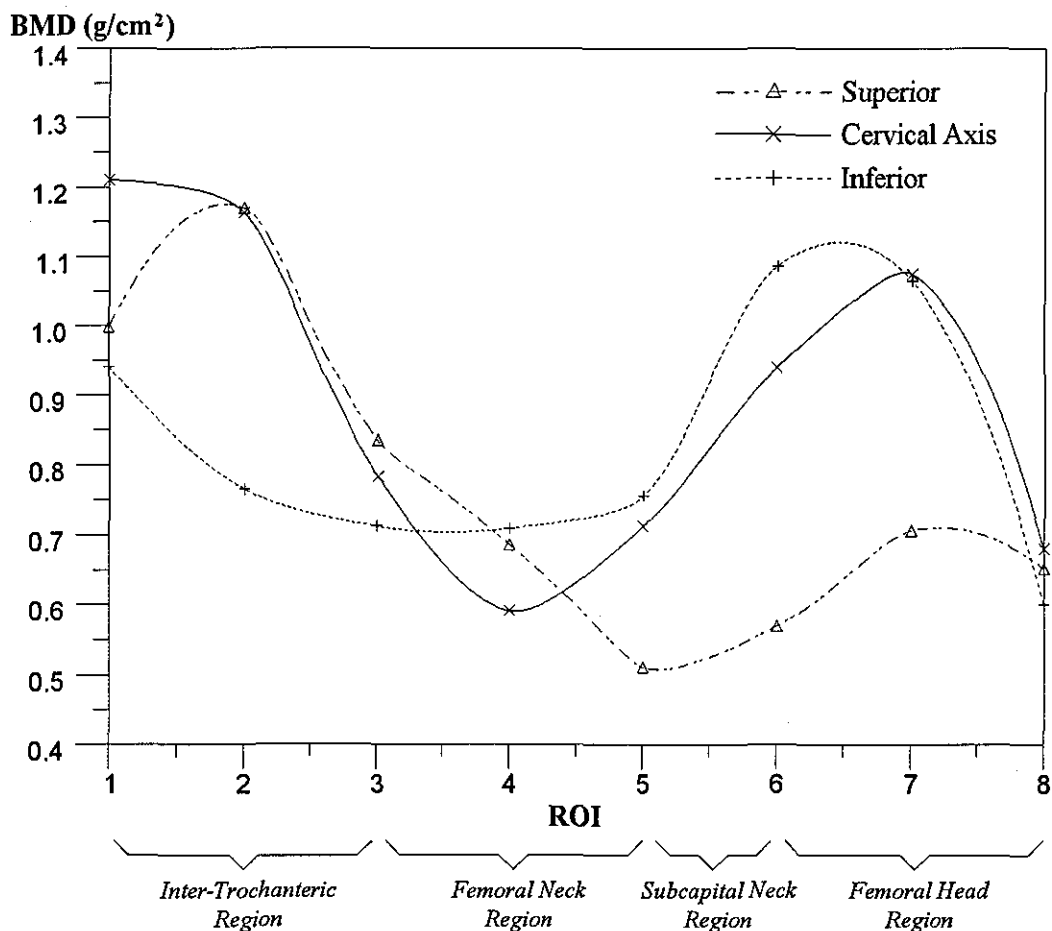
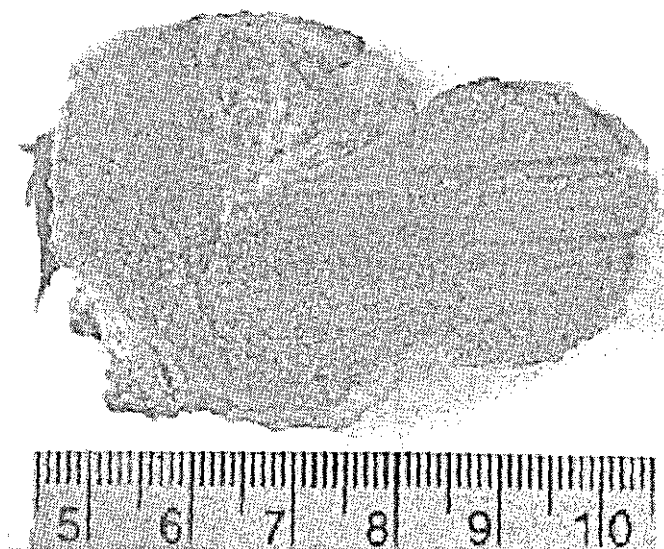


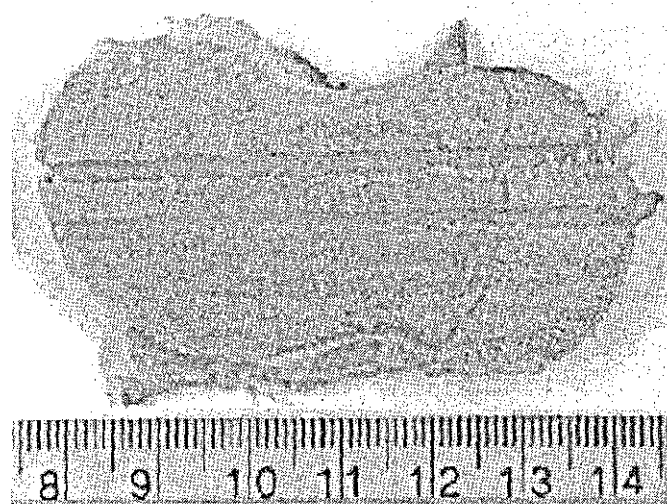
Fig. 9.6 Typical profiles of BMDs with respect to ROIs as indicated in figure 7.10a

The inclusion of the bone thickness, shown in figure 9.7, to obtain BMD in g/cm^3 at the same ROIs as those in figure 9.6 has produced different BMD profiles. Figure 9.8 shows the new BMD profiles. The inclusion of bone thickness allows for the variation of the cross-sectional geometry of the proximal femur to be considered. A notable change can be seen in the regions of the inter-trochanter and the femoral neck from the superior section to the cervical axis. The significance of including the bone thickness lies in the correlation between the BMD and the average drilling force in the direction of the cervical axis, as discussed in Section 9.2.3.

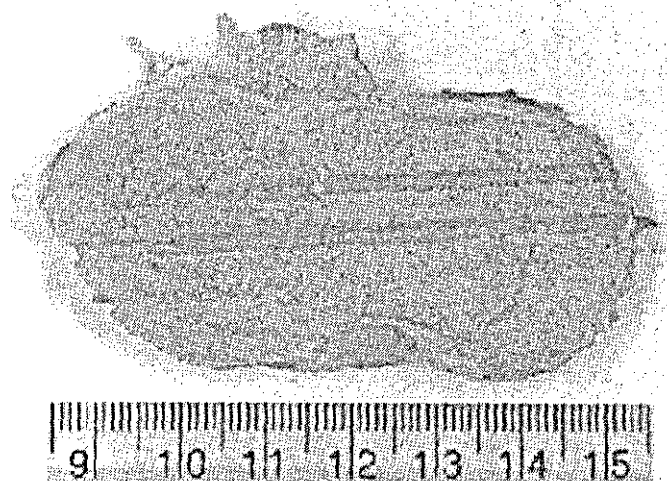
The results show that the differences in the BMD represent a variation in the bone strength of the proximal femur. The section between the cervical axis and the inferior is shown to be the most reliable section in producing a consistent BMD profile. In the extreme superior and inferior sections to the cervical axis, the BMDs may have been largely affected by the outer layer of cortical bone.



(a)



(b)



(c)

Fig. 9.7 Illustrations of the changes in the bone thickness according to sections: (a) Superior, (b) Cervical Axis (Medial), (c) Inferior

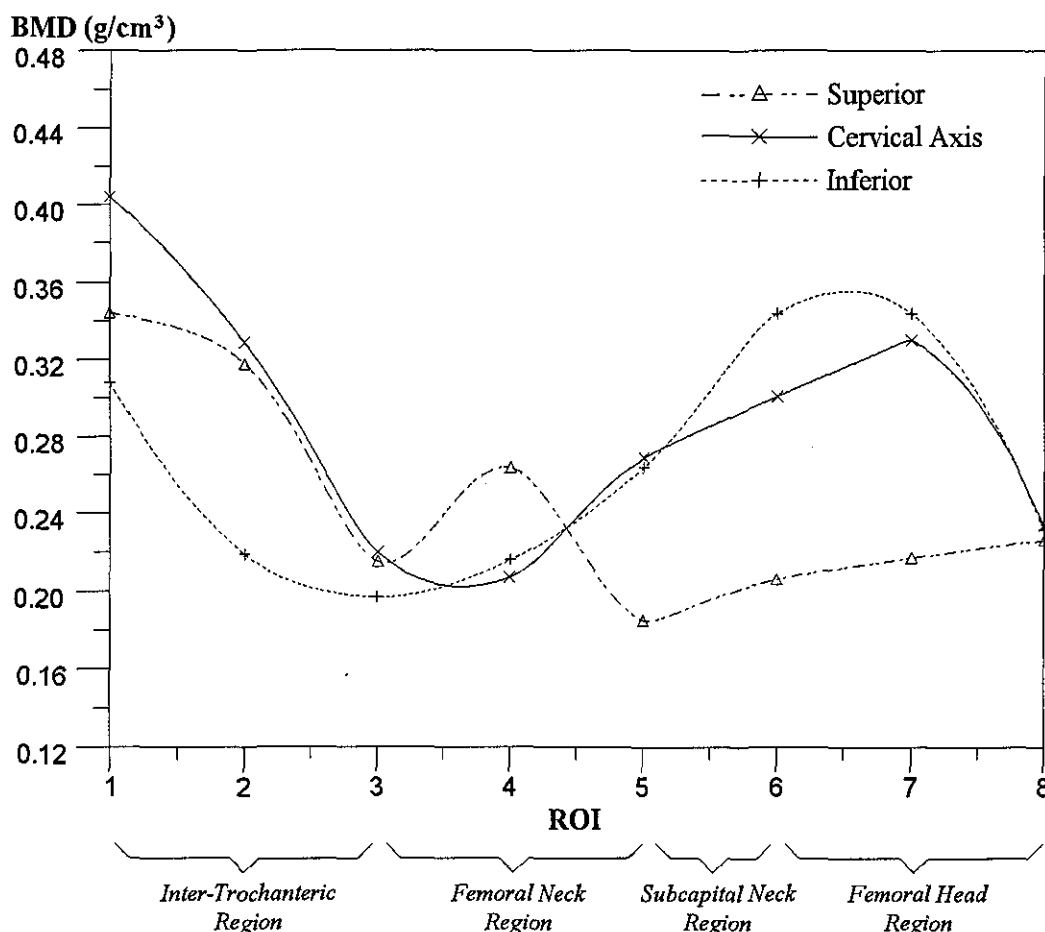


Fig. 9.8 Profiles of BMDs in g/cm^3 with respect to ROIs as indicated in figure 7.10a

9.2.2 Profiles of the Average Drilling Force

The drilling trajectories in the cervical axis direction are classified into superior, cervical axis and inferior sections, shown in figure 9.9a. These sections are further divided into anterior, lateral-medial and posterior zones, shown in figure 9.9b. Typical average drilling forces profiles corresponding to the BMD profiles (figure 9.6) are presented in figure 9.10. The actual drilling force profiles are given in Appendix 7.4.

When drilling in the superior section, the force profiles for the anterior and the lateral-medial zones, shown in Fig. 9.10a, have been found to be different in terms of force magnitude and distribution of strength. The average drilling profile for the posterior zone was not included because the drilling trajectory was diverted as the drill bit broke through the femoral head. In addition, the variation of average forces in the anterior and the lateral-medial zones has been shown to have little significance in the correlation between average drilling forces and BMDs.

The average force profiles for the cervical axis and inferior sections, as shown in figures 9.10b and 9.10c, share many similarities in the anterior and lateral-medial zones. However, the drilling forces are generally lower in the inferior section. In addition, a slight increase in the force magnitude from the anterior zone towards the posterior zone can be observed between the regions of the femoral neck and the femoral head. The forces from the inter-trochanteric region to the subcapital neck region have been found to be relatively low and are generally between the values of 0 N and 10 N. While the highest drilling forces have been obtained from the region of the femoral head.

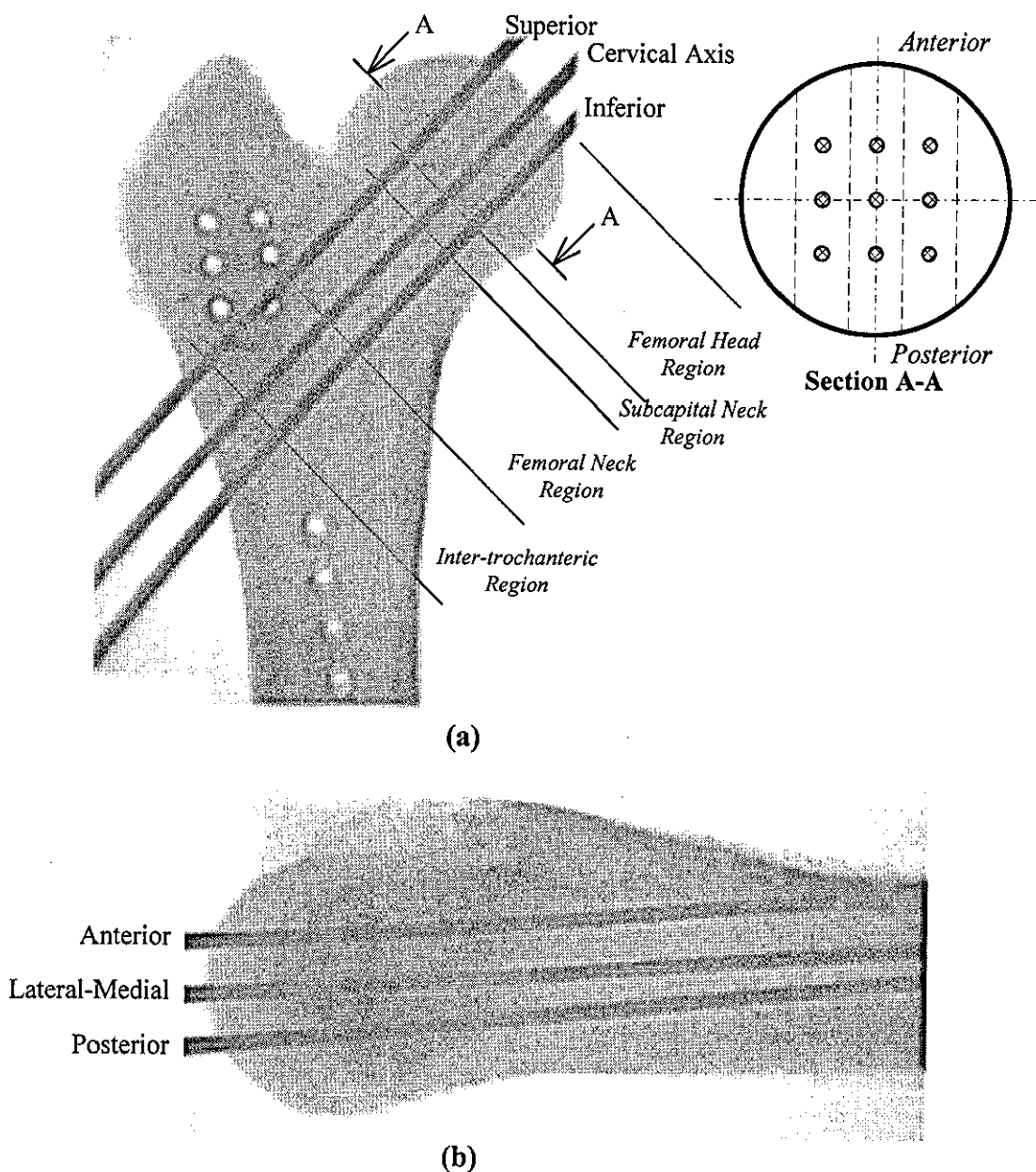


Fig. 9.9 Drilling trajectories in the direction of the cervical axis of a porcine proximal femur shown by the x-ray images: (a) AP view, (b) Lateral view

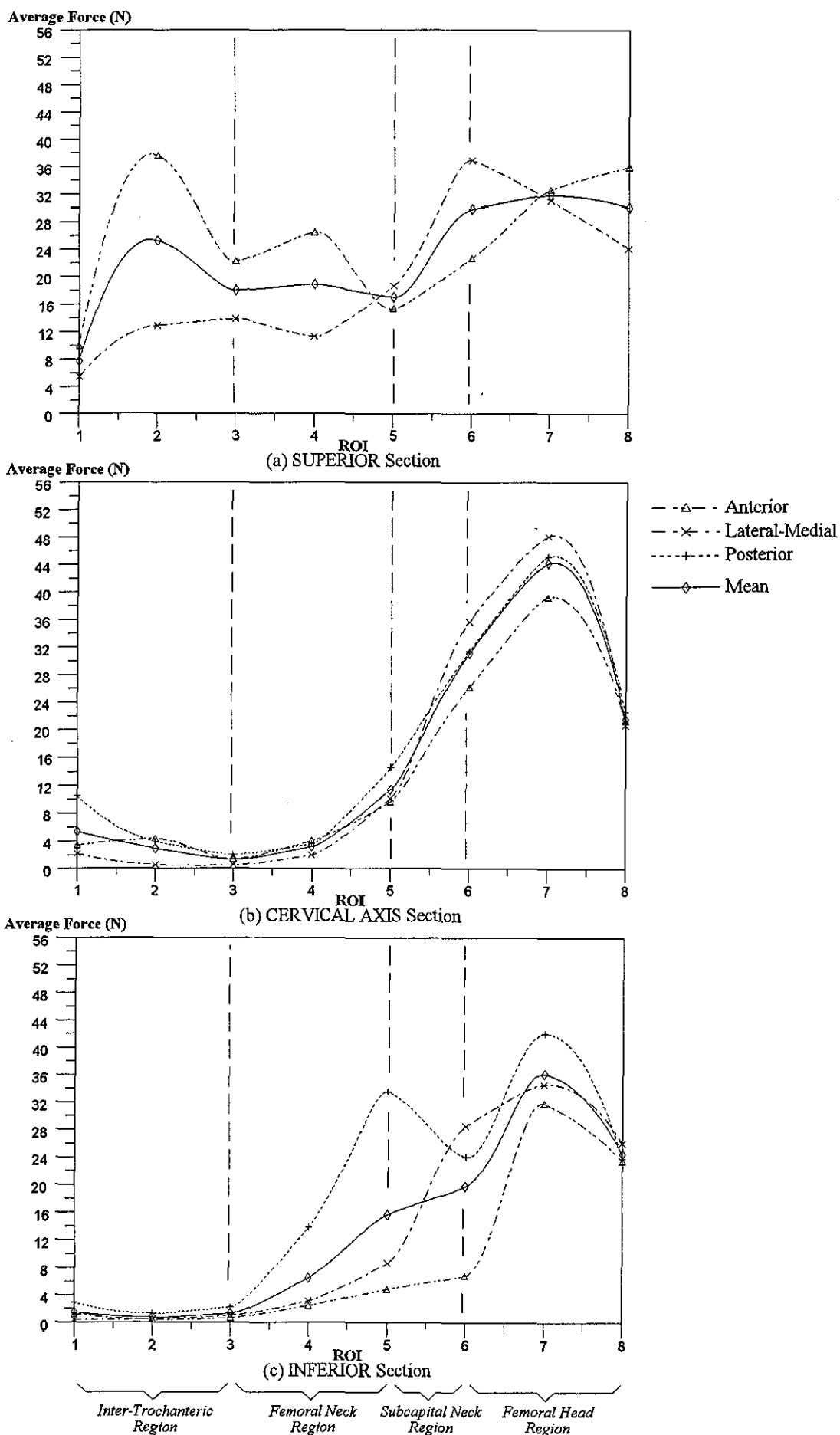


Fig. 9.10 Typical profiles of average drilling forces with respect to ROIs

Consistency in the force profiles has been found only between the cervical axis and the inferior sections. This includes the anterior and lateral-medial zones for the corresponding sections. The higher forces in the inter-trochanteric region of the superior section may be caused by the epiphyseal line. The presence of red marrow in the cervical axis and inferior sections may account for the low drilling forces in the inter-trochanteric region. In addition, the effects of trabeculae orientation in the direction of the cervical axis coupled with low bone density may partly explain the low forces in the femoral neck region.

As mentioned in Section 9.1.1, the measured drilling force includes a component of frictional force. The frictional forces between the drill bit and the bone at different regions, shown in figure 9.11, increase with the depth of drilling. The maximum average frictional force has been found to be less than 0.8 N at the maximum depth of drilling. This value of friction, which is of low magnitude, has little effect on the drilling force at the femoral head region. However, the effect of friction is considerable in the regions of the inter-trochanter and the femoral neck (ROI number 1, 2, 3 and 4) because the drilling forces obtained in these regions are relatively low. Apart from friction, the other contributing factors which may have introduced errors to the measurements of drilling forces are drill bit clogging and the flow of blood from the bone, as explained in Section 9.1.1.

9.2.3 Correlation between Average Drilling Force and BMD

The correlation between the average drilling force and BMD (in g/cm^2) in the direction of the cervical axis has been found to be significantly different from the correlation in the AP direction. Furthermore, the relationships along the cervical axis have been found to be very site specific. In order to minimise the correlation error, the average force and the BMD of the first and the last ROIs, which are located near the edges of the inter-trochanteric and the femoral head regions respectively, have been omitted. Comparison using figures 9.6 and 9.10 of the BMD and the average drilling force profiles respectively provides some indication of why mixed relationships have been obtained. In the superior section to the cervical axis, no significant relationship has been found and the slopes for average forces at the anterior, lateral-medial and posterior zones with respect to the BMD vary from positive to negative. Therefore, the following discussion regarding the correlation between average drilling forces and BMDs will

refer only to the cervical axis and the inferior sections. The ROIs in these two sections are mainly located in the regions of the femoral neck and the femoral head.

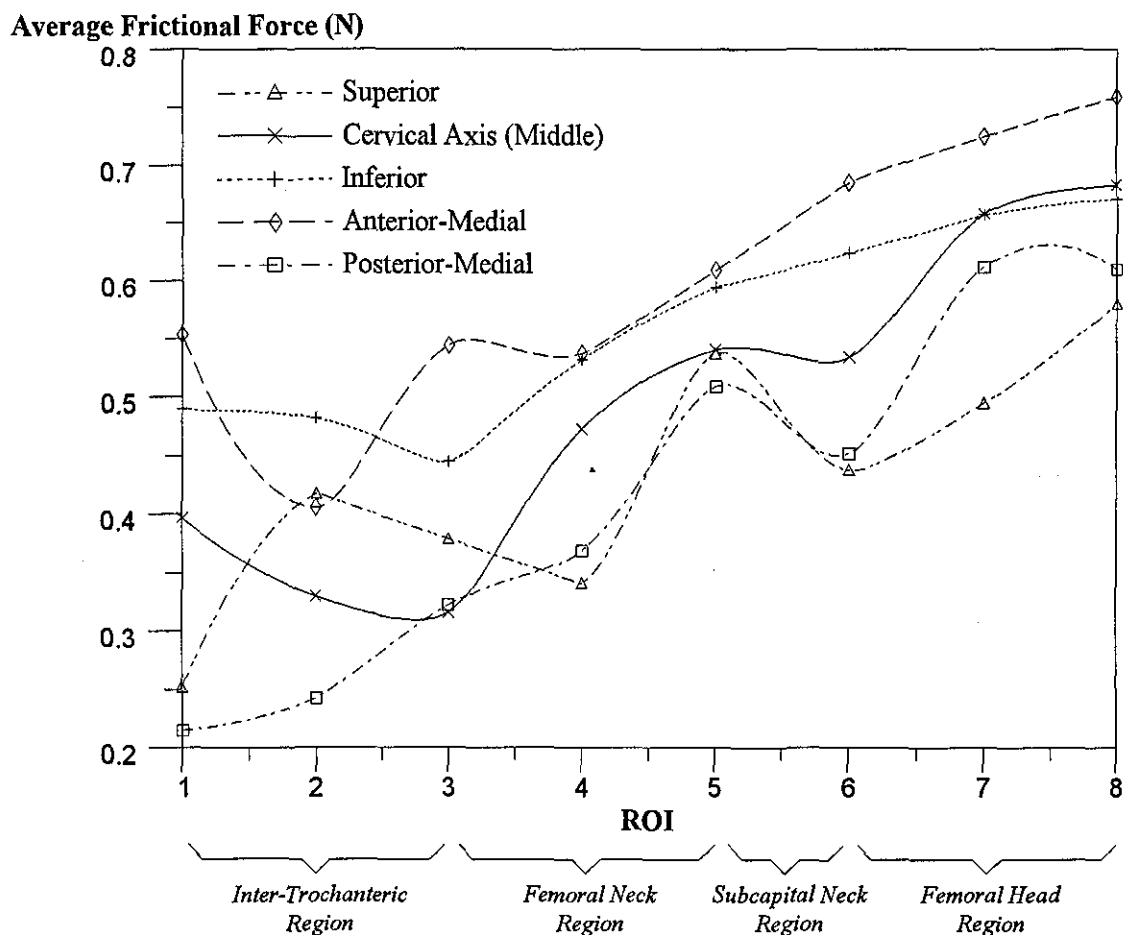


Fig. 9.11 Profiles of average frictional forces at different sections with respect to ROI

A positive relationship begins to develop as the ROIs shift towards the inferior direction of the cervical axis. However, the average forces have been found to have a large overlap with the BMDs. The relationships obtained from the cervical axis and the inferior sections, shown in figure 9.12, have been found to be positive although there are some variations in the slope between the anterior, lateral-medial and posterior zones. The use of bone cross-sectional thickness to obtain BMD in g/cm^3 , shown in figure 9.7, has been found to produce an improvement in the correlation coefficient of the relationships. This can be seen in figure 9.13.

It has been shown in figure 9.12 that a certain correlation exists only from the regions of the femoral neck to the femoral head in the lower half of the proximal femur. However, the ratio between the highest and the lowest values of BMD (figure 9.6) is much lower than that of the

highest and lowest average drilling forces (figure 9.10). This may be the main factor behind such a large overlap between the BMD and the average force in the correlation.

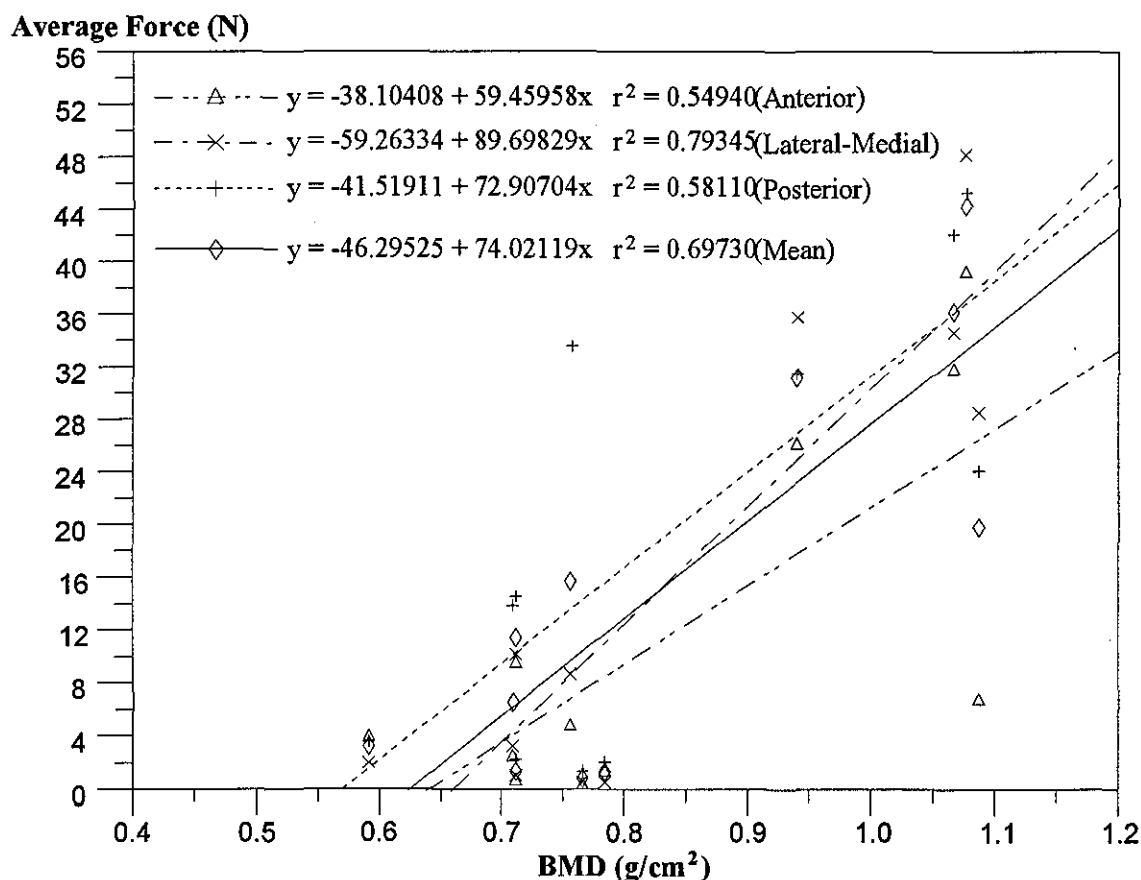


Fig. 9.12 Correlation between average drilling forces and BMDs in g/cm² at the cervical axis and the inferior sections in the regions of the femoral neck and the femoral head

The extremely low average drilling forces between regions of the inter-trochanter and the subcapital femoral neck have been shown to correspond to a minimum level of BMDs of the bone. This would possibly mean that the cortical shell at these regions accounts for the majority of the BMD measurements. Meanwhile, the maximum average forces around the region of the femoral head correspond to the maximum BMDs. In the inter-trochanteric region, the thickness of the bone has a significant effect on the BMD, and as a result, the BMD does not indicate the actual strength of the cancellous bone within.

Although the drilling forces and the BMDs have been shown to be relatively low (approaching zero) in the femoral neck region, the importance of the cancellous bone with the bone marrow cannot be overlooked. Martens *et al.* (1983) conducted an experiment to evaluate the contribution of cancellous bone to the overall strength of the proximal femur. By removing

cancellous bone at the centre of the inter-trochanteric, femoral neck and femoral head regions, it was found that the strength of the proximal femur reduced to approximately half the original strength.

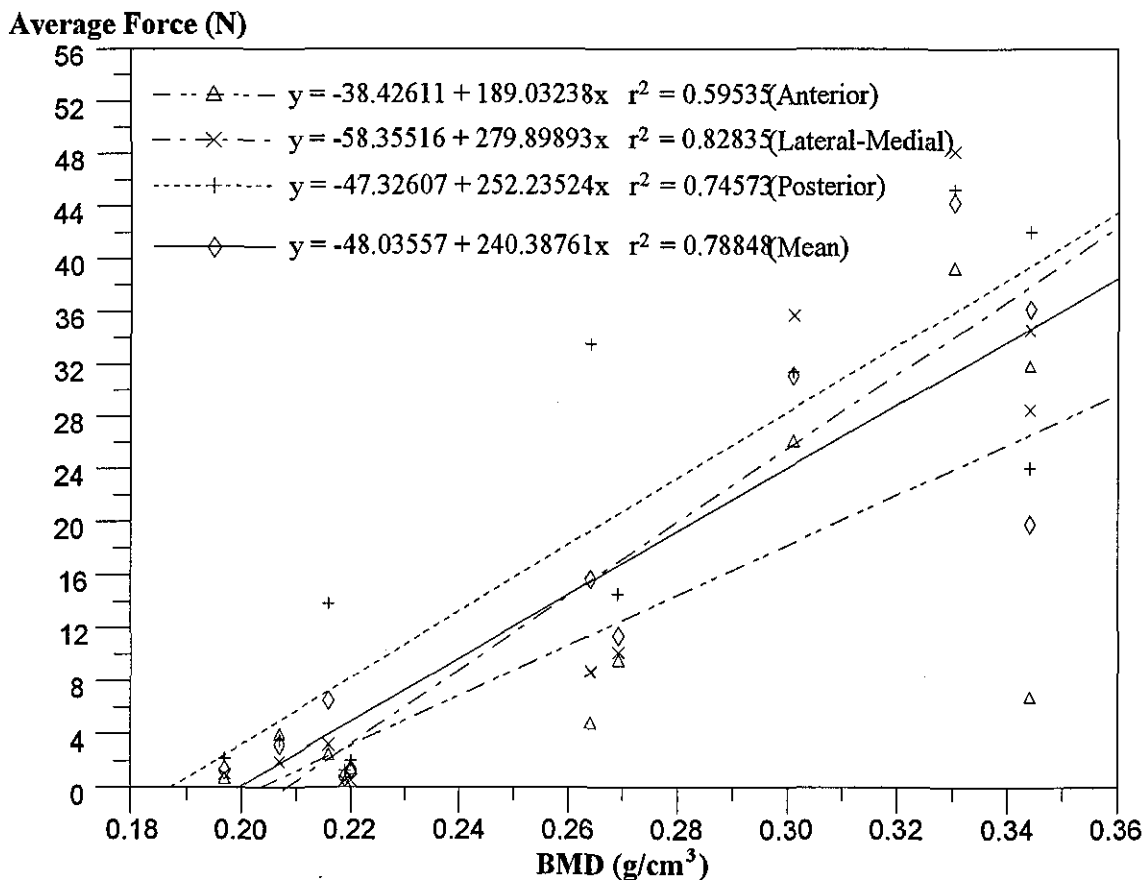


Fig. 9.13 Correlation between average drilling forces and BMDs in g/cm^3 at the cervical axis and the inferior sections in the regions of the femoral neck and the femoral head

The effects of trabecular orientation in the femoral neck region have been briefly examined by a separate drilling experiment in the direction perpendicular to the cervical axis, as shown in figure 9.14. Figure 9.15 shows the average drilling forces in the lateral-medial zone within the ROIs, also indicated by numbers in figure 9.14, corresponding to figure 7.10a. Based on the results presented, there has been little evidence of the effects of the trabecular orientation on the average drilling force. The notable difference is in the average forces at the inferior section, which have been found to be relatively low.

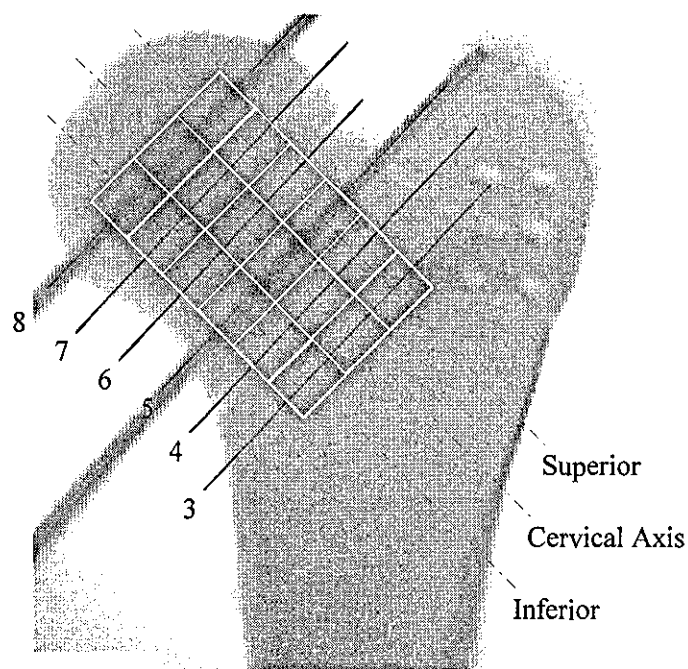


Fig. 9.14 Drilling trajectories in the direction perpendicular to the cervical axis of a porcine proximal femur

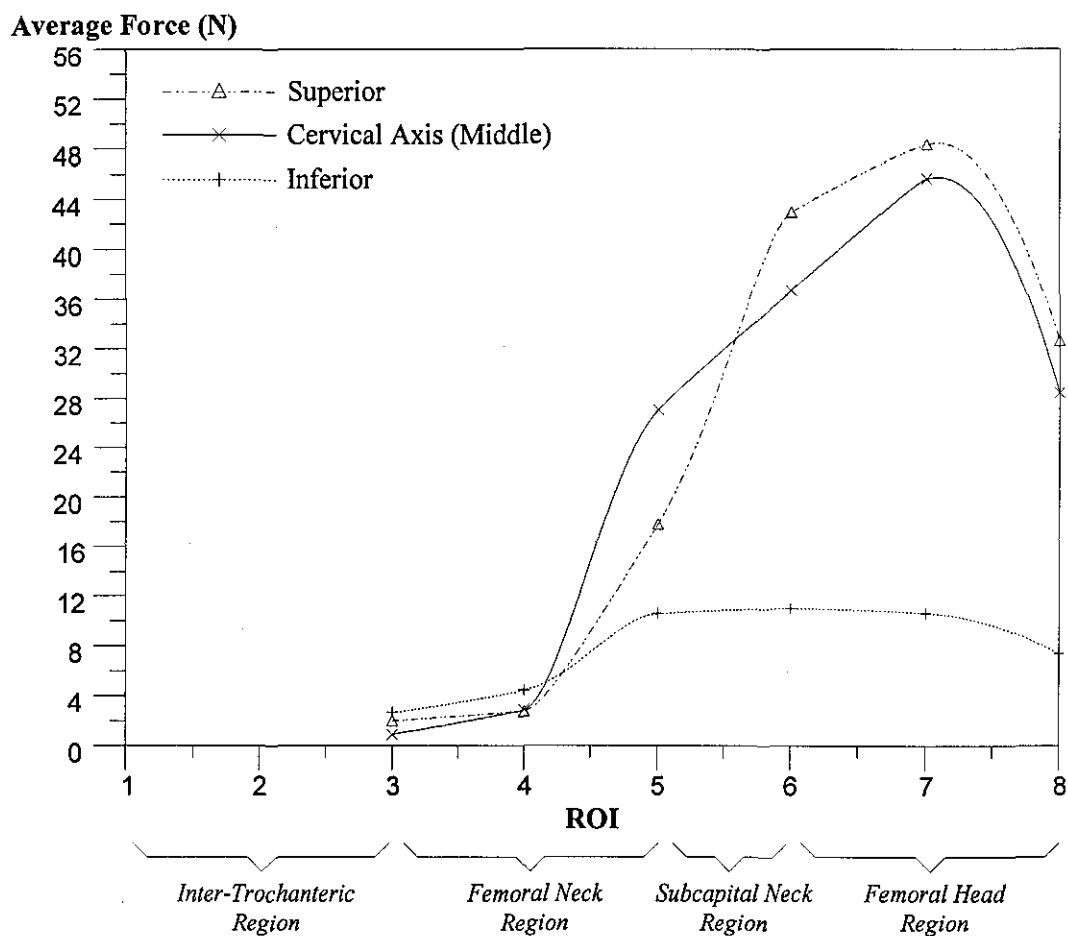


Fig. 9.15 Profiles of average drilling forces at the lateral-medial zone in the direction perpendicular to the cervical axis with respect to ROI

9.3 Discussion

There have been very few investigations related to drilling of the proximal femur. The changes in the drilling forces, indicated by the present investigation and by Chagneau and Levasseur (1992), have been shown to provide a form of quantification of the bone strength. Drilling forces presented by Shuaib and Hillery (1995) have shown a vast difference between the cortical and cancellous bone. This is not the case in this present investigation and the results presented by Karalis and Galanos (1982). The main reason for the vast difference could be explained by the different drill bits used and the specimens of femoral head obtained from patients undergoing hip arthroplasty (Shuaib & Hillery, 1995), which could have an adverse effect on the cancellous bone strength.

The investigation reported in this thesis has found that the strength of the cortical bone (femoral shaft) indicated by the drilling force cannot be applied to the strength estimation of the cancellous bone (proximal femur) and *vice-versa* for a corresponding BMD, as shown in figure 9.5. This is due to the extremely large difference in the level of correlation between the average force and the BMD between the two types of bone. Therefore, cortical bone cannot be considered as dense cancellous bone; this was also stated by Rice *et al.* (1988). The results reinforce the findings of Rice *et al.* (1988) and Keller (1994) related to the prediction of mechanical properties (compressive strength and modulus of elasticity) between cancellous and cortical bones for a corresponding apparent density.

The relationship in the direction of AP between the BMD and the average drilling force of the proximal femur has been found to be positive with a good coefficient of correlation. This is comparable to the osteopenetration results presented by Bentzen *et al.* (1987) and Petersen *et al.* (1996) on human proximal tibiae. However, bone drilling has several advantages over the use of osteopenetrometer introduced by Hvid *et al.* (1984). Bone drilling is extensively used in orthopaedic surgery, while osteopenetration is not part of standard surgical procedures. Through automation, the evaluation of bone strength can be carried out with bone drilling. The forces involved in bone drilling are far lower than the penetration forces for the same feed rate. As a result, the drilling equipment will be easier to set-up and handle. The start of drilling will be easier than direct penetration of a needle which would involve extremely high forces in order

to overcome the outer layer of cortical bone. Furthermore, the friction involved in drilling has been shown to be minimal.

The evaluation of bone strength is not confined only to the femoral neck, the Ward's triangle (figure 4.7) and the femoral head. The results from this investigation show that it is possible to predict the strength of the proximal femur from the strength of the greater trochanter. This is indicated in figure 9.1, where the correlation between average drilling forces and BMDs at the greater trochanter is similar to the correlation at the femoral head. A similar relationship (linear) was found by Leichter *et al.* (1988) between the BMD measurement of the greater trochanter and the average shear stress at failure (obtained from mechanical testing) of the femoral neck. Therefore, a possible relationship may be present between bone drilling and mechanical testing for the estimation of bone strength. Also, BMD, as shown in figure 9.1, has been found to account for approximately 70-80 % of the average drilling force, which is within the range of bone strength reported in many studies (Wahner & Fogelman, 1995; Petersen *et al.*, 1996).

A good correlation in the direction of the cervical axis, as shown in figure 9.12, has been found only in the regions of the femoral neck and the femoral head. Improved correlation has been shown when bone thickness, which is related to the changes in the cross-sectional geometry (figure 9.7), is included. Therefore, some of the poor relationships between mechanical properties and BMDs, presented by Cody *et al.* (1996), may be partially due to the omission of bone thickness, and also due to the inclusion of some locations of ROIs near the edges of the femoral head region. At the edges of the femoral head, the BMDs obtained are relatively low in magnitude, as shown in figure 9.6.

In addition, the correlation may have been further affected by the direction of drilling in the present study or the direction of loading in the case of mechanical properties (Cody *et al.* 1996). Bone densitometry can only provide BMD measurement of the proximal femur in the AP direction. Therefore, the direction of drilling or loading orthogonal to this AP direction affects the correlation as there is a significant variation in the strength across the proximal femur in the AP direction (figure 9.3). A comparison between the correlation in the direction of the AP (figure 9.1) and the cervical axis (figure 9.12) show a large difference in the slope of

correlation. The slope of correlation in the cervical axis direction is steeper than the AP slope, which indicates that a different correlation is obtained.

This investigation indicates that bone drilling can be used for the evaluation of the strength of bone. Unlike mechanical compression tests, the physiologic boundary conditions of the proximal femur are maintained to a certain extent during drilling experiments. The profiles of drilling forces obtained also show that bone drilling provides better spatial resolution than both the densitometric measurements and the mechanical tests. However, a number of limitations of this investigation have been identified.

- (i) The number of samples used in the correlation is relatively small.
- (ii) The specimens are limited to porcine bones of the same age. Using porcine bones of the same age, however, may help to eliminate the age variable in the correlation.
- (iii) Matching the ROIs of the average drilling force and of the BMD is difficult, and the correlation could have been adversely affected as a result of matching errors.
- (iv) The effects of drill bit clogging and blood flow may have influenced the drilling forces.
- (v) The method of clamping in this investigation may have also affected the drilling forces.

In spite of the limitations of this study, a positive trend for the evaluation of bone strength has been found between the BMD and the average drilling force.

In summary, it has been shown that force data from bone drilling can be used to indicate the strength of bone. In this preliminary investigation, a linear relationship has been found to exist between the drilling forces and the BMD measurements. However, in order to develop bone drilling as a diagnostic method for bone strength evaluation, further investigations involving direct mechanical tests on bone materials are required to establish strength relationships between bone drilling forces and bone strength. Bone drilling forces are also functions of drill bit shape, diameter, feed rate and drill bit rotational speed. Therefore, generalised relationships for bone drilling may be needed to cover the different drill bit shapes, diameters and drilling conditions.

CHAPTER 10

CONCLUSIONS

The conclusions, which have been drawn from the work, the analysis of the results and the discussions are presented in this chapter.

10.1 Contribution of the Research

This research has demonstrated the significant contribution of automation/mechatronics technology to orthopaedic surgery, in two key areas, associated with the drilling of bone. The two key areas of contribution have been identified as the enhancement of safety and the evaluation of bone strength based on the characteristics of bone drilling of the femoral shaft and the proximal femur respectively. The enhancement of safety refers to the imminent detection, and thus avoidance, of drill bit break-through. The use of a modified Kalman filter to produce a reliable and repeatable trend has significantly reduced the problems associated with drill bit break-through, especially, in the presence of system compliance and inherent fluctuation of drilling force. The presence of a trend enables this method to be implemented easily, safely and in real time into automated drilling systems.

In the evaluation of bone strength related to cancellous bone, the average drilling force has been found to have a positive relationship with the bone mineral density (BMD). This relationship is found to depend on the drilling direction. The correlation of BMD to the average drilling force in the anterior-posterior (AP) direction, which has a high coefficient of correlation, is not interchangeable with the direction of the cervical axis. The contribution of this research is aided by the development of a novel drilling experimental rig which enables bone drilling tests to be carried out in a controlled environment at both the femoral shaft and the proximal femur sites.

10.2 Conclusions from the Research

Based on the experimental results and the discussions, the following conclusions are drawn:

- (i) The system compliance, which results in a reduced rate of penetration, has a significant effect on the profiles of drilling force. This is indicated by the false perception of the thickness of the cortical walls and the medullary cavity of the femoral shaft. At break-through, the spring-back action due to the system compliance can cause excessive protrusion of the drill bit.
- (ii) The force difference between successive samples (FDSS), which detects sharp changes in the force profile, is greatly affected by the inherent drilling force fluctuation caused generally by the variation of the bone structural density. This results, therefore, in false break-through indication. The change of drill bit rotational speed is also generally detectable during break-through, but the fluctuation in the measurements of rotational speed is higher than the drilling force measurements.
- (iii) Using a modified Kalman filter on the FDSS and the rotational speed, a robust and a more consistent trend is established by ironing out the fluctuations of the FDSS and the drill bit rotational speed. The trends created by the modified Kalman filter are safe and simple to apply to the detection of drill bit break-through. Early detection of break-through can also be achieved with the modified Kalman filter. However, the use of the modified Kalman filter on the rotational speed (K-Speed) is not reliable at low speeds. The use of only Kalman filtered FDSS (K-FDSS) has been shown to be adequate for a reliable detection of imminent break-through.
- (iv) In the direction of the AP, the relationship of the cancellous bone at the greater trochanter and the femoral head between the BMD and the average drilling force is linear with a high coefficient of correlation. The strength of the cancellous bone derived from drilling forces cannot be applied to the strength estimation of the cortical bone or *vice-versa* for a given BMD due to the huge difference in the level of correlation.

- (v) The profiles of the BMD and the average drilling force in the direction of the cervical axis (orthogonal to the AP direction) is evidently different, especially in the superior section to the cervical axis and the inter-trochanteric region. Positive linear relationship between the BMD and the average drilling force along the cervical axis is found only in the region of the femoral neck and the femoral head. The use of bone thickness on the BMD corresponding to the region of interest (ROI) improves the linear correlation with the average force.
- (vi) The correlation of the BMD and the average drilling force depends on the direction of drilling. The slope of correlation differ significantly between the direction of the AP and the cervical axis.
- (vii) The implementation of automation/mechatronics technology into the drilling of bone enables information regarding the drilling characteristics to be made available for the enhancement of safety and the evaluation of bone strength.

CHAPTER 11

RECOMMENDATIONS FOR FUTURE WORK

The recommendations for future work in relation to the application of automated/mechatronic bone drilling for the enhancement of safety and the evaluation of bone strength are presented in this chapter.

11.1 The Enhancement of Safety

The magnitude of maximum Kalman filtered force difference between successive samples (K-FDSS) can be used to indicate levels of system compliance (i.e. compliant, medium or stiff). High value of K-FDSS indicates a stiff system, while a low value represents a compliant system. With this information, the detection method of drill bit break-through can be improved by developing an algorithm to provide a controlled penetration especially in highly compliant system.

The use of the modified Kalman filter for improving the detection of drill bit break-through requires further experiments at different system compliances. Further analysis of the K-FDSS data in conjunction with force data may result in possible estimation of the system compliance. This would enable an even earlier detection of imminent drill bit break-through.

Laboratory trials using the Kalman filter technique in an operating environment would need to be conducted. This will help to evaluate the effectiveness of the technique and provide some relevant specifications for the development of a new drilling unit.

Finally, a new mechatronic drilling system for orthopaedic surgery can be developed in conjunction with a control algorithm with the ability to detect imminent drill bit break-through and to provide a controlled penetration.

11.2 The Evaluation of Bone Strength

The number of samples used in this investigation is relatively small, and as a result, rogue data can have a significant effect on the correlation. In order to verify the relationship between BMD and average drilling force, a lot more experimental measurements are needed.

The present investigation has used porcine femurs to show the correlation between BMD and average drilling force. However, the characteristics of BMD and drilling force may be different in the human femurs. Therefore, sufficient number of experiments need to be conducted on human femurs in order to establish the relevant relationships. In addition, the experimental rig may have to be modified to cater for human femurs.

The correlation between BMD and average drilling force of cortical bone from the femoral shaft can be improved by conducting experiments on porcine bones of different age and/or on bones of different species.

The size of the ROI, which depends on the pixel size of the BMD scanner type, may be further reduced possibly to give a more accurate representation of the BMD profile. This may result in increased matching errors and the solution to this may be to use a template based on the AP x-ray image taken after the drilling experiments for each bone.

The effects of trabecular orientation on the drilling forces need to be further investigated since bone strength at the proximal femur depends, partly, on the structural integrity of the cancellous bone. This can help to establish a link between the AP direction and the cervical axis direction since the correlation of BMD with average drilling force depends on the direction of drilling.

Consideration has to be given to the problem of drill bit clogging due to the large drilling depth. This is to ensure that possible correlations are not adversely affected by the drill bit clogging. In addition, the flow of blood in the proximal femur during drilling may have an effect on the drilling forces.

With the introduction of bone drilling, a triangular relationship consisting of the drilling strength, the BMD and the mechanical strength can be established for the improvement of the evaluation of bone strength. The determination of the mechanical strength can either be in the form of a compression test on the cancellous bone of the proximal femur or in the form of a non-failure bending test on the proximal femur. The compression test provides the strength in terms of ultimate strength and modulus of elasticity, while the non-failure bending test, which emulates the anatomical loading of the pelvis, indicates strength by the amount of deformation or displacement for a given load.

The possible outcome from the triangular relationship is the derivation of a bone strength index or number based on the analysis of drilling data. This index could represent the strength in terms of density and the trabecular orientation specific to the location within the bone. The development of such a method could be applicable to cancellous bone at other sites of the body beside the proximal femur.

Finally, a new mechatronic drilling system can be developed as an *in vivo* diagnostic tool for the evaluation of bone strength and the identification of diseased bones based on the strength index. The aim is to assist orthopaedic surgeons in the decision making related to the treatment of a fracture and the management of post-operative treatment, as well as to evaluate the success rate of the surgical procedure or treatment. It must be noted that the mechatronic device for the evaluation of bone strength can be designed such that it may also be utilised for imminent detection and avoidance of drill bit break-through.

REFERENCES

- Abouzgia, M.B. and James, D.F. (1995) Measurements of shaft speed while drilling through bone. *J. Oral Maxillofac. Surg.*, **53**, 1308-1315.
- Adams, J.E. (1992) Osteoporosis and bone mineral densitometry. *Current Opinion in Radiol. - Musculoskeletal Radiol.*, **4**, 11-20.
- Albright, J.A., Johnson, T.R. and Saha, S. (1978) Principles of internal fixation. *Orthopaedic Mechanics - Procedures and Devices* (edited by Ghista, D.N. and Roaf, R.), pp.123-229. Academic Press, London.
- Allotta, B., Belmonte, F., Bosio, L. and Dario, P. (1995) A mechatronic tool for drilling in orthopaedics. In Proceedings of the 2nd. International Workshop on *Mechatronics in Medicine and Surgery*, pp.92-107.
- Arshinov, V. and Alekseev, G. (1976) *Metal Cutting Theory and Cutting Tool Design*, pp.245-272, Mir Publishers.
- Bechtol, C.O., Ferguson, A.B. and Laing, P.G. (1959) *Metals and Engineering in Bone and Joint Surgery*, pp.127-146, Williams & Wilkins, Baltimore.
- Beck, T.J., Ruff, C.B., Warden, K.E., Scott Jr., W.W. and Rao, G.U. (1990) Predicting femoral neck strength from bone mineral data: A structural approach. *Invest. Radiol.*, **25**, 6-18.
- Bentzen, S.M., Hvid, I. and Jørgensen, J. (1987) Mechanical strength of tibial trabecular bone evaluated by x-ray computed tomography. *J. Biomechanics*, **20**, 743-752.
- Bonfield, W. and Li, C.H. (1968) The temperature dependence of the deformation of bone. *J. Biomechanics*, **1**, 323-329.
- Bouazza-Marouf, K., Browbank, I. and Hewit, J.R. (1995) Robotic-assisted internal fixation of femoral fractures. *Proc. Instn Mech. Engrs, Part H, Journal of Engineering in Medicine*, **209**, 51-58.
- Bozic, S.M. (1979) *Digital and Kalman filtering*, pp.100-108, Edward Arnold.
- Brear, K., Currey, J.D., Raines, S. and Smith, K.J. (1988) Density and temperature effects on some mechanical properties of cancellous bone. *Engng in Medicine*, **17**, 163-167.
- Brett, P.N., Baker, D.A., Reyes, L. and Blanshard, J. (1995) An automatic technique for micro-drilling a Stapedotomy in the flexible stapes footplate. *Proc. Instn Mech. Engrs, Part H, Journal of Engineering in Medicine*, **209**, 255-262.

- Brown, T.D. and Ferguson, A.B. (1980) Mechanical properties distributions in the cancellous bone of the human proximal femur. *Acta Ortho. Scand.*, **51**, 429-437.
- Bucholz, R. and Browner, B (1990) *Surgery of the Musculoskeletal System*, (edited by McCollister Evarts, C.), pp. 2695-2729, Churchill Livingstone.
- Chagneau, F. and Levasseur, M. (1992) Mechanical analysis of bone structures by Dynamostratigraphy. *Eur. J. Mechanics A/Solids*, **11**, 551-571.
- Chesnut III, C.H. (1993) Noninvasive Methods for Bone. *The Osteoporotic Syndrome - Detection, Prevention and Treatment* (edited by Avioli, L.V.), pp. 77-87, Wiley-Liss.
- Cody, D.D., McCubbrey, D.A., Divine, G.W., Gross, G.J. and Goldstein, S.A. (1996) Predictive value of proximal femoral bone densitometry in determining local orthogonal material properties. *J. Biomechanics*, **29**, 753-761.
- Coetzee, J.C. and Van Der Merwe, E.J. (1992) Exposure of surgeons-in-training to radiation during intramedullary fixation of femoral shaft fractures. *SAMJ*, **81**, 312-314.
- Compston, J.E., Cooper, C. and Kanis, J.A. (1995) Bone densitometry in clinical practice. *BMJ*, **310**, 1507-1510.
- Cooper, C. (1990) Bone mass throughout life: Bone growth and involution. *Osteoporosis: Pathogenesis and Management* (edited by Francis, R.M.), pp.1-26, Kluwer Academic Publishers.
- Cummings, S.R., Black, D.M., Nevitt, M.C., Browner, W., Cauley, J., Ensrud, K., Genant, H.K., Palermo, L., Scott, J. and Vogt, T.M. (1993) Bone density at various sites for prediction of hip fractures. *Lancet*, **341**, 72-75.
- Cunningham, J.L., Fordham, J.N., Hewitt, T.A. and Speed, C.A. (1996) Ultrasound velocity and attenuation at different skeletal sites compared with bone mineral density measured using Dual Energy X-Ray Absorptiometry. *Br. J. Radiol.*, **69**, 25-32.
- Dandy, D.D. (1989) *Essential Orthopaedics and Trauma*, Churchill Livingstone.
- Dario, P., Guglielmelli, E. and Allotta, B. (1994) Robotics in medicine. In IEEE/RSJ/GI International Conference on *Intelligent Robots and Systems*, **2**, pp.739-752.
- Davis, J.K., Jackson, C.J. and Scott, I. (1980) The relationship between feed rate and point angle of a twist drill bit when drilling bone. *Engng. in Medicine*, **9**, 137-142.
- De Laet, C.E.D.H., Van Hout, B.A., Burger, H., Hofman, A. and Pols, H.A.P. (1997) Bone density and risk of hip fractures in men and women: Cross sectional analysis. *BMJ*, **315**, 221-225.

- Duboeuf, F., Jergas, M., Schott, A.M., Wu, C.Y., Glüer, C.C. and Genant, H.K. (1995) A comparison of bone densitometry measurements of the central skeleton in post-menopausal women with and without vertebral fracture. *Br. J. Radiol.*, **68**, 747-753.
- Edmondston, S.J., Singer, K.P., Day, R.E., Breidahl, P.D. and Price, R.I. (1994) *In vitro* relationships between vertebral body density, size, and compressive strength in the elderly thoracolumbar spine. *Clin. Biomech.*, **9**, 180-186.
- Ernst, H. and Haggerty, W.A. (1958) The Spiral point - A new concept in drill point geometry. *Trans. ASME*, **80**, 1059-1072.
- Eriksson, A.R., Albrektsson, T. and Albrektsson, B. (1984) Heat caused by drilling cortical bone: Temperature measured *in vivo* in patients and animals. *Acta Orthop. Scand.*, **55**, 629-631.
- Evans, F.G. (1973) *Mechanical Properties of Bone*, Charles C Thomas Publisher.
- Farnworth, G.H. and Burton, J.A. (1974) Optimization of drill geometry for orthopaedic surgery. In Proceedings of the 14th International Conference on *Machine Tool Design and Research Conference*, Paper No.28, pp.227-233.
- Faulkner, K.G., Glüer, C.C., Majumdar, S., Lang, P., Engelke, K. and Genant, H.K. (1991) Noninvasive measurements of bone mass, structure, and strength: Current methods and experimental techniques. *Am. J. Roentgenol.*, **157**, 1229-1237.
- Feeney, M., Masterson, E., Keogh, P. and Quinlan, W. (1997) Risk of pelvic injury from femoral neck guidewires. *Arch. Orthop. Trauma Surg.*, **116**, 227-228.
- Galloway, D.F. (1957) Some experiments on the influence of various drill performance. *Trans. ASME*, **79**, 191-231.
- Gardner, J.F. and Peel, M.M. (1979) *Introduction to Sterilisation and Disinfection*, Churchill Livingston.
- Glüer, C.C., Wu, C.Y. and Genant, H.K. (1993) Broadband Ultrasound Attenuation signals depend on trabecular orientation: An *in vitro* study. *Osteoporosis Int.*, **3**, 185-191.
- Goldstein, S.A. (1987) The mechanical properties of trabecular bone: Dependence of anatomic location and function. *J. Biomechanics*, **20**, 1055-1061.
- Goulet, R.W., Goldstein, S.A., Ciarelli, M.J., Kuhn, J.L., Brown, N.B. and Feldkamp, L.A. (1994) The relationship between the structural and orthogonal compressive properties of trabecular bone. *J. Biomechanics*, **27**, 375-389.
- Grimm, M.J. and Williams, J.L. (1997) Assessment of bone quantity and 'quality' by ultrasound attenuation and velocity in the heel. *Clin. Biomech.*, **12**, 281-285.

- Hagiwara, S., Yang, S.O., Glüer, C.C., Bendavid, E. and Genant, H.K. (1994) Non-invasive bone mineral density measurement in the evaluation of osteoporosis. *Rheumatic Disease Clinics of North Am.*, **30**, 651-669.
- Heidrich, F. (1993) Limitations of bone densitometry. *Am. Family Physician*, **48**, 25-27.
- Hodgskinson, R. and Currey, J.D. (1993) Separate effects of osteoporosis and density on the strength and stiffness of human cancellous bone. *Clin. Biomech.*, **9**, 262-268.
- Howorth, F.H. (1980) Air flow patterns in the operating theatre. *Engng in Medicine*, **9**, 87-92.
- Hutchings, H. (1995) *Interfacing with C*, pp.158-176, Butterworth-Heinemann, Oxford.
- Hvid, I., Andersen, K. and Olesen, S. (1984) Cancellous bone strength measurement with the Osteopenetrometer. *Engng in Medicine*, **13**, 73-78.
- Jacobs, C.H., Pope, M.H., Berry, J.T. and Hoaglund, F.T. (1974) A study of the bone machining process - Orthogonal cutting. *J. Biomechanics*, **7**, 131-136.
- Jacobs, C.H., Berry, J.T., Pope, M.H. and Hoaglund, F.T. (1976) A study of the bone machining process - Drilling. *J. Biomechanics*, **9**, 343-349.
- Jaeger, J.C. and Cook, N.G.W. (1979) *Fundamentals of Rock Mechanics*, Chapman and Hall, London.
- Karalis, T. and Galanos, P. (1982) Research on the mechanical impedance of human bone by a drilling test. *J. Biomechanics*, **15**, 561-581.
- Kassler, M. (1993) Robotics for health care : A review of the literature. *Robotica*, **11**, 495-516.
- Keaveny, T.M., Borchers, R.E., Gibson, L.J. and Hayes, W.C. (1993) Trabecular bone modulus and strength can depend on specimen geometry. *J. Biomechanics*, **26**, 991-1000.
- Keller, T.S. (1994) Predicting the compressive mechanical behaviour of bone. *J. Biomechanics*, **27**, 1159-1168.
- Kwong, L.M., Johanson, P.H., Zinar, D.M., Lenihan, M.R. and Herman, M.W. (1990) Shielding of the patient's gonads during intramedullary interlocking femoral nailing. *J. Bone Jt. Surg.*, **72-A**, 1523-1526.
- Leichter, I., Simkin, A., Margulies, J.Y., Bivas, A., Roman, I., Deutsch, D. and Weinreb, A. (1988) Can the weight-bearing capacity of the femoral neck be estimated by physical measurements on the greater trochanter. *Engng in Medicine*, **17**, 59-62.
- Linde, F., Hvid, I. and Madsen, F. (1992) The effect of specimen geometry on the mechanical behaviour of trabecular bone specimens. *J. Biomechanics*, **25**, 359-368.
- Lotz, J.C., Gerhart, T.N. and Hayes, W.C. (1990) Mechanical properties of trabecular bone from the proximal femur: A quantitative CT study. *J. Comput. Assist. Tomogr.*, **14**, 107-114.

- Marshall, D., Johnell, O. and Wedel, H. (1996) Meta-analysis of how well measures of bone mineral density predict occurrence of osteoporotic fractures. *BMJ*, **312**, 1224-1259.
- Martens, R., Van Audekercke, R., Delport, P., De Meester, P. and Mulier, J.C. (1983) The mechanical characteristics of cancellous bone at the upper femoral region. *J. Biomechanics*, **16**, 971-983.
- Massey, B.S. (1986) *Measures in Science and Engineering: Their Expression, Relation and Interpretation*, pp.102-153, Ellis Horwood Limited, Chichester.
- Matthews, I.P., Gibson, C. and Samuel, A.H. (1994) Sterilisation of implantable devices. *Clin. Materials*, **15**, 191-215.
- Matthews, L.S. and Hirsch, C. (1972) Temperatures measured in human cortical bone when drilling. *J. Bone Jt. Surg.*, **54-A**, 297-308.
- Matthews, L.S., Green, C.A. and Goldstein, S.A. (1984) The thermal effects of skeletal fixation - Pin insertion in bone. *J. Bone Jt. Surg.*, **66-A**, 1077-1083.
- Moris, M., Peretz, A., Tjeka, R., Negaban, N., Wouters, M. and Bergmann, P. (1995) Quantitative Ultrasound bone measurements: Normal values and comparison with bone mineral density by Dual X-Ray Absorptiometry. *Calcif. Tissue Int.*, **57**, 6-10.
- Müller, M.E., Allgöwer, M., Schneider, R. and Willenegger, H. (1991) *Manual of Internal Fixation - Techniques Recommended by the AO-ASIF Group*, 3rd. Edition, Springer-Verlag, Berlin.
- Mundy, G.R. (1995) *Bone Remodelling and its Disorders*, Martin Dunitz, London.
- Nigg, B.M. and Herzog, W. (1994) *Biomechanics of the Musculo-Skeletal System*, pp.47-78, John Wiley & Sons, Chichester.
- Noordeen, M.H.H., Lavy, C.B.D., Briggs, T.W.R and Roos M.F. (1993) Unrecognised joint penetration in treatment of femoral neck fractures. *J. Bone Jt. Surg.*, **75-B**, 448-449.
- Ong, F. R. and Bouazza-Marouf, K. (1998) Drilling of bone: A robust automatic method for the detection of drill bit break-through. *Proc. Instn Mech. Engrs, Part H, Journal of Engineering in Medicine*, **212**. (in Appendix 6 and to be published)
- Oxford Jr., C.J. (1955) On drilling of metals 1 - Basic mechanics of the process. *Trans. ASME*, **77**, 103-114.
- Perez, E.D. (1994) Hip fracture: Physicians take more active role in patient care. *Geriatrics*, **49**, 31-37.

- Petersen, M.M., Jensen, N.C., Gehrchen, P.M., Nielsen, P.K. and Nielsen, P.T. (1996) The relation between trabecular bone strength and bone mineral density by dual-photon and dual-energy x-ray absorptiometry in the proximal tibia. *Calcif. Tissue Int.*, **59**, 311-314.
- Piekarski, K (1978) Structure, properties and rheology of bone. *Orthopaedic Mechanics - Procedures and Devices* (edited by Ghista, D.N. and Roaf, R.), pp.1-20. Academic Press, London.
- Preising, B., Hsia, T.C. and Mittelstadt, B. (1991) A literature review: Robotics in medicine. *IEEE Engng in Medicine and Biol.*, June, 13-22.
- Rho, J.Y., Zerwekh, J.E. and Ashman, R.B.(1994) Examination of several techniques for predicting trabecular elastic modulus and ultimate strength in the human lumbar spine. *Clin. Biomech.*, **9**, 67-71.
- Rice, J.C., Cowin, S.C. and Bowman, J.A. (1988) On the dependence of the elasticity and strength of cancellous bone on apparent density. *J. Biomechanics*, **21**, 155-168.
- Riley, S.A. (1989) Radiation exposure from fluoroscopy during orthopaedic surgical procedures. *Clin. Orthop. Rel. Res.*, **248**, 257-260.
- Saha, S., Pal, S. and Albright, J.A. (1982) Surgical drilling: Design and performance of an improved drill. *Trans. ASME, J. of Biomech. Engng*, **104**, 245-252.
- Sanders, R., Koval, K.J., DiPasquale, T., Schmelling, G., Stenzler, S. and Ross, E. (1993) Exposure of the orthopaedic surgeon to radiation. *J. Bone Jt. Surg.*, **75-A**, 326-330.
- Sartoris, D.J. (1994) Clinical Value of Bone Densitometry. *Am. J. Roentgenol.*, **163**, 133-135.
- Schoenfeld, C.M., Lautenschlager, E.P. and Meyer Jr., P.R. (1974) Mechanical properties of human cancellous bone in the femoral head. *Med. Biol. Engng*, **12**, 313-317.
- Schultz, A.B. (1992) Mobility impairment in the elderly: Challenges for biomechanics research. *J. Biomechanics*, **25**, 519-528.
- Shaw, M.C. and Oxford Jr., C.J., (1957) On drilling of metals 2 - The torque and thrust in drilling. *Trans. ASME*, **79**, 139-148.
- Shuaib, I. and Hillery, M. (1995) Forces generated in guide-wires when drilling human bone. *Proc. Instn Mech. Engrs, Part H, Journal of Engineering in Medicine*, **209**, 157-162.
- Singh, M., Nagrath, A.R. and Maini, P.S. (1970) Changes in the trabecular pattern of the upper end of the femur as an index of osteoporosis. *J. Bone Jt. Surg.*, **52-A**, 457-467.
- Smith, M.D., Cody, D.D., Goldstein, S.A., Cooperman, A.M., Matthews, L.S. and Flynn, M.J. (1992) Proximal femoral bone density and its correlation to fracture load and hip-screw penetration load. *Clin. Orthop. Rel. Res.*, **283**, 244-251.

- Smyth, P.P., Adams, J.E., Whitehouse, R.W. and Taylor, C.J. (1997) Application of computer texture analysis to the Singh Index. *Br. J. Radiol.*, **70**, 242-247.
- Sneath, R.S. (1964) The determination of optimum twist drill shape for bone. *Biomechanics and Related Bioengineering Topics*, Proc. Symp. Glasgow, pp.41-45, Pergamon Press, Oxford.
- Tothill, P., Fenner, J.A.K. and Reid, D.M. (1995) Comparisons between three dual-energy X-ray absorptiometers used for measuring spine and femur. *Br. J. Radiol.*, **68**, 621-629.
- Turner, C.H., Peacock, M., Timmerman, L., Neal, J.M. and Johnston Jr., C.C. (1995) Calcaneal ultrasonic measurements discriminate hip fracture independently of bone mass. *Osteoporosis Int.*, **5**, 130-135.
- Van De Graaff, K.M. and Fox, S.I. (1992) *Concepts of Human Anatomy and Physiology*, 3rd Edition, Wm. C. Brown.
- Van Egmond, D.B., Hovius, S.E R., Van Der Meulen, J.C. and Den Ouden, A. (1994) Heat recording at tips of Kirschner wires during drilling through human phalanges. *J. Hand Surg.*, **19A**, 648-652.
- Wahner, H.W. and Fogelman, I. (1995) *The Evaluation of Osteoporosis: Dual Energy X-Ray Absorptiometry in Clinical Practice*, Martin Dunitz, London.
- Wallace, W.A. (1983) The increasing incidence of fractures of the proximal femur: An orthopaedic epidemic. *Lancet*, **231**, 1413-1414.
- Weiss, N.A. (1993) *Elementary Statistics*, 2nd Edition, pp.580-625, Addison-Wesley.
- Wiggins, K.L. and Malkin, S. (1976) Drilling of bone. *J. Biomechanics*, **9**, 553-559.
- Williams, R.A. (1974) A study of the drilling process. *Trans. ASME - J. Engng for Industry*, **96**, 1207-1215.
- Williams, P.L. and Warwick, R. (1980) *Gray's Anatomy*, 36th Edition, Churchill Livingstone.
- Yamada, H. (1970) *Strength of Biological Materials* (edited by Evans, F.G.), pp.19-80, Williams & Wilkins, Baltimore.
- Zegunis, V., Toksvig-Larsen, S. and Tikuisis, R. (1993) Insertion of K-wires by hammer generates less heat: A study of drilling and hammering K-wires into bone. *Acta Orthop. Scand.*, **64**, 592-594.

Appendix 1

Exemplar of Orthopaedic Surgical Procedures for Femoral Fracture Fixation

The aim of this appendix is to provide a general description of fractures and fracture treatment related to the femur. An outline of two particular femoral fracture treatment procedures and the difficulties involved are also presented.

A1.1 Fractures of the Femur

Fractures of the femur or any long bones are classified into three sections: (i) the proximal which is the upper end of the femur, (ii) the shaft (diaphysis), and (iii) the distal which is the lower end of the femur. Typical features of these sites are shown in figure A3.1 of Appendix 3. These fractures are further categorised into three types, A, B and C shown in figure A1.1, according to the location of the fracture at a particular bone section or segment (Müller *et al.*, 1991). The types of fracture, (i) at the proximal femur are (A) trochanteric, (B) neck and (C) head, (ii) at the shaft are (A) simple, (B) wedge and (C) complex, and (iii) at the distal femur are (A) extra-articular, (B) partial articular and (C) complete articular.

Each type of fracture is then divided into three groups, which gives a total of 9 groups shown in figure A1.1, to represent the fracture characteristics (Müller *et al.*, 1991). For example, type A is classified as A1, A2 and A3 groups; type B is classified as B1, B2 and B3 groups; and type C is classified as C1, C2 and C3 groups. Finally these groups are put into three sub-groups, indicated by .1, .2 and .3, according to the three characteristic variations within the group. Thus, there are 27 sub-groups for each bone segment. The scale of severity of the fracture is arranged in an ascending order according to morphologic complexities of the fracture, and difficulties inherent in the prognosis and treatment. For example, A1 indicates the simplest fracture with the best prognosis and C3 indicates the most difficult fracture with the worst prognosis. A comprehensive classification of fractures of long bones can be found in the 'Manual of Internal Fixation' by Müller *et al.* (1991).

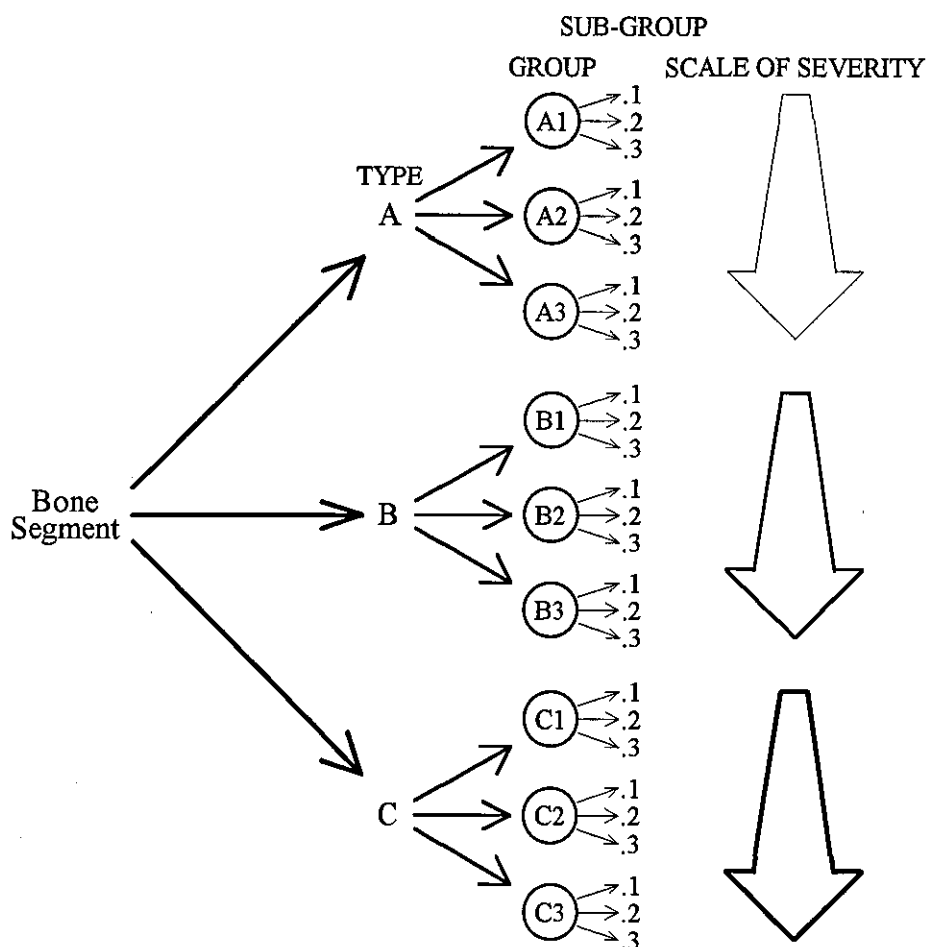


Fig. A1.1 Classification of fractures of long bones (Müller *et al.*, 1991)

Fractures of the proximal and the shaft of the femur, as shown in figure A1.2, have been selected to demonstrate the potential of a robotic system in orthopaedic surgery assistance (Bouazza-Marouf *et al.*, 1995). The proximal femur or hip fractures are often referred to as fractures of the neck and the trochanter (figure A1.2a). These fractures, which lead directly to mobility impairment, are commonly associated with the elderly suffering from osteoporosis (Wallace, 1983; Schultz, 1992; Compston *et al.*, 1995). Osteoporosis is a metabolic disease characterised by a reduction in bone strength in terms of bone density and bone quality. The reduced bone strength, therefore, increases the risk of fracture in the event of a fall. Fractures of the femoral shaft are normally associated with accidents and sports related injuries as a result of a high impact force to the bone.

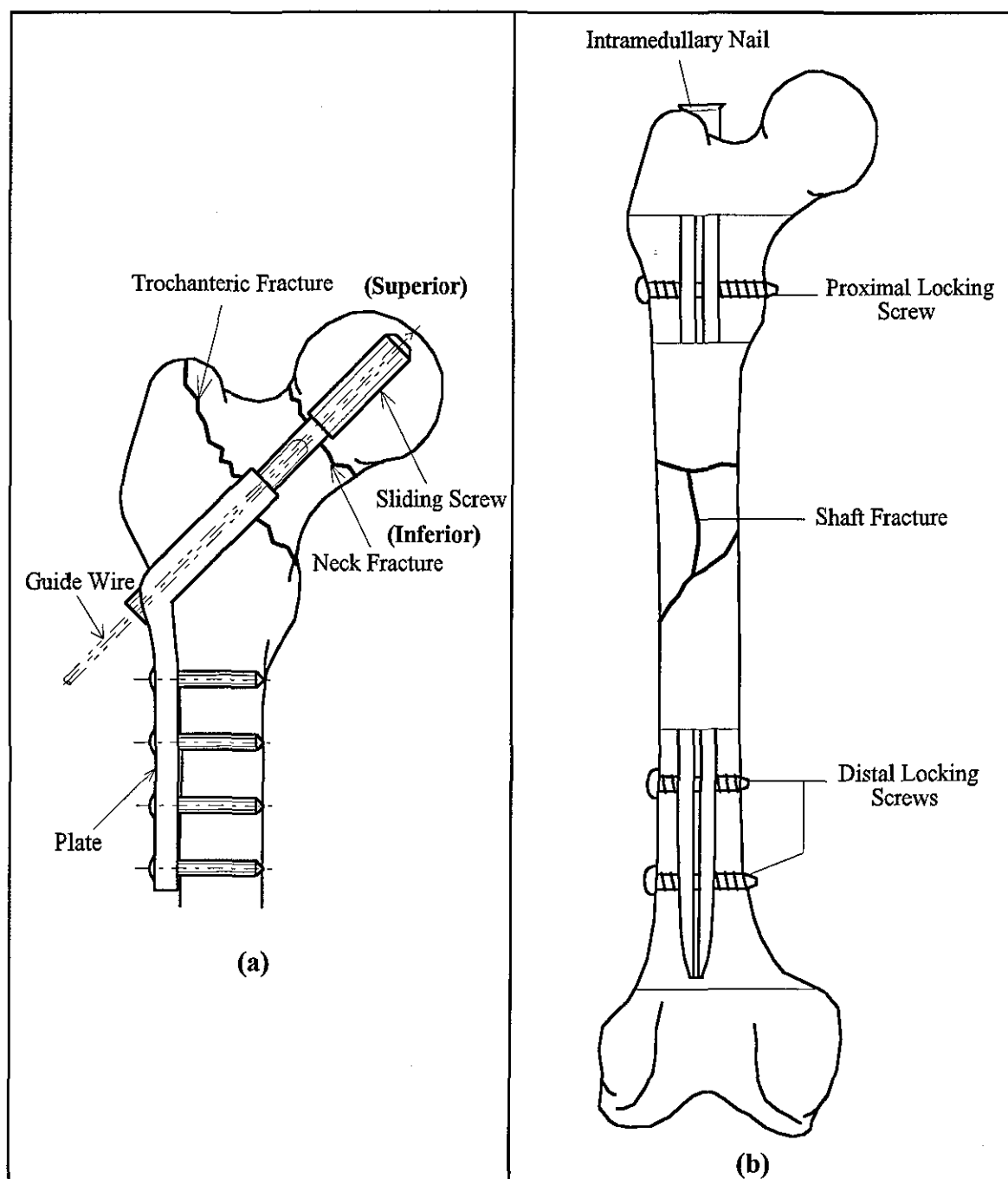


Fig. A1.2 Fracture fixation of the femur (Bouazza-Marouf *et al.*, 1995)

A1.2 Internal Fixation of Proximal Femur Fractures

The fracture of the proximal femur is normally treated with internal fixation using the compression screw and plate arrangement shown in figure A1.2a. This fixation procedure begins with the patient being placed in a supine position on the fracture table. Then, an anatomic reduction of the fracture, using fluoroscopic images from a mobile x-ray (C-arm) unit,

is performed by applying traction, abduction and rotation through the fracture table. Before making an incision on the affected site, appropriate draping is carried out to ensure sterility of the operative area. The incision has to give adequate exposure of the bone to permit the placement of the plate. A guide wire is then partially inserted into the bone manually using an angle guide. Two x-ray images, posterior-anterior (PA) and lateral views, are taken to ascertain the position and the orientation of the guide wire. If the optimum placement of the guide wire is not achieved, the process of inserting the guide wire is repeated. When the optimum placement is obtained, the guide wire is driven to a depth just before breaking through the femoral head. The guide wire is left in position to act as a guide for the subsequent enlarging and reaming of the hole, and insertion of the screw. The hole is enlarged and reamed using a triple reamer (drill bit) and the cannulated compression screw is inserted to the correct depth as indicated by the guide wire. Both the reamer and the screw have a hollow internal (central) canal to allow them to be slid along the guide wire. The position of the screw is fluoroscopically checked before the barrelled plate is placed over the screw. The plate is then secured to the cortical bone by means of screws along the femoral shaft. Finally, the guide wire is removed and the traction is released.

The main difficulty related to this internal fixation procedure is obtaining the optimal orientation of the guide wire placement. Incorrect placement of the guide wire leads to less than optimum position of the compression screw and as a result, failure of the fixation in the form of screw cut-out of the femoral head may occur when load is applied. Therefore, multiple attempts in the guide wire insertion may be required to obtain the optimum placement. Because this guide wire insertion is blind in nature, surgeons have to rely heavily on fluoroscopic guidance and visualise a three-dimensional object using two orthogonal x-ray images (PA and lateral). The advantages of fluoroscopic guidance are gained at the expense of increased radiation exposure especially on the surgeon's hand. The hazard of radiation exposure is more pronounced among surgically inexperienced surgeons due to the long learning curve (Coetzee, 1992). Although the radiation from the C-arm is relatively low, radiation exposure is a cumulative process, and as a consequence, there is no safe dose.

The proposed method of measuring and analysing the drilling force is intended to assist the surgeon by providing additional information regarding the strength of the bone along the drilling trajectory. This information can be used to select appropriate treatment of internal fixation and

to suggest the need for more protective post-operative treatment (Smith *et al.*, 1992), as well as to assess the success rate associated with internal fixation.

A1.3 Internal Fixation of Femoral Shaft Fractures

The treatment of femoral shaft fractures is often associated with closed intramedullary nailing, as shown in figure A1.2b. Intramedullary nails are long hollow metal tubes which are inserted from the proximal end of a long bone into the medullary cavity. This method of internal fixation provides the best fracture stabilisation and does not require a secondary procedure as compared to plaster-casting and external fixation (Bucholz & Browner, 1990). Furthermore, a decreased length of hospitalisation has also been noted in the intramedullary nailing when compared to traction and plaster-casting methods. Because of the complexity in the types of shaft fractures, pre-operative planning and intra-operative planning play an important role towards the success of intramedullary nailing.

The patient is placed either in supine or lateral position on the fracture table and a closed reduction is performed with the help of a C-arm. After draping the affected site, an incision is made for adequate exposure of the proximal femur's greater trochanter. A hole is made in line with the longitudinal shaft axis and a centering pin is inserted into the medullary canal. The centering pin acts a guide for the cannulated cutter to open the medullary canal. The centering pin and the cutter are then removed. Assuming that the alignment of bone fragments is maintained, a reaming rod with an offset or a curved ball tip is inserted, as far as possible, to the distal end of the femur under fluoroscopic guidance on both PA and lateral planes. If minor residual displacement of the fracture is present, the offset ball tip reaming rod can facilitate realignment. Otherwise, a smaller intramedullary nail is inserted to act as a lever for the realignment of major fracture fragments in order to facilitate the insertion of the reaming rod. Further reaming is carried out using a flexible cannulated reamer through the reaming rod, which acts as a guide, until a desired diameter is obtained. The reaming rod is replaced by a guide rod when the reaming process is completed. A nail of the appropriate diameter and length is then selected and inserted, as far as possible, into the medullary canal. Using a ram or a mallet, the nail is driven into the medullary canal to a correct depth in controlled strikes.

After the laborious process of inserting the nail, the next stage is to insert interlocking screws to prevent rotation of the femur's proximal and distal fragments. Inserting the proximal interlocking screw is relatively easy and this is achieved by using a mechanical targeting device. However, the insertion of distal interlocking screws is much more complicated due to the bending and torsional deformation of the nail during insertion. Thus, it is practically impossible for mechanical targeting devices to locate the distal holes which are hidden behind the cortical wall of the femoral shaft. The difficulty in locating these distal holes can be overcome by using hand-held aiming devices or the free-hand aiming method in conjunction with fluoroscopic guidance. This procedure of locating the distal holes is very skill demanding and exposure to x-ray radiation on the surgeon's hand is inevitable. Therefore, the hazard of radiation exposure is more pronounced among surgically inexperienced surgeons due to the long learning curve (Coetzee, 1992).

The proposed method of safety enhancement is aimed at assisting the surgeon in preventing or minimising excessive protrusion or over-travel of drill bit during break-through so as to minimise tissue damage. The measurement and analysis of drilling forces can also give an indication of the material, in which the drill bit is penetrating. In the case of inserting distal interlocking screws, the material can either be cortical bone or metal (intramedullary nail). This can, therefore, further enhance the safety of the drilling procedure associated with robotic assisted orthopaedic surgery in addition to the drilling trajectory planned by the vision interface system. The robotic system with a vision interface system is described in Appendix 2.

Appendix 2

Description of the Robotic System for Orthopaedic Surgery Assistance

The general description of the prototype robotic system for orthopaedic surgery assistance, which is outlined in Section 2.2.2, is presented in this appendix.

A2.1 Prototype Robot Manipulator and Controller

The design of the prototype manipulator, shown in figure A2.1, is to meet both the safety and the sterility requirements, as well as the physical size limitation imposed by the operating procedure. The manipulator has of four degrees of freedom (DOF) for the positioning of a drill feed unit (Bouazza-Marouf *et al.*, 1995). There are two cartesian (linear) joints and two rotational joints for the four DOFs. The linear motions are horizontal (joint 1) and vertical (joint 2), while the rotational motions are pan (joint 3, rotation about the vertical axis) and tilt (joint 4, rotation about the horizontal axis). The drill feed unit (joint 5) is a linear joint. All the joints are driven by stepper motors through two different mechanisms. The drill feed, horizontal, tilt and vertical motions are driven through backlash-free ballscrews, while the pan motion is driven through a backlash-free Harmonic Drive gearbox. Interfacing of the motor drivers to a personal computer (PC) is achieved through a digital I/O board, which enables the manipulator to be controlled by the PC. At present, the software program for controlling the robot manipulator is written in Borland C++ V4.0 programming language.

Apart from the drill feed joint, all other joints are locked in position through the application of brakes. The systems used on the horizontal, tilt and vertical joints are commercially available fail-safe electromagnetic brakes which operate to stop the ballscrews from rotating, when the electrical power is switched off. The size of these brakes depends on the lead or pitch of the ballscrew. Almost all commercial electromagnetic and mechanical brakes or clutches have inherent backlash due to the clearances between/at the rotating and sliding components. However, backlash in the electromagnetic brakes is reduced to a minimum using shims of

appropriate thickness. Backlash in the brake could have a detrimental effect on the accuracy and precision of the whole system.

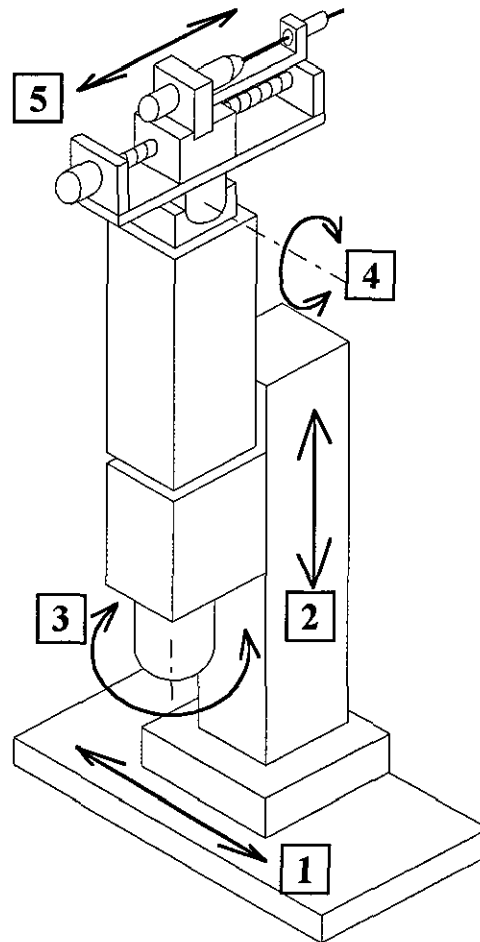


Fig. A2.1 Prototype robot manipulator

Although, backlash-free brakes and clutches are commercially available at a very high cost, they are not suitable for the particular construction of the pan joint. A problem exists in the pan joint as a result of the long extension of the drill feed unit from the pan rotating axis and the expected high drilling forces. The brake for the pan joint has, therefore, been specially designed to meet the braking requirements of high torque and to be free of backlash. The assembly drawing of the pan and brake unit can be found in Appendix 8.1. In addition to the backlash-free feature, the pan brake utilises a toggle mechanism activated by a pneumatic cylinder to obtain a high braking torque. This toggle mechanism also provides a safety feature which ensures that the brake, once activated, remains in force even when the power (electrical or pneumatic) is cut-off.

The positional feedback for all the joints is obtained from angular and linear potentiometers. These analogue measurements are filtered using fourth-order analogue Butterworth filters in order to reduce/eliminate noise and avoid aliasing before being interfaced to a PC through a commercial analogue to digital converter (ADC). Two levels of safety limits are implemented in the robotic system for protection against mechanical overdrive. The initial level, enforced by software limits as a front line protection, enables the motion of the system to be halted prior to the hardware level of limit switches being activated, which would then require the resetting of the system.

Finally, an end effector, which is mounted on the carriage of the feed motion, is required to enable the robotic system to perform drilling. The assembly drawing of the end effector, which consists of a drill holder, a drill feed unit and a force sensor, can be found in Appendix 8.2. Measurement of drilling thrust force by the force sensor is obtained from strain gauges attached to a cantilever plate. The drill holder provides a mounting for an air drill. This has a drill bit guide to prevent deflection caused by slippery and uneven bone surfaces, hence maintaining the desired drilling trajectory. Further description of the end effector is given in Section 7.1.1. Due to sterility issues, the drill holder was specially designed to withstand sterilisation by steam (autoclaving¹) using suitable materials for both standard and manufactured components. It was also designed to be easily located and clamped onto the drill feed unit without the loss of positional accuracy, even with a sterilised drape over the drill feed unit. Although the use of air drills complies with current practice in orthopaedic surgery, industrial air drills, ARO Series 20, were used for experimental purposes instead of the autoclavable surgical air drills.

Although the robot manipulator can move to any line in space within the working envelope, the drilling trajectory would not be known without the information of the fractured bone location. This information can only be obtained from an integrated vision system.

¹ Autoclaving, which is easily available and relatively inexpensive, is an effective method of killing all types of micro-organisms (Gardner & Peel, 1979).

A2.2 Vision Interface System

In order to obtain the position of an object, such as a bone, or a line in three-dimensional space with respect to the manipulator, a vision interface system is integrated with a mobile x-ray unit and a calibration frame (Bouazza-Marouf *et al.*, 1995). This vision interface is a digital image processing system (DIPS) that consists of a frame grabber, a display monitor and supporting image processing software. The vision system performs four main tasks, namely to digitise and store the video signal transmitted from the x-ray unit image intensifier/television system, to correct for image distortion, to perform drilling trajectory planning and to provide a surgeon interface. In addition, the position feedback from the drill feed enables the progress/position of the drill bit to be continuously monitored and displayed without further use of fluoroscopy.

The digitised image suffers a form of spatial distortion known as 'pincushion distortion', which is caused by mapping a projected x-ray image from a curved surface on to a flat output. Therefore, measurements can only be made after correction of the distorted images has been performed. Image correction is achieved through a calibration frame which has plates of perspex with radio-opaque reference markers, such as ball bearings, in rectilinear grid pattern. The mechanical design of a particular type of calibration frame is given in Appendix 8.3. Since the spacing between markers are known, the image distortion can be corrected by image processing software to produce actual coordinate measurements. With the calibration frame, which is easily detachable, being connected to the manipulator, the coordinate measurements from the vision system can be transformed into coordinate measurements with respect to the base of the manipulator. Subsequently, the location of the bone or the drilling trajectory is downloaded to the controller and converted into joint commands for the robot manipulator.

A2.3 Procedure of Robotic Assisted Orthopaedic Surgery

The accuracy and repeatability of the robot manipulator combined with the visual information extracted from x-ray images by the vision system reflect the great potential robotic systems have in the field of surgery assistance. However, the benefits of a robotic system could mean certain changes in the conventional surgical procedures to accommodate new equipment and to adopt new operating procedures.

A general procedure of using the robotic system for one particular type of orthopaedic surgical procedure, the repair of hip fractures, is as follows:

- (i) After positioning the patient on the orthopaedic traction table, the surgeon proceeds to fracture reduction by applying traction.
- (ii) The manipulator is positioned as close to the fracture site as possible so that the fractured bone is in full view within the calibration frame.
- (iii) After the x-ray unit is in position, two near orthogonal fluoroscopic images are acquired and stored by the frame grabber.
- (iv) Calibrations are carried out to correct image distortion and ascertain the coordinate measurements of the bone in three dimension.
- (v) An incision is made on the patient, after the calibration frame has been removed, and the fracture site is adequately exposed using a retractor. It should be ensured that the manipulator is not being displaced.
- (vi) Subsequently, the surgeon indicates the desired path of the guide wire on two images, the PA and lateral, that are displayed one at a time.
- (vii) The indicated path of the guide wire is displayed for the surgeon to check and confirm.
- (viii) The desired trajectory computed by the vision system is converted into joint commands for the manipulator which is then driven to the required drilling position and locked in position, leaving the drill feed free to traverse forward.
- (ix) The surgeon initiates the drilling procedure.
- (x) Before proceeding further with the drilling, the surgeon checks and confirms the drilling trajectory by taking another pair of fluoroscopic images.

Appendix 3

Bone

The objective of this appendix is to provide background to the science of bone structure, properties and function in support of this research. A general description of the functions and chemical composition of the bone is given. The active mechanism of bone regeneration, which is governed by three types of bone cell, is discussed. The bone structure is also described in terms of macro and micro levels in this appendix. As orthopaedic surgery is normally associated with fracture of bone, a brief description of the fracture stabilisation and healing of bone is provided. Finally, the physical properties of bone are discussed with respect to bone disorders and, in particular, its mechanical properties.

A3.1 The Functions of Bone

Bone is a highly vascular, dynamic and living composite material of organic and inorganic (mineral) components with minute liquid filled pores. Because bones are the main structural elements of the body, hard inorganic and resilient organic components are intimately blended in the bone tissue to provide almost equal resistance to both tension and compression. At gross level, the ability of bones to resist mechanical forces is a function of the mechanical properties and architecture of bones. As a result, bone offers remarkable hardness, resilience and strength.

The functions of the bone can be categorised into mechanical and physiological. Mechanically, bones form a supporting framework to transmit forces for physical activity and for the protection of internal organs. As a supporting framework, bones require adequate anatomic shape and stiffness according to the anatomic location and loading conditions as bones are subjected to forces exerted not just by the physical activity but also by the muscle and the body. In addition, bones, acting as lever systems, provide attachments for ligaments and tendons.

The physiological functions of bone involve the formation of blood cells (hematopoiesis) and storage of salts or calcium (mineral homeostasis) to provide a mineral reservoir for the body.

The process of hematopoiesis takes place in the red marrow which is largely found in the pores of cancellous bone.

A3.2 The Chemical Composition of Bone

Bone consists of organic and inorganic components. The composition, properties and distribution of these two components have a significant effect on the mechanical properties of bone. In mature bone, the organic component makes up 30-40% and the mineral component forms 60-70% of the dry weight of the bone, and water constitutes 20% of the total weight (Williams & Warwick, 1980). The organic component contains approximately 95% collagen (a protein material) fibres which provides some resilience (flexibility) and toughness to bone. While the remaining organic component consists of various bone proteins.

The inorganic component, which is deposited on the organic (collagen) matrix, consists of calcium and phosphate salts in the form of hydroxyapatite to give the bone its strength, hardness and some rigidity. It also provides a mineral reservoir for the body where approximately 95% of the body mineral is stored. Mineral salts in the serum (blood plasma) are essential for a number of body functions and therefore, regulating mineral balance in serum always comes first before the mineral requirement of bone. This is carried out by withdrawing the mineral component from the bones.

A3.3 Bone Cells

Bone has a remarkable capacity for regeneration due to the continuous process of bone removal (resorption), formation and maintenance in a phenomenon known as bone remodelling (Mundy, 1995; Nigg & Herzog, 1995). This dynamic process of bone remodelling is governed by three types of major bone cells: osteoclasts, osteoblasts and osteocytes. Osteoclasts are cells that are responsible for the resorption of bone by releasing mineral (calcium) from the bone matrix into the serum. Meanwhile, osteoblasts, the bone forming cells, are responsible for the synthesis of collagen matrix and later the mineralisation of the newly formed bone matrix. The mature

mineralised bone matrix, known as osteocytes, is assumed to be responsible for maintaining bone tissue by controlling local mineralisation and mineral exchange between bone and serum.

The process of bone remodelling either allows the bone to maintain its existing mass or results in a reduction of bone mass. The remodelling sequence is initiated by the activation of osteoclasts on a previously inactive bone surface. For a period of approximately two weeks, the continuous bone resorption activity produces a resorption cavity. It is then followed by a process of bone formation through osteoblasts to fill or repair the resorption cavity over a period of approximately three months. The relationship between processes of bone resorption and bone formation is, therefore, extremely critical in maintaining bone mass during bone remodelling. An increase in the bone resorption with respect to the bone formation would imply a loss in bone mass.

A3.4 The Structural Composition of Bone

The bones in the body can be classified according to shape, namely long, short, flat, irregular and sesamoid (Williams & Warwick, 1980; Nigg & Herzog, 1994). The bone drilling investigation in this thesis concentrates on a long bone, for instance the femur (figure A3.1). In general, the bone consists of two basic structural components: the cortical (compact) bone and the cancellous (spongy and trabecular) bone. The human skeleton is represented by approximately 80% cortical bone and 20% cancellous bone (Hagiwara *et al.*, 1994). Cortical bone is a solid and dense material, and is resistant to bending. This type of bone forms the wall of the shaft (diaphysis) and external surfaces of bones. Depending on the mechanical requirements, the thickness of the cortical bone varies between and within bones (Nigg & Herzog, 1995). For example, the shaft construction of long bones is thinner but still maintains the same compressive stress throughout the length of the shaft (Piekarski, 1978). In addition, this type of construction increases the bending ability of the shaft.

Cancellous bone, however, has an irregular structure of interconnecting plates and columns like a porous structure called trabeculae, as shown in figure A3.2. This type of construction is quite suitable for absorbing energy and transmitting compressive stresses, as well as for reducing the weight of the bone. The spaces between the interconnecting trabeculae are filled with red

(hemopoietic) marrow. Cancellous bone is mainly found in the vertebrae, in the epiphysis (bulbous end) of long bones (for example, the proximal and distal ends of a femur shown in figure A3.1), and between two layers of cortical bone in the flat and short bones. In terms of mechanical properties, such as elasticity modulus and compressive strength, cancellous bone is inferior to cortical bone. Therefore, the construction of cancellous bone has to be thicker to absorb energy and to transmit compressive stresses, especially at the ends of long bones which support bearing surfaces of joints (Piekarski, 1978). Cancellous bone also has a higher metabolic (turnover) rate due to its greater surface area as compared to cortical bone, rendering cancellous bone more responsive to changes in the mineral storage (Cooper, 1990).

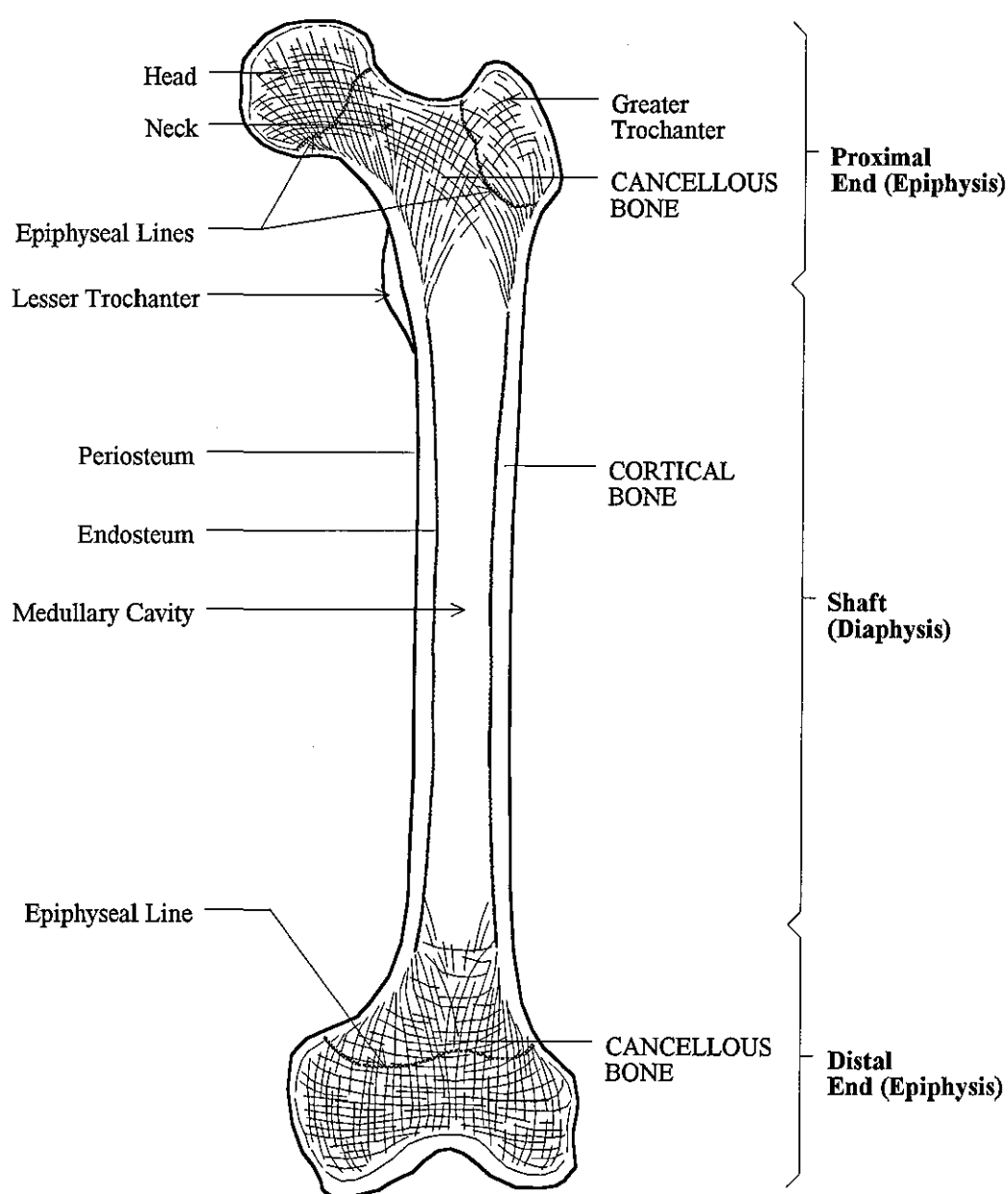


Fig. A3.1 Bone structural distribution of a femur (long bone)



Fig. A3.2 Structure of cancellous bone (Williams & Warwick, 1980)

A3.5 The Microstructure of Bone

The microstructure of bone can be classified into three types: woven bone, primary bone and secondary bone (Nigg & Herzog, 1995; Williams & Warwick, 1980). Woven bone is a non-lamellar bone, and the orientation of the collagen fibres in woven bone is irregular and hence has less bone density. The term 'lamellar' describes a pattern of lamination and often refers to the regular microstructure of mature or adult bone. Woven bone is related to the formation of bone during embryonic life and found in isolated patches in adults. However, woven bone is most commonly found during the healing process of a fractured bone, whereby it acts as a temporary source of mechanical strength and support for the development of mature (lamellar) bone.

Both lamellar and non-lamellar bones are found in primary bone. Unlike woven bone, primary bone requires an existing hard tissue or cartilage model for bone formation. There are three main types of primary bone which are morphologically, mechanically and physiologically different. The first type is known as primary or circumferential lamellar bone, and it is found encircling the inner and outer surfaces of the bone. Since primary lamellar bone has a large surface area in close proximity to marrow and blood, functional requirement of blood cell

formation and mineral balance in serum takes precedence over mechanical requirement. Plexiform bone is the second type, but it is commonly found in bones of fast growing large animals, such as the cow, which demand rapid growth for mechanical strength. The plexiform bone also has a highly oriented microstructure. The third type called primary osteons, which are first formed, are non-lamellar parallel-fibred bone. Osteons are sets of thin plates of bony tissue, called lamellae, arranged in concentric rings around a vascular canal. Primary osteons are developed through sequential filling with mineralised collagen matrix and narrowing of vascular spaces of woven bone. At the same time, the collagen matrix becomes a more parallel-oriented structure and forms into concentric rings of lamellae with a central vascular canal.

Secondary bone, which is lamellar bone, is a product of bone remodelling to replace existing bone tissue, which includes woven bone (when it exists) and primary bone, with new bone. This new bone tissue is known as secondary osteons or Haversian systems and is typically found in cortical bone. The main difference between primary and secondary osteons is the presence of cement (reversal) lines on secondary osteons due to bone remodelling. Cement lines, which demarcate the outer limits of each Haversian system, indicate the limit of bone resorption and the start of bone formation during bone remodelling. Other differences include smaller vascular canals and fewer lamellae in primary osteons than secondary osteons. The microstructure of Haversian systems is shown in figure A3.3. Haversian systems are irregular cylindrical units that consist of concentric lamellae of bone tissue which surround a central Haversian canal containing minute blood vessels and a nerve. Small spaces called lacunae, which contain osteocytes, are distributed between these lamellae. Since osteocytes have a function of maintaining bone tissue, fine radiating channels called canaliculi connect lacunae with each other and with the Haversian canal to transport nutrients. The Haversian canals are linked with the periosteum, endosteum and each other via oblique and perpendicular perforating channels known as Volkmann's canals. Between the Haversian systems, there are angular intervals occupied by interstitial bone that comprises remnants of woven bone, primary osteons and older remodelled secondary osteons. All Haversian and most interstitial systems have a boundary of cement line to indicate the limit of bone resorption.

Cortical bone consists of Haversian systems that are oriented parallel to the shaft of long bones, while the trabeculae of cancellous bone are made up of fragmented superimposed lamellae with numerous intervening cement lines. Only certain large trabeculae contain small Haversian

systems. Nutrients for the trabeculae are provided by blood vessels in the red marrow filled cancellous bone and these blood vessels do not penetrate the trabeculae.

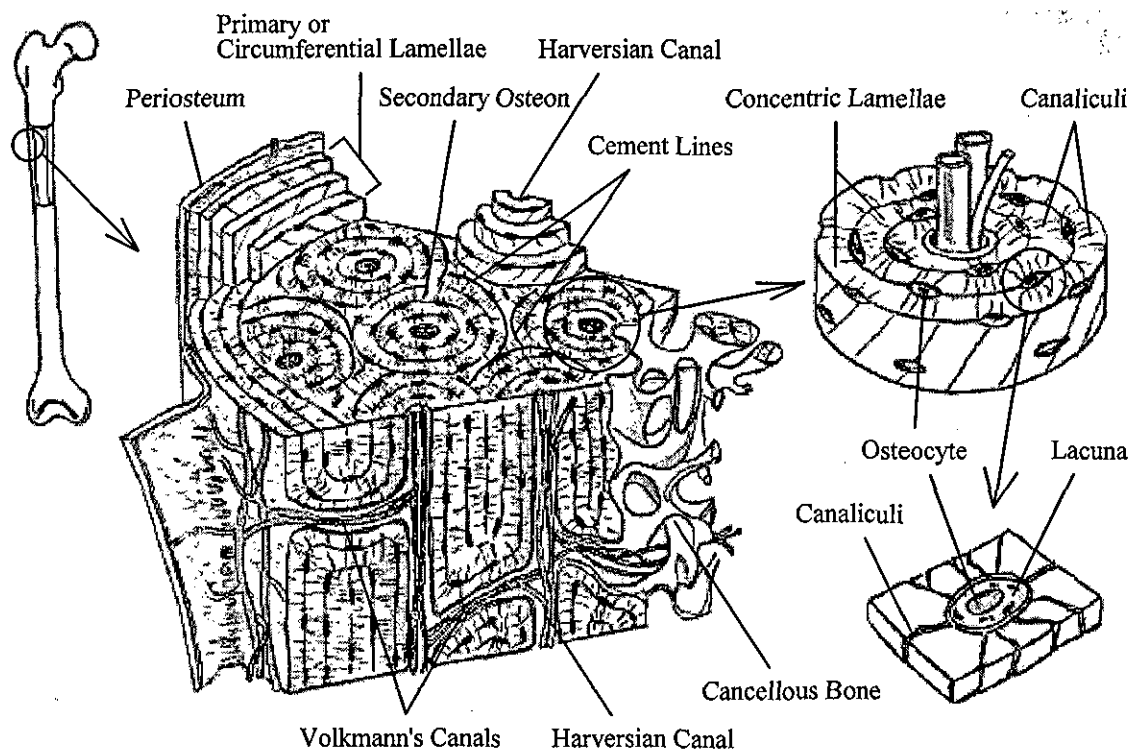


Fig. A3.3 Microstructure of bone

A3.6 Fracture Stabilisation and Healing of Bone

When a bone fractures, its functionality is lost. Means of reducing bone fragments to their anatomic position and stabilising the fracture have to be carried out in order to effect the process of bone healing. The aim of reducing the fracture is to provide for optimal recovery of function and to minimise malalignment, while fracture stabilisation maintains the position of the reduced bone fragments and offers a temporary support while the bone heals. Stabilisation can be achieved through traditional traction and plaster-casting, and either internal or external fixation of the fractured bone.

Soon after a fracture, the surrounding periosteum is normally torn and the repair process begins with the coagulation of blood which flows from ruptured blood vessels into the fracture area to form hematoma. It is followed by rapid formation of callus or woven bone to bridge the fracture gap as well as to provide temporary strength and support. Gradually, the callus

undergoes the process of bone remodelling to produce lamellar bone. The outcome of this fracture healing process depends partly on the quality of the fracture reduction and stabilisation, and partly on the orientation of loads applied.

A3.7 The Physical Properties of Bone

In the previous sections, bone is described in terms of anatomy and physiology. The physical importance of bone lies in the study of bone strength, and the effects of metabolic (nutritional) and hormonal (endocrine) disorders on the physical properties of bone. The determination of mechanical properties of bone can provide an indication on the extent of reduction in bone strength due to bone disorders.

Effects of Metabolic and Hormonal Disorders on Bone

Hormonal disorders greatly affect the development of bone where hypersecretion and hyposecretion of growth hormone can lead to gigantism and dwarfism respectively. Metabolic effects, however, have a significant impact on the mechanical properties of bone, and often lead to gross deformation of bone and increased risk of fracture as a result of reduction in bone strength.

The most prominent metabolic disorder is osteoporosis which is characterised by a continuous loss or increased porosity of bone tissue, without affecting the organic and mineral content in the remaining bone, due to increased osteoclasts activity than normal during bone remodelling. An abnormally large resorption cavity is created by osteoclasts, but the filling of this cavity carried out by osteoblasts is incomplete. Although bone loss is age-related, osteoporosis accelerates the rate of bone loss which undermines the normal material and structural integrity of the bone. Therefore, osteoporosis is the main cause of increased bone fragility and risk of fracture among the elderly population.

Another type of metabolic disorder related to the elderly population is called Paget's disease whereby the process of bone remodelling becomes excessive and abnormal (Mundy, 1995).

This increased activity of both osteoblasts and osteoclasts is irregular and results in different areas of bone formation and resorption. There is also another bone disorder called osteomalacia or softening of bone which is described by the failure of mineralisation during bone formation (Mundy, 1995). This is caused by the deficiency of Vitamin D which influences the intestinal absorption of calcium and phosphate. Prolong osteomalacia coupled with weight-bearing can lead to gross deformity of bone.

Mechanical Properties of Bone

The mechanical properties of bone are determined by methods applied to engineering materials which are homogeneous and isotropic. Since bone is a composite and anisotropic material, only some formulae are applicable (Evans, 1973; Jacobs *et al.*, 1976). The literature on the mechanical properties of both cortical and cancellous bone has been well established.

Mechanical properties of bone can be represented by modulus of elasticity, compressive strength, tensile strength and density. The elastic modulus of cortical bone is approximately 10% of steel although this value varies according to the direction of loading due to anisotropy. The strength of cancellous bone is at least one order of magnitude smaller than cortical bone. In addition, bone storage, condition of the bone (either wet or dry), anatomical site, temperature and to some extent microscopic structure have a significant effect on the determination of mechanical properties. Therefore, large variation in the values of mechanical properties has been shown in the literature for both cortical and cancellous bones. Further discussion on the mechanical properties of cancellous bone is found in Chapter 4 Section 4.3.1.

In this investigation, the experimental tests were carried out on porcine femurs as pig bones share certain similarities in mechanical properties to human bones. The mechanical properties of human and porcine femoral cortical bones are shown in Table A3.1 (Yamada, 1970). Other values of mechanical properties of human femoral cortical bone have been shown to vary between: 80-150 MN/m² for tensile strength, 131-224 MN/m² for compressive strength, and 5-28 GN/m² for tensile modulus of elasticity (Nigg & Herzog, 1995).

Unlike cortical bone, cancellous bone has an intricate architectural organisation to achieve physiologic optimisation for maintaining mechanical integrity with minimum mass. This architectural organisation of cancellous bone, coupled with variations in specimen geometry and testing conditions, causes a large variation in the mechanical properties determined by various researchers. The compressive elastic modulus for cancellous bone of the proximal femur varies from 20.68 MN/m² to 2248 MN/m², while compressive strength varies from 0.21 MN/m² to 16.2 MN/m² (Martens *et al.*, 1983; Goldstein, 1987). Such large variation in the mechanical properties creates difficulty in defining the strength of cancellous bone. Furthermore, the mechanical properties of cortical and cancellous bone are not interchangeable, and the extrapolation of strength and elastic modulus from the cancellous bone to predict those of the cortical bone or vice-versa have been consistently unsuccessful (Rice *et al.*, 1988; Keller, 1994).

Mechanical Properties (Femoral Cortical Bone)	Human (Age Group)		Pig
	20 - 39 years	60 - 69 years	
Ultimate Tensile Strength (MN/m ²)	121.64±1.08	86.33±2.35	86.33±1.47
Tensile Modulus of Elasticity (GN/m ²)	17.56	-	14.62
Ultimate Compressive Strength (MN/m ²)	166.77±4.22	145.19±2.26	98.1±0.69
Compressive Modulus of Elasticity (GN/m ²)	10.40	-	4.81
Ultimate Torsional Strength (MN/m ²)	57.09±1.08	48.95±1.18	-
Torsional Modulus of Elasticity (GN/m ²)	3.43	2.94	-

Table A3.1 Mechanical properties of human and pig cortical bones (femur)

Appendix 4
Modelling of Drilling Unit Bone Support System
(with reference to Section 5.2)

The drilling unit bone support system, shown in figure 5.1, can be represented by a spring mass model, as shown in figure A4.1, when damping is ignored. The equation of motion of the spring mass model is:

$$m \frac{d^2 y(t)}{dt^2} = F(t) - ky(t)$$

which upon Laplace transformation, with zero initial conditions, gives:

$$ms^2 Y(s) = F(s) - kY(s)$$

$$\frac{Y(s)}{F(s)} = \frac{1}{ms^2 + k}$$

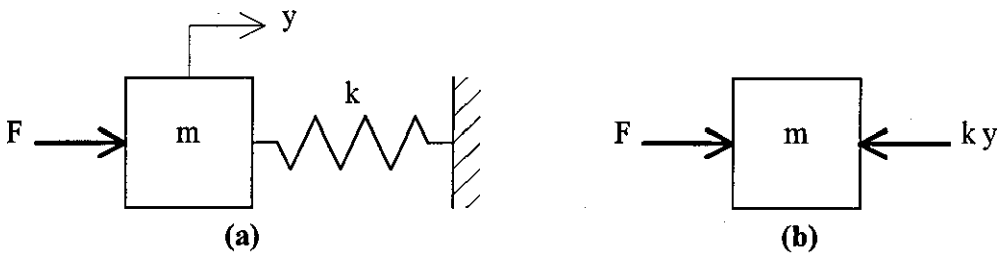


Fig. A4.1 (a) A spring mass model, (b) Free body diagram of the mass

The spring mass model would, therefore, vibrate for infinite time (a continuous sinusoid of frequency = $\sqrt{(k/m)}$) in response to a disturbance. However, the friction in the bearings and the friction between the drill bit and bone during drilling provide a damping force to the model. Assuming viscous damping (and ignoring coulombic friction), the system can be modelled as shown in figure A4.2. The equation of motion of the spring mass damper model is:

$$m \frac{d^2 y(t)}{dt^2} = F(t) - C \frac{dy(t)}{dt} - ky(t)$$

which upon Laplace transformation, with zero initial conditions, gives:

$$ms^2 Y(s) = F(s) - CsY(s) - kY(s)$$

$$\frac{Y(s)}{F(s)} = \frac{1}{ms^2 + Cs + k}$$

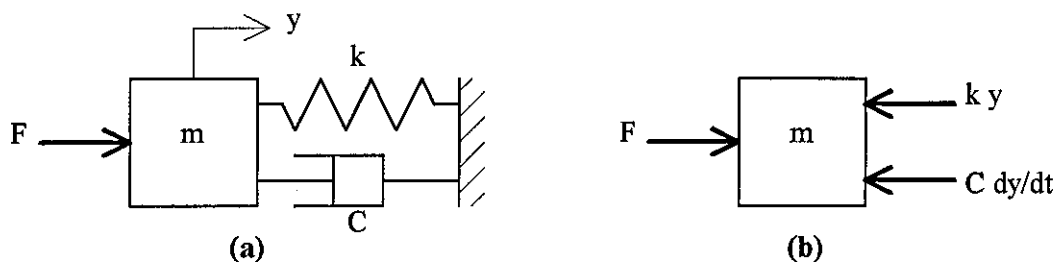


Fig. A4-2 (a) A spring mass damper model, (b) Free body diagram of the mass

As a result of the inherent damping in the model, the response to a disturbance becomes similar to a decaying sine. The decaying sine of the system is shown in figure A4.3 in response to a unit step input. This response is based on the system mass, m , of 7 kg, a damping coefficient, C , of 2 Ns/m and a spring stiffness coefficient, k , of 2800 N/m (2.80N/mm).

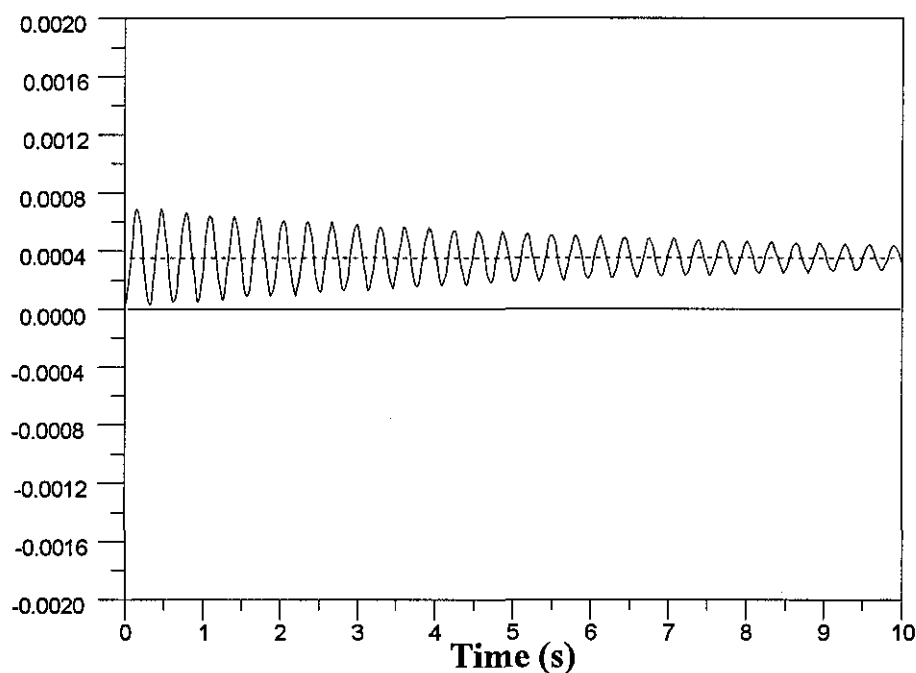


Fig. A4.3 The response of the spring mass damper system to a unit step input

Appendix 5

Modelling of Cross-Sectional Chip Area at Drill Bit Break-Through

This appendix presents the derivation of a model to represent drill bit break-through. The model is based on the changes in the cross-sectional area of the chip, cut by the drill bit, as a function of time which is related to the feed rate.

The chip is assumed to be produced along the cutting edge during drilling, as shown in figure A5.1. The aim of modelling the cross-sectional chip area is to show the variation in the chip area at imminent drill bit break-through.

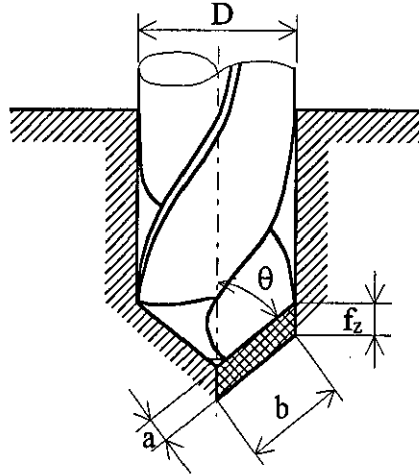


Fig. A5.1 Cross-sectional area of the chip (Arshinov & Alekseev, 1976.)

From figure A5.1, the drill feed per lip, f_z , is:

$$f_z = \frac{f}{2} \text{ mm/rev} \quad (\text{A5-1})$$

where: f is the feed rate (mm/rev).

The thickness, a , of the undeformed chip per lip measured from the perpendicular direction to the drill lip disregarding the chisel edge is given by:

$$a = f_z \sin \theta = \frac{f}{2} \sin \theta \text{ mm}$$

where: θ = is the half drill bit point angle.

The width, b , of the undeformed chip measured along the lip is:

$$b = \frac{D}{2\sin\theta} \text{ mm}$$

where: D is the drill bit diameter (mm).

The total cross-sectional area, $TCSA$, of the undeformed chip per lip over one revolution is:

$$TCSA = a.b = \frac{Df}{4} \text{ mm}^2 \quad (\text{A5-2})$$

The drill bit break-through process involves three stages of chip formation, as shown in figure A5.2. In the first stage, the chip area begins to reduce at a feed rate of f , as the drill bit begins to break-through. At time t (s) after the start of break-through, the cross-sectional area is reduced by an area $A_1(t)$ at Stage 1, which is given by:

$$A_1(t) = \frac{1}{2}(fnt)(fnt\tan\theta) = \frac{(fnt)^2}{2}\tan\theta \text{ mm}^2$$

where: n is the rotational speed (rev/s) of the drill bit.

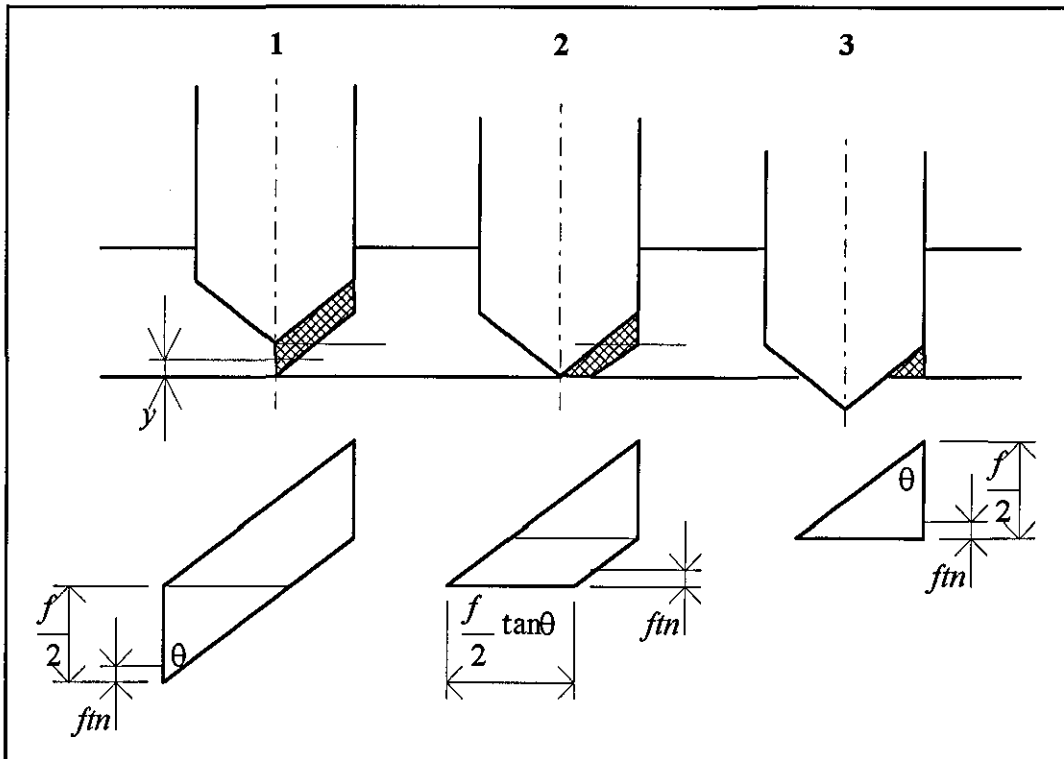


Fig. A5.2 Three stages of chip area formation during drill bit break-through

The cross-sectional area of the chip becomes:

$$CSA_1(t) = \frac{Df}{4} - \frac{(fnt)^2}{2} \tan\theta \text{ mm}^2 \quad (\text{A5-3})$$

At the start of Stage 2, the cross-sectional area of the chip is:

$$TCSA_2 = \frac{Df}{4} - \frac{f^2}{8} \tan\theta \text{ mm}^2 \quad (\text{A5-4})$$

and the area is reducing by:

$$A_2(t) = fnt \left(\frac{f}{2} \tan\theta \right) \text{ mm}^2$$

Therefore, the cross-sectional area of the chip decreases to give:

$$\begin{aligned} CSA_2(t) &= \frac{Df}{4} - \frac{f^2}{8} \tan\theta - A_2(t) \\ &= \frac{Df}{4} - \frac{f^2}{8} \tan\theta - \frac{f^2 nt}{2} \tan\theta \text{ mm}^2 \end{aligned} \quad (\text{A5-5})$$

At the start of Stage 3, the cross-sectional area of the chip is:

$$TCSA_3 = \frac{f^2}{8} \tan\theta \text{ mm}^2 \quad (\text{A5-6})$$

The cross-sectional area of the undeformed chip varies in a triangular form.

$$\begin{aligned} CSA_3(t) &= \frac{1}{2} \tan\theta \left(\frac{f}{2} - fnt \right)^2 \\ &= \frac{1}{2} \tan\theta \left(\frac{f^2}{4} - f^2 nt + (fnt)^2 \right) \text{ mm}^2 \end{aligned} \quad (\text{A5-7})$$

The time taken to complete Stage 1 is obtained by equating equations A5-3 and A5-4, i.e.:

$$CSA_1(t) = TCSA_2$$

This gives:

$$\begin{aligned} n^2 t_1^2 &= \frac{1}{4} \\ \therefore t_1 &= \frac{1}{2n} \end{aligned} \quad (\text{A5-8})$$

The time taken to complete Stage 2 from Stage 1 is obtained by equating equations A5-5 and A5-6, i.e.:

$$CSA_2(t) = TCSA_3$$

This gives:

$$\therefore t_2 = \frac{D}{2fn} \cot \theta - \frac{1}{2n} \quad (A5-9)$$

The time taken to complete Stage 3 from Stage 2 is obtained by equating equation A5-7 to zero, i.e.:

$$CSA_3(t) = 0$$

This gives:

$$\therefore t_3 = \frac{1}{2n} \quad (A5-10)$$

Therefore, the time-varying cross-sectional area of the chip at the three stages obtained from the equations above are given by:

$$CSA(t) = \begin{cases} \frac{Df}{4} - \frac{(fnt)^2}{2} \tan \theta & 0 < t \leq \frac{1}{2n} \\ \frac{Df}{4} - \frac{f^2}{8} \tan \theta - \frac{f^2 nt}{2} \tan \theta & \frac{1}{2n} < t - \frac{1}{2n} \leq \frac{D}{2fn} \cot \theta \\ \frac{1}{2} \tan \theta \left(\frac{f^2}{4} - f^2 nt + (fnt)^2 \right) & \frac{D}{2fn} \cot \theta < t - \frac{D}{2fn} \cot \theta \leq \frac{D}{2fn} \cot \theta + \frac{1}{2n} \end{cases}$$

Appendix 6

A Recursive Kalman Filter

This appendix presents the process of minimising the mean-squared error in order to establish the relationship between two time-varying parameters, $a(n)$ and $b(n)$, of the recursive Kalman filter.

To show the derivation of an optimum Kalman filter (Bozic, 1979), a first-order recursive algorithm is used and is given by:

$$\hat{y}(n) = a(n)\hat{y}(n-1) + b(n)x(n) \quad (\text{A6-1})$$

where: $\hat{y}(n)$ represents the best estimate of the actual or pure signal $y(n)$, $x(n)$ is the current input which can be affected by noise, and $a(n)$ and $b(n)$ are two time-varying parameters.

Therefore, the error $e(n)$ of this estimation is:

$$e(n) = \hat{y}(n) - y(n) \quad (\text{A6-2})$$

$$e(n) = a(n)\hat{y}(n-1) + b(n)x(n) - y(n) \quad (\text{A6-3})$$

The relationship between the two time-varying parameters, $a(n)$ and $b(n)$, is determined through the minimisation of the mean-squared error. The mean-squared error $\rho(n)$ is given as:

$$\begin{aligned} \rho(n) &= E[(\hat{y}(n) - y(n))^2] = E[e(n)^2] \\ &= E[(a(n)\hat{y}(n-1) + b(n)x(n) - y(n))^2] \end{aligned} \quad (\text{A6-4})$$

where: E represents the operation to evaluate the mean or expected value of a data set.

For minimisation, the mean-squared error is differentiated with respect to $a(n)$ and $b(n)$ and is then equated to zero:

$$\frac{\partial \rho(n)}{\partial a(n)} = 2E[a(n)\hat{y}(n-1) + b(n)x(n) - y(n)]\hat{y}(n-1) = 0 \quad (\text{A6-5})$$

$$\frac{\partial \rho(n)}{\partial b(n)} = 2E[a(n)\hat{y}(n-1) + b(n)x(n) - y(n)]x(n) = 0 \quad (\text{A6-6})$$

Equations A6-5 and A6-6 can be alternatively written, using equation A6-3, as:

$$E[e(n)\hat{y}(n-1)] = 0 \quad (\text{A6-7})$$

$$E[e(n)x(n)] = 0 \quad (\text{A6-8})$$

Equation A6-5 is used to establish the relationship between $a(n)$ and $b(n)$ and is written as:

$$E\{[a(n)\hat{y}(n-1) + b(n)x(n) - y(n)]\hat{y}(n-1)\} = 0 \quad (\text{A6-9})$$

Add and subtract $a(n)y(n-1)$ for the above equation A6-9 to give:

$$E\{[a(n)[\hat{y}(n-1) - y(n-1)] + a(n)y(n-1)]\hat{y}(n-1)\} = E\{[y(n) - b(n)x(n)]\hat{y}(n-1)\} \quad (\text{A6-10})$$

In order to derive the optimum Kalman filter, the signal to be estimated, $y(n)$, and the present noisy input signal, $x(n)$, can be represented by an assumed model of signal generation and its measurement, as shown in figure A6.1. The signal generation model consists of a first-order recursive digital filter driven by a zero-mean white noise source to give similar noise spectral properties to those of the actual signal. Random noise in the signal during measurement or observation is represented by the additive zero-mean white noise in the measurement model.

The pure random signal $y(n)$ is generated according to the dynamical equation:

$$y(n) = ay(n-1) + w(n-1) \quad (\text{A6-11})$$

where: the parameter a acts as a time-constant for the signal generation.

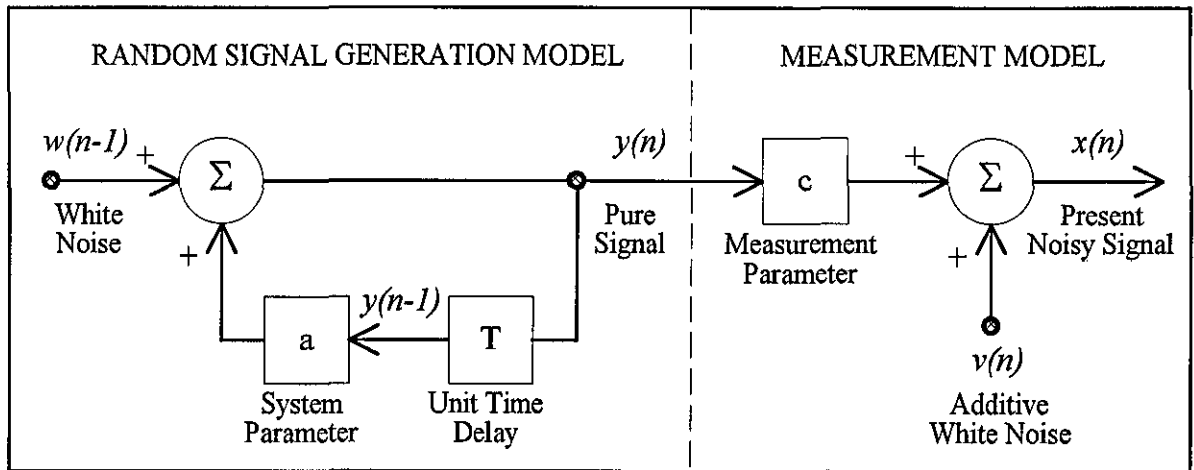


Fig. A6.1 Model of random signal generation and measurement/observation (Bozic, 1979)

Subsequently, the noisy signal $x(n)$ is produced by modifying the pure signal through a measurement parameter c and additive white noise, as shown in figure A6.1. Therefore, a linear measurement model equation is given as:

$$x(n) = cy(n) + v(n) \quad (\text{A6-12})$$

Substitute equations A6-11 and A6-12 to equation A6-1 to give:

$$\hat{y}(n) = a(n)\hat{y}(n-1) + acb(n)y(n-1) + cb(n)w(n-1) + b(n)v(n) \quad (\text{A6-13})$$

At time $(n-1)$, the above equation A6-13 is expressed as:

$$\hat{y}(n-1) = a(n-1)\hat{y}(n-2) + acb(n-1)y(n-2) + cb(n-1)w(n-2) + b(n-1)v(n-1) \quad (\text{A6-14})$$

Substitute equation A6-2 for $(n-1)$ and equation A6-12 to equation A6-10 on the left-hand-side and right-hand-side respectively to give:

$$a(n)E[e(n-1)\hat{y}(n-1) + y(n-1)\hat{y}(n-1)] = E\{[y(n)[1 - cb(n)] - b(n)v(n)]\hat{y}(n-1)\} \quad (\text{A6-15})$$

With reference to equation A6-15, the term $E[e(n-1)\hat{y}(n-1)] = 0$ is obtained using equation A6-7 for previous time of $(n-1)$. The second term $E[v(n)\hat{y}(n-1)] = 0$ is due the estimate at time $(n-1)$ is not correlated with the measurement noise at time (n) , which is shown in equation A6-14. As a result, the above equation A6-15 reduces to:

$$a(n)E[y(n-1)\hat{y}(n-1)] = [1 - cb(n)]E[y(n)\hat{y}(n-1)] \quad (\text{A6-16})$$

Using the signal generation model A6-11, the above equation A6-16 is given as:

$$a(n)E[y(n-1)\hat{y}(n-1)] = [1 - cb(n)]E\{[ay(n-1) + w(n-1)]\hat{y}(n-1)\} \quad (\text{A6-17})$$

The term $w(n-1)$ in equation A6-17 is not related to $\hat{y}(n-1)$, which is shown in figure A6-14, and thus, $E[w(n-1)\hat{y}(n-1)] = 0$. As a result the above equation A6-17 becomes:

$$a(n)E[y(n-1)\hat{y}(n-1)] = a[1 - cb(n)]E[y(n-1)\hat{y}(n-1)]$$

Therefore:

$$a(n) = a[1 - cb(n)] \quad (\text{A6-18})$$

Substitute equation A6-18 to equation A6-1 to give the equation of a Kalman filter:

$$\hat{y}(n) = a\hat{y}(n-1) + b(n)[x(n) - ac\hat{y}(n-1)] \tag{A6-19}$$

Equation A6-19 in system block diagram is shown in figure A6.2. The present output $\hat{y}(n)$ of a Kalman filter is the sum of two weighted terms. The first term is taken as the previous best estimated output; the second is taken as a correction term which depends on the current measurement/input, $x(n)$, which can be affected by noise and the previous estimate $\hat{y}(n-1)$. Although the gain parameter $b(n)$ is time-varying, it can be assumed that it converges to a steady value as the Kalman filter reaches steady-state operation. This steady-state value for $b(n)$ can be evaluated using equations A6-1, A6-4, A6-7, A6-8 and A6-12 (Bozic, 1979). Therefore, the Kalman filter may be taken as an elementary first-order low-pass recursive filter.

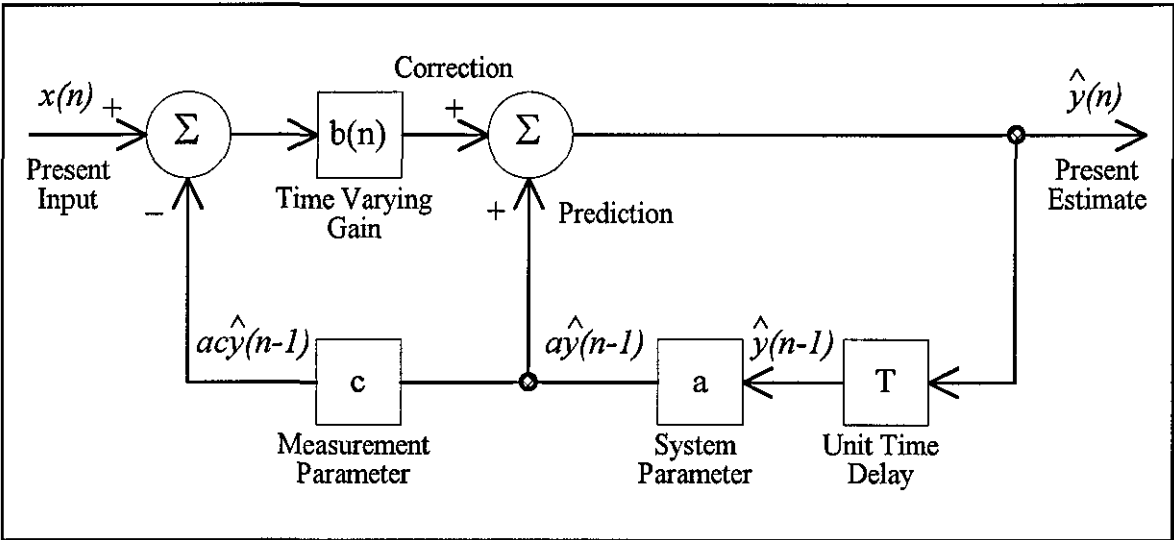


Fig. A6.2 Recursive Kalman filter in system block diagram (Bozic, 1979)

Appendix 7

Journal Paper to be published in the

Proc. Instn Mech. Engrs, Part H, Journal of Engineering in Medicine, Vol. 212, 1998.

Drilling of bone: a robust automatic method for the detection of drill bit break-through

F. R. Ong and K. Bouazza-Marouf

Experimental Results related to Chapter 9

This appendix presents results related to Chapter 9. The first three sections consist of measurements of bone mineral density from a Lunar DPX-alpha instrument. The last section presents the profiles of drilling force along the cervical axis, as outlined in Section 7.2.3.

A8.1 BMD Measurements at the Greater Trochanter and the Femoral Head

The measurements of BMD at the greater trochanter of three porcine proximal femurs are shown in figures A8.1.1, A8.1.2 and A8.1.3.

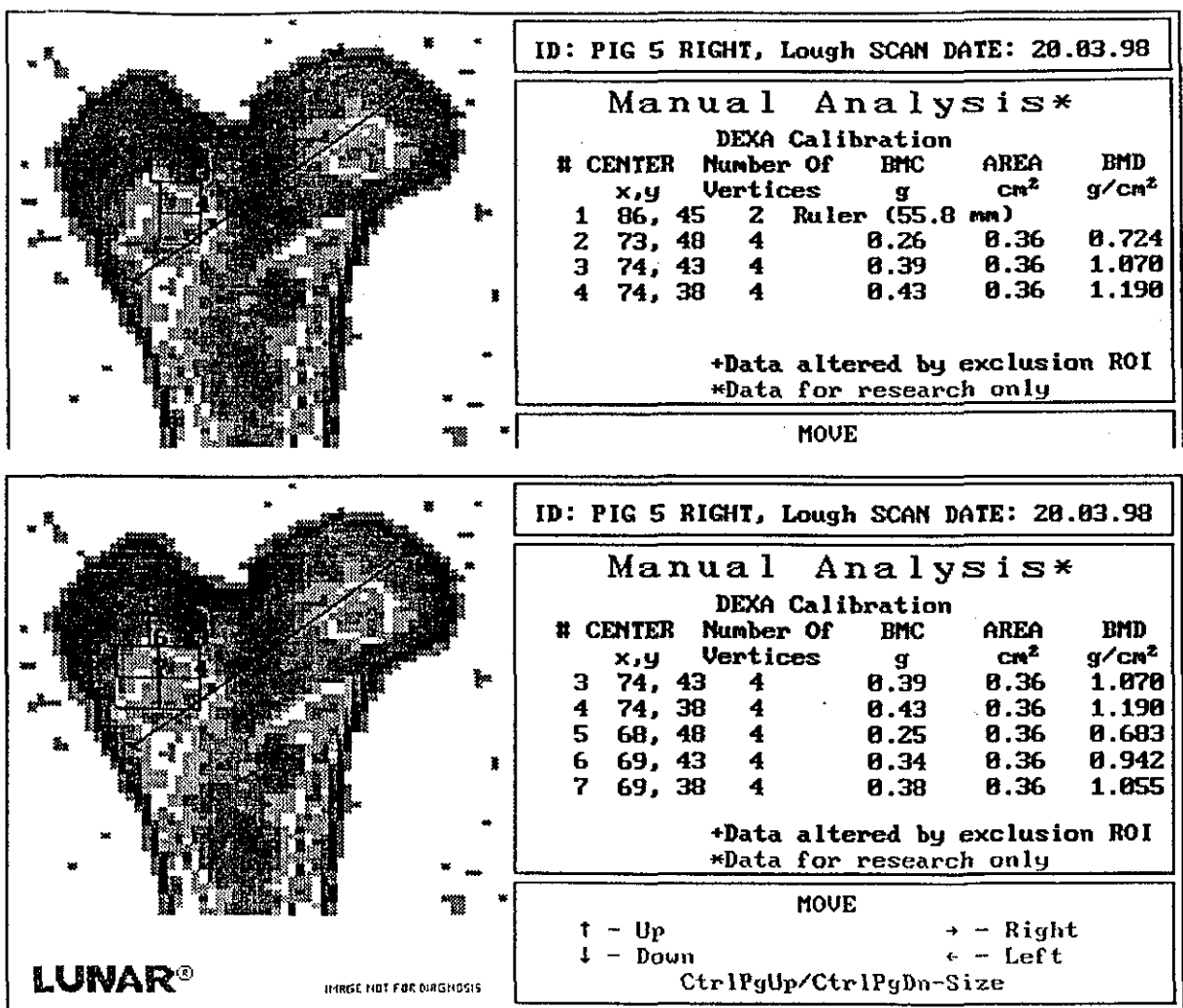


Fig. A8.1.1 BMD measurements at the greater trochanter of porcine femur (1)

The measurements of BMD at the femoral head of two porcine proximal femurs are presented in figures A8.1.4 and A8.1.5.

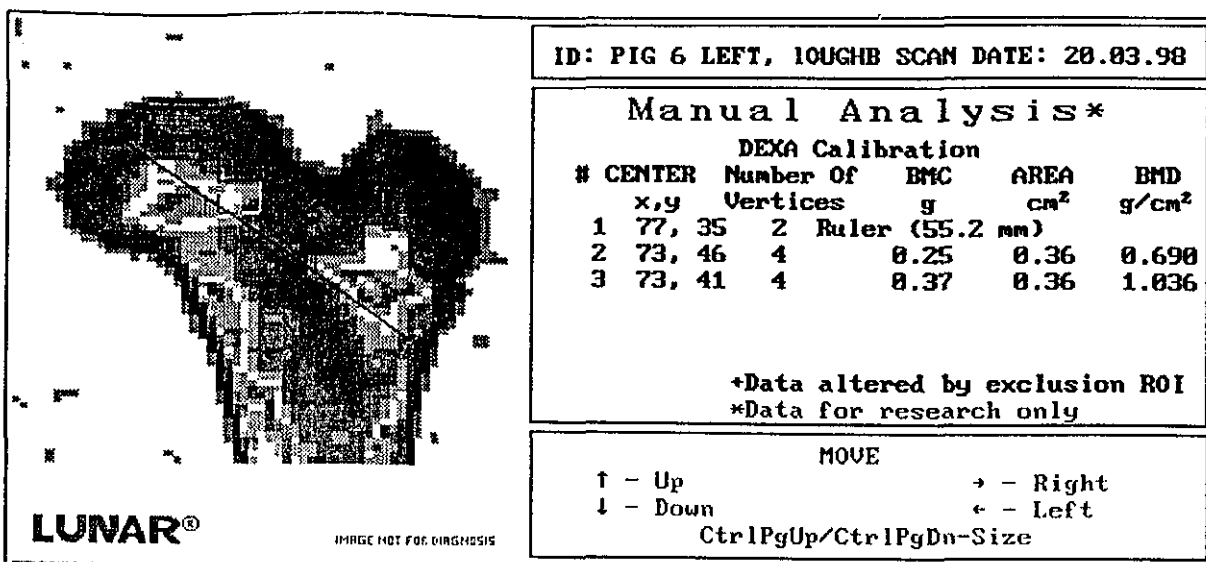
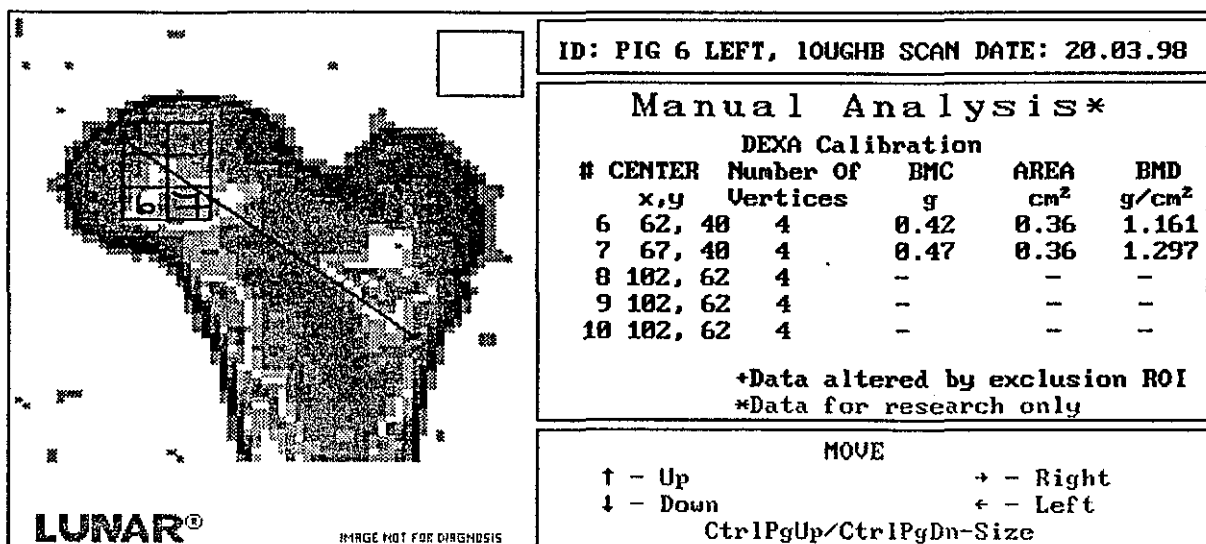
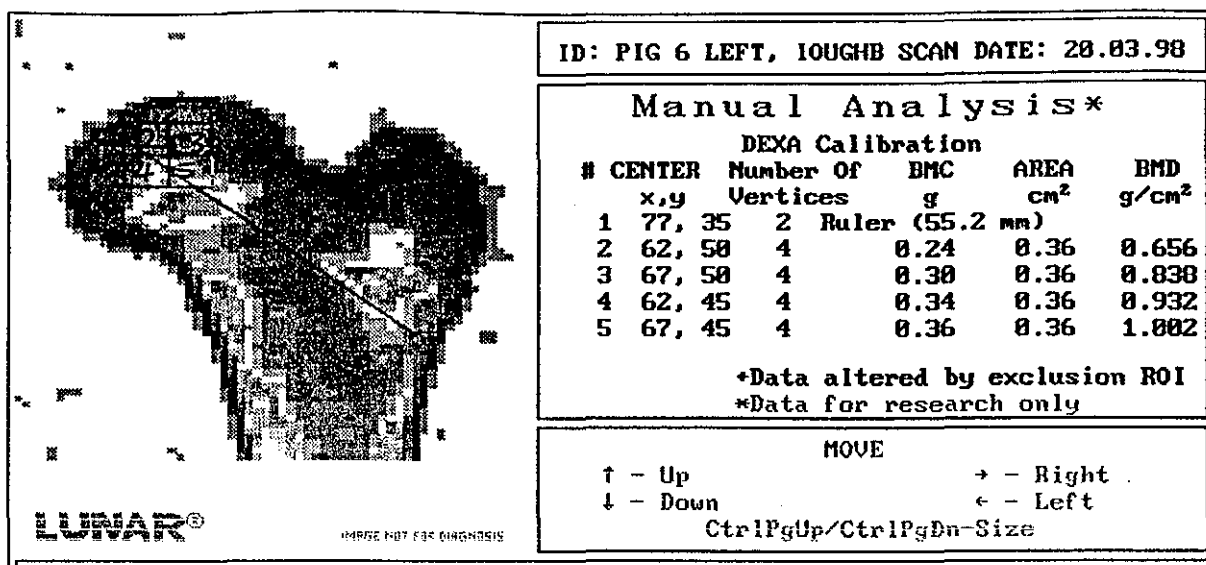
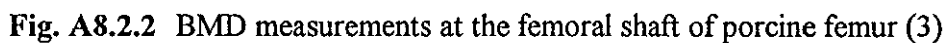
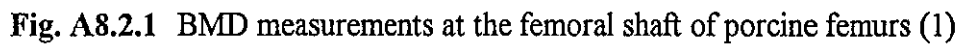


Fig. A8.1.4 BMD measurements at the femoral head of porcine femur (2)

The measurements of BMD at the femoral shaft of three porcine proximal femurs are shown in figures A8.2.1, A8.2.2 and A8.2.3.



The measurements of BMD along the cervical axis of a porcine proximal femur, according to the ROIs shown in figure 7.10a, are shown in figures A8.3.1, A8.3.2 and A8.3.3.

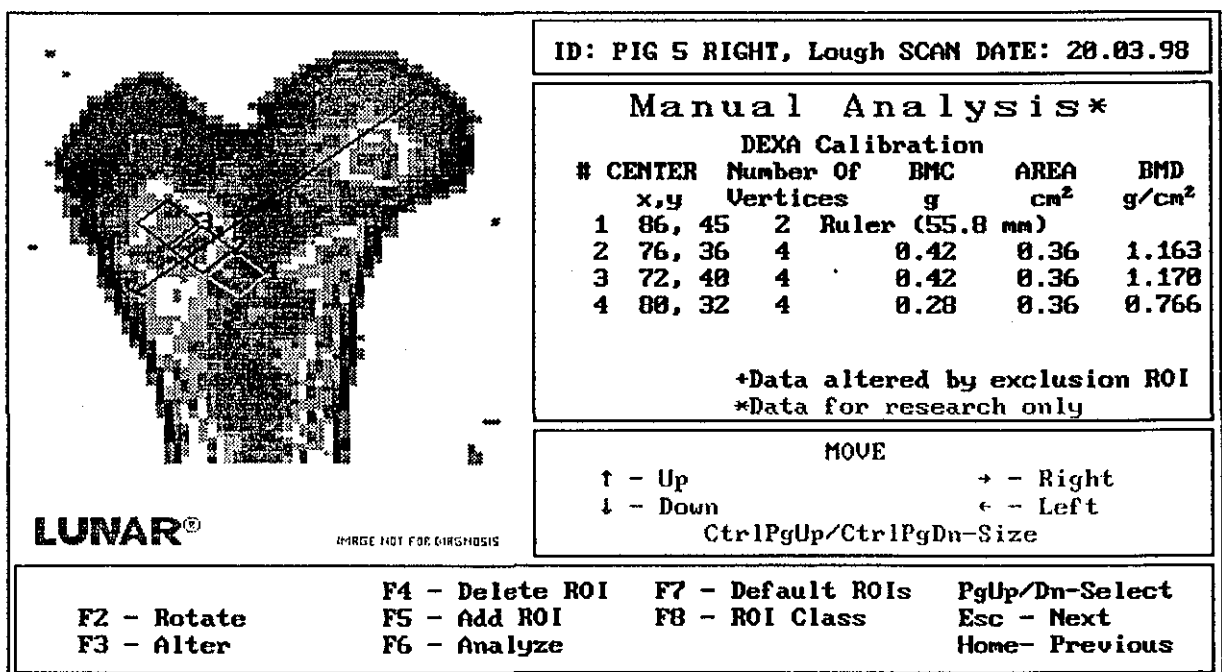
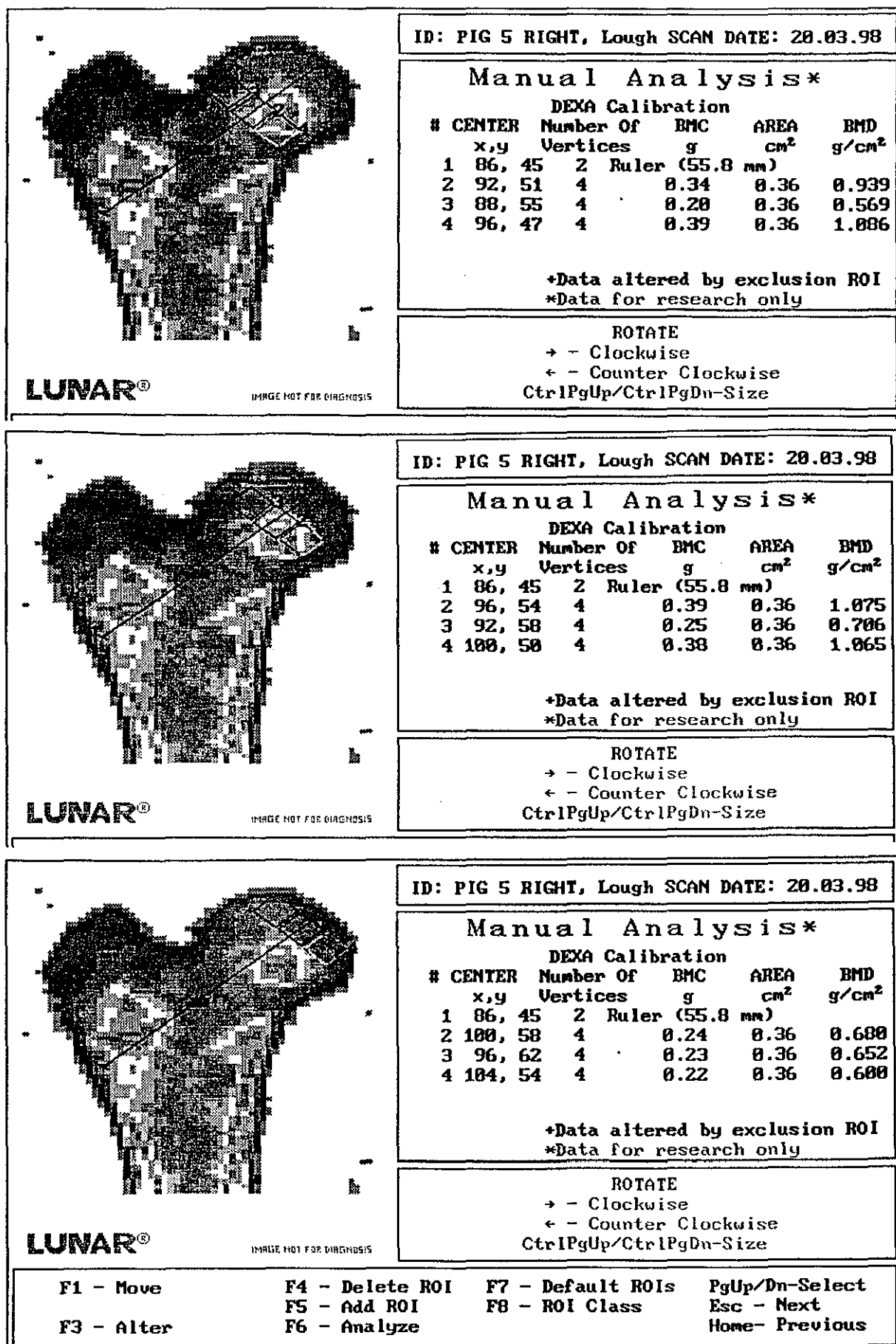


Fig. A8.3.1 BMD measurements along the cervical axis of a porcine femur (ROIs 1 & 2)




LUNAR® IMAGE NOT FOR DIAGNOSIS

ID: FIG 5 RIGHT, Lough SCAN DATE: 20.03.98

Manual Analysis*

DEXA Calibration

#	CENTER x,y	Number Of Vertices	BMC g	AREA cm ²	BMD g/cm ²
1	86, 45	2	Ruler (55.8 mm)		
2	96, 54	4	0.39	0.36	1.075
3	92, 58	4	0.25	0.36	0.706
4	100, 50	4	0.38	0.36	1.065

+Data altered by exclusion ROI
*Data for research only

ROTATE
→ - Clockwise
← - Counter Clockwise
CtrlPgUp/CtrlPgDn-Size



LUNAR® IMAGE NOT FOR DIAGNOSIS

ID: FIG 5 RIGHT, Lough SCAN DATE: 20.03.98

Manual Analysis*

DEXA Calibration

#	CENTER x,y	Number Of Vertices	BMC g	AREA cm ²	BMD g/cm ²
1	86, 45	2	Ruler (55.8 mm)		
2	100, 58	4	0.24	0.36	0.680
3	96, 62	4	0.23	0.36	0.652
4	104, 54	4	0.22	0.36	0.600

+Data altered by exclusion ROI
*Data for research only

ROTATE
→ - Clockwise
← - Counter Clockwise
CtrlPgUp/CtrlPgDn-Size

F1 - Move	F4 - Delete ROI	F7 - Default ROIs	PgUp/Dn-Select
F3 - Alter	F5 - Add ROI	F8 - ROI Class	Esc - Next
	F6 - Analyze		Home- Previous

Fig. A8.3.3 BMD measurements along the cervical axis of a porcine femur(ROIs 6, 7 & 8)

A8.4 Actual Profiles of Drilling Force in the Direction of the Cervical Axis

The profiles of drilling force at a porcine proximal femur along the cervical axis are presented in accordance with the sections of the superior, the cervical axis and the inferior, shown in figures A8.4.1, A8.4.2 and A8.4.3. Each section is further classified into zones of the anterior, the lateral-medial and the posterior, as shown in figures 7.10a and 9.9. The drilling forces were obtained using an industrial twist drill bit of diameter 2.5 mm, which is driven at a feed rate of 90 mm/min and a rated drill bit rotational speed of 1000 rev/min.

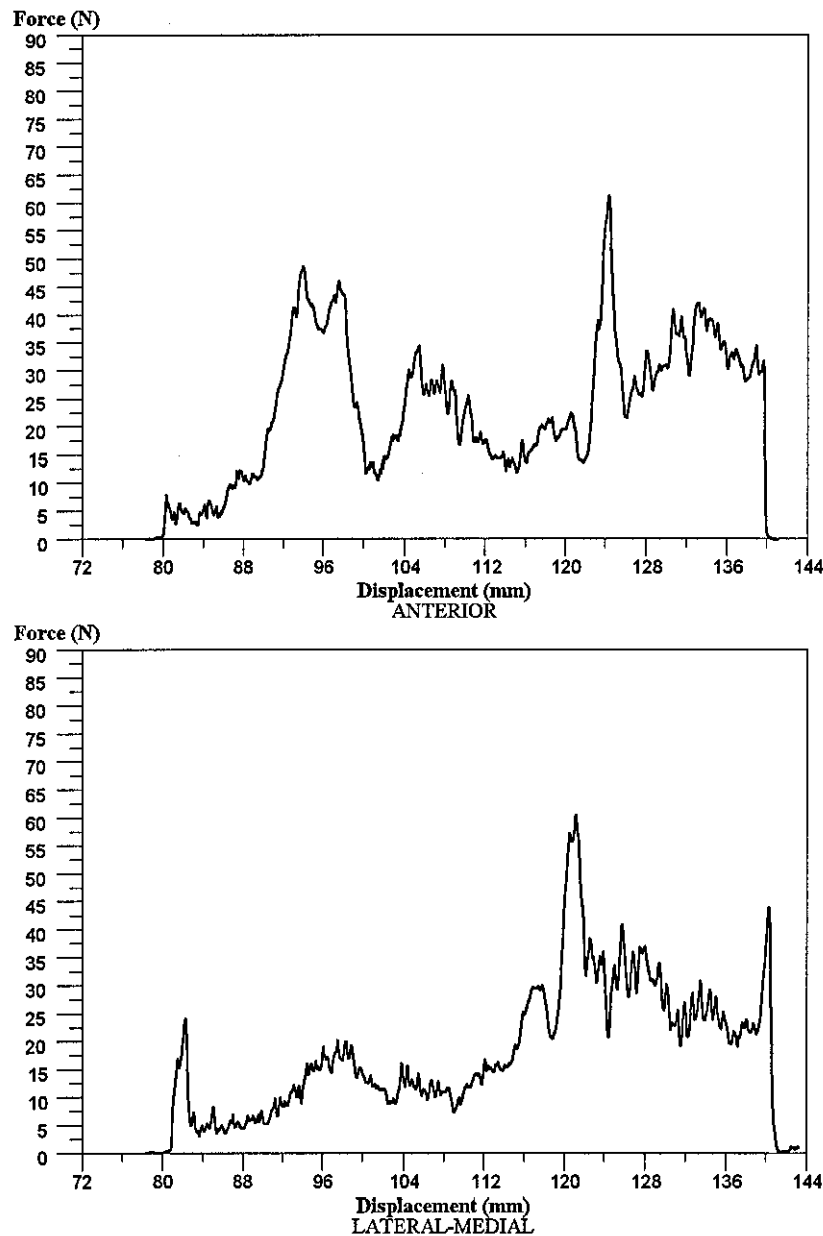


Fig. A8.4.1 Profiles of drilling forces at the superior section to the cervical axis of a porcine proximal femur (Feed Rate = 90 mm/min; Rated Speed = 1000 rev/min)

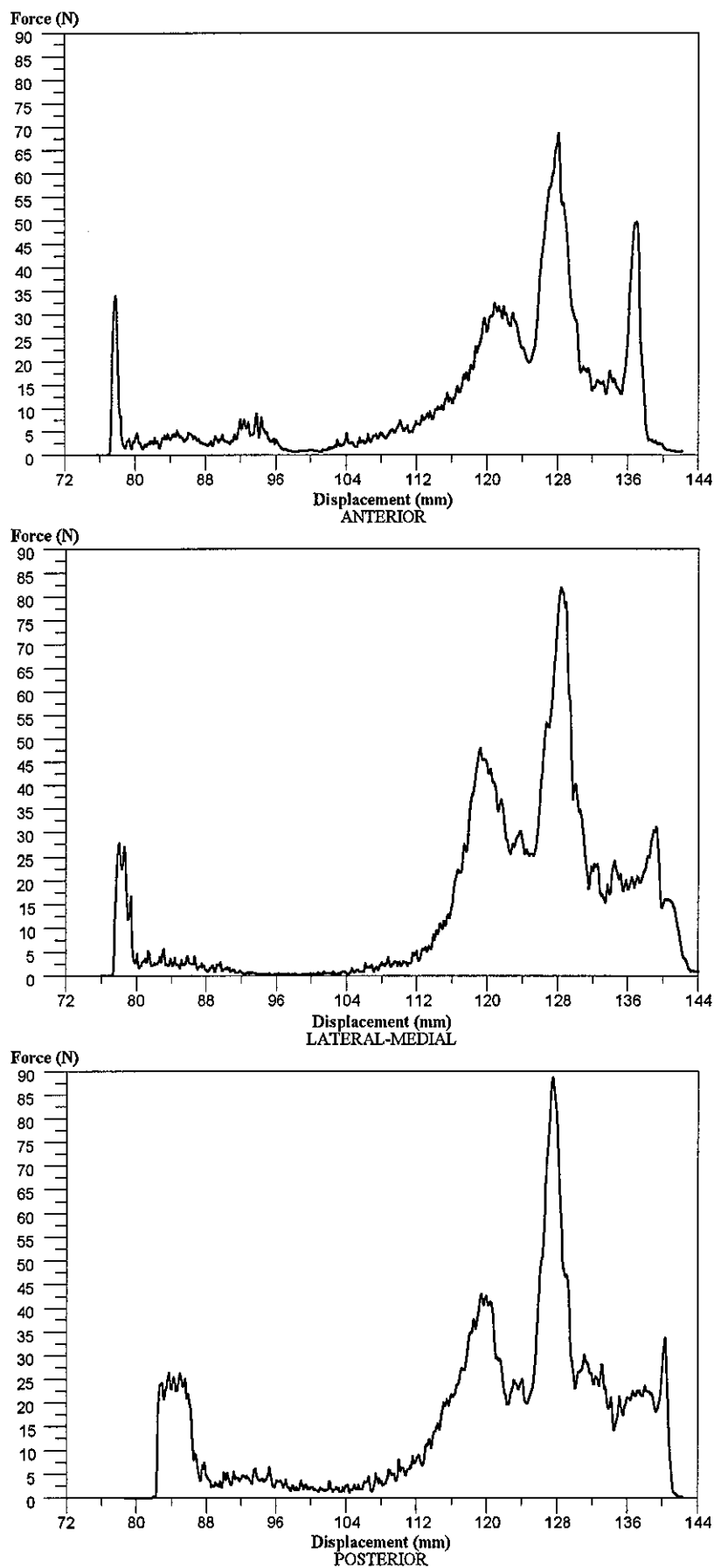


Fig. A8.4.2 Profiles of drilling forces along the cervical axis of a porcine proximal femur (Feed Rate = 90 mm/min; Rated Speed = 1000 rev/min)

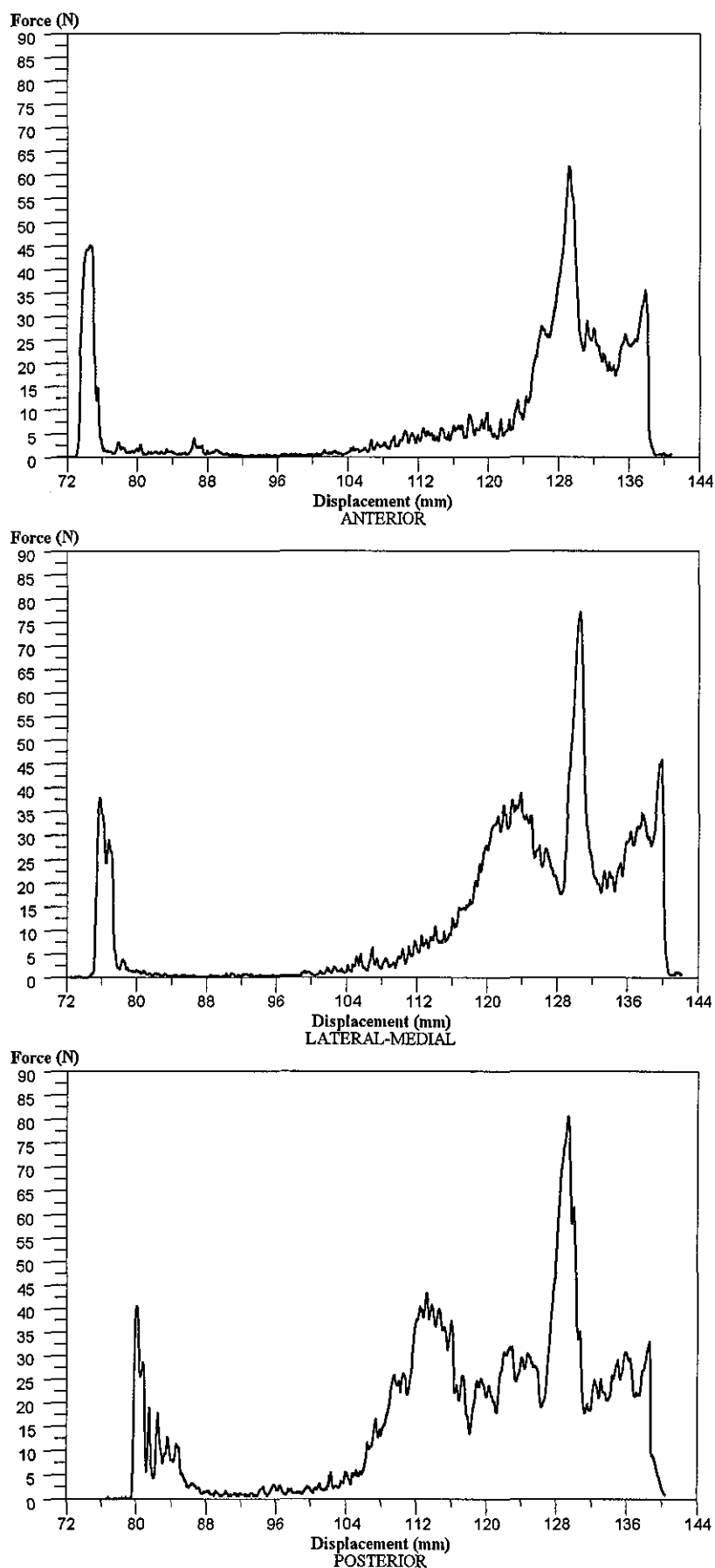


Fig. A8.4.3 Profiles of drilling forces at the inferior section to the cervical axis of a porcine proximal femur (Feed Rate = 90 mm/min; Rated Speed = 1000 rev/min)

Appendix 9
Mechanical Design - Drawings

A9.1 The Pan Joint with Brake Unit

PLANS TAKEN FROM HERE

A9.2 The End Effector

STOR-A-FILE IMAGING LTD

PLANS TAKEN FROM HERE

Date: 12/02/08

Authorised by: Simon Cockbill

Issue 2

Page 1 of 1

If in hard copy, this page is UNCONTROLLED and only valid on date of issue 22-Feb-08

A9.3 A Calibration Frame

STOR-A-FILE IMAGING LTD

PLANS TAKEN FROM HERE

Date: 12/02/08

Authorised by: Simon Cockbill

Issue 2

Page 1 of 1

If in hard copy, this page is UNCONTROLLED and only valid on date of issue 22-Feb-08

A9.4 The Drilling Experimental Rig

PLANS TAKEN FROM HERE

